

THESE DE DOCTORAT DE

L'UNIVERSITE DE NANTES
COMUE UNIVERSITE BRETAGNE LOIRE

ECOLE DOCTORALE N° 602
Sciences pour l'Ingénieur
Spécialité : « *Génie des Procédés et Bioprocédés* »

Par

«Arturo-Vladimir HEREDIA-MARQUEZ»

**«Optimization of Biofuel production in
Solar conditions by Microalgae»**

Thèse présentée et soutenue à «Saint-Nazaire», le « 06 novembre 2020 »

Unité de recherche : Laboratoire GEPEA, UMR-CNRS 6144

Thèse N° :

Rapporteurs avant soutenance :

Elisabeth BADENS
Pascal GUIRAUD

Professeur des universités HDR, Aix-Marseille Université
Professeur des universités HDR, INSA

Composition du Jury :

Président :	Elisabeth BADENS	Professeur des universités HDR, Aix-Marseille Université
Examineurs :	Arnaud ARTU Nabil GRIMI	PhD Procédés Microalgues, TOTAL Maître de conférences HDR, U. de Technologie de Compiègne
Dir. de thèse :	Jeremy PRUVOST	Directeur GEPEA, UMR-CNRS 6144
Co-dir. de thèse :	Luc MARCHAL	Professeur des universités HDR, Université de Nantes
Co-dir. de thèse :	Olivier Gonçalves	Maître de conférences HDR, Université de Nantes

Résumé de la thèse en français

Optimisation de la production de biocarburants par les microalgues en conditions solaires

Vladimir HEREDIA
Université de Nantes - GEPEA

Le changement climatique et la croissance de la société qui exige toujours plus de ressources sont deux des principaux défis de l'humanité. La production d'énergie propre et durable en est justement un des plus grands enjeux. Dans ce contexte, la production de biocarburants liquides par les microalgues est censée contribuer à la régulation des *climate drivers* (changements liés à l'effet de serre), tout en produisant une partie de l'énergie nécessaire aux besoins de la société.

Le bioéthanol et le biodiesel produits à partir de microalgues utilisent les métabolites accumulés par la cellule (carbohydrates de type sucres et lipides de type TAG) lors de conditions de croissance défavorables, telles que l'absence d'azote dans le milieu ou les fortes intensités lumineuses reçues par la culture. Cependant, actuellement, le processus de production nécessite être optimisé pour lever des verrous du passage à grande échelle et pour produire plus d'énergie qu'il n'en consomme. Cela concerne principalement la quantité de sucres et de lipides produits par le procédé de culture, ainsi que les technologies et leur efficacité, tout au long de la chaîne de production.

Au cours de ces travaux seront étudiés et optimisés des protocoles de culture solaire pour la production de métabolites énergétiques. Les effets sur les changements cellulaires les plus marquants tels que la teneur en lipides et en sucres, et les changements de la résistance mécanique cellulaire lors de la limitation azotée seront étudiés. Les impacts de ces changements sur les étapes de récupération des molécules énergétiques d'intérêt seront également analysés et optimisés. De même, les principales variables opérationnelles de l'extraction des lipides par voie humide seront également optimisées (*ie.* le rapport solvant/culture, le type de solvant, le temps de séjour pour la destruction des cellules). Pour terminer, l'impact de ces résultats sera évalué selon différents scénarios dans un modèle de valorisation énergétique globale.

Les souches de microalgues ont des réponses différentes à la carence en azote dans le milieu, il a été proposé au chapitre 2 de déterminer comment la souche s'adapte à quatre niveaux consécutifs de limitation azotée en mode continu (56%, 46%, 29% et 13% d'azote).

Lors d'une culture sous récolte et illumination en continu, la concentration en biomasse de *N. gaditana* est passée de 2,13 kg/m³ en conditions non limitées (200%_{NO₃}) à 0,89kg/m³ en limitation à 13%_{NO₃}. La concentration en biomasse n'a été pas affectée de façon linéaire par rapport à la limitation azotée. Une réduction de la concentration d'azote de 200%_{NO₃} à 56%_{NO₃} ne réduit que de 3% la concentration en biomasse. En revanche, une limitation plus forte de 29%_{NO₃} à

13% NO_3 a réduit la concentration en biomasse de 36%. La tendance au final est très proche de celle d'une autre microalgue d'intérêt, également considérée dans cette thèse pour comparaison, à savoir *P. kessleri* dont l'étude est présentée par Kandilian *et al.* [2019]. Une différence notable entre les deux souches est liée au niveau de stress nécessaire pour accumuler leurs molécules de réserve énergétique. Il semble que *P. kessleri* accumule préférentiellement des sucres par rapport aux TAG dans toutes les conditions. Par ailleurs, même si *N. gaditana* accumule légèrement plus de sucres dans des conditions de limitation moyenne (56% et 46% NO_3) et plus de TAG dans des conditions de limitation fortes (29% et 13% NO_3), l'accumulation est globalement équilibrée entre les deux types de réserve lorsqu'on compare avec *P. kessleri*.

L'effet combiné sur la croissance de la biomasse et sur la composition des réserves énergétiques chez *N. gaditana* a permis d'obtenir les valeurs maximales de productivité en sucres et en TAG à un niveau de limitation de 56% NO_3 , équivalentes à 3,41 et 2,19 $\cdot 10^{-3}$ Kg/m².j (SE 0,17 et 0,19) respectivement. La productivité en sucres n'a pas beaucoup varié dans la limitation à 56% NO_3 par rapport à l'expérience non limitée (200% NO_3). Cependant, elle a chuté de manière significative aux niveaux de limitation inférieurs, passant de 2,28 $\cdot 10^{-3}$ Kg/m².j à 46% NO_3 à 1,19 $\cdot 10^{-3}$ Kg/m².j à 13% NO_3 (SE 0,12 et 0,11 respectivement). La productivité en TAG est restée pratiquement inchangée pour les limitations à 56%, 46% et 29% NO_3 , atteignant des valeurs de 2,19, 1,87 et 1,94 $\cdot 10^{-3}$ Kg/m².j (SE 0,19, 0,18, 0,07) respectivement. Bien que le niveau de limitation à 13% NO_3 ait déclenché la teneur la plus élevée (24,2% X), la productivité en TAG a atteint 1,56 $\cdot 10^{-3}$ Kg/m².j (SE 0,16), dû ici à une productivité en biomasse plus faible. Par rapport à *P. kessleri* tel que rapporté par Kandilian *et al.* [2019], la différence la plus forte est observée dans la productivité en sucres en raison d'une forte teneur en sucres (environ 64%) dans les limitations azotée pour *P. kessleri*. La productivité la plus élevée est atteinte à 7,8 $\cdot 10^{-3}$ Kg/m².j pour une limitation de 46% NO_3 .

Il a également été analysé l'effet de la limitation azotée sur le taux de destruction cellulaire de la culture. Cette étape est en effet importante lors de l'extraction en voie humide des TAG. Une culture non limitée de *N. gaditana* peut être détruite à 75% en un seul passage par homogénéisation à haute pression à 1750 bar. Cette valeur est maintenue avec une faible limitation à 56% NO_3 . Mais ensuite, dans la limitation à 46% NO_3 , le taux de destruction τ_D a diminué à 63% pour finalement représenter 17% pour la limitation la plus faible. La concentration cellulaire comme explication à ce phénomène a été rejetée puisque la préparation de l'échantillon a toujours été établie pour obtenir un concentration en biomasse à 1kg/m³. La modification de la composition et de l'épaisseur de la paroi cellulaire pourrait expliquer ce résultat, engendrant une résistance plus élevée des cellules [Beacham *et al.*, 2014, Janssen *et al.*, 2019b, 2020, Scholz *et al.*, 2014, Zhang and Volkman, 2017].

La destruction cellulaire des microalgues cultivées dans des conditions de carence en azote est un facteur important pour la récupération des TAG et des sucres intracellulaires lors du traitement

de la biomasse humide. Nos résultats montrent au final que même si la productivité est élevée pour certains niveaux de limitation, tous les composés ne pourraient pas être récupérés si la cellule résiste à la destruction, réduisant alors l'efficacité de récupération globale des lipides. Les résultats obtenus ont donc des conséquences sur l'ensemble de la consommation énergétique dans le processus de production de biocarburants.

L'autre information est que nos résultats ont souligné que les niveaux de limitation azotée appliqués peuvent avoir un impact différent sur la productivité en TAG et sucres de différentes souches de microalgues. À certains niveaux de limitation, la production de sucres sera supérieure à celle en TAG, ou *vice versa*. Cela pourrait donc avoir au final une incidence sur la quantité et le type d'énergie qui peut être obtenue sous la forme de biocarburants. Pour cette raison, une analyse théorique sur l'énergie potentiellement récupérable (E_P) a été discutée.

Nannochloropsis gaditana a atteint une valeur maximale d'énergie récupérable pour le biodiesel et le bioéthanol de 67,8 et 18,7 J/m²·j respectivement, pour une quantité correspondante d'énergie récupérable totale E_P de 86,6 J/m²·j. Cela a été atteint pour la limitation à 56% $_{NO_3}$. À titre de comparaison, la quantité d'énergie potentiellement récupérable E_P pour *P. kessleri* est de 128 J/m²·j à la limitation 46% $_{NO_3}$ [Kandilian *et al.*, 2019] avec 47 J/m²·j correspondant à l'énergie obtenue à partir du bioéthanol et 81 J/m²· à partir du biodiesel.

En conclusion du chapitre 2, *Nannochloropsis gaditana* a montré une productivité en sucres plus faible que *Parachlorella kessleri*. *P. kessleri* a un potentiel plus important si l'on considère une double valorisation en biocarburants (biodiesel et bioéthanol), où il serait donc possible d'obtenir plus d'énergie pour la même quantité de biomasse sèche (en raison de la grande accumulation de sucres et de TAG). En revanche, *N. gaditana* est intéressant uniquement en ce qui concerne la production de biodiesel du fait d'une production en TAG plus élevée que celle en sucres. Cependant, si on considère l'effet marqué de la limitation azotée sur la destruction cellulaire, une étude complète sur l'optimisation de la production et de la récupération de TAG, ainsi que sur les processus et les variables connexes à la production de biodiesel, reste nécessaire pour exploiter le potentiel de *N. gaditana* pour la production de biocarburants.

Le chapitre 3 porte sur l'optimisation de la production en TAG de *Nannochloropsis gaditana* en culture continue et limitation azotée sous cycles jour-nuit simulés. Une telle optimisation n'est en effet pas triviale, en raison du changement d'état physiologique au cours de ces conditions de culture variables.

La première approche testée dans ce chapitre a consisté à rechercher la concentration initiale minimale de nitrate N_0 au taux de dilution maximal qui permet simultanément d'accumuler des TAG et de maintenir la croissance des cellules sans lessiver le système pendant les cycles jour-nuit simulés. Lorsque le taux de dilution est supérieur à 0,02h⁻¹, les cultures sont lessivées, même à des

concentrations en nitrate plus élevées. Avec un taux de dilution égal ou inférieur à $0,013 \text{ h}^{-1}$, un régime périodique stable est atteint avec de l'azote résiduel N_t proche de zéro (environ $0,03 \text{ mM}$ pour $56\%_{NO_3}$, $0,11 - 0,06 \text{ mM}$ pour $46\%_{NO_3}$ et $0,2 - 0,10 \text{ mM}$ pour $29\%_{NO_3}$). Ces différences sont principalement basées sur l'effet combiné du taux de dilution et du taux de croissance résultant de chaque limitation. Les productivités en TAG les plus élevées ont été constatées pour les cultures ayant une concentration initiale d'azote de $29\%_{NO_3}$ pour différents taux de dilution. Le système à $0,013 \text{ h}^{-1}$ a atteint $2,9$ et $2,3 \cdot 10^{-3} \text{ kg/m}^2 \cdot \text{j}$ de productivité surfacique en TAG aux heures de prélèvement au coucher et lever du soleil respectivement. De même, le système à $0,005 \text{ h}^{-1}$ a obtenu une productivité surfacique en TAG légèrement supérieure avec $3,0$ et $2,5 \cdot 10^{-3} \text{ kg/m}^2 \cdot \text{j}$ pour les mêmes heures d'échantillonnage.

Une fois que la stabilité du PBR sous cycles jour-nuit et limitation à $29\%_{NO_3}$ en mode continu à $0,005 \text{ h}^{-1}$ a été atteinte, une optimisation supplémentaire a été menée. L'objectif était d'ajouter ponctuellement des nitrates (NaNO_3) tout en évitant son accumulation pendant le cycle, afin d'augmenter le temps passé par les cellules en carence. Pour atteindre cet objectif, la quantité connue de NaNO_3 consommée en 24 h a été ajoutée séparément par rapport au milieu, en une seule dose et en début de journée.

Il a été observé que les teneurs en TFA et TAG ne variaient pas autant que dans les expériences précédentes pendant la période nocturne. En revanche, le taux de destruction variait de façon plus importante. Cela pourrait être lié à la modification de la paroi des cellules via la présence d'algebans, qui pourraient être impactés par la dynamique lumière/obscurité et/ou par la carence en azote. Ils pourraient jouer un rôle dans la composition de la paroi cellulaire. Cela reste à étudier, en analysant par exemple, les modifications des hydrocarbures à longue chaîne dans la composition des parois cellulaires au cours des cycles jour-nuit.

Les productivités volumétrique et surfacique en TAG ont été calculées respectivement entre $27,0$ et $20,2 \cdot 10^{-3} \text{ kg/m}^3 \cdot \text{j}$, et $0,8$ à $0,6 \cdot 10^{-3} \text{ kg/m}^2 \cdot \text{j}$. Ces résultats sont très proches de ceux obtenus avec des batchs en extérieur en cycles jour-nuit simulés, mais avec un meilleur taux de destruction des cellules. Les productivités en TAG récupérables ont été mesurées stables autour de $12,6 \cdot 10^{-3} \text{ kg/m}^3 \cdot \text{j}$ ($\text{SE}=3,7$, $n=3$) ($0,4 \cdot 10^{-3} \text{ kg/m}^2 \cdot \text{j}$).

En plus de cette expérience, la moitié de la dose d'azote pour 24 h a été fournie dans les mêmes conditions (données non présentées). L'objectif était de voir si des concentrations d'azote plus faibles auraient un impact sur la teneur en TAG. Étonnamment, après stabilisation, les teneurs en lipides totaux et en TAG n'ont pas changé de manière significative ($12,4\%$ et $12,1\%$ respectivement ; $\text{SE}=0,23\%$ et $0,82\%$, $n=2$) mais la concentration en biomasse a diminué à $0,7 \text{ kg/m}^3$ ($2,5$ et $2,1 \text{ kg/m}^3$ pour les protocoles continus et ponctuels à dose complète, respectivement). En réduisant à la moitié les besoins en azote, la productivité surfacique en TAG a diminué à $0,3 \cdot 10^{-3} \text{ kg/m}^2 \cdot \text{j}$, ce qui correspond également à la moitié de la productivité surfacique en TAG de la dose complète.

En comparant la productivité en TAG obtenue sous apport ponctuel (soit $0,8 \cdot 10^{-3}$ kg/m²·j) avec la productivité en limitation azotée sous apport continu (3 à $2,5 \cdot 10^{-3}$ kg/m²·j), la productivité la plus élevée (et la teneur la plus élevée en TAG) a été obtenue avec l'apport continu ; avec 70% d'augmentation par rapport aux protocoles d'apport ponctuel (90% pour la moitié de l'apport). Si on compare aux essais de culture batchs avec carence en azote, une augmentation similaire est obtenue. Ces résultats permettent de supposer qu'un faible excès d'azote dans le milieu, par rapport à une culture totalement carencée, est bénéfique pour la synthèse de TAG. Il est possible que certaines voies de translocation ou de synthèse *de novo* soient activées/désactivées pour permettre à la cellule de survivre pendant les cycles jour-nuit. Par conséquent, la baisse de productivité en cas d'ajout ponctuel pourrait être due au fait que les cellules privilégient leur survie plutôt qu'accumuler des TAG, puisque les cellules ont juste la quantité d'azote suffisante; ce qui ne se produit pas lorsque les cellules ont un peu plus d'azote que nécessaire pendant le protocole de limitation avec apport continu.

Le chapitre 4 a été consacré à l'étude de la récupération des TAG en voie humide, celle-ci s'étant montrée efficace sur le plan énergétique [Angles *et al.*, 2017, Dong *et al.*, 2016, Ghasemi Naghdi *et al.*, 2016, Lee *et al.*, 2012, Taher *et al.*, 2014]. Les analyses ont été menées sur *N. gaditana* en étudiant les opérations d'extraction en voie humide: broyage à billes et extraction centrifuge continue. Du fait de sa résistance mécanique plus élevée et de son aptitude à produire des TAG en quantité significative, cette espèce est une candidate intéressante pour optimiser le procédé global du biodiesel par voie humide.

Tout d'abord, l'optimisation de la destruction cellulaire réalisée sur la biomasse de deux cultures (l'une non-carencée et l'autre carencée en azote) a permis de calculer le temps de séjour nécessaire au broyeur à billes pour détruire 80% des cellules. Ces valeurs sont de 4,8 min pour une culture non-carencée et 5,8 min pour la culture carencée, du fait de la diminution de la fragilité cellulaire observée au chapitre 2.

Ensuite, le meilleur des trois solvants proposés a été choisi en fonction de la quantité de TAG récupérée dans la biomasse carencée en azote. Le Me-THF et l'EtoAc ont montré une efficacité d'extraction similaire $\eta_{E,TAG}$: jusqu'à 88% et 82% respectivement. L'heptane est le moins efficace, avec 34 %. Dans tous les cas montrés dans cette étude, les TAG ont représenté 89% des lipides totaux, ce qui montre que les solvants utilisés n'ont aucune sélectivité pertinente vis-à-vis des TAG.

En utilisant la destruction cellulaire en combinaison à l'extraction, il a pu être étudié l'affinité des solvants une fois que les molécules TAG étaient déjà libérées dans le milieu. Cela a permis de maximiser le rendement de l'extraction et donc de réduire la quantité de solvant utilisée. Le Me-THF a été au final choisi comme le plus efficace des trois solvants.

Un plan d'expériences type Box-Benhken a été choisi comme méthode d'optimisation des prin-

cipaux paramètres d'extraction centrifuge continue, pour réduire le nombre de tests et analyser simultanément les interactions multiparamétriques. Il comprenait 15 unités d'observation (UO) pour trois facteurs indépendants et une variable réponse: 12 UO dérivées de variables indépendantes autour de 3 autres UO en tant que répliques du point central. La valeur optimale obtenue avec cette méthode, ainsi que les résultats du broyage à billes, ont eu pour objectif d'obtenir des informations pertinentes sur l'efficacité globale de la méthode d'extraction par voie humide dans le contexte du biodiesel.

D'abord, des pré-tests ont défini la plage opérationnelle de concentration en biomasse entre 2 et 10 g/L afin d'éviter autant que possible l'émulsification. Ensuite, les variables et les plages choisies pour le dispositif d'extraction centrifuge ont été choisies pour chaque paramètre opératoire: concentration en biomasse X (provenant du broyeur à billes) 2, 5, 10 g/L ; débit de solvant (Me-THF) et d'alimentation S et F , 5, 7,5, 10 mL/min chacune. Les échantillons de chaque OU ont été analysés pour déterminer le rendement de l'extraction des lipides totaux/TAG ($\eta_{E,i}$).

Après exploitation par le logiciel Design Expert, les données se sont avérées correspondre à un modèle d'ordre quadratique. La réalisation d'une ANOVA a montré que les sources du premier ordre (A:concentration en biomasse, B:taux de solvant et C:taux d'alimentation) semblent avoir moins d'importance que les sources du second ordre (AB, AC, BC, A^2 , B^2 et C^2). En ignorant les variables additives, la source AB (Coeff_{TFA} : 0,230, Coeff_{TAG} : 0,236) s'est avérée avoir l'effet proportionnel le plus important sur le rendement de l'extraction $\eta_{E,i}$, suivie par un effet proportionnel inverse sur la relation entre S et F (Coeff_{TFA} : -0,118, Coeff_{TAG} : -0,135). Cela signifie simplement que si l'on veut récupérer davantage de lipides, il faut utiliser un débit de solvant S plus élevé, mais cet effet est diminué si le débit de culture F augmente par rapport à S . Aussi une concentration en biomasse élevée nécessitera plus de temps et un contact d'interface plus élevé avec le solvant, ce qui peut être obtenu en réduisant la vitesse d'alimentation pour l'extraction centrifuge continue.

Le logiciel Design Expert fournit également un outil permettant de localiser numériquement le point optimal pour les trois sources simultanées. En utilisant un risque d'erreur $\alpha = 0,05$ et pour une efficacité d'extraction maximale dans le modèle, on a constaté que $\eta_{E,TFA} = 0,93$ à $X = 8,3$ g/L, $S = 9,2$ mL/min, $F = 5,0$ mL/min et $\eta_{E,TAG} = 0,84$ à $X = 7,9$ g/L, $S = 8,9$ mL/min, $F = 5,4$ mL/min. Ces deux points d'efficacité sont conformes aux analyses précédentes. À noter que ces valeurs sont issues du 80% de lipides libérés lors de l'opération de broyage à billes précédente.

Au point optimal obtenu avec le plan d'expérience, la consommation spécifique de solvant pour l'extraction centrifuge continue a pu être déterminée à $\Gamma_{Me-THF} = 213,8$ g_{Me-THF}/g_{TAG}. Au final, un rendement optimal d'extraction en voie humide de 73% a été obtenu avec le broyage à billes combiné à l'extraction centrifuge continue (utilisant le Me-THF).

Les résultats de l'extraction centrifuge continue pourraient être améliorés. Une intensification supplémentaire de l'étape d'extraction serait nécessaire pour combiner le changement d'échelle et

la réduction de la consommation de solvant, ainsi que pour résoudre les problèmes d'émulsification pour la production de biodiesel. Ces travaux ont aussi démontré la relation entre les niveaux de stress azoté, la concentration en biomasse et la libération de matière intracellulaire avec formation d'émulsion. Cela a mené à identifier une zone de travail à éviter lors de l'extraction centrifuge continue. À cet effet, des recherches supplémentaires sur l'optimisation de l'hydrodynamique dans la chambre d'extraction centrifuge continue pourraient permettre de travailler avec des concentrations en biomasse plus élevées, ce qui augmenterait l'efficacité globale du procédé.

Le chapitre 5 a eu pour but de conduire un analyse énergétique de l'ensemble de la production de biodiesel en utilisant les protocoles optimisés, les concepts proposés et les résultats des chapitres précédents. En parallèle, la co-production de bioéthanol a également été incluse dans une approche de bioraffinage énergétique supplémentaire.

L'ensemble du processus de production a été divisé en blocs opérationnels : Production de biomasse (Prod-100), récupération des métabolites (Rec-200), conversion du biodiesel (BioD-300) et conversion du bioéthanol (BioE-400). En particulier, le bloc de production de biomasse comprend le Photobioréacteur (PBR-101) et la Centrifugation (C-102) ; le bloc de récupération des métabolites comprend le Broyage à billes (BM-201) et l'Extraction centrifuge continue (CX-202) ; le bloc de conversion du biodiesel comprend une première Récupération de solvant (D-301), puis la Transestérification (R-302) et la Récupération de biodiesel (D-302); et enfin le bloc de conversion du bioéthanol couvre l'unité de Fermentation (R-401) et la Récupération d'éthanol (D-402).

Les cinq cas de simulation pour une production de 1 Tn/an de biomasse de microalgues ont été établis de la manière suivante :

Cas 1: Le bloc Prod-100 est un photobioréacteur Flat-Panel FP-PBR de 10 cm de profondeur, injection d'air pour le mélange de la culture, avec contrôle de température par refroidissement évaporatif passif PEC, [Nwoba *et al.*, 2020]. Il correspond à la culture de *Nannochloropsis gaditana* en mode continu/chemostat (taux de dilution D 0,01 h⁻¹), lumière continue (250 $\mu\text{mol}/\text{m}^2\cdot\text{s}$) et limitation azotée (56%_{NO₃}) selon les résultats du chapitre 2,

Cas 2: Le bloc Prod-100 est un FP-PBR de 10 cm de profondeur avec injection d'air pour le mélange de la culture. Le contrôle de la température a été ici considéré en utilisant l'unité de verre isolant (IGU, insulated glass unit), avec un générateur intégré d'énergie photovoltaïque, comme présenté par Nwoba *et al.* [2020]. Le même protocole de culture que celui utilisé dans le Cas 1 a été appliqué : culture de *N. gaditana* en mode continu/chemostat (D 0,01 h⁻¹), lumière continue (250 $\mu\text{mol}/\text{m}^2\cdot\text{s}$) et limitation azotée (56%_{NO₃}) pour *N. gaditana*,

Cas 3: Un photobioréacteur à haute productivité volumétrique HVP-PBR de type Algofilm [Pruvost *et al.*, 2016] a été simulé pour le bloc Prod-100. Le HVP-PBR a été considéré comme ayant une profondeur de 2 mm, une injection d'air pour le mélange de la culture, le verre isolant IGU pour le contrôle de la température et la cogénération d'énergie photovoltaïque. Comme pour les Cas 1 et 2, ce scénario comprenait le même protocole de culture pour la culture de *N. gaditana*, *ie.* *N. gaditana* sous mode continu/chemostat (D , $0,01 \text{ h}^{-1}$), lumière continue ($250 \mu\text{mol}/\text{m}^2\cdot\text{s}$) et limitation azotée ($56\%_{\text{NO}_3}$),

Cas 4: La quatrième simulation comprenait un HVP-PBR de 2 mm de profondeur, l'injection d'air pour le mélange de la culture, le système IGU pour le contrôle de la température et la cogénération d'énergie photovoltaïque. Dans ce cas, le protocole continu en conditions solaires utilisé pour la culture *N. gaditana* était basé sur le protocole proposé dans le chapitre 3. Il fait appel à l'utilisation simultanée d'une production continue à un taux de dilution D de $0,005 \text{ h}^{-1}$, de la limitation azotée à $29\%_{\text{NO}_3}$ et de l'apport de lumière en cycles jour-nuit simulés avec une densité de flux photonique moyenne de $269 \mu\text{mol}/\text{m}^2\cdot\text{s}$, et

Cas 5: Pour le dernier scénario, le Prod-100 a utilisé la même unité PBR (HVP-PBR de 2 mm de profondeur, injection d'air, IGU+photovoltaïque) que pour le Cas 4, mais il a été envisagé une culture de *Parachlorella kessleri* produisant une grande quantité de TAG et de sucres sur la base des résultats obtenus par Kandilian *et al.* [2019] ; *ie.* fonctionnement en mode continu sous un taux de dilution D de $0,01 \text{ h}^{-1}$, lumière continue à $250 \mu\text{mol}/\text{m}^2\cdot\text{s}$ et limitation azotée à $46\%_{\text{NO}_3}$.

L'analyse des technologies de culture pour le bloc de production a d'abord été étudiée. Dans des conditions idéales (unités de procédé considérées 100% efficaces), le FP-PBR+PEC ne peut atteindre que 0,07 avec donc un bilan énergétique largement négatif. Cela contraste avec la valeur idéale du FP-PBR+IGU+PV à 0,84 ; plus proche de la neutralité énergétique ($\text{NER}=1$). Lors de l'introduction du HVP-PBR+IGU+PV (Cas 3), le NER_{BioD} a considérablement augmenté, avec une valeur idéale de 53,6. La principale différence entre ces deux derniers concerne la cogénération d'énergie photovoltaïque et l'économie de l'apport d'énergie pour le contrôle de la température. La même tendance a pu être constatée quand les efficacités réelles (pas les idéales) ont été considérées dans les mêmes systèmes de culture : Le FP-PBR+PEC a atteint 0,04, le FP-PBR+IGU+PV a obtenu 0,8 tandis que le système photovoltaïque HVP-PBR+IGU+ a toujours le rapport le plus élevé avec 50,7.

On peut clairement constater que le système FP-PBR+PEC (Cas 1) est énergétiquement non durable en raison de son système de contrôle de la température (parallèlement au fait qu'il consomme également des quantités importantes d'eau pour le refroidissement ; non pris en compte

dans ce travail). En ce qui concerne le PBR, seule l'utilisation d'un verre isolant avec des panneaux photovoltaïques peut augmenter considérablement le ratio énergétique, avec le surplus d'énergie qui peut être utilisé pour soutenir d'autres opérations tout au long du processus de production.

Ensuite, en ajoutant l'ensemble des opérations de traitement de la biomasse au système de culture FP-PBR+PEC, le NER_{BioD} 100% a diminué de 0,07 à 0,03 (le NER_{BioD} 100% suppose 100% d'efficacité sur toutes les unités du procédé pour donner une approximation de l'énergie potentiellement récupérable après traitement). La même tendance se produit avec l'ajout du IGU et du PV (FP-PBR+IGU+PV) : l'ensemble des unités de traitement réduit le NER_{BioD} 100% eff. de 0,84 à 0,25. Au contraire, l'excédent d'énergie généré par le FP-PBR+IGU+PV pourrait être utilisé pour supporter certaines des opérations du traitement. En ajoutant simplement le bloc de récupération du métabolite Rec-200 à ce dernier, le NER_{BioD} 100% eff. est toujours positif passant de 53,6 à 1,7 ; et de 50,7 à 1,6 en considérant les pertes d'efficacité ; *ie.* environ 30 fois moins avec le bloc Prod-100 seulement. Ensuite, en ajoutant le bloc conversion de biodiesel (BioD-300), le NER_{BioD} 100% eff. est passé à 0,50 (0,47 avec les pertes d'efficacité). Cela met en évidence l'impact élevé du traitement de la biomasse sur le procédé de production de biocarburants, même si le bloc de production a un surplus important d'énergie. Les systèmes produisant de l'énergie photovoltaïque (40 870 MJ/an) peuvent compenser une partie de cette énergie, mais cela ne suffit pas encore à rendre le procédé globale (NER_{BioD}) positif. En conséquence, on peut conclure que le refroidissement par évaporation passive (PEC) et l'ajout de l'énergie photovoltaïque au système Flat-Panel (FP+PEC ou FP+IGU+PV) sont encore loin de fournir des économies d'énergie suffisantes pour améliorer le NER_{BioD} dans le processus de production global.

Le chapitre 3 a proposé un protocole intéressant basé sur la production continue sous limitation azotée et les cycles jour-nuit. Ce protocole est également plus proche des conditions réelles de fonctionnement en extérieur (*ie.* culture solaire). Ce protocole a été combiné dans le Cas 4 avec le système photovoltaïque HVP-PBR+IGU+ pour être comparé avec le protocole établi dans le Cas 3, qui comprend également le mode continu et la limitation azotée dans le même système de culture mais sous lumière continue.

Dans un premier temps, si l'on considère uniquement la production de biodiesel, la biomasse résultant du protocole en extérieur a une teneur en TAG de 30%_X, soit le double de celle du protocole en lumière continue. Une teneur en TAG plus élevée pour le premier protocole permet de produire un volume de biodiesel deux fois plus important (196 L/an, 6 746 MJ/an) que pour le second protocole (98 L/an, 3 369 MJ/an).

Si le NER_{BioD} est calculé pour le processus de production de biodiesel selon les deux protocoles mentionnés dans les Cas 3 et 4, il en résulte un procédé énergétiquement efficace ($NER > 1$) pour les blocs d'opération Prod-100 + Rec-200. En particulier, le NER_{BioD} obtenu pour la production continue avec limitation azotée sous cycles jour-nuit a été de 51,5 pour le bloc Prod-100 ; ce chiffre

est tombé à 1,7 lorsque le processus du traitement Rec-200 a été ajouté. Toutefois, le processus complet jusqu'à l'obtention du biodiesel a permis d'obtenir un NER_{BioD} de 0,67 (NER_{BioD} 100% eff. de 0,71). Ces valeurs sont similaires à celles déjà examinées pour le protocole et le système du Cas 3, mais avec l'avantage que le protocole du cas 4 prend en compte les cycles jour-nuit pour une production réaliste de biocarburants en extérieur.

Ensuite, en considérant l'ajout de la conversion du bioéthanol aux simulations (Cas 4), le $NER_T(+E_{BioE})$ (calculé sur l'ensemble de la sortie énergétique) augmente légèrement à 0,68 pour le processus de production global (NER_{BioD} 100% eff. de 0,74). Si l'énergie photovoltaïque n'est pas prise en compte dans les calculs, le $NER_T(-E_{photovoltaïque})$ diminuerait fortement à 0,07, révélant à nouveau l'importance de la cogénération d'énergie photovoltaïque dans le bloc Prod-100. À noter aussi que les calculs n'ont pas considéré l'énergie nécessaire à la récupération du bioéthanol après fermentation. Au final, la récupération de 48 L/an de bioéthanol augmente la valorisation du produit du processus 24%, pour finalement produire 244 L/an (pour 1 Tn/an de biomasse); *ie.* 7 754 MJ/an en combustibles liquides uniquement et 75 259 MJ/an en incluant l'énergie photovoltaïque.

Même si les ratios énergétiques nets pour tous les cas simulés sont inférieurs à 1 pour la double production de biocarburant, les travaux présentés ici ont permis d'identifier les principales unités de procédé à forte consommation énergétique et leur effet sur le processus global, ainsi que l'importance de la coproduction d'autres sources d'énergie (photovoltaïque et simultanément biodiesel et bioéthanol) dans l'énergie finale du processus et le ratio énergétique net. Dans une approche de bioraffinage orientée vers l'énergie, la double production de biocarburant semble intéressante à étudier plus en détails; elle pourrait contribuer à diminuer les coûts du processus et à valoriser plus largement la biomasse.

Tout au long de ce manuscrit, plusieurs aspects clés du processus de production de biocarburants et de leurs interactions ont été abordés de façon intégrée. Parmi les principaux résultats à souligner:

- Effet important de la souche choisie en fonction de son potentiel énergétique;
- Protocole de production continue avec limitation azotée et cycles jour-nuit simultanés;
- Aperçu des changements physiologiques (résistance mécanique et consommation de TAG) des microalgues lors des cycles jour-nuit et carence azotée ainsi que leur impact direct sur le traitement de la biomasse pour la récupération de molécules d'intérêt en voie humide;
- et le potentiel de double récupération des biocarburants grâce à des technologies de culture et du traitement de la biomasse pour améliorer le rapport énergétique net final et la valorisation de la biomasse algale en biocarburant.

Les dernières simulations présentées révèlent toutefois que les technologies proposées sont

encore loin de la neutralité énergétique. Cependant, les technologies récentes et les nouveaux protocoles de culture et de traitement de biomasse présentés ici nous rapprochent un peu plus de l'objectif de production d'énergie durable et ainsi aider à résoudre les défis de l'environnement et de la société moderne.

Vita

2007 - 2012 Biotechnology Engineering,
Instituto Politecnico Nacional
Mexico City, Mexico

2015 - 2020 Ph.D., Bioprocess Engineering
Université de Nantes, GEPEA Laboratory,
Saint-Nazaire, France

Related publications

1. Heredia, V., Pruvost, J, Goncalves, O., Marchal L. (Submitted). Optimization of lipid recovery from *Nannochloropsis gaditana* via wet-centrifugal extraction. Algal Research.
2. Heredia, V., Marchal L., Goncalves, O., Pruvost, J. (In process). Optimization of continuous TAG production in solar nitrogen limited culture by *Nannochloropsis gaditana*. Algal Research
3. Kandilian, R., Taleb, A., Heredia, V., Cogne, G., and Pruvost, J. (2019). Effect of light absorption rate and nitrate concentration on TAG accumulation and productivity of *Parachlorella kessleri* cultures grown in chemostat mode. Algal Research, 39(October 2018), 101442.
4. Bouillaud, D., Heredia, V., Castaing-Cordier, T., Drouin, D., Charrier, B., Gonçalves, O., . . . Giraudeau, P. (2019). Benchtop flow NMR spectroscopy as an online device for the in vivo monitoring of lipid accumulation in microalgae. Algal Research, 43(July), 101624.

Conference presentations

1. Heredia, V., Goncalves, O., Marchal, L., Pruvost, J., Optimization of Lipids Production by *Nannochloropsis gaditana* in Outdoor Conditions: Influence of Physiology over TAG Recovery using Wet-Biomass Extraction Process. International Conference on Algal Biomass Biofuels and Bioproducts 2019. June 19, 2019. Poster
2. Heredia, V., Cueff, M., Hervé, L., Marchal, L., Goncalves, O., Pruvost, J., Microalgal Triglycerides recovery during Day/Night Cycles: Physiological influence over Downstream. 5th European Congress of Applied Biotechnology. September ,15-19, 2019. Poster.
3. Heredia, V., Marchal L., Goncalves, O., Pruvost, J., Direct microalgae solar culture influence on final lipid recovery: doe approach. AlgaEurope18, December 2018. Poster
4. Heredia, V., Marchal L., Goncalves, O., Pruvost, J., Optimization of microalgae solar culture coupled at lipid wet extraction in biodiesel production. 6th Congress of the International Society for Applied Phycology. June 2017. Oral
5. Heredia, V., Marchal, L., Cueff, M., Hervé, L., Goncalves, O., Pruvost, J., Tryglyceride recovery from microalgae grown in diurnal cycles: Physiological influence over Downstream process efficiency. IWAAlgae2019. July, 1-2, 2019. Oral.
6. Farjon, J., Bouillaud, D., Charrier, B., Drouin, D., Heredia, V., Goncalves, O., Giraudeau, P., Compact NMR spectroscopy and advanced pulse sequences: the perfect union for the online and real time monitoring of bioprocesses. European RFMF Metabomeeting 2019.

Acknowledgements

The present work reflects the efforts of not only myself but also all the personal and colleagues of GEPEA/ALGOSOLIS; not only in the science-academic aspect, but also in the personal.

First of all, I want to thank to Pr. Jeremy Pruvost, my thesis advisor and head of the GEPEA/ALGOSOLIS laboratory, for his guidance during all my thesis work. Without doubt your personality has transcended the science field and got me inspired in the daily life. Sincerely, I thank you for your trust, support and availability face to your other several duties. Merci Chef!

Likewise, I want to thank my co-advisors Pr. Luc Marchal and Pr. Olivier Gonçalves. They have been invaluable in their technical and scientific advice. I want to thank you both for offering me new perspectives and your infinite kindness. Merci aussi Chefs!

I thank to Pr. Laurent Pilon for his invaluable professional advice during my internship at UCLA.

I want to also thank to the two emeritus GEPEA directors I had the pleasure to meet: Jack Legrand and Pascal Jaouen, for their work in managing the laboratory and for welcoming me to initiate my PhD.

I also want to thank my dissertation jury: Pascal Guiraud, Elisabeth Badens, Nabil Grimi and Arnaud Artu for reviewing and commenting on my PhD work.

Then, I want to also acknowledge the intensive work of all the permanent staff at the GEPEA laboratory and ALGOSOLIS platform, specially Delphine Drouin, Raphaëlle Touchard, Emmanuel Dechandol, Helen Marec, Laura Herve, Benjamin Le Gouic, Guillaume Roelens, Carole Broussard, Marie-Pierre Fuchs, Jordan Tallec, Sebastien Chollet and Lucie Van Harver

Similarly, I would like to thank to CONACyT for the financial support during these 5 years.

Au cours de mon parcours de doctorat, j'ai eu le plaisir de connaître et de travailler avec différentes promotions de collègues. Des gens avec lesquels j'ai non seulement partagé des connaissances, mais aussi des histoires, des amitiés, des tragédies et trop joie. Merci à :

Antoine Soulies

Antoinette Kazbar

Arnaud Artu

Astrid de Luca

Aumaya Taleb

Charlene Tobie

Erika Clavijo (y Camilo)

Myriam Phelippe

Razmig Kandilian

Remy Coat

Sebastien Jubeau

Sergio Rios

Tomas Rinaldi

Valeria Montalescot

Alexandra Busnel

Eglantine Todisco

Elsa Gerard

Jeremy Monlyade (et Fany)

Lisa Zaouk

Marlene Bonnanfant (et Antoine)

Philippe Moussion

Rémi Nghiem Xuan (et Adrick)

Rosine Zinkoné

Antoine Decamp

Armel Noubissie

Danielle Pro

Dounia Makoure

Guillaume Tanguy

Ikha Safitiri

Imma Gifuni

Liliana Villafana (y Sean)

Fernando Ferrel

Flora Girard

Hengsim Phuong

Joris Sebile

Julien Louveau

Kashif Hussain

Shuli Liu

Sikandar Almani

... et un grand merci également à tous les stagiaires et au personnel non permanent que j'ai rencontré.

De manera importante, quiero agradecer a mi madre y a mi hermano. Esto también es suyo. Sus sacrificios y esfuerzos me ayudaron a solventar muchas situaciones difíciles en épocas tempranas. Esa sangre forjó los pilares que hoy me sostienen, gracias por sus fuerzas, apoyo y amor incondicional.

También quiero agradecer a Ale por estar ahí en la distancia y darme fuerzas en la etapa del cierre; incluso si tampoco ha sido fácil para ti. Te ACA.

Agradezco a Alan y Majo por esas noches antiestress de juegos y su ayuda para solventar mis últimos días; a Mariela por seguir siendo mi amiga en la distancia y en las circunstancias; y a Alexis por seguir ahí no importado con quienes estemos ni en dónde.

Aussi aux personnes en dehors de la recherche même, qui ont donné un contrepoids à ma vie et que, en conséquence, m'ont aidé à trouver un équilibre à de nombreux moments: Elina et sa belle famille pour l'énorme support au tout début de la thèse; Laetita et Céline pendant les danses au coucher du soleil; Agathe pour inspirer le début du chemin; M. Souchet pour son soutien et sa compréhension; et Erick pour m'avoir appris à monter et tomber.

Contents

1	Introduction	1
1.1	Climate Change	1
1.1.1	Causes of Climate change	3
1.1.1.1	Greenhouse Effect	3
1.1.2	Consequences	6
1.1.3	An answer?: Humanity Goals	8
1.2	Fuels and Biofuels	9
1.2.1	Biofuels Generations	14
1.2.1.1	First Generation	14
1.2.1.2	Second Generation	15
1.2.1.3	Third Generation	15
1.2.1.4	Fourth Generation	16
1.2.2	BioDiesel production from lipids transesterification	16
1.2.3	BioEthanol production from carbohydrates Fermentation	17
1.3	Biofuels from microalgae	18
1.3.1	The microalgal cell	19
1.3.1.1	Feeding the cell: CO ₂ , Nitrogen and Light	21
1.3.1.2	Energy storage: lipid and sugar	24
1.3.1.3	More energy storage: Stressing the cell	27
1.3.2	Culturing Microalgae	29
1.3.2.1	Photobioreactor systems	29
1.3.2.2	Culture system operation	32
1.3.2.3	Outdoor cultivation and light influence	35
1.3.3	Dowstream processing: From Microalgae to Biofuels	41
1.3.3.1	Wet pathway	41
1.3.3.2	Cell Disruption	41
1.3.3.3	Centrifugal Extraction	42
1.3.4	BioDiesel and BioEthanol: Considerations	43

1.3.5	Interesting Subproducts from the Biochemical Conversion	45
2	Energy-rich microalgae biomass for liquid biofuels: influence of strain selection and culture conditions	47
2.1	Introduction	48
2.2	Methods	49
2.2.1	Strains	49
2.2.2	Culture medium	50
2.2.3	Culture systems	50
2.2.4	Cell disruption rate and cell counting	51
2.2.5	Dry Weight measures	51
2.2.6	Pigment content	52
2.2.7	Total Fatty Acid and Triacylglycerol content	52
2.2.8	Total carbohydrates content	52
2.2.9	Nitrate concentration measurement	53
2.2.10	Potentially recoverable energy calculation	53
2.3	Results and Discussions	54
2.3.1	Response of <i>N. gaditana</i> to Nitrogen depletion in day-night cycles	54
2.3.2	<i>N. gaditana</i> culture under nitrogen limitation and continuous mode	57
2.3.2.1	Nitrogen Uptake and Stress index	57
2.3.2.2	Main biomass compounds	58
2.3.2.3	Cell resistance	61
2.3.3	Potentially recoverable energy	62
2.4	Conclusions	63
3	Optimization of continuous TAG production in solar nitrogen limited culture by <i>Nannochloropsis gaditana</i>	65
3.1	Introduction	66
3.2	Materials and Methods	69
3.2.1	Culture medium	69
3.2.2	Outdoor Reactors	69
3.2.3	Indoor Reactor	69
3.2.4	Day-night cycles	70
3.2.4.1	Actual solar cycles	70
3.2.4.2	Simulated Cycles	70
3.2.5	Experimental layout	71
3.2.6	Cell disruption rate	72

3.2.7	Dry Weight measures	72
3.2.8	Stress Index	73
3.2.9	Total Fatty Acid/Triacylglycerol content measurement	73
3.2.10	Nitrate concentration measurement	73
3.3	Results and Discussion	74
3.3.1	Released TAG in batch mode and day-night cycles	74
3.3.1.1	Depleted batch culture at actual Day-Night cycles	74
3.3.1.2	Depleted batch culture at simulated Day/Night cycles	76
3.3.2	Released TAG during continuous N-limited culture and simulated day-night cycles	79
3.3.2.1	Minimal initial NO_3^- concentration for TAG accumulation	79
3.3.2.2	TAG production under punctual NO_3^- addition	82
3.4	Conclusions	85
4	Optimization of lipid recovery from <i>Nannochloropsis gaditana</i> via wet-centrifugal extraction	87
4.1	Introduction	88
4.2	Materials and Methods	90
4.2.1	Microalgal Cultures	90
4.2.2	Dry-Weight Analysis	90
4.2.3	Bead Milling	91
4.2.4	Quantification of Cell Disruption	91
4.2.5	Total Fatty Acid (TFA) and Triacylglycerol (TAG) extraction efficiency and quantification	91
4.2.5.1	<i>Solvent Choice and Standard Extractions</i>	91
4.2.5.2	<i>Continuous Centrifugal Extraction</i>	92
4.2.5.3	<i>Centrifugal Partition Extraction</i>	93
4.2.6	Response surface methodology for Continuous Centrifugal Extraction	93
4.3	Results and Discussion	94
4.3.1	Final Culture Conditions	94
4.3.2	Cell Disruption Optimization	94
4.3.3	Choice of Solvent for Extraction	96
4.3.4	Centrifugal Partition Extraction	96
4.3.5	Response surface methodology for Continuous Centrifugal Extraction optimization	97
4.4	Conclusion	102

5	Energy-driven biorefinery approach for double Biofuel recovery from microalgae	103
5.1	Introduction	104
5.2	Materials and Methods	106
5.2.1	Process description and System boundaries	106
5.2.2	Operation Units description	109
5.2.2.1	Photobioreactor, PBR-101	109
5.2.2.2	Centrifugation, C-102	110
5.2.2.3	Bead-Milling, BM-201	111
5.2.2.4	Centrifugal Continuous Extraction, CX-202	111
5.2.2.5	Solvent Recovery, D-301	112
5.2.2.6	Transesterification, R-302	113
5.2.2.7	Fermentation, R-401	113
5.2.2.8	BioEthanol and BioDiesel recovery, D-402 and D-303	114
5.2.3	Output Calculations	114
5.2.4	Simulation Cases Description	116
5.3	Results and Discussion	117
5.3.1	Analysis of Culture system impact	117
5.3.2	Analysis of culture protocol adn double biofuel conversion	122
5.3.2.1	Outdoors culture protocol	122
5.3.2.2	Double Biofuel valorization	123
5.4	Conclusion	125
6	General Conclusion	127

List of Figures

1.1	Geological temperature on Earth	2
1.2	Global average radiative forcing in 2005	4
1.3	Climate change: CO ₂ concentration through time.	5
1.4	Scenarios in the CO ₂ mitigation	10
1.5	Average annual global primary energy demand growth by fuel, 2010-2018	11
1.6	Biofuels forecast 2017-2023.	13
1.7	Common stoichiometry for BioDiesel and BioEthanol	17
1.8	Biofuel Process schema from microalgae.	20
1.9	Light and Dark reactions.	21
1.10	Carbon buffer reaction and their association to changes in pH in water dilution.	22
1.11	TAG Synthesis.	25
1.12	Photobioreactors culture systems for microalgae culture	33
1.13	Common operations mode in microalgal culturing	34
1.14	Light attenuation effect on photosynthetic growth.	38
1.15	Light attenuation effect on photosynthetic growth.	39
1.16	Global diagram for BioEthanol and Biodiesel downstream	40
1.17	Bead milling equipment	41
1.18	Centrifugal Extraction device	43
2.1	<i>P. kessleri</i> and <i>N. gaditana</i> microscopic images	50
2.2	Physiological changes of <i>N. gaditana</i> under day-night cycles in depleted conditions.	55
2.3	Comparison of areal productivity for batch under two light regimes <i>P. kessleri</i> and <i>N. gaditana</i>	56
2.4	Comparison of cell disruption rate for two physiological state for <i>N. gaditana</i> and <i>P. kessleri</i>	56
2.5	Areal productivities for TAG and carbohydrates of <i>N. gaditana</i> and <i>P. kessleri</i> at steady state in several levels of nitrogen limitation	60
2.6	Potentially recoverable energy values for <i>N. gaditana</i> and <i>P. kessleri</i>	62

3.1	Flat-panel airlift PBRs systems used for outdoor and indoor cultivations	70
3.2	Culture conditions, biomass concentration and disruption rate under outdoor conditions for replete and deplete cultures	75
3.3	Released TAG under day-night simulated cycles	76
3.4	Residual NO_3^- concentration at the periodic regimes of multiple dilution rates during simulated day-night cycles.	79
3.5	Residual NO_3^- concentration at the periodic regime during simulated day-night cycle for two dilution rates.	81
3.6	Culture changes for punctual addition of NO_3^- in continuous mode during day-night cycles.	83
4.1	Physiological state and disruption kinetics at bead milling	94
4.2	pH value of microalgae suspension after bead milling	95
4.3	Triacylglycerol extraction efficiency for the three solvents used	96
4.4	Raw experimental data and model plots for extraction efficiency, $\eta_{E,i}$	98
4.5	Box-Benhken RSM contour graphs for extraction efficiency, $\eta_{E,i}$	99
5.1	Mass and Energy scheme for the double biofuel recovery simulation	107

List of Tables

1.1	World Biofuels Production for 2017, 2018 and 2019.	12
1.2	Advantages and limitations of open ponds and photobioreactors	30
1.3	Important equations for continuous and batch microalgae cultures.	36
1.4	Main BioDiesel and Bioethanol properties.	44
2.1	Biochemical comparison of <i>P. kessleri</i> and <i>N. gaditana</i> at the end of simulated DnC culture (11 days)	54
2.2	Physiological changes of <i>N. gaditana</i> and <i>P. kessleri</i> at steady state for several levels of nitrogen limitation	59
2.3	Values use for the calculation of the Recoverable fuel energy.	61
3.1	Biomass concentration and TFA and TAG content obtained in periodic regime during simulated day-night cycles for two dilution rates.	80
4.1	Main physicochemical properties of heptane, ethyl acetate and 2-methyl-tetra-hydrofuran	92
4.2	Analysis of variance (ANOVA) for response surface quadratic model.	99
4.3	Regression coefficients estimates for equations obtained in modeling wet extraction efficiency.	100
5.1	Description of Operation at the Production stage.	109
5.2	Simulated characteristics for the PBR-101 unit	116
5.3	Liquid biofuel produced volumes and Input/Output Energies for five simulation cases	118
5.4	Net Energy Ratio for the five simulation cases	121

Chapter 1

Introduction

1.1 Climate Change

*Climate change is the biggest challenge
of our generation (all humans living this period of time).
Not solving our contributions to climate change,
will condemn our future as specie of this world*

All the out-of-trend alterations on climate (atmosphere, ocean, and ice sheets and sea ice) that persist for an extended period of time, is considered as climate change [IPCC, 2007]. Climate changes are natural on Earth, and variations can occur in a daily, seasonally, yearly or much longer-time frame [Bond *et al.*, 1997, Hansen and Sato, 2012, IPCC, 2007]. In fact, human civilization developed during the last 10,000 years (an interglacial period) where Earth's temperature and sea level have been unusually stable (Fig. 1.1) [Hansen and Sato, 2012]. However, last records show that actual climate changes are faster compared to historical trends [Hansen and Sato, 2012, IPCC, 2014, Willeit *et al.*, 2019, WMO, 2020].

The modern human society has showed its capacity to be the only specie on Earth able to change the environment. As any other biological organism, the consumption of *energy and mass* has been a key factor for human development. From hunting and farming to genetic engineering for feeding a hungry world; from fire and vapor to fossil fuels; we have passed from living in caves to build our own caves of hundreds meters high and even planning on living out of Earth.

The consequences of all this human activity are notorious [IPCC, 2007, 2014, WMO, 2019, 2020] and include: extinctions (including the Holocene ones) and noticeable changes in biodiversity and its rhythms, re-distribution of life on the surface (species adaptation and agriculture), nocturnal enlightening, redistribution of minerals as consequence of extraction industry, erosion and sedimentation and remarkable changes in Earth chemical composition (appearance of radioisotopes, and high levels greenhouse gases (GHGs)). Such changes have led scientific community to propose

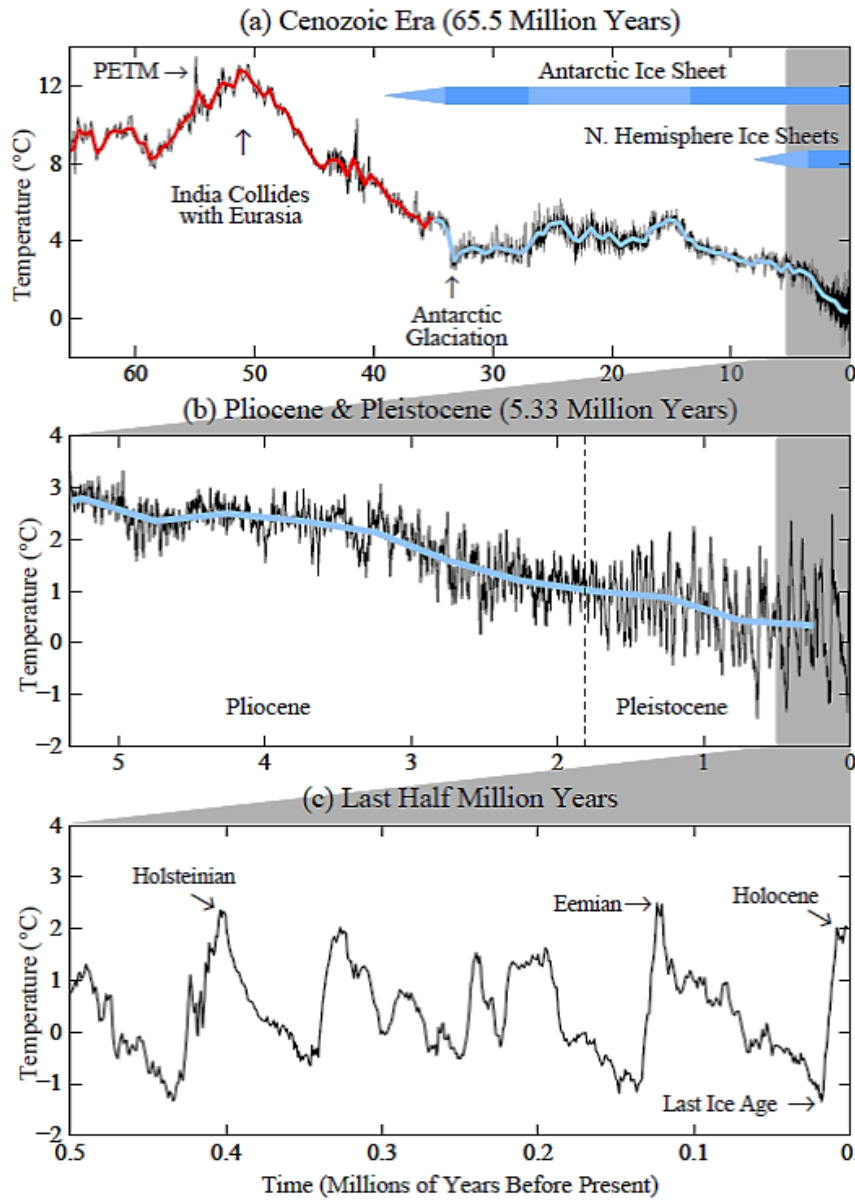


Figure 1.1: Geological temperature on Earth (taken from Hansen and Sato [2012]). Pliocene/Pleistocene is expanded in (b) and the last half million years in (c). High frequency variations in black, red and blue curves have 500 ky resolution. PETM is the Paleocene Eocene Thermal Maximum. Blue bars indicate ice sheet presence, with dark blue for ice sheets near full size. Holsteinian and Eemian are known in paleoclimate literature as Marine Isotope Stages 11 and 5e.

a new geological epoch: *The Anthropocene*. It is confoundable in period time but is distinct from Holocene (11 700 years ago). This geological epoch pretends to consider the impact of human activity on the planet [Zalasiewicz *et al.*, 2010].

1.1.1 Causes of Climate change

Climate is affected by the so-called *climate drivers* or *climate forcing* which, by natural or anthropogenic origins, can retain some of the solar irradiance. They include: 1) variations in the solar energy reaching Earth, 2) changes in the reflectivity of Earth's atmosphere and surface and 3) changes in the greenhouse effect. Beside climate drivers, also exist the *climate feedbacks*, which can amplify or dampen (positive or negative feedback) the response to a given climate forcing. They include: 4) clouds and water vapor, 5) precipitation, 6) greening of the forest and 7) ice albedo.

Direct anthropogenic emission of water vapor (a greenhouse gas) makes a negligible contribution as climate driver. However, water vapor is the largest climate feedback, affecting equilibrium climate. Cloud feedbacks reflect about one-third of the total amount of sunlight that hits the Earth back into space. A warmer climate could cause vapor retention in the atmosphere, leading to increase cloudiness and so the sunlight reaching the surface. Less heat would get absorbed, which could slow the increased warming. Studies reveal that increasing a five percent the cloud reflectivity (with for example natural aerosols), could be possible to compensate the GHGs increase from the modern industrial era. However, it is also possible that long-term decreases in cloudiness could have major impacts [Voiland, 2010]. Because of in recent years the effects of clouds have been just measured, cloud feedbacks remain the largest source of uncertainty [IPCC, 2007].

1.1.1.1 Greenhouse Effect

The Sun is the main source of energy of Earth. From wind and waves to the chemical bounds in organic material and fossil fuels, all are related directly or indirectly to the Sun. However, not all energy emitted by the star arrive to Earth; it depends of multiple factors. When talking about intrinsic (to Earth) factors, it can be noticed that some energy can be reflected by surface, clouds or ice; then, if the planet absorbs the same amount of energy that it reflects, its average temperature remains stable. On the other hand, for extrinsic factors, the energy arriving to the planet may be also due to Earth's tilt, gradual changes in Earth's rotation [Berger, 1988] or even sun's activity cycles. However, none of these extrinsic factors have been proved to have a significant effect on the recent warming observed [IPCC, 2007]. The heat coming from the Sun is mainly retained by the atmosphere in a phenomena named greenhouse effect. The greenhouse effect is natural on Earth, it keeps temperature friendly to life. Without it, life never could have appeared and the entire planet would be freezing.

Most of the solar energy absorbed or radiated by Earth is modulated by the atmosphere and it

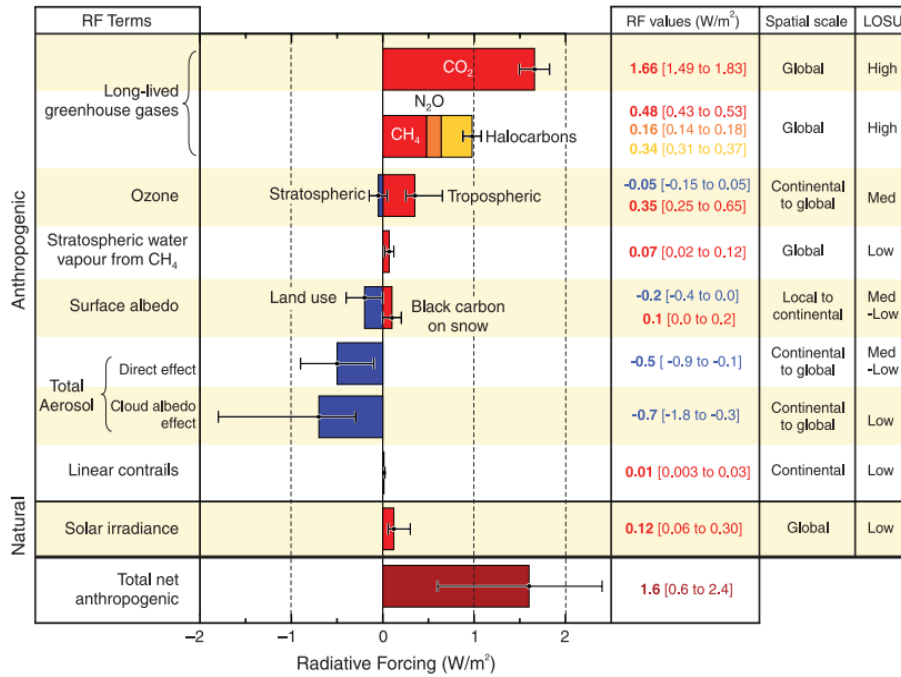


Figure 1.2: Global average radiative forcing (RF) in 2005 with respect to 1750 for CO₂, CH₄, N₂O and other important agents and mechanisms, together with the typical geographical extent (spatial scale) of the forcing and the assessed level of scientific understanding (LOSU). Aerosols from explosive volcanic eruptions contribute an additional episodic cooling term for a few years following an eruption. The range for linear contrails does not include other possible effects of aviation on cloudiness. Taken from IPCC [2007].

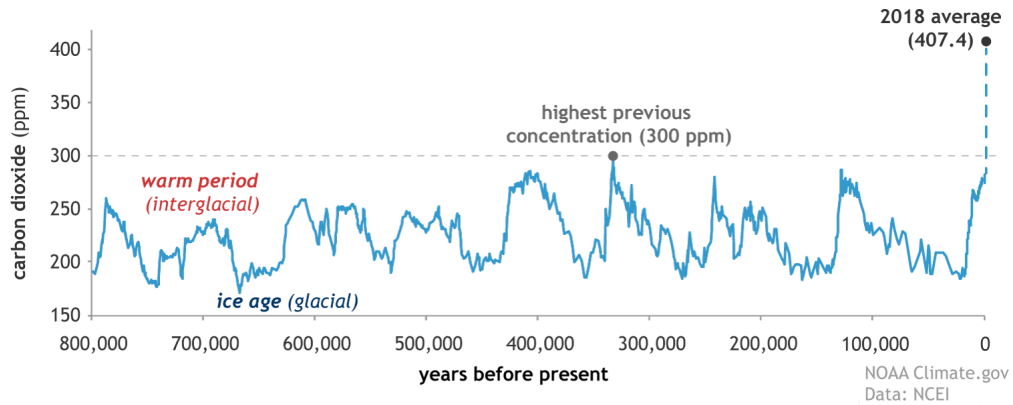
depends on its composition. The atmospheric warming potential depends on the radiative properties of each component and so its concentration. Main GHGs are water vapor, carbon dioxide (CO₂), methane(CH₄), nitrous oxide (N₂O) and 3 types of industrial gases (hydrofluorocarbures (HFC), perfluorocarbons (PFC) and sulfur hexafluoride (SF₆)) [IPCC, 2007]. Carbon dioxide, methane, nitrous oxide, CFC-12 and CFC-11 account for about 96% of the direct radiative forcing^a.The remaining 4% is contributed by an assortment of 15 minor halogenated gases including HCFC-22 and HFC-134a. Just from 1990 to 2017, the radiative forcing due to GHG's increased 41%. CO₂ has accounted for about 80% of this value [IPCC, 2007, 2014].

The actual increase in GHGs concentration, has been *extremely likely* to be driven by human activities related to economic and population growth^b [IPCC, 2014]. Since Industrial Revolution^c, (Fig. 1.3b) human activities as burning coal-oil for fuel and deforestation, have increased the abundance of the heat-trapping gases and amplified the greenhouse effect. Global increases in CO₂ concentrations are due primarily to fossil fuel use and land-use change (this latter with a significant

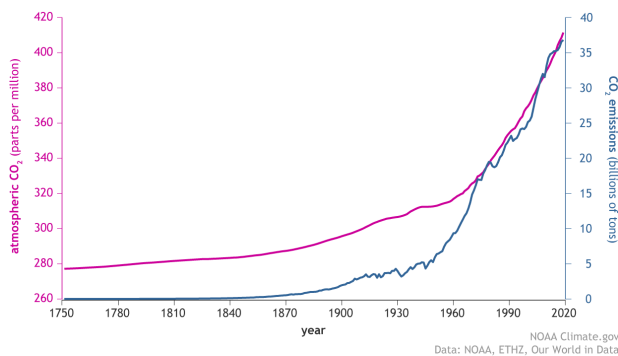
^aAs Earth absorbs energy from the sun, it must eventually emit an equal amount of energy to space. The difference between incoming and outgoing radiation is known as a the *radiative forcing*. Climate drivers can trigger feedbacks that intensify or weaken the original radiative forcing. Radiative forcing measures that factor of influence [IPCC, 2007, 2014].

^bPopulation size, economic activity, lifestyle, energy use, land use patterns, technology and climate policy.

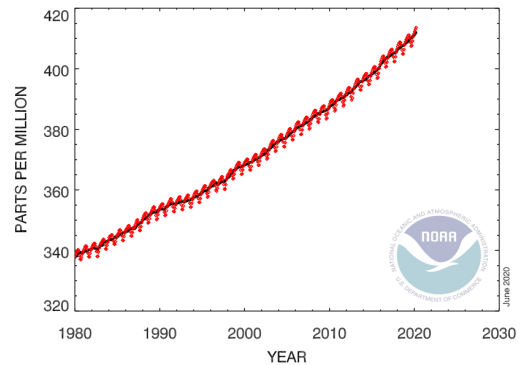
^cHistorically, Industrial revolution is the period from 1760 to 1840-1840. IPPC has considered 1850 as the reference year in the CO₂ management effort.



(a) CO₂ through epochs



(b) CO₂ since industrial revolution



(c) CO₂ for the last decades

Figure 1.3: Climate change: CO₂ concentration through time. A) Global atmospheric carbon dioxide concentrations (CO₂) in parts per million (ppm) for the past 800,000 years to 2018; B) Pre-1978 and actual (2020) changes in the CO₂; C) Last changes in atmospheric CO₂ concentration (ppm) since 1980 to 2020. The highest and present value (march 2020) is 413.67 ppm. Graphic sources taken from Lindsey [2020]

but smaller contribution). The increase in CH₄ concentration is predominantly due to agriculture and fossil fuel use too. The increase in N₂O concentration is primarily due to agriculture [IPCC, 2007, Lindsey, 2020].

Recent mesures [IPCC, 2014, Lindsey, 2020] shows that the current CO₂ average concentration is around 413.67 ppm (Fig. 1.3C). It is difficult to see the implications of the increased CO₂ concentration: a change from 340 ppm to 410 ppm in 40 years seems to be not relevant. But when is compared to historical registers, a new panorama appears. In figures 1.3A and B, it is shown the CO₂ concentration since 800 thousands of years (data taken from ice cores) and from since 1750. In a glance since 1950, CO₂ has been alarmingly increasing. For the period between 1750 and 2011, half of CO₂ emissions have occurred just in the last 40 years. CO₂ emissions in that frame-time, mainly came from fossil fuel combustion and industrial processes, and contributed about 78% to the total GHGs emission increase between 1970 and 2010, with a contribution of similar percentage over the 2000–2010 period [IPCC, 2007, 2014].

Furthermore, CO₂ accumulation looks even more higher when comparing to levels in Earth's history. Since thousands of years, belong the natural cycles, CO₂ oscillated just between 180-300 ppm. Lindsey [2020] mentioned that the present CO₂ values are the highest in 650,000 years. Moreover, also recent studies showed that may be the highest since 3 millions years ago, with a global temperature of not more than 2°C over preindustrial levels [Willeit *et al.*, 2019] (Fig. 1.1). And furthermore, models also shows that the actual fossil fuel consumption risks of taking us, by the year 2250, to CO₂ values not seen since 50 million years ago (*ie.* 2,000 ppm) [Foster *et al.*, 2017]. This implies that if humankind fails in strategies to reverse CO₂ emissions and implant more sustainable activities, the entire planet will experience climatic conditions not seen since last geological epochs.

1.1.2 Consequences

In 2006, Al-Gore^d filmed "An Inconvenient Truth", a documentary about the effects of climate change. The politician, exposed those days data which sustained the effect of doing nothing to solve the situation: longer dry seasons, harder hurricanes, rains, plagues and changes in rain patterns. By the time it seemed like climate change would be something left for next generations to live.

However, just during the last years, our generation has witnessed unprecedented changes in climate. It has been shown [IPCC, 2014, WMO, 2019] that most of the natural hazards that affected nearly 62 million people in 2018, were associated with extreme weather and climate events. About 35 million people were hit by floods. In 2018 the hurricane Florence and Hurricane Michael were just two of 14 "billion dollar disasters" US. Also super Typhoon Mangkhut affected 2.4 million

^dAmerican politician and environmentalist who served as the 45th vice president of the United States from 1993 to 2001.

people mainly in the Philippines. More than 1,600 deaths were linked to heat waves and wildfires in Europe, Japan and US. Kerala in India suffered the heaviest rainfall and worst flooding in nearly a century. In 2018 lot of places in the world set fire.

The last statement of World Meteorological Organization (WMO) reports the following state of climate[WMO, 2020]:

1. The global mean temperature for 2019 was $1.1\pm 0.1^{\circ}\text{C}$ above pre-industrial levels. The year 2019 is likely to have been the second warmest in instrumental records. Since the 1980s, each successive decade has been warmer than any preceding one since 1850. Global atmospheric mole fractions of greenhouse gases reached record levels in 2018 with CO_2 at 407.8 ± 0.1 ppm, CH_4 at 1869 ± 2 ppb and N_2O at 331.1 ± 0.1 ppb. These values constitute, respectively, 147%, 259% and 123% of pre-industrial levels. Early indications show that the rise in all three GHGs continued in 2019.
2. The year 2019 saw low sea-ice extent in both the Arctic and the Antarctic. The daily Arctic sea-ice extent minimum in September 2019 was the second lowest in the satellite record. In Antarctica, variability in recent years has been high with the long-term increase offset by a large drop in extent in late 2016. Extents have since remained low, and 2019 saw record-low extents in some months. 2040 could be the first year without ice in poles.
3. The ocean absorbs around 90% of the heat that is trapped in the Earth system by rising concentrations of GHGs. Ocean heat content, reached record- high levels again in 2019. Over the decade 2009–2018, the ocean absorbed around 23% of the annual CO_2 emissions, lessening the increase in atmospheric concentrations. However, CO_2 absorbed in sea water, acidificates the ocean. Oceans observations from the last 20 to 30 years, show a clear decrease in average pH at a rate of 0.017–0.027 pH units per decade since the late 1980s.
4. As the ocean warms, it expands and sea level rises. Sea level has increased throughout the altimeter record, but recently sea level has risen at a higher rate due partly to increased melting of ice sheets in Greenland and Antarctica. In 2019, the global mean sea level reached its highest value since the beginning of the high-precision altimetry record (January 1993).

If the actual rhythm of anthropogenic contributions is not strongly reduced, it is probable that our own capacity to seed rice, corn and wheat, will be reduced; including such changes as earlier timing of spring events, such as leaf-unfolding, bird migration and egg-laying; and poleward and upward shifts in ranges in plant and animal species [IPCC, 2007, 2014]. Climate change brings out not just consequences for earth: in a warmer world, the accessibility to water, fresh food, raw materials and energy efficiency could be more complicated.

Human activities have caused approximately 1°C of global warming above pre-industrial levels, and are expected to reach 1.5°C between 2030 and 2052 if the actual trend continues. The risks

associated to reach that global temperatures, are high but lower than reaching 2°C. It has to be noted that anthropogenic emissions from pre-industrial period to date, will persist for centuries to millennia, but these emissions alone are unlikely to cause further warming than 0.5°C. However reaching and sustaining net zero global anthropogenic CO₂ emissions and declining the radiative forcing of the rest of GHGs would halt anthropogenic global warming on through the next decades [IPCC, 2018].

"There is no longer any time for delay" wrote A. Guterres^e in the last report of the WMO Statement on the State of the Global Climate [WMO, 2019]. We are too many in the planet already, and if we pretend to coexists in this planet, we need to change habits as individuals and unified society.

1.1.3 An answer?: Humanity Goals

*Technologies carried out by any country
seeking to solve climate change
must be at the service of the international community.
The causes have been global
and the solution also requires a global interaction*

The *Paris Agreement* took place at the United Nations Climate Change Conference 2015 (COP 21, Paris, France). It is the first legally binding documents in the history of global climate [United-Nations, 2015]. Nations agreed to use the best available science for mitigate the anthropogenic impact in climate. With this, they also recognize that food security must be protected, the future of hunger must be prevented and food production systems must be made less vulnerable to the adverse effects of climate change.

As part of the international efforts for responding to the 1.5°C global warming alert and avoid the over-accumulation of GHGs, 45% of CO₂ athropogenic emissions should be reduced in 2030; and in 2050 they might be disappeared. [IPCC, 2018].

Two complementary strategies for reacting to climate change have been established: *Mitigation* and *Adaptation*^f. Adaptation aim to reduce the impact of climate change in society, but the effectiveness is limited, specially considering the greater scenarios of rates and magnitudes of climate change. For these maneuvers to be more effective, it is required to diminish the risk of those scenarios for the long-term with a sustainable development perspective which also will enhance future options and preparedness. Mitigation actions have both co-benefits and risks but not as higher as those associated to climate change itself. The pathways to mitigation require a substantial CO₂

^eUnited Nations Secretary-General

^fAdaptation is the process of adjustment to actual or expected climate and its effects in order to either lessen or avoid harm or exploit beneficial opportunities. Mitigation is the process of reducing emissions or enhancing sinks of GHGs, so as to limit future climate change.

reduction of the anthropogenic emissions in the few decades and near zero emissions of CO₂ and other GHGs by the end of the century. The goal scenario for maintain below 2°C by 2100 is 530 ppm or lower of atmospheric CO₂ which represent a mitigation of annual GHGs emissions (relative to 2010 levels) of -30% or higher (Fig. 1.4) [IPCC, 2014, 2018].

The considered major CO₂ emissions sector to mitigate are: *Transport, Buildings, Industry, Energy supply* and *Agriculture, Forestry and Other Land Use (AFOLU)*.

Mitigation options are available in every major sector. Mitigation can be more cost-effective if using an integrated approach that combines: a) measures to reduce energy use and the greenhouse gas intensity of end-use sectors, b) decarbonize energy supply, c) reduce net emissions and d) enhance carbon sinks in land-based sectors [IPCC, 2014].

Carbon Dioxide Removal (CDR)^g is fundamental in many mitigation scenarios. CDR are needed to be deployed on large-scale and over a long time period to significantly reduce CO₂ concentrations in the scenarios where the CO₂ budget or the 1.5°C are overshoot. Bioenergy with Carbon Dioxide Capture and Storage (BECCS) and removal in the AFOLU are the only CDR methods included in these scenarios, which uses will depend on the overshooting grade. In a glance, BECCS are expected to remove 364-662 Gt CO₂ in without or with a limited overshoot; or 1191 Gt CO₂ for a higher overshoot scenario [IPCC, 2018].

There exist evidence suggesting that bio-energy production options with low life-cycle emissions, can reduce GHG emissions; these outcomes are site-specific, relying on the efficient integrated 'biomass-to-bioenergy systems', sustainable land use management and governance. The deployment of such technologies includes bottlenecks for the large-scale deployment including concerns on land, food security, water resources, biodiversity conservation and livelihood [IPCC, 2014].

1.2 Fuels and Biofuels

The International Energy Agency (IEA) reports [IEA, 2019] that energy consumption worldwide grew by 2.3% in 2018^h (Fig. 1.5ⁱ), and nearly twice the average rate of growth since 2010, driven by a robust global economy as well as higher heating and cooling needs in some parts of the world. Despite the economic expansion of 1.8%, demand increased by only 0.2% in Europe, mainly due to the increase in energy efficiency by Germany which resulted in a 2.2% drop in energy demand, with oil demand decreasing by more than 6%. Demand in France and the United Kingdom increased moderately [IEA, 2019].

^gCarbon Dioxide Removal (CDR) and Solar Radiation Management (SRM) belongs to the Geoengineering approach, proposed by the IPCC 2014 aimed to deliberately alter the climate system in order to alleviate the impacts of climate change.

^hAs a result carbon emission increased 1.7% (33.1 Gt CO₂) in 2018.

ⁱA toe is defined as the amount of energy release by burning one tonne of crude oil. It accounts approximately 45 GJ or 11.630 MWh

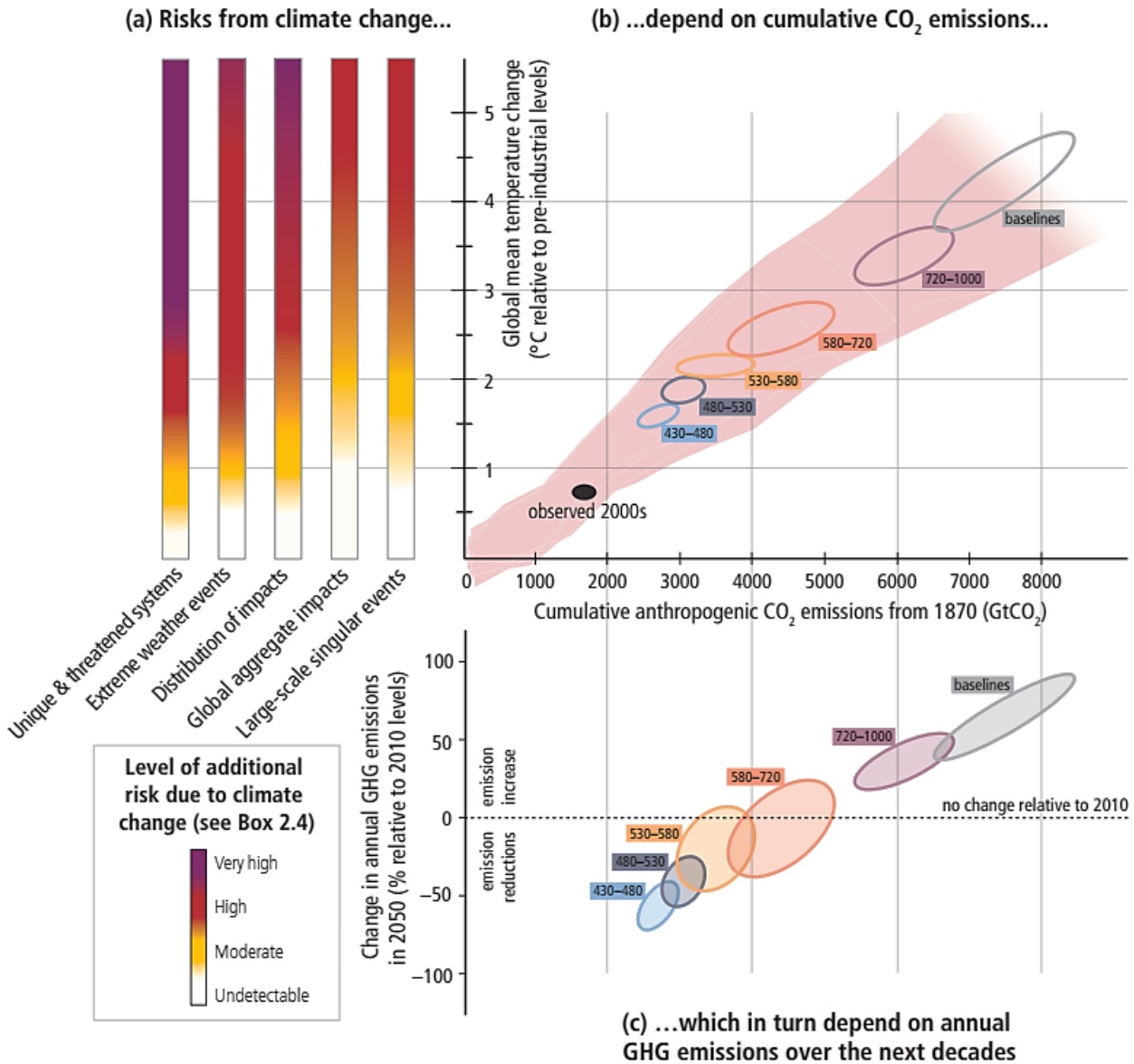


Figure 1.4: Scenarios in the CO₂ mitigation. The relationship between risks from climate change, temperature change, cumulative CO₂ emissions and changes in annual GHG emissions by 2050. Limiting risks (a) would imply a limit for cumulative emissions of CO₂ (b), which would constrain annual emissions over the next few decades (c). Panel (a) reproduces the five Reasons For Concern. Panel (b) links temperature changes to cumulative CO₂ emissions (in GtCO₂), from 1870. They are based on a simple climate model (median climate response in 2100) for the baselines and five mitigation scenario categories (six ellipses). Panel c shows the relationship between the cumulative CO₂ emissions (in GtCO₂) of the scenario categories and their associated change in annual GHG emissions by 2050, expressed in percentage change (in percent GtCO₂-eq per year) relative to 2010. Set de Images taken from [IPCC, 2014]

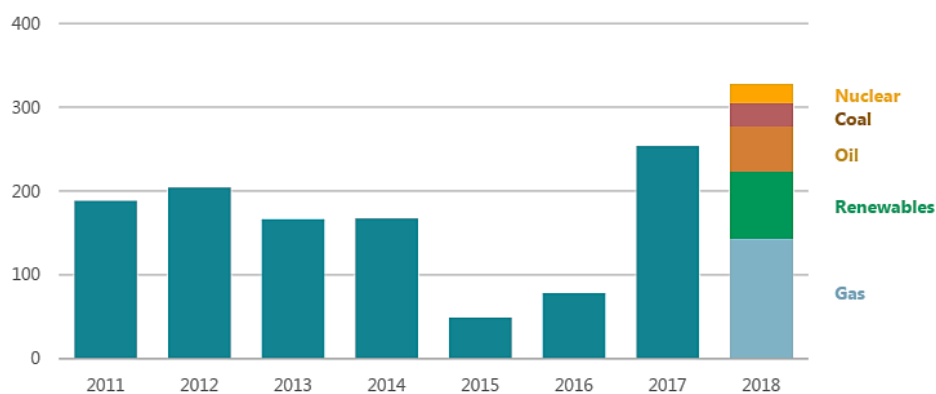


Figure 1.5: Average annual global primary energy demand growth by fuel, 2010-2018. Bar units are for megatone's (Mtoe). Values for: Gas, 143 Mtoe; Renewables, 81 Mtoe; Oil, 54 Mtoe; Coal, 27 Mtoe; and Nuclear, 23 Mtoe. Taken from IEA [2019]

Likewise, around the globe, oil demand^j grew 1.8%, 1.1% and 0.88% at the end of 2017, 2018 and 2019 respectively (69.7 mb/d in 2019). At the time of this work, IEA estimates that 2020 might be, at least since 2009 recession, the first time when demand contracts with -0.1% annual change at the end of year. However is very likely that the COVID-19 in 2019 events, will create uncertainty to the forecast in the oil market. A *rebound* effect could be expected in the demand for the period 2021-2025 [IEA, 2020]. Subsequently, diesel accounted for 30% of world oil demand growth in 2018. Around three-quarters of the global demand is accounted by the transport consumption. Diesel/gasoil final demand during 2018-2019, increased in Asia-Oceania and Europe passing from 1.89 to 1.90 and 6.44 to 6.46 millions barrels per day respectively; meanwhile Americas decreased from 5.32 to 5.26 millions barrels per day. France demand trend decreases to 0.7 millions barrels per day at the end of 2019^k [IEA, 2020]. In this context, nations are searching for new strategies to reduce their dependence to fossil fuels and to switch to more ecofriendly technologies. For the 2017 to 2018 period, all the renewable energies increased by 4%, accounting for almost one-quarter of global energy demand growth in 2018 (see Fig. 1.5) [IEA, 2019]. The IEA reported for the last forecast 2017-2023, that bioenergies will lead growth in renewable energy consumption. Around 30% of the growth in renewables consumption is expected to come from modern bioenergy in the form of solid, liquid and gaseous fuel due to bioenergy's considerable use in heat and its growing consumption and in transport (Fig. 1.6a).

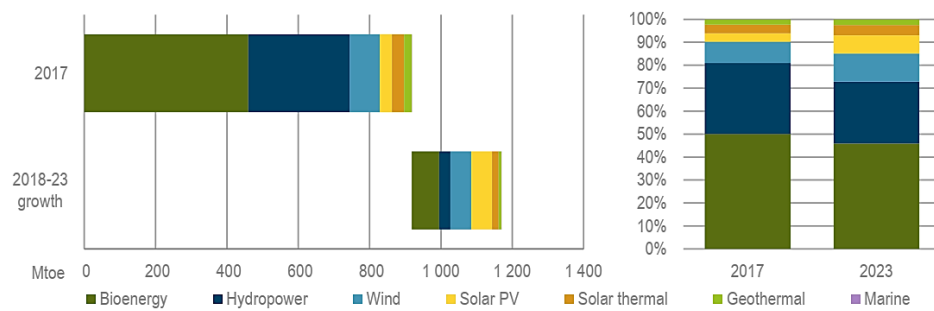
Global biofuels production increased 6.5% in 2019 (See Table 1.1). Biofuels are part of the global efforts for reducing climate change [Hamje *et al.*, 2014, IPCC, 2014, Ponton, 2009, WMO, 2019]. Biofuels may be comprised as part of BECCS for the Energy supply, Transport and Building mitigation sectors [IPCC, 2007, 2014, 2018].

^jOil demand refers to total liquid demand, including biofuels

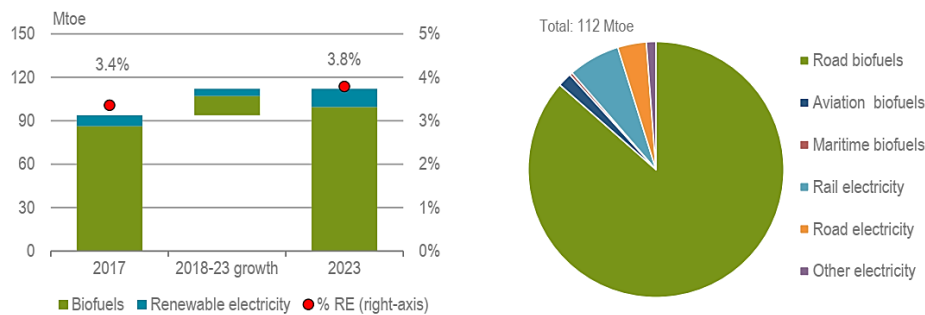
^kIn France, 73.2%, 9.5%, 5.3%, 5.3%, 3.1% and 0.7% were consumed in transport, residential, commercial and public services, agriculture/forestry, industry and fishing respectively (2017)

Table 1.1: World Biofuels Production for 2017, 2018 and 2019. Data taken from [IEA, 2020].

	2017		2018		2019	
	thousand barrels per day					
	Ethanol	BioDiesel	Ethanol	BioDiesel	Ethanol	BioDiesel
OECD Americas	1062	111	1078	126	1064	119
<i>Unites States</i>	1032	104	1048	121	1029	113
<i>Other</i>	30	7	30	5	35	6
OECD Europe	88	265	96	275	87	286
<i>France</i>	13	47	21	52	15	52
<i>Germany</i>	14	62	14	65	13	66
<i>Italy</i>	-	13	-	15	-	18
<i>Spain</i>	7	34	9	33	9	35
<i>United Kingdom</i>	11	-	9	-	4	-
<i>Other</i>	42	109	43	110	45	117
OECD Asia Oceania	3	12	5	12	5	16
<i>Australia</i>	3	1	4	1	4	1
<i>Other</i>	0	11	1	12	1	15
Total OECD	1153	388	1178	413	1156	421
Total Non-OECD	627	293	718	315	818	401
<i>Brazil</i>	478	74	547	92	621	102
<i>China</i>	56	-	56	-	69	-
<i>Argentina</i>	19	56	19	47	19	43
Other	74	163	95	176	109	257
Total Ethanol/BioDiesel	1780	681	1897	728	1974	822
Global Biofuels	2461		2625		2796	



(a) Bioenergy in renewable energies



(b) Biofuels in renewable energies

Figure 1.6: Biofuels forecast 2017-2023. It can be seen in a) the renewable energy consumption by technology for the forecast; and in b) the renewable energy in transport by fuel (left) and renewable consumption by transport mode in 2023 (right). Taken from [IEA, 2018].

Two main types of liquid biofuels are in production at the 2020 onset¹: *BioDiesel* and *Biotehanol*. Their production has been increasing during the last years due to the use of already matured conventional technologies. In 2019 production grew 4% for BioEthanol and 12% for BioDiesel (1974 and 822 thousand barrels per day respectively (See Table 1.1). BioDiesel production during 2019 was led by United States with 14% of the total, followed by Brazil, Germany and France (12%, 8% and 6% respectively, Table 1.1) [IEA, 2020]. In the same manner, for 2019, BioEthanol production was also led by United States with the 52% , followed by Brazil with 31% of the total (Table 1.1) [IEA, 2020]. United states growth was supported by an abundant corn crop and high capacity utilisation by domestic ethanol facilities. Brazil's ethanol production was boosted by low international sugar prices that favoured ethanol output.

As it can be seen, the biofuel production is dominated by the United States and Brazil which is mostly destined for domestic consumption. In both countries, fuel ethanol and BioDiesel are blended with fossil transport fuels. In Brazil unblended fuel ethanol also competes directly with gasoline at the pump. However, as production costs for biofuels, gasoline and diesel vary by country, most of the differences in policy measures and the break-even oil price for ethanol and BioDiesel, affect biofuel competitiveness in both countries [IEA, 2018].

Advanced biofuel^m markets are developing in areas that have established policy mechanisms

¹Biogas could also be considered, but for the aim of this work, it will not be analyzed.

^mFor a wider definition of conventional and advanced biofuels, see the end of the section 1.2.1

to foster research, development and deployment. Over three-quarters of announced and under-construction advanced biofuel plants using less mature technologies are in Europe, India and the United States, where policy frameworks to support deployment are in place

The future of biofuels is promising. The European Renewable Energy Directive requires that 14% of transport fuel come from renewable energies by 2030 ⁿ. In the IEA forecast 2017-2023, just for the transport, biofuel production is expected to continue to increase, rising 15% to 165 billion litres (L) by the end of 2023. However, biofuels might only represent less than 4% of total transport energy demand in 2023. Even next to the fast and continuous electric mobility expansion market, biofuels are expected to still hold almost 90% share of total renewables in transport sector energy demand in 2023 (Fig. 1.6b) [IEA, 2018].

1.2.1 Biofuels Generations

Three biofuels generations can be grouped according to the nature of the feedstock used in the production process.

1.2.1.1 First Generation

Fuel obtained from the direct conversion of feedstock already available as the major constituent in the original source, without any or only with a minor pre-treatment. This is the case of all the sugars and oil contained in grains from food crops. This type of fuels are valued either by effectiveness to be blended with oil-based fuels in the internal combustion engine, or their performance to be used in new engine technologies or flexible fuel vehicles. Most of the actual global production is based in type of biofuel, including BioEthanol, BioDiesel and biogas [Alalwan *et al.*, 2019]. However there have existed lots of concerns about their sustainability. First, the debate on if the well-to-fuel pathway is actually capable to mitigate GHGs since some biofuels from this generation can produce net negative gains (*ie.* releasing more carbon than during the feedstock cultivation)[Ponton, 2009]. Indeed, Edwards *et al.* [2014] concluded that current government aspirations are beyond levels that existing arable lands can actually produce. This leads to the third concern related to croplands: biodiversity and food supply. Looking for more arable land could be either counter-productive for GHG mitigation because of deforestation (next to the effect of losing biodiversity for monoculture and species migration/extinction), or counter-productive of the croplands used for food supply (a higher demand of biofuels leads to an increase in the volumes of crops being diverted away from the global food market). On the latter is estimated that 7 million square kilometers of land (about the size of Australia) could be devoted to energy crops by only using this biofuel generation [IPCC, 2018].

ⁿ10% per renewable energy in transport by 2020 with 7% cap for conventional biofuels. Further information in IEA [2018]

1.2.1.2 Second Generation

Biofuels from the second generation took relevance after the issues of the first generation and aim to overcome them. These biofuels are produced using feedstocks not directly available or not being the major constituent of the original source, and/or requiring a major transformations for their recovery. Examples of the feedstocks used in the second generation are: non-food crops (poplar trees, willow and eucalyptus, miscanthus, switchgrass, reed canary grass, and wood) or agriculture waste, both mainly treated as lignocellulosic material; organic waste, used cooking oil, mature waste oil and animal fat waste. Only 2nd generations of biofuels have been considered in the mitigation section of IPCC [2007]. This is due to that net carbon from their combustion may be neutral or even negative [Alalwan *et al.*, 2019] and also because some lignocellulosic and waste material are not in competition with food croplands. However the main drawback is that the feedstock (mostly issued as by-products) can only provide a limited proportion of biofuels demand. Similarly, if non-food crops lands were only dedicated to biofuel production, the competition for use of land for food became again an issue.

1.2.1.3 Third Generation

Microorganisms are cultivated as feedstocks for the third generation of biofuels. By the conjunction of biotechnology and engineering concepts it is possible to biologically synthesize the raw-molecules normally found in the conventional feedstocks of the first and second generations (like the triglycerides or simpler carbohydrates), which is known as *de novo* synthesis. The third generation of biofuels are based on improvements in the production and metabolism of biomass. BioEthanol and BioDiesel from microalgae or bacteria are the most common examples [Ali *et al.*, 2019, Ho *et al.*, 2013, Scholz *et al.*, 2013, Yang *et al.*, 2016, Yousuf, 2012]. The third biofuel generation have gained relevant attention for energy production but also for all the by-products of high added value that can be recovered [Leong *et al.*, 2018]. They have several important properties such as requiring less space to grow, high metabolite content (the actual feedstocks), the ability to grow in both artificial and natural environments, and for some, the fact of being ecofriendly [Alalwan *et al.*, 2019]. Microorganism can also be grown using land and water unsuitable for food production. Industrialization of microbial technology for biofuel production is questionable due to life cycle assessment and techno-economic feasibility of the processes [Leong *et al.*, 2018]. Despite the high biomass and metabolite productivities, the cost of glucose represents around 80% of the total fee penalty of growth medium for some microbial biofuels [Alalwan *et al.*, 2019]. It makes some cultivation economically unattractive. However, it is possible to use inexpensive (or even recycling) carbon sources like sugars from industrial and agricultural waste, crude glycerol from other BioDiesel industries, cellulosic materials and cane molasses and CO₂ from flue gas Alalwan *et al.* [2019], Cuellar-Bermudez *et al.* [2015], Dineshababu *et al.* [2019].

Third generation of biofuels might be implemented already but optimization on nutrient supply for starvation for stress, energy net gains and tecno-economics aspects are still required to be massively produced [Leong *et al.*, 2018].

1.2.1.4 Fourth Generation

There exists some scientific advancements on route to produced the so called fourth generation of biofuels. Contrary to third generation biofuels, such developments are still in laboratory scale and their industrial deployment is far to be ready. These new biofuels take advantage of the most recent advancements in metabolic engineering, genetic modification and synthetic biology. They aim to uncouple or enhance the metabolism of the cell to over-express metabolites. This generation could consider examples like biofuels obtained from modified bacteria [de Farias Silva and Bertuccio, 2016, Dien *et al.*, 2003], modified microalgae [Beer *et al.*, 2009, de Farias Silva and Bertuccio, 2016] or enzymatic coupling [Orijel *et al.*, 2020].

A second categorization for biofuels can be introduced as *Conventional* and *Advanced*. The advanced biofuels are defined by IEA [2018] as all those sustainable fuels produced from non-food crop feedstocks (and non competitive with their agricultural lands) which are capable of significantly reducing lifecycle GHG emissions (related to the corresponding fossil fuel alternative) and which do not cause adverse sustainability impacts. Opposite defined, the conventional are those using food crop feedstocks to produce fuels with the corresponding consequences.

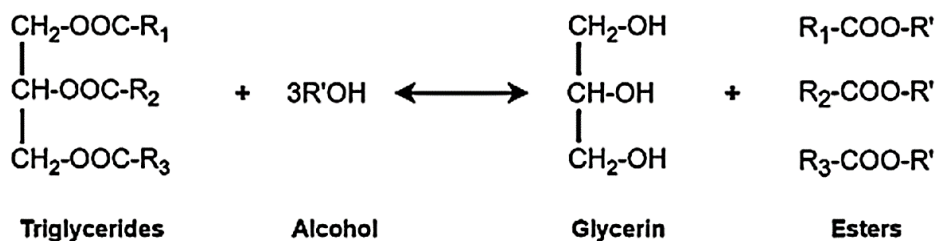
Advanced biofuels can be also classified based on the maturity of the technology used to produce them. IEA [2018] presents the term *novel advanced biofuels* for advanced biofuels from technologies that have not yet been fully commercialized. This distinction is made to highlight the status of technologies that require ongoing support to tackle financial, technical and market barriers.

1.2.2 BioDiesel production from lipids transesterification

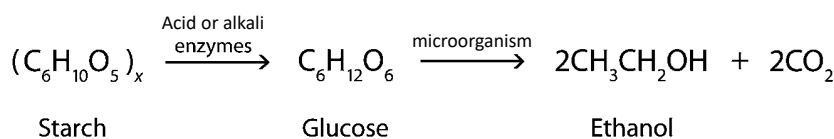
Oils from rape seed, sunflower seed, soy beans, palm, animal carcass, tallow, waste cooking oil and algal oil are all suitable for transesterification although BioDiesel from some oils need to be blended with conventional diesel fuel.

BioDiesel is produced by a chemical reaction called transesterification^o. The transesterification process is well-established; Oil feedstock (triglycerides) reacts with an alcohol (usually methanol) to produce Fatty Acid Methyl Ester (FAME) and glycerol. Stoichiometry is showed in the figure 1.7a. During this process the tri-glyceride molecule is successively split into di-glyceride and mono-glyceride, to finally release the glycerol molecule. Reaction may be catalyzed at 60°C by action

^oalso called methylation since methanol is used as reactant



(a) Transesterification



(b) Hydrolysis + Fermentation

Figure 1.7: Common stoichiometry for BioDiesel and BioEthanol.

of acid, alkalis or lipase enzymes, but alkali-catalyzed reaction is 4000 times faster. Under this conditions reaction can last 90 min to complete. Reaction yield can be improved by using dry reactants (which leads to soap formation; saponification) and oil feedstock clean of free fatty acids.

Industrially yield may be improved by increasing the amount of the alcohol up to 6 mol of methanol [Faried *et al.*, 2017, Fukuda *et al.*, 2001]. Methanol can be substituted by ethanol to produce an Ethyl Ester (FAEE). Assuming ethanol is from bio-origin, this has the advantage of boosting the "renewability" of the fuel. However, FAEE is unlikely to be produced extensively in practice [Edwards *et al.*, 2013].

There are also some by-products from the residue after pressing some seeds (also known as cake which leads to a commercial product known as meal) and the glycerine produced during transesterification. Meal is used today as animal feed that also can be used for biogas production. Glycerine is used in many food and cosmetics applications, as well as for paints, resins and antifreeze or to be used as animal feed. It can be also be used to produce biogas or even hydrogen [Edwards *et al.*, 2013].

1.2.3 BioEthanol production from carbohydrates Fermentation

BioEthanol is another well established technology. It can be produced from a variety of crops and other biomass resources by fermentation of sugars (carbohydrates). Virtually any source of carbohydrates can be used but the more common actually used are starch (from potato, wheat, barley,

corn or algae) or sugars (from sugar cane, sugar beet or algae). BioEthanol can be occasionally used as neat, but it is more often blended with conventional gasoline.

Sugar are directly converted but more elaborated compounds need first to be hydrolyzed. Hydrolysis can occur by action of enzymes or acids or bases [Harun and Danquah, 2011, Harun *et al.*, 2011, Ho *et al.*, 2013]. Once the carbohydrates are more available, microorganisms can convert the carbohydrates into ethanol. The basic stoichiometry is showed in the figure 1.7b. At the end of the fermentation step, low concentrations of alcohol are produced in the water substrate; consequently distillation is used for purification but such a process inputs a considerable amount of energy [Edwards *et al.*, 2013].

Traditionally, yeast as *Saccharomyces cerevisiae*, have been used for fermentation [Otterstedt *et al.*, 2004, Scholz *et al.*, 2013]. But also bacteria like *Zymomonas mobilis* have shown many desirables industrial biocatalyst characteristics, such as high specific productivity, high alcohol tolerance and a broad pH range for production [Swings and De Ley, 1977, Yang *et al.*, 2016]. Many other microorganisms may be used in biofuel production, but the choice has to consider limitations as economical production, industrial robustness, substrate utilization, productivity and yield [Yang *et al.*, 2016]. Some bacteria have been subjected to genetic modifications to increase their performance via bio ethanol production [Dien *et al.*, 2003].

The acid hydrolysis and fermentation in separated steps is often highly effective. In the same manner Ho *et al.* [2013] has shown the feasibility of simultaneous saccharification and fermentation (SSF) using microalgal feedstock; achieving similar yields than the separate hydrolysis and fermentation.

1.3 Biofuels from microalgae

Biofuels from microalgae may have been considered as part of the *novel advanced biofuels* of the third generation. Two scenarios support the production of biofuels with microalgae: from: a) Contribute to energy free-fossil-fuel transition and b) CO₂ mitigation as part of the BECCS strategies. In fact, at the onset of the XXI century, biofuels like biodiesel were expected to be more cost competitive to existing fossil fuels, even with potential to produce more energy per acre than conventional crops [Chisti, 2007]. Most of the common issues related to biofuel production from 1st and 2nd generations, are avoided when culturing microalgae, like land, food security, water resources, biodiversity conservation and livelihoods.

From a general perspective, microalgae just require a light source, mostly inorganic nutrients sources and water; and with them many products can be obtained. Microalgae cultivation can take some important value from:

- a) wastewater (mainly nitrogen and phosphorus), with potential for treatment of organic efflu-

ents;

- b) cultivation in brackish water on non-arable lands, and then it may not incur land-use change, minimizing associated environmental impacts;
- c) CO₂ fixation directly from the source, by the integration with smokestacks from other industries, and then participating in the circular industry;
- d) all year round production, productivity of microalgae cultures exceeds the yield of the best oilseed crops;
- e) the biorefinery approach, that might allow to recover secondary and high added value metabolites, very useful in other industries;

Although all the benefits, some aspects in the entire process still require some improvements. When culturing microalgae for biofuels, it has to be observed:

- a) that species selection must meet requirements for biofuel production while ideally allowing extraction of valuable by-product to make more economically feasible the process;
- b) to attain higher photosynthetic efficiencies through the development of optimized production systems;
- c) the risk of negative energy balance after accounting for requirements in for operations units;
- d) the lack of data for large scale plants;
- e) to save water and other important materials for the production;

Algae-based production to produce bioenergy products may not be foreseen to be economically viable in the near to intermediate term. Some technical, cost and sustainability barriers need to be solved before launching into larger production scales. Resource (water, land, energy) and nutrients (N, P) remain key drivers for economic and environmental sustainability. The energy balance is especially relevant for this topic, since microalgae cultures can involve large energy needs.

1.3.1 The microalgal cell

There exist about 35 000 species of microalgae which have been describe to date [Borowitzka and Moheimani, 2013]. Commonly, algae is classified according to cytological and morphological characters [Richmond, 2004]. In algae there exists:

- a) Prokaryotes for Cyanobacteria (*Cyanophyta* and *Prochlorophyta*, and
- b) Eukaryotes for *Rhodophyta*, *Rhodophyta*, *Chlorophyta*, *Dinophyta*, *Chrysophyta*, *Prymnesiophyta*, *Bacillariophyta*, *Xanthophyta*, *Eustigmatophyta*, *Rhaphidophyta* and *Phaeophyta*.



Figure 1.8: Biofuel Process schema from microalgae.

Each major division and classes can differ significantly from each other, and the choice of certain strain for use at production levels, might rely on the kinds of metabolites produced by, and their ability to produce such in stress conditions or harsh environments. Equally important, features related to processing and recovery of metabolites are interesting for the downstream process.

As mentioned before, *mass and energy* are key for any living organism. Microalgae are organisms that can assimilate their nutrients by several ways, including [Richmond, 2004]:

- a) *Autotrophy*, for producers of complex organic molecules by the use of inorganics sources. Where *Photoautotrophy*, for those wich convert radiant energy into biologically energy molecules and synthesize organics compounds using that energy and CO_2 or carbonates as a source of carbon; and *obligate Photoautotrophy* for those that cannot grow in the dark. By far, most algae belong to this category, although many require minimal quantities of organic compounds for growth, such as vitamins.
- b) *Heterotrophy*, mass and/or energy needs is obtained from organic compounds produced sometimes by other organisms. Where *Photoheterotrophy*, require light as energy source to be able to consume organic compounds (the organic compounds may also satisfy the energy requirements of the algae); *Auxotrophy*, where the algae require small quantities of essential organic compounds like vitamins and amino acids.
- c) *Mixotrophy*, for algae needing both organic and inorganic compouds (CO_2) for growth.

Media formulations aims to simulate the fresh, brackish or sea water where microalgae usually

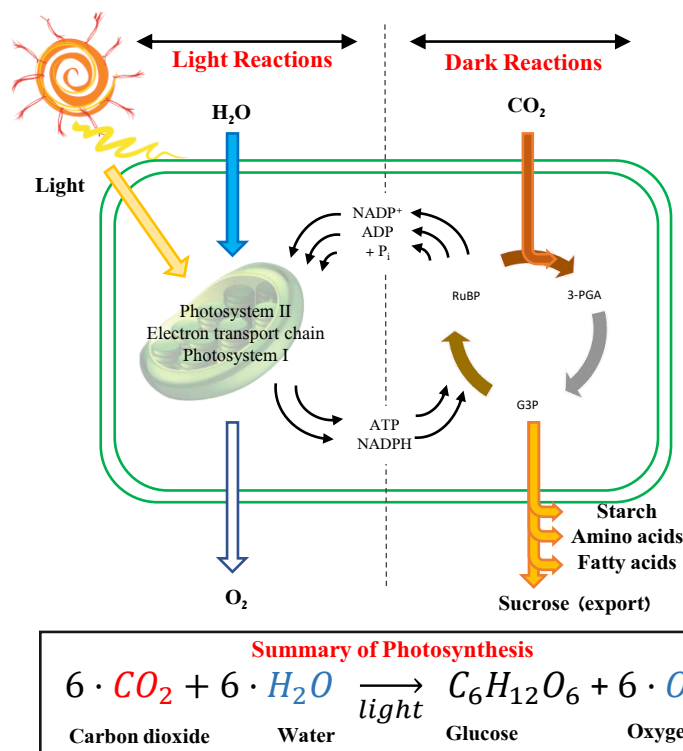


Figure 1.9: Light and Dark reactions in the microalgal cell. Organic molecules intermediaries represented in the Calvin cycle, are: ribulose-1,5-bisphosphate (RuBP), 3-phosphoglyceric acid (3-PGA) and glyceraldehyde-3-phosphate (G3P)

grow, but by optimizing the concentration of elements needed to sustain the non-limited growth. There are several media formulations for mineral supplying, all involving mixtures of around 30 elements of organic or inorganic sources, different ranges of pH and total salts content; all according to the specific microalgae requirements [Richmond, 2004].

1.3.1.1 Feeding the cell: CO₂, Nitrogen and Light

Light. Photon, an elemental particle, is carrier of electromagnetic energy. The amount of energy carried by, depends on the so-called wave frequency and this, on its wavelength. Thus, visible light as an electromagnetic wave, also carries energy in the 380-750 nm wavelength spectrum. This energy can be captured by microalgae using special organelles called chloroplast.

The light absorption by microalgae is dependent on the light wavelength [Janssen, 2002, Krzemińska *et al.*, 2014, Legrand, 2013]. Photosynthetic pigments contained in the chloroplast, also referred as light harvesting antenna, capture photons over different spectral bands of the light spectrum. They are the first actors in the light capture during the photosynthesis. The amount and type of pigments allow microalgae to seize efficiently solar energy under diverse kinds of environments [Legrand, 2013].

Photosynthesis can be divided in two set of reactions: *Light reactions* and *Dark reactions* (Fig. 1.9). During light reactions, by the photolysis of water, electrons are transferred to reduce the

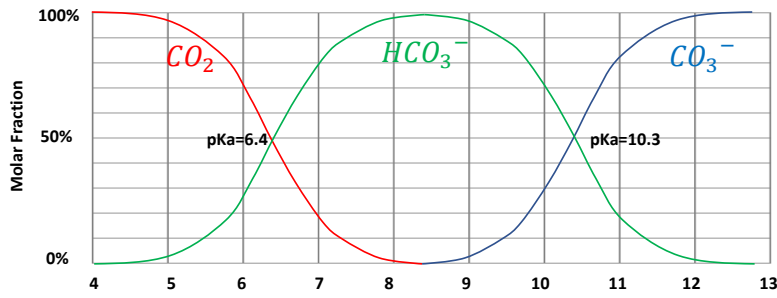
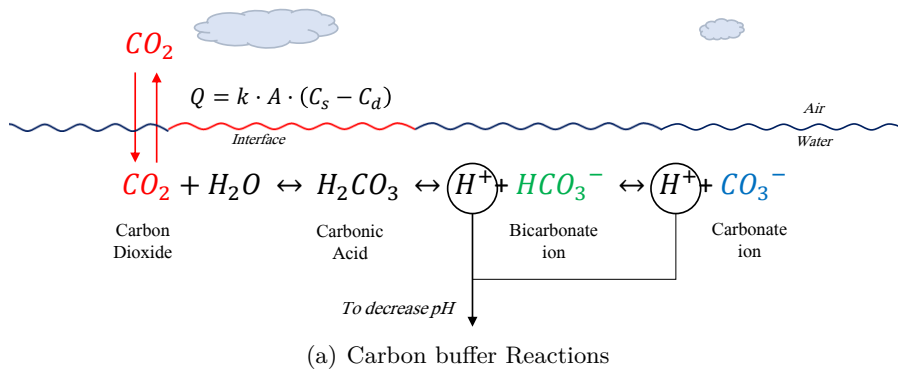


Figure 1.10: Carbon buffer reaction and their association to changes in pH in water dilution. For gas transfer equation, Q is the mass flux of CO_2 , k the mass transfer coefficient, A is the gas-liquid interface area, C_s the saturation concentration of dissolved CO_2 in the liquid equilibrium with the partial pressure of CO_2 in the gas phase, and C_d is the instantaneous concentration of dissolved CO_2 in the liquid.

NADP^+ and ADP molecules, into NADPH and ATP . Once enough energy from light has been converted into biochemical energy, the cell can launch the dark reactions to fix CO_2 .

Cornet *et al.* [1992] and Kandilian *et al.* [2014] introduced the Mean Volumetric Rate of Energy Absorption (MVREA) which represents the rate of light energy absorption by microalgae cells, by accounting for the cumulative effect of biomass concentration, the spectral mass absorption cross-section (related to the pigment content) and the local spectral fluence rate (light attenuation through the culture medium). This value has been used to predict and compare the growth kinetics and biomass or lipid productivities of microalgae cultures.

CO₂. Microalgae can fix CO_2 from three different sources, namely: CO_2 from the atmosphere; CO_2 in discharge gases from heavy industry, and; HCO_3^- from soluble carbonates. For autotrophic microalgae production, the consumption of the carbon source, and so the cell growth, rely on the availability of this in the medium. The diffusion of only atmospheric CO_2 into open ponds, for example, can at most sustain productivities around $10 \text{ g/m}^2 \cdot \text{d}^{-1}$ [Richmond, 2004]. The availability of CO_2 in the medium is governed by the gas transfer equilibrium (atmosphere-medium) and the carbon buffer reactions (Fig. 1.10a), and they are present in freshwater or sea water environments. By the latter reactions, the pH it is naturally regulated between 7.75 and 8.2 in oceans and some

lakes.

However, it is usual to observe pH increase during microalgae cultivation where there is no CO₂ addition, reaching pH values > 9.5 in dense algal cultures outdoors by mid-day. Such increase means that most of the inorganic carbon is in form of bicarbonate or carbonate (Fig. 1.10b) and there is none or little CO₂. This, implies that during CO₂ fixation, OH⁻ accumulates in the medium [Richmond, 2004]. There is also the possibility of carbonate salts precipitating at the high pH [Borowitzka and Moheimani, 2013].

Microalgae use the Dark reactions of photosynthesis to capture CO₂. During this set of reactions, CO₂ is fixed by action of Ribulose-1,5-bisphosphate carboxylase/oxygenase (Rubisco) enzyme in the Calvin cycle. The energy for this reactions comes from NADPH and ATP previously synthesized in the light reactions. Stoichiometrically, 3 mol of CO₂ are used to produce a single molecule of Glyceraldehyde 3-phosphate (G3P). These molecule is the first component in the synthesis of amino acids, lipids and more complex carbohydrates.

Oxygen (O₂) is a product of photosynthesis and also competes with CO₂ as a substrate for Rubisco in a process called Photorespiration [Borowitzka and Moheimani, 2013, Richmond, 2004]. In this process, Rubisco^P functions as an oxygenase, to form phosphoglycolate. After dephosphorylation, the resulting glycolate is converted, in several steps, to serine, ammonia and CO₂. However, the change of the Rubisco function can only occur when there are high concentration of O₂ and low concentration of CO₂ (*ie.* O₂/CO₂ ratio) whereas a low O₂/CO₂ ratio favours carboxylation.

Nitrogen. After carbon, nitrogen is the most important nutrient contributing to biomass growth. It is a constituent in all structural and functional proteins such as peptides, enzymes, chlorophylls, energy transfer molecules and genetic materials. When culturing microalgae nitrogen is mostly supplied as nitrate (NO₃⁻), but also as ammonia (NH₄⁺) and urea.

Under both autotrophic and heterotrophic conditions, ammonium is transported across the membrane by a group of proteins belonging to the ammonium transporter family, a group of evolutionarily related proteins commonly found in bacteria, yeasts, algae and higher plants [Wilhelm *et al.*, 2006]

The nitrogen source for growth is different from species to species, and the biochemical composition can also depends on the chosen source. Thus, the choice of the source is crucial to maximize the productivity of the target product, such as lipids and carbohydrates. Similarly, it have been shown that when nitrogen is limited in culture medium, microalgae slow down cell growth rate and increase their lipid or carbohydrate content, reducing protein synthesis [Ho *et al.*, 2014]. Nitrogen or phosphate limitation reduces the ability to use photosynthetically fixed carbon for protein

^PRubisco has low affinity to CO₂, its Km (halfsaturation) being roughly equal to the level of CO₂ in air. Thus, under high irradiance, high oxygen level and reduced CO₂, the reaction equilibrium is shifted towards photorespiration [Richmond, 2004].

synthesis, but does not prevent the formation of photosynthetic storage products [Berges *et al.*, 1996].

1.3.1.2 Energy storage: lipid and sugar

Lipids are constituents of membrane components, storage products, metabolites and sources of energy. Lipid content may account from 2% up to 50% in a dry weight basis [Richmond, 2004].

In plants, biosynthesis of fatty acids and glycerolipids involves cooperation of two subcellular organelles, plastids and the endoplasmic reticulum (ER), and for eukaryotic algae this is probably also the case [Borowitzka and Moheimani, 2013] (Fig. 1.11). PDAT (Phospholipid:diacylglycerol acyltransferase) is one of the enzyme involved in Triacylglycerol synthesis. It catalyses conversion of phospholipid and 1,2-diacylglycerol, into lysophospholipid and triacylglycerol products. Likewise, this enzyme has been also found to be essential for vigorous growth under favorable culture conditions and for membrane lipid degradation with concomitant production of TAG for survival under stress [Yoon *et al.*, 2012].

Lipids can be divided into non-polar (neutral) and polar lipids. The major part of neutral lipids in microalgae are triglycerides (TAG) and free fatty acids, a common source of energy and carbon storage; whereas in polar lipids it can be found glycerides (glycolipids and phospholipids), constituents of cell membrane and intracellular organelle membranes.

Algal lipids are typically composed of glycerol, carbohydrates or bases esterified to fatty acids having carbon numbers in the range of C₁₂–C₂₂ [Richmond, 2004]. Among those fatty acids, it can be found:

1. C_{14:0} (*Myristic Acid*): Named after nutmeg (*Myristica fragrans*), which is 75% trimyristin.
2. C_{15:0} (*Pentadecanoic acid*). It is not commonly found in nature, but is found in trace amounts in daily products like as in cow's milk fat (1.2%).
3. C_{16:0} (*Palmitic acid*): This is the most common saturated fatty acid found in animals, plants and microorganisms. It is the second fatty acid that is produced during lipogenesis. From this, it can be elongated other fatty acids of longer chains or with double bonds (insaturations). It is the most abundant in meats (after oleic acid, which is monounsaturated) and milk fats (butter, cheese and cream) and in vegetable oils such as coconut and palm oil.
4. C_{16:1n-7} (*Palmitoleic acid*): It is synthesized through palmitic acid by the action of the enzyme delta-9 desaturase, a common component of acyl-glycerides in human adipose tissue. It is present in all tissues, but is found in higher concentrations in the liver.
5. C_{18:0} (*Stearic acid*): Also found in many animal and vegetable oils and fats.

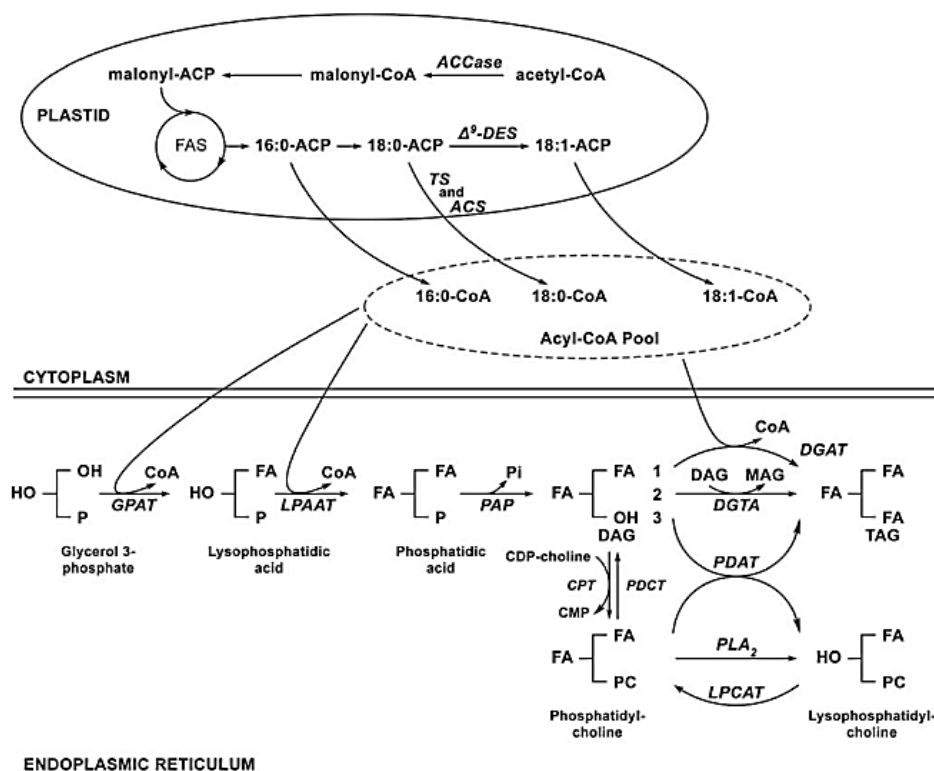


Figure 1.11: TAG Synthesis. Simplified scheme of TAG biosynthesis in plants. ACCase acetyl-CoA carboxylase, ACP acyl carrier protein, ACS acyl-CoA synthase, CPT CDP-choline:1,2-diacylglycerol cholinephosphotransferase, D9-DES D9-desaturase, DGAT DAG acyltransferase, DGTA diacylglycerol:diacylglycerol transacylase, FAS fatty acid synthase, GPAT glycerol 3-phosphate acyltransferase, LPAAT lysophosphatidate acyltransferase, LPCAP lysophosphatidylcholine acyltransferase, PAP phosphatidate phosphohydrolase, PDAT phospholipid:diacylglycerol acyltransferase, PLA₂ phospholipase A₂, TE acyl-ACP thioesterase, PDCT phosphatidylcholine:diacylglycerol cholinephosphotransferase. Taken from [Borowitzka and Moheimani, 2013].

6. $C_{18:2n-6}$ (*Linoleic acid*): Mostly found in cell membrane lipids (plants, animals). It is one of the two families of essential fatty acids. Oleic means "related to or derived from olive oil/oleic acid, because it can be produced oleic acid after saturation of the omega-6 bond.
7. $C_{18:3n-3}$ (*Alpha-Linolenic Acid*): Highly concentrated in certain vegetable oils. It is present in the membranes of the tilacoids of some plant leaves. It is an omega-3 polyunsaturated fatty acid. Omega-3 fatty acids such as a-linolenic acid are important structural components of cell membranes. When incorporated into phospholipids, they affect cell membrane properties such as fluidity, flexibility, permeability and the activity of membrane-bound enzymes. It is also one of the two essential acids.
8. $C_{20:5n-X}$: Mainly associated with galactolipids, the major membrane constituents of tilacoids [Fábregas *et al.*, 2002]. They are important membrane lipids in plants, where they replace phospholipids to preserve phosphate for other essential biological processes. For example, chloroplast membranes contain large amounts of monogalactosyldiacylglycerols (MGDG) and digalactosyldiacylglycerols (DGDG).

Similar to lipids, carbohydrates are important molecules constituents of microalgal structure and energy storage. In microalgae, 15 – 60% of biomass normally accounts for carbohydrate content, and are a direct product of CO₂ fixation in the Calvin cycle during photosynthesis (Fig. 1.9).

Carbohydrates of algae can be found in the form of starch (present in plastids), cellulose, glycogen, sugars, and other polysaccharides (present in the cell-wall) or agar. The carbohydrates may play many roles in the cell. They can be present in cell walls, providing structural support as intracellular carbohydrates acting as storage molecules (energy sources to drive other metabolic processes) or act as protectants for the survival under stress [Borowitzka and Moheimani, 2013, Richmond, 2004]

Although the microalgal carbohydrates have a low heating value (15.7 kJ/g), those carbohydrates are used for the production of biohydrogen, bioethanol, and biobutanol, because of the availability of high levels of fermentable sugars (low-hemicellulose, and zero-lignin content). For more complex sugars such as polysaccharides a pre-treatment can be needed for recovering simpler carbohydrates structures. Also, based on the microalgal species, carbohydrate content and composition may vary [Alam *et al.*, 2020]. The preference for the accumulation for energy storage molecule depends on the species. For example, cyanobacteria normally accumulates carbohydrates as glycogen, while microalgae do as starch (amylopectin-like polysaccharide).

1.3.1.3 More energy storage: Stressing the cell

Stress is the disturbance of homeostasis due to the action of stimulus impacting algal cell (light, temperature, nutrients, shear force, etc.). Once cells have restored homeostasis by acclimation and possibly adaptation^q, they are no longer stressed [Borowitzka, 2018]. If environmental conditions are always changing (like in batch cultures or day-night cycles, among others), there is not a single and constant physiological state; the organism is always trying to acclimate.

Different types of stresses (or combination of them) can trigger several types of responses in the algal cell. Cultures in photobioreactors, for example, are usually formulated such that mass nutrients and light are supplied in excess to ensure that they never become the rate-limiting factor. However, for specific applications, lights or nutrients may purposefully be supplied in limiting concentrations, causing the cell to acclimate to the new environment and thus changing its physiology and composition for a beneficial effect on the final valorization.

As mentioned before, in the biofuels industry, TAG and carbohydrates are mainly targeted for BioDiesel and BioEthanol respectively. The accumulation of these molecules by above the basal content, can be triggered mainly by action of high light intensities and nutrient limitation (nitrogen) [Kandilian *et al.*, 2019]. Other stressors like temperature, salinity or pH can also promote the accumulation of organic carbon compounds [Bonnefond *et al.*, 2016, Breuer *et al.*, 2013, Renaud *et al.*, 1995, Ruangsomboon, 2012, Vítová *et al.*, 2016]. In conditions such as nitrogen starvation, carbohydrates and lipids, may account up to 60% or 65% of dry microalgae, respectively [de Farias Silva and Bertucco, 2016, Taleb *et al.*, 2016].

It has to be noted the difference between nitrogen *limitation* and *depletion*. Limitation is meant for a reduction in the basal nitrogen amount in the medium, but not zero. Either cell growth and TAG/carbohydrates content may be not maximal, but are still present in a diminished range. Meanwhile, nitrogen depletion is meant for cultures in total absence of a nitrogen source where it is expected that cell growth might be minimal but TAG/carbohydrates content might be maximal.

Equally important, it is to note two approaches to starve the cell: *sudden starvation* or *progressive starvation* [Van Vooren *et al.*, 2012]. During progressive starvation, cells are left to naturally consume the nitrogen source until it is exhausted. For a sudden starvation, cells usually from an optimal physiological state, are separated from the optimal growth medium (*eg.* by centrifugation and rinsing) of optimal medium, and suddenly replaced in a nitrogen depleted (or limited) medium.

Among the consequences of nitrogen starvation, there is the reduction of the amount of pigments in the cell, as well as the increase in the carotenoid/chlorophyll A ratio [WATSON and OSBORNE, 1979]. Similarly, it also directly affects photochemical energy conversion because of decreases in protein synthesis that appear to affect chloroplastic proteins (and thus the proteins of PSI and

^qAcclimation is defined as the change of the macromolecular composition of an organism that occurs in response to a change in the environment and requiring changes in gene expression; meanwhile adaptation considers the change in genotype in response to a change in the environment [Borowitzka, 2018]

PSII reaction centers). In these cases, the carbon fixed in photosynthesis, is diverted from the path of protein synthesis to that leading to either lipid-or carbohydrate synthesis. Photosynthesis during nitrogen limitation still continues, albeit at a reduced rate, up to some limit in nitrogen concentration [Pruvost *et al.*, 2009, 2011b, Richmond, 2004, Van Vooren *et al.*, 2012].

This is the reason why higher lipid content are usually found to be associated to the lowest biomass productivities [Van Vooren *et al.*, 2012]. Despite this, it has been suggested that exists an optimal point during nitrogen limitation where starved biomass growth is enough to not compromise the metabolite productivity [Brennan and Owende, 2010, Kandilian *et al.*, 2019, Li *et al.*, 2013].

Some algal species increase their carbohydrate rather than their lipid content under nitrogen limited conditions. For cultures of *Chlorella* genus under nitrogen starvation, for example, some strains were found to accumulate large amounts of starch whereas others accumulated neutral lipids instead [Borowitzka and Moheimani, 2013, Richmond, 2004]. Likewise, Li *et al.* [2013] found that microalgae producing starch as a source of primary energy reserve usually have low lipid concentration. However, starch conversion may also contribute to the accumulation of neutral lipids during nutrient limitation.

As well, some culture strategies can take advantage of the stress effect on the cells. For *Parachlorella*, Li *et al.* [2013] reported the culture media dilution up to 10 times to reduce the amount of nutrients and thus biomass concentration. Consequently higher light intensities were received by the cell while introducing nitrogen starvation, which is key for triggering the accumulation of organic carbon compounds. For Van Vooren *et al.* [2012], during the sudden starvation, the operative parameter was the initial concentration of biomass: High concentrations of biomass may shadow the culture, limiting the availability of light cells (light attenuation) and then reducing lipid photosynthetic production. On the contrary, for progressive nitrogen starvation, the initial nitrogen concentration is the main operating parameter of the culture. The initial nitrogen directly affects the biomass concentration evolution during the culture, and then light transfer conditions. This leads to the existence of an optimum initial nitrogen concentration which leads to maximal TAG productivity values . Likewise Kandilian *et al.* [2014] also proposed the importance of an optimal MVREA where cells pass from low TAG productivities to higher values.

1.3.2 Culturing Microalgae

*"Crianse sobre el agua de la laguna de México
 unos como limos muy molidos [...]
 cógenlos los indios con unos redejoncillos de malla muy menuda [...]
 y échalos alli á secar [...].
 Cómenlo mucho los indios y
 tiene se buenos anda [...]
 por todos los mercaderes de la tierra como nosotros [...]
 es bien sabroso"*
Memoriales, by Toribio de Motolinia^r

The use of microalgae is not recent. The ancient Aztec empire (1321-1521, in the actual capital of Mexico) had a diet complement with Tecuitlatl (presumably *Arthrospira platensis*). During that time, this cyanobacteria bloomed on the surface of the brackish zone in the ancient Texcoco lake. Tenochtitlan, a neighboring city of around 250 000 people, was discharging most of its sewage into the lake, supplying some of the nutrients needed to grow. Tecuitlatl was harvested using a fine mesh at certain time of the year, then it was dried in the sun and reduced to a fine powder. The blue-green powder, had a salty flavor which could be consumed as seasoning, or mixed with other ingredients to form bread-like. It was exported out of the Aztec empire and, even the Spanish conquistadors were fascinated by the taste and preparation of this "strange blue-green paste" [Farrar, 1966].

Ever since, the culture, harvesting and final processing dedicated to cyanobacteria or microalgae, has substantially improved.

1.3.2.1 Photobioreactor systems

Photobioreactor (PBR) is the equipment used for culturing microalgae. The ideal culturing system should be able of controlling efficiently the growing conditions (pH, temperature, light source and mineral nutrients and CO₂ supply, and others), but also be economically viable, practical, easy to scale-up and useful to different microalgae applications and environments.

If the PBR is open to environment it is named *open pond*, whereas if not, it is named *closed*. There may also exist several variations in PBR design, but they can be grouped in four types accordingly to their geometry : *Raceway ponds*, *Tubular photobioreactor*, *Flat panel photobioreactor* and *Column photobioreactor* (Fig. 1.2):

Raceway ponds. A Raceway pond (Fig. 1.12a) is named after the loopy path described by water in such reactor. It consist fo a shallow ditch dug or an artificial pool, covered (or not) with

^r"There breeds upon the water of the lake of Mexico a sort of very fine slime [...] the Indians gather it with a very fine-meshed net [...] and they throw it down to dry [...]. The Indians eat a lot of it, and it keeps so well that they go[...] to all the markets of the land and us [...] it is very tasty"

Table 1.2: Advantages and limitations of open ponds and photobioreactors. Taken from Brennan and Owende [2010].

Production system	Advantages	Limitations
Raceway pond	<ul style="list-style-type: none"> Relatively cheap Easy to clean Utilises non-agricultural land Low energy inputs Easy maintenance 	<ul style="list-style-type: none"> Poor biomass productivity Large area of land required Limited to a few strains of algae Poor mixing, light and CO₂ utilisation Cultures are easily contaminated
Tubular photobioreactor	<ul style="list-style-type: none"> Large illumination surface area Suitable for outdoor cultures Relatively cheap Good biomass productivities 	<ul style="list-style-type: none"> Some degree of wall growth Fouling Requires large land space Gradients of pH, dissolved oxygen and CO₂ along the tubes
Flat plate photobioreactor	<ul style="list-style-type: none"> High biomass productivities Easy to sterilise Low oxygen build-up Readily tempered Good light path Large illumination surface area Suitable for outdoor cultures 	<ul style="list-style-type: none"> Difficult scale-up Difficult temperature control Small degree of hydrodynamic stress Some degree of biofilm
Column photobioreactor	<ul style="list-style-type: none"> Compact High mass transfer Low energy consumption Good mixing with low shear stress Easy to sterilise Reduced photoinhibition and photo-oxidation 	<ul style="list-style-type: none"> Small illumination area Expensive compared to open ponds Shear stress Sophisticated construction

plastic sheers draped up the sloping earth embankments. During production, culture medium is supplied in front of a paddlewheel and then circulated through the loop to the harvest extraction point. It is possible to supply more CO₂ if needed by submerged injectors, even if regularly the CO₂ is satisfied [Brennan and Owende, 2010]. The construction is relatively inexpensive compared with others systems, but it is influenced by the characteristics of the ground. Regularly, raceway PBR are operated with only 15 cm water depth, otherwise a severe reduction in flow and turbulence would occur. Because of limitations, low areal productivities in comercial raceways of around 12 - 13 g/m²·d are usually obtained [Brennan and Owende, 2010, Richmond, 2004].

Tubular photobioreactor. One the most common designs in commercial algal production. Tubular PBR are systems (Fig. 1.12b) of several transparent tubes (generally 0.1 m or less in diameter) joined by U-bends forming a one one several levels of connected flat loops. There exists models where light supply comes axially from a inner embedded tube, but most of the industrial systems use sunlight. When using sunlight, the array of capture may be aligned horizontally, vertically, inclined or as a helix. They are usually constructed with glass or special plastics. The circulation of the culture may be by either pumping the entire culture through the system or just agitated by air injection (airlift). When the culture is airlifted, the gas used may be a mixture of CO₂ with air, allowing mass transfer to the liquid medium as well as providing a mechanism for mixing. Similarly, it exists other systems of gas exchange for tubular PBR where gas and nutrients take place in a separated vessel. Agitation and mixing are very important to encourage gas exchange in the tubular PBR [Borowitzka and Moheimani, 2013, Brennan and Owende, 2010]. The productivity of this kind photobioreactors has been showed to be higher than raceway ponds (operated in parallel); achieving areal productivity of 20-30 g/m²·d [Richmond, 2004].

Column photobioreactor. Vertical tubular reactors (or column reactors, Fig. 1.12c) are simple, low cost, compact and easy to operate systems. Mixing is achieved by injecting compressed CO₂-air mixtures from the bottom. They offer the an efficient mixing, with high volumetric gas-liquid mass transfer rates and controllable growth conditions. Vertical columns are transparent walls made of glass, glass fibre or plastic of up to 2.5 meters high and 30-50 cm in diameter. The tube may be constricted at the bottom (where it is aerated) to prevent algal settling. Similar to tubular reactors, they can be illuminated either from a concentric inner tube or externally. Low productivities outdoors may be obtained in solar conditions due to the large angle of exposition to sunlight along the height of the column. Thus a substantial amount of solar energy may be reflected and not available for growth. As consequence, productivities lower than tubular PBR may be obtained [Brennan and Owende, 2010, Richmond, 2004].

Flat panel photobioreactor. Flat panel reactors (Fig. 1.12d) are often used to grow pho-

totrophic microorganisms at laboratory level, due to the manageability of light control on the designed surfaces. However, despite their apparent simplicity, few such systems have been used for mass cultivation. The reactors are usually made of transparent materials with variable but reduced thicknesses (even millimeters). The systems can also be oriented and tilted at different angles (Vertical or inclined) depending on the intensity or direction of the light source. They can also be arranged in several closely packed modules (Fig. 1.12f) for attaining higher areal productivities by larger surface area exposed to illumination. In vertical or inclined arrangements, they are usually agitated by airlift with CO₂ and air mixtures, for ensuring at the same time adequate mixing, a good mass transfer capacity, and limiting biofouling on the reactor walls. Temperature control may be achieved by water spraying (evaporative cooling) or by heat exchangers. Flat photobioreactors also present low accumulation of dissolved oxygen and high photosynthetic efficiency achieved when compared to tubular versions. Because flat panels PBR may maximize light capture, they can also achieve maximal biomass productivities up to 20-30 g/m²·d [Borowitzka and Moheimani, 2013, Brennan and Owende, 2010, Pruvost *et al.*, 2017, Richmond, 2004].

As a major interest, the concept of Flat Panel culture can be developed towards thinner culture systems. Reducing thickness to just few centimeters or even below, as for the Algofilm-PBR [Pruvost *et al.*, 2017], leads to the High Volumetric Productivity photobioreactors (HVR-PBR, Fig. 1.12e) which may attain highers biomass concentration (11-30 kg/m³).

1.3.2.2 Culture system operation

Independently of the technology used, photobioreactors can be operated in *batch mode*, *fed-batch mode*, *continuous mode* and *semi-continuous mode* for culturing microalgae (Fig. 1.13). For all operation modes, light can be supplied continuously or in day-night cycles. Some of the equations and parameters used for the operation modes are represented in the table 1.3.

Batch mode. In batch mode, culture medium is just supplied once at the beginning of the culture (time t_0) and eventually some nutrients are exhausted by cell development. It is a closed system with no mass inlets or outlets. The culture is only harvested at the end of the batch, which is usually during the stationary phase (t_f). During TAG/carbohydrates production two batches can be coupled. The first batch, may aim to produce biomass under optimal growing conditions just before the beginning of stationary phase. Then the cells can be washed and replaced in a second reactor for sudden starvation.

Fed-batch mode. A fed-batch culture can be understood as sequential batch cultures in the same PBR vessel; *ie.* there is a physical inlet flow with no outlet (or vice versa). At the beginning of the operation, the PBR is filled with an operative volume significantly less than the attended at the final time t_f . Then, cellular growth is monitored as for a batch mode. When the culture

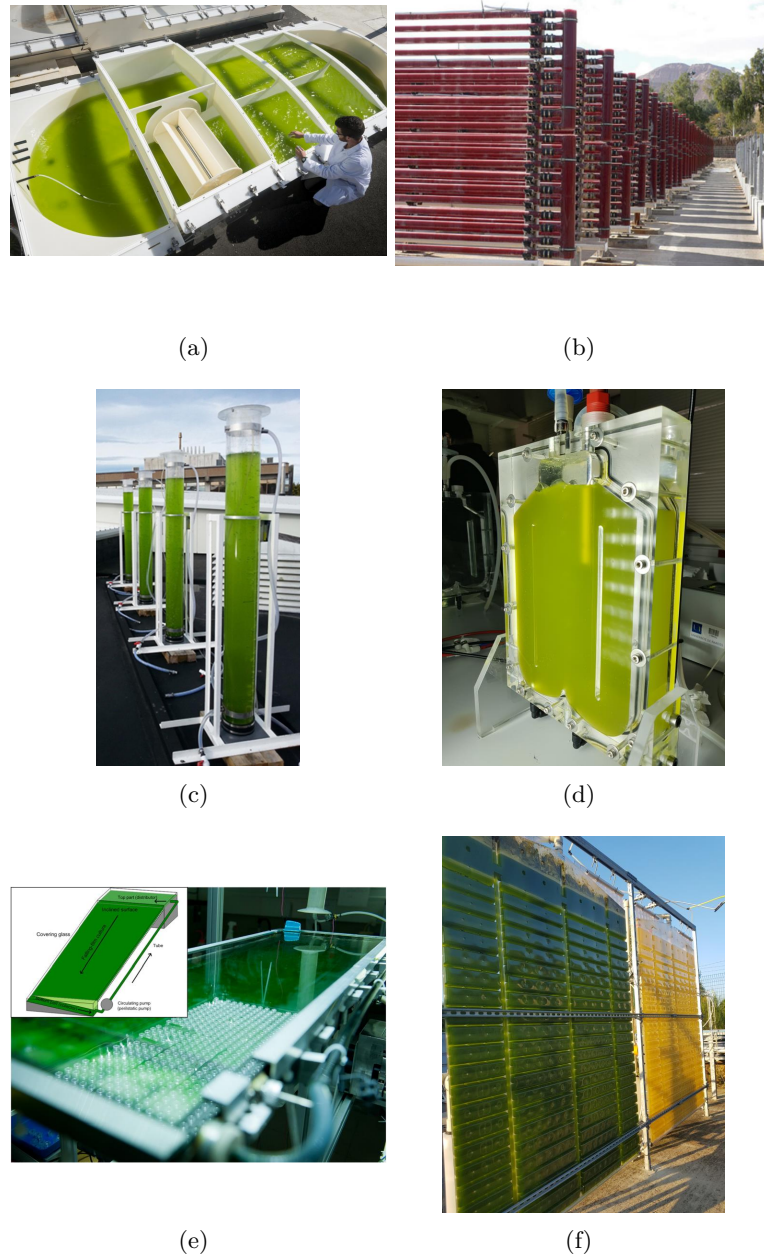


Figure 1.12: Photobioreactors culture systems for microalgae culture. a) Raceway open pond [CNRS, 2020]; b) Tubular [Borowitzka and Moheimani, 2013]; c) Column [Plouviez *et al.*, 2017]; d) Lab scale Flat Panel; e) Algofilm-High Volumetric Productivity Flat Panel [Pruvost *et al.*, 2017]; f) Subitec modules.

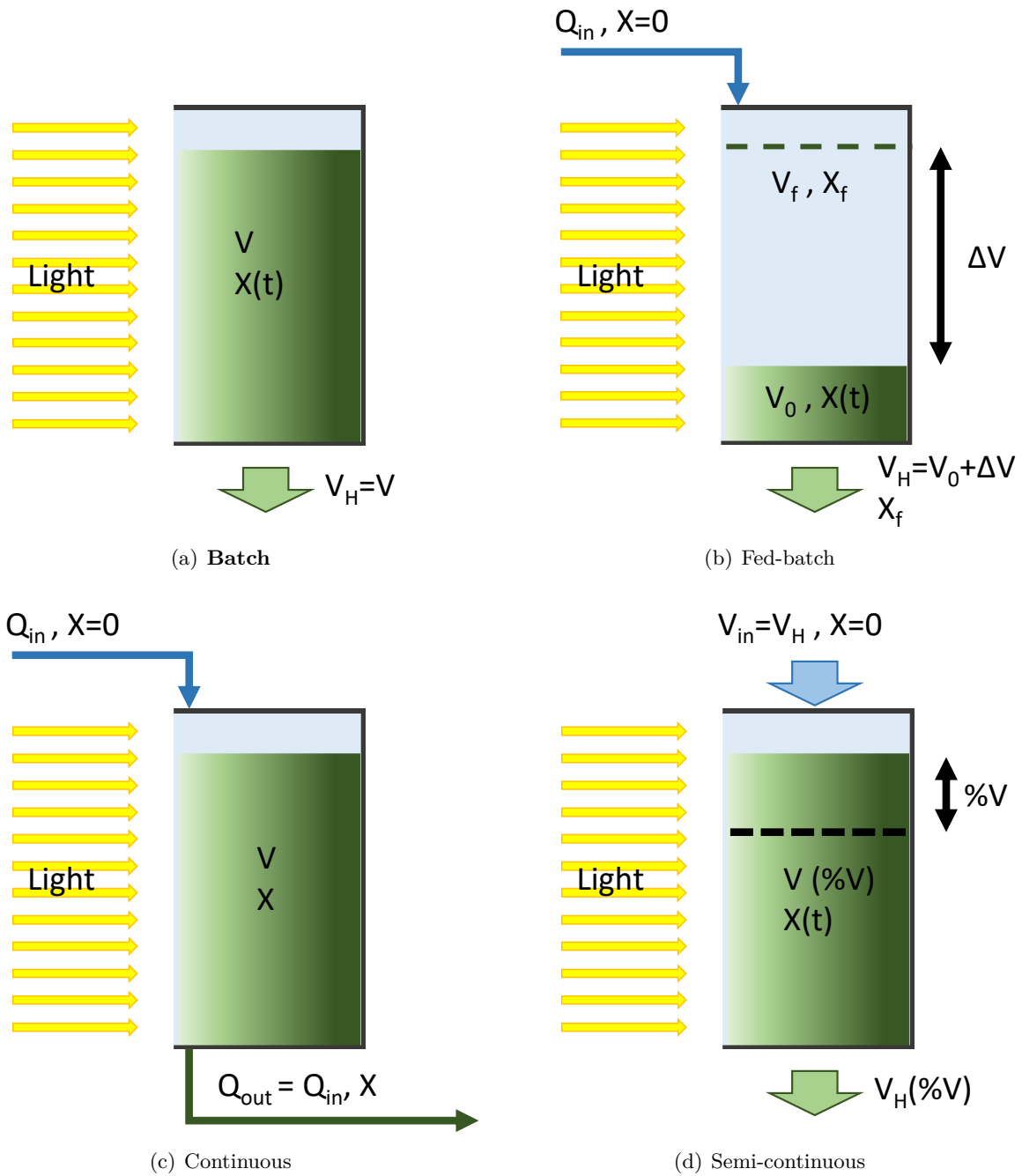


Figure 1.13: Common operations mode in microalgal culturing. Variables are Q for flow rate; X for biomass concentration; V for volume; Subscripts are *in* for inlet; *out* for outlet; *f* for final values; *0* for initial; V_H for harvesting volume; especial variable $\%V$ for replenishment percentage.

achieved the required state, fresh media is re-supplied into the PBR, and a second batch is started. This can be repeated as many times as the vessel volume and the percentage of refilling, allow it.

Continuous mode. Continuous mode is meant for the continuous medium supply and culture harvest. There are both inlets and outlets where the total inlet mass flows is equal to the total outlet mass flows, so that there is no mass accumulation. The operative criteria is the dilution rate (D , 1/h). Supplied media can be optimal, limited or depleted. Cells are expected to achieved an steady state were the monitored variables are unchanging. This steady state has a feedback with the dilution rate. If the monitored variables are related to any physiology aspect of the cell the system is also called a *chemostat*; but if the monitored variable is the turbidity of the culture (regularly measured by the outgoing light from the culture), then the culture may be named *turbidostat*.

Semi-continuous mode. It is a variation of continuous mode. Instead of a continuous supply of medium and culture harvesting, in a semi-continuous mode, the culture is harvested and replenished punctually at established vessel percentages; *ie.* there is a punctual inlet and outlet, but not continuous in time.

Batch and fed-batch operations last as long as cells consume the medium, whereas continuous and semi-continuous modes, can potentially be maintained for longer periods in optimized conditions. During the latter modes, biomass production and TAG/carbohydrates accumulation may occur simultaneously in the same reactor, whit negligible period of maintenance. Therefore, semi-continuous or continuous processes could result in a stable and robust process with higher productivities compared to the classical batch approach [Benvenuti, 2016].

1.3.2.3 Outdoor cultivation and light influence

When culturing outdoors, productivity could be affected by: a) evaporation which, even though has a favorable effect over temperature, may also change the ionic composition of growth medium, b) biological contamination or predation, especially if it is an open PBR, c) drastic temperature changes during day-night cycles and seasons, d) CO_2 loss, out from reactor which may limit carbon availability in the culture medium, e) losses in stirring efficiency due to larger volumes, resulting in deficient nutrient availability and lower gas-liquid mass transfer rates (oxygen and CO_2), and f) full dependency for weather and its irradiation fluctuations during day-night cycles [Brennan and Owende, 2010].

About the latter, light can fluctuate enormously according to geographic regions but also during day time and seasons. As light is the source of energy in phototrophic organisms, it impacts on the growth rates (μ), photosynthesis efficiency and metabolite accumulation; and all of them in global

Table 1.3: Important equations for continuous and batch microalgae cultures. A^* and V^* are for illuminated surface and volume respectively (m^2 and m^3); V_R is for reactor volume (m^3); L is for thickness of the reactor (m); D is for diameter (m); Q_{in} is for inlet flow rate (m^3/h) and $\%_j$ is for the content of j metabolite in the cell in a dry weight base.

Specific illuminated area, a_s (1/m)		
$a_s = \frac{A^*}{V_R}$	$a_s = \frac{1}{L}$	$a_s = \frac{2}{D}$
General	Flat geometry	Cylinder geometry
Volumetric illuminated fraction, γ		
$\gamma = \frac{V^*}{V_R}$	$\gamma = \frac{A^*}{V_R} \cdot L$	$\gamma = a_s \cdot L$
Continous mode PBR		
$D = \frac{Q_{in}}{V_R}$	$\tau = \frac{V_R}{Q_{in}}$	
Dilution rate (1/h)	Residence time	
<i>Volumetric Productivity</i>	<i>Surface Productivity</i>	
for biomass, X	$P_X = D \cdot X = \frac{X}{\tau}$	$S_X = P_X \cdot \frac{V_R}{A} = \frac{P_X}{a_s}$
for metabolite, $\%_j$	$P_j = P_X \cdot \%_j$	$S_j = \frac{P_j}{a_s}$
<i>X and $\%_j$ are the values measured at steady state</i>		
Batch mode PBR		
<i>Volumetric Productivity</i>	<i>Surface Productivity</i>	
for biomass, X	$P_X = \frac{X_f - X_0}{t_f - t_0}$	$S_X = P_X \cdot \frac{V_R}{A} = \frac{P_X}{a_s}$
for metabolite, $\%_j$	$P_j = \frac{\%_j \cdot X_f - \%_j \cdot X_0}{t_f - t_0}$	$S_j = \frac{P_j}{a_s}$
<i>X and $\%_j$ are the values measured at time t</i>		

productivity.

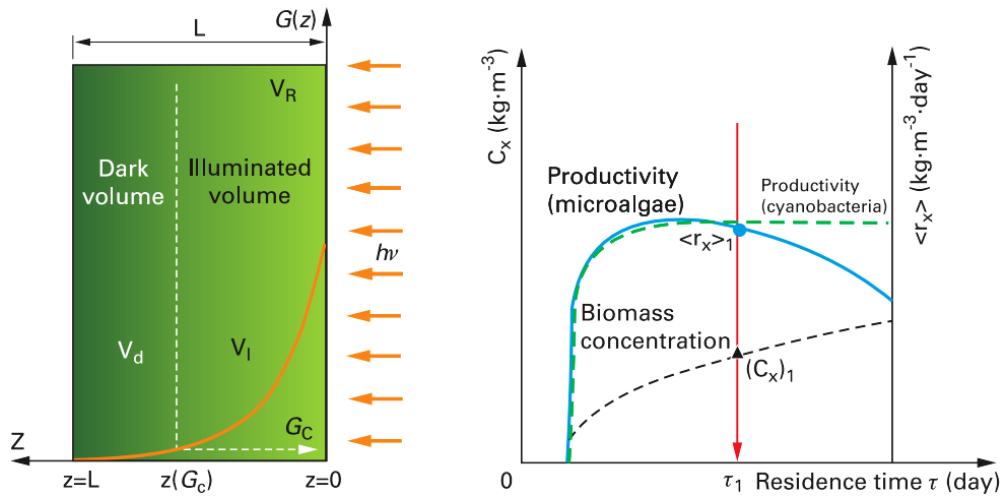
When a PBR is exposed to light, the closest cells layers are the first absorbing incoming light. This will result in a "shadowing-like effect" for cells in the subsequent layers of the culture, which will be enhanced as well by the depth of the reactor. This is called *light attenuation* and is influenced by pigment concentration and light scattering biomass properties [Cornet *et al.*, 1992, Kandilian *et al.*, 2014].

As the pigment concentration in the PBR varies (commonly along to biomass concentration or by the physiological state of the cell), it is also observed a response in light attenuation, the rate of light energy absorbed (measured by the mentioned MVREA) and the volumetric illuminated fraction in the PBR (γ).

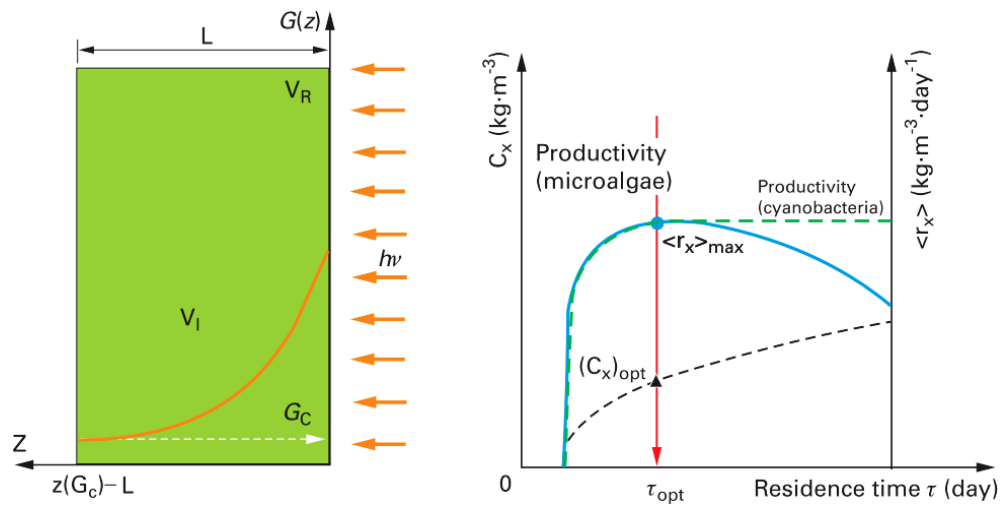
During the steady state of continuous cultures, it is possible to establish different dilution rate and observe the relation between biomass concentration and light attenuation (Fig. 1.14). High biomass concentrations (normally at larger dilution rates) will create a large dark volume fraction in the reactor and full light absorption, $\gamma < 1$ (Fig. 1.14a). In very diluted cultures and with usually no high pigments concentrations, part of the incident light is transmitted through the culture and lost for the photoreaction processes; it creates a kinetic light regime with $\gamma > 1$ (Fig. 1.14c). An optimal dilution rate may set the conditions to the so called luminostat regime, where $\gamma = 1$, there is full light absorption and no dark volume in the culture (Fig. 1.14b).

Similarly, according to figure 1.15, if light received (represented by irradiance) is below the saturation limit (G_{sat}), cell growth (represented by specific growth rates μ) will increase with light (*photolimitation*). However, when cell are exposed to high light irradiances, they will *photosaturate*, reducing then the specific growth rate, increasing energy dissipation, and thus diminishing PBR productivity. Equally important, if cells receive equal or less light than its compensation irradiance (G_c), cell will begin to consume some of the energy reserve molecules (TAG/carbohydrates) to maintain cell growth. The overall growth rate in the culture volume is then the combined result of the photosynthetic response which is locally influenced by the available light along the depth of the culture.

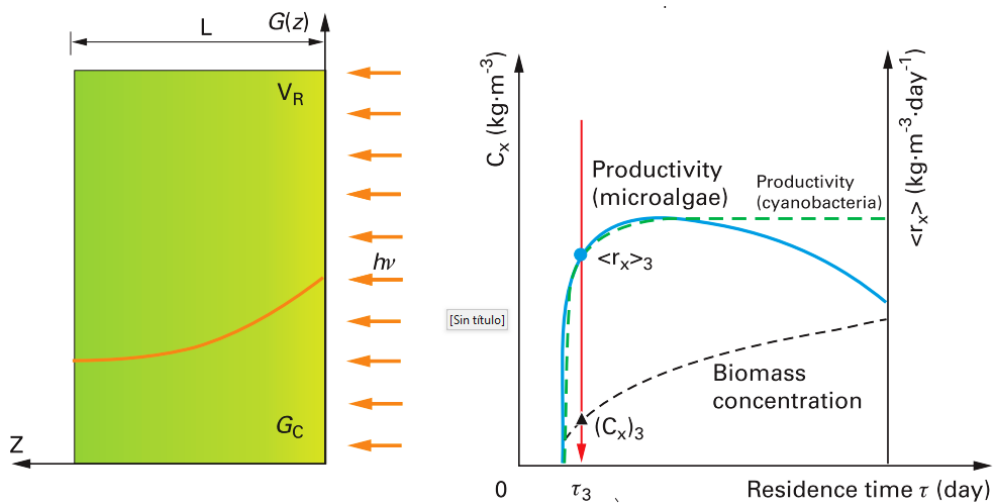
Moreover, Kandilian *et al.* [2014] and Kandilian *et al.* [2019] demonstrated the relationship between total fatty acid productivity and the main volumetric rate of light energy absorbed (MVREA). These results shows that nitrogen starvation only does not guarantee a large total fatty acid production rate and it may be limited also by the MVREA. Increasing the MVREA beyond its optimal value resulted in a decrease in the daily total fatty acid productivity and the reduction in pigment content; without which, it was not possible to achieve complete light absorption in the PBR during nitrogen starvation. Therefore, the process was biologically limited by the maximum lipid accumulation allowed in cells: a maximum total fatty acid productivity of 4.5 g/m²·d corresponding to MVREA equal to 13 $\mu\text{mol/g}_X\cdot\text{s}$



(a) Full light absorption, $\gamma < 1$



(b) Luminostat, $\gamma = 1$



(c) Kinetic regimes, $\gamma > 1$

Figure 1.14: Relation between the light absorption conditions (represented by the irradiance field G_z) and corresponding mean biomass volumetric productivities ($\langle r_x \rangle$). The three typical cases of light-attenuation conditions are represented: a) full light absorption, b) luminostat and c) kinetic regimes. Taken from Pruvost and Cornet [2012]

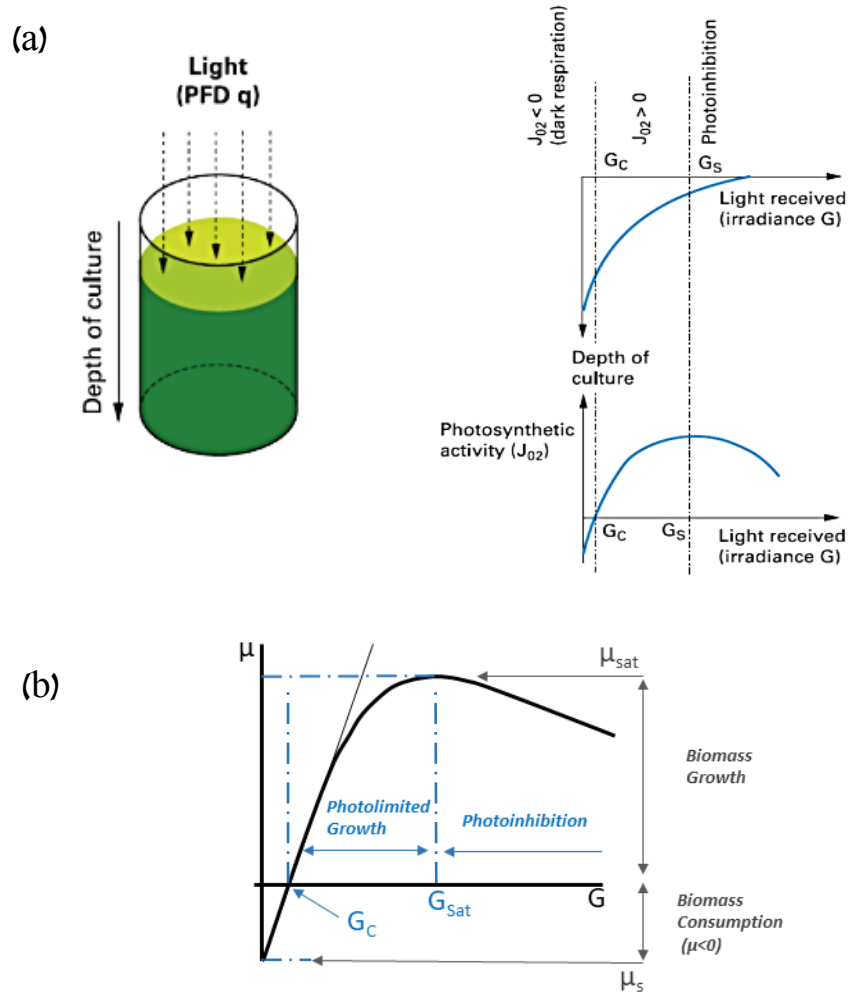


Figure 1.15: Light effect on photosynthetic growth. a) Relation between light attenuation and photosynthetic growth in microalgal cultivation systems. Taken from Pruvost and Cornet [2012]; b) Shows the growth rate response of microalgae to irradiance. J_{O_2} is the Photosynthetic activity; μ_{sat} is for specific growth rates for photosaturation (maximal); μ_{sat} is respiration point; G_{sat} stands for saturation irradiance; and G_C is the compensation irradiance (G in $\mu\text{mol}/\text{m}^2\cdot\text{s}$ and μ in $1/\text{h}$).

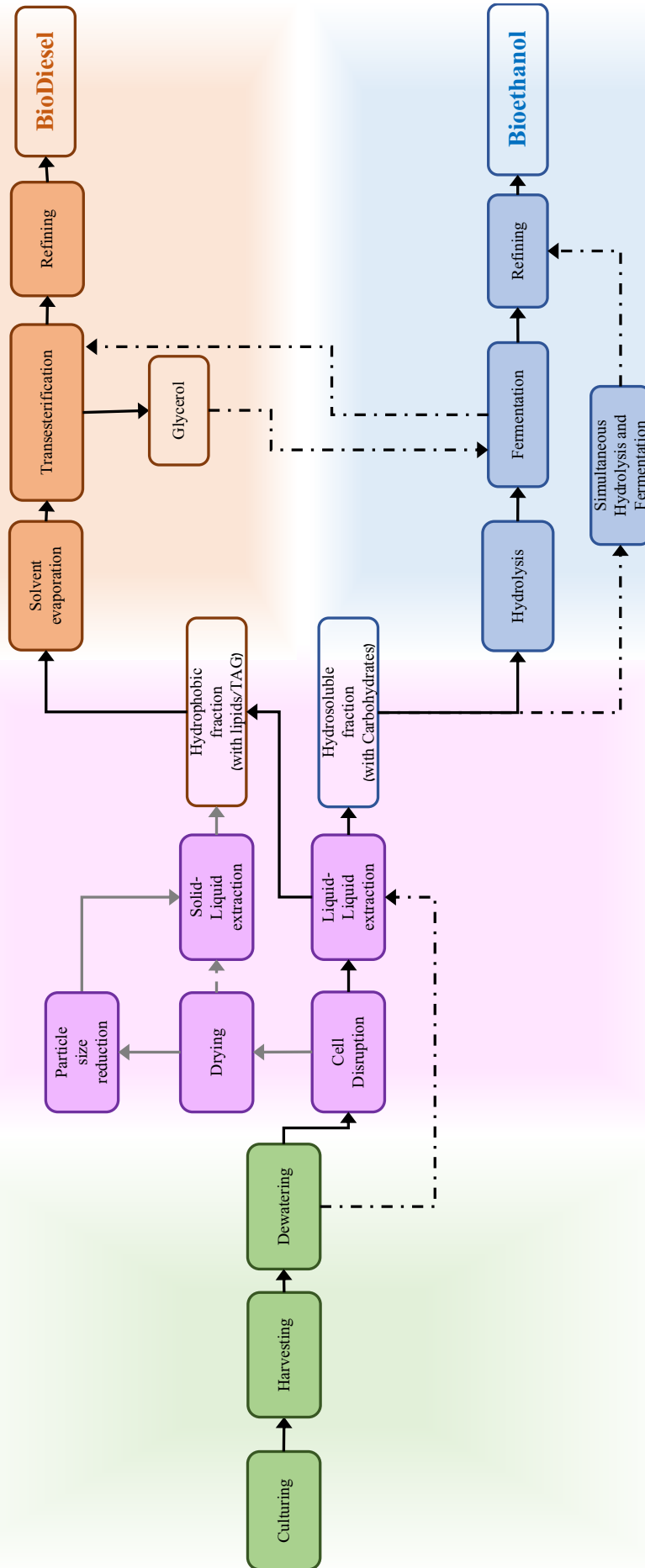


Figure 1.16: Global diagram for BioEthanol and Biodiesel downstream. Green color highlights the culturing stages, violet the recovery stages, orange the BioDiesel conversion and blue BioEthanol conversion. Black arrows suggests the main pathway and dotted lines are for interesting alternatives. Full boxes stand for operation units and empties for products. [Fariied *et al.*, 2017, Halim *et al.*, 2012a, Harun *et al.*, 2010, Ho *et al.*, 2013, Karemore and Sen, 2016].

1.3.3 Downstream processing: From Microalgae to Biofuels

1.3.3.1 Wet pathway

After producing TAG and carbohydrates molecules in the cells, they need to be recovered for further conversion. There exists several methods to accomplish this task [Fariel *et al.*, 2017, Halim *et al.*, 2012a], however the, so called, *Wet pathway*^s is of interest to recover and separate TAG and carbohydrates from microalgal biomass. It considers the prior release of the intracellular material into the medium through cell disruption, and then its extraction from the liquid phase. Particularly, the recovery of TAG, as hydrophobic compounds, may take advantage of their affinity for different solvents during liquid-liquid extraction. Their separation also allows to increase carbohydrate availability for a further conversion into BioEthanol.

1.3.3.2 Cell Disruption

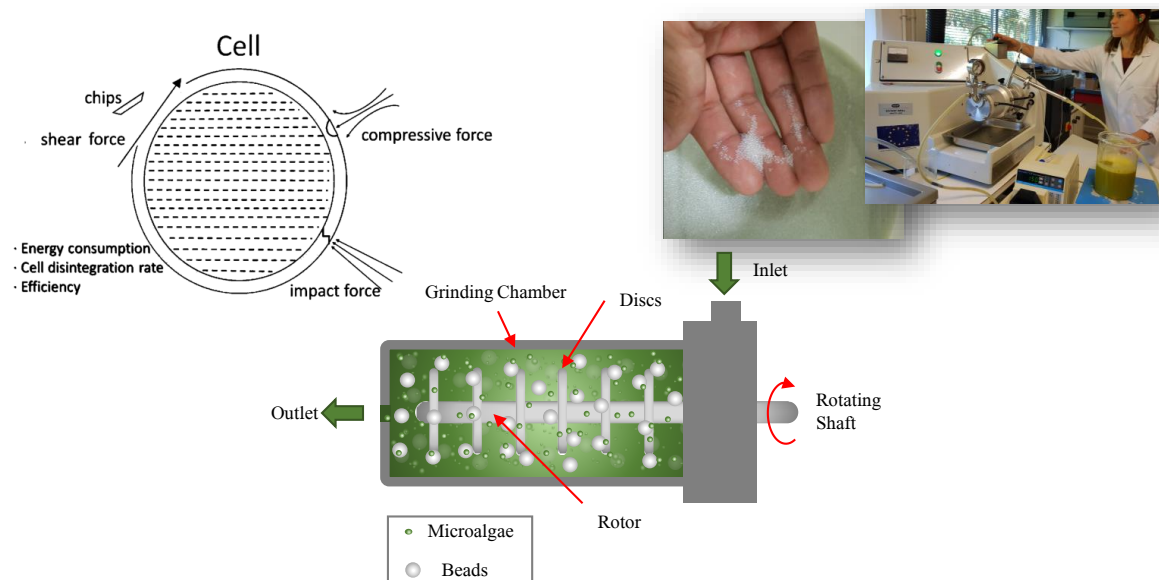


Figure 1.17: Bead milling: Forces acting on the cell during bead milling [Pan *et al.*, 2017], diagram of components and real pictures.

Cell wall separates the intracellular medium from the environment, leaving inside all the interest compounds. The thickness and chemical composition of microalgal cell wall, significantly changes in response to the growth environment [Kim *et al.*, 2016]. The most common compounds in microalgal cell wall are lipids, cellulose, lignin, tannins, protein, glycoprotein and polysaccharide, but these can variate among species [Lee *et al.*, 2017, Scholz *et al.*, 2014]. Some species are suggested to also contain algaenan in the cell wall; a term comprising lipid-related aliphatic species (also present in some plants) which confer extreme resistance to shear stress, chemical degradation and solvent

^sThis method raised as a contrary option to the *Dry pathway* in lipid recovery, where cell are not disrupted and, after a drying treatment, biomass pass to solid-liquid extraction. During the process energy is invested for heating and to facilitate the extraction and solvent recycling. This may impact the global energy efficiency by investing more energy than produced.

difussion [Angles *et al.*, 2017, Blokker *et al.*, 1998, Kim *et al.*, 2016, Scholz *et al.*, 2014, Zhang and Volkman, 2017]. Therefore considering cell fragility (and also cell size) and selecting the adequate method to disrupt it, is key in the recovery process. Costs, energy consumption (correlated to the processed volume), pumpability, efficiency and biomass requirements, has to be considered during the choice.

The methods to disrupt cell wall can be grouped in: a) Bio-chemical (comprising chemical and enzymatic methods), and b) Physical-mechanical (for electric, ultrasounds, microwaves, milling and homogenization). Mechanical methods may be the most suitable for large scale cell disruption due to the technological readiness level and efficiency, despite their high specific energy consumption [Montalescot *et al.*, 2015]. Mechanical methods are nowadays a preferred option face to bio-chemical methods [Balasundaram *et al.*, 2009]. Among them bead milling has been studied recently for the wet-pathway [Angles *et al.*, 2017, Montalescot *et al.*, 2015, Zinkoné *et al.*, 2018].

Bead milling principle is based on the mechanical stress induced by the interaction^t between beads and the microalgal cells (Fig. 1.17). Discs, axially coupled to a shaft, turn inside a grinding chamber. The latter is filled (but not fully) with beads (of glass, zirconium or other material of interest) of around 1 mm diameter. Filling volumes can vary between 35% up to 90% of the total chamber. Then culture is supplied into the chamber and, once culture also charges the chamber, the shaft rotates to induce kinetic energy into the beads which will interact with the cells. If the size and amount of beads, rotating shaft speed, residence time of the culture and biomass concentration are optimal, the cell wall might be broken up, releasing the intracellular compounds.

1.3.3.3 Centrifugal Extraction

When the metabolites are released outside the cell, it is needed to separate and recover the interest compounds. Solvent extraction of lipids for a single phase has been already wide reviewed [Bojczuk *et al.*, 2017, Chua and Schenk, 2017, Dong *et al.*, 2016, Halim *et al.*, 2012a, Harris *et al.*, 2018, Ryckebosch *et al.*, 2014, Taher *et al.*, 2014]. However, there exists another approach to separate and recover compounds with different miscibility in two different phases: *Centrifugal extractions*.

Centrifugal extraction technologies follow guidelines of process intensification. This is a well-established hybrid technology that combine, by the use of high rotary g-forces (between 200 and 2000 RCF), liquid-liquid extraction and phase separation.

Devices are regularly axially symmetrical constructed. For Continuous Centrifugal Extractor module (Fig. 1.18), the housing of the centrifuge is acting as a stator while in the inner part, a rotor, is spinning. In the gap between rotor and stator, two phases (culture an solvent; light and heavy phases) are introduced either separately or previously mixed. Then the rotation creates extremely high shear forces resulting in a very good mixing and then mass transfer between those phases.

^tImpact, torsion, shearing and rolling are some of them

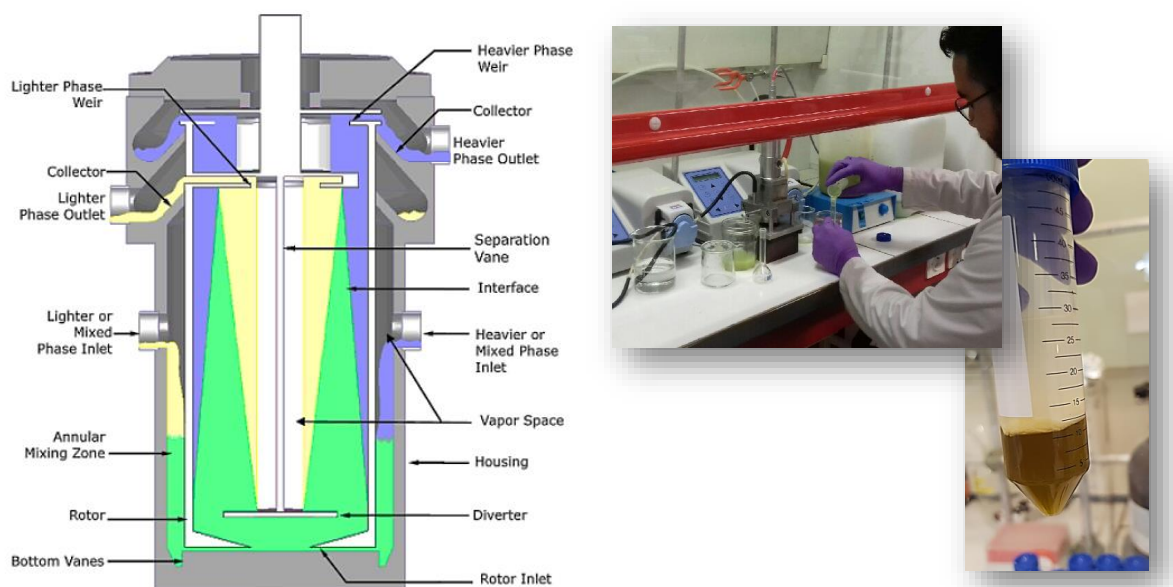


Figure 1.18: Centrifugal Extraction: Diagram of the device (taken [Seyfang *et al.*, 2019]) from and real pictures. The figure illustrates the mixed fluid in green, the lighter phase fluid in yellow, and the heavier phase fluid in blue.

Inside the rotor, the mixed fluid is forced upward to the outlets. On the way from the bottom to the top of the rotor the light phase (lower density) is accumulated at the center of the rotor whereas the heavy phase (high density) is accumulated closer to the rotor wall. Each fluid is recovered in its own collector ring and then leaves the separator through the heavy and light phase outlets. The extremely high g-forces and rotational speed benefit the mass transfer for the extraction. It has also been mentioned that extraction centrifuges have very small footprint combined with an excellent throughput per volume ratio [Seyfang *et al.*, 2019].

To be noted that for liquid-liquid extraction in the biofuel context, the solvent used has to be poorly soluble in water and with an environment impact as low as possible. Some solvents or mixtures of solvents, like those soluble in water ($\text{CHCl}_3:\text{MeOH}$), may have also a lysis effect on the cells; removing the need of the cell disruption. In this case extraction will be only limited by the solid-liquid-liquid mass transfer.

1.3.4 BioDiesel and BioEthanol: Considerations

Requested final characteristics for BioEthanol and BioDiesel are shown in the figure 1.4.

At the end of fermentation and further distillation, BioEthanol is still carrying large amounts of water and impurities. If they are not fully removed, they may have a corrosive effect on fuel combustion systems. Corrosion may cause damage to the components in the fuel system (since these components are made steel and zinc-aluminum alloys), fuel pumps and fuel tanks. [Khuong *et al.*, 2016]. Therefore, distillation or other purification process, is required to remove water and impurities in the diluted alcohol product after fermentation (usually 10 - 15% ethanol). This is why,

Table 1.4: Main BioDiesel and Bioethanol properties. Taken from [Khuong *et al.*, 2016, Xu *et al.*, 2006]

Property	BioDiesel from microalgal oil	Diesel fuel	ASTM biodiesel standard
Density (kg/m ³)	864	838	860 - 900
Viscosity (mm ² /s, at 40 °C)	5.2	1.9 - 4.1	3.5 - 5.0
Flash point (°C)	115	75	Min 100
Solidifying point (°C)	-12	-50 -10	-
Cold filter plugging point (°C)	-11	-3.0 (max -6.7)	Summer max 0; Winter max -15
Acid value (mg KOH/g)	0.374	Max 0.5	Max 0.5
Heating value (MJ/kg)	41	40 - 45	-
H/C ratio	1.81	1.81	-
BioEthanol			
Density (kg/m ³)	790		
Viscosity (mm ² /s, at 40 °C)	1.13		
Oxygen (% mass)	34.7		
Cetane number	5, 8		
Octane number	110		
Latent heat of vaporization (MJ/kg)	0.91		
Heating value (MJ/kg)	25.22, 26.70		
Flash point (°C)	13		
Auto ignition temperature (°C)	332.8, 366.0		
Water content (mg/kg)	2024		
Stoichiometric fuel/air ratio	1/9.01		

even if Bioethanol production is a well-established technology, just some engines can run under full ethanol fuel or very high blends. In Europe, regulations (EN228) recommend to blend Bioethanol with gasoline up to 10% [Edwards *et al.*, 2014].

Contrary, BioDiesel can be used without problems in standard diesel engines in blends up to 7% with conventional diesel fuel. This is allowed in the EN590 diesel fuel specification [Edwards *et al.*, 2014]. However algal BioDiesel properties is bounded to the properties of the TAG molecules produced. For example, too much insaturations (+2n) in the fatty acids make the product more susceptible to oxidation and with a lower freezing point. This has an impact on the BioDiesel combustion for conventional diesel engines. However, for use in the aviation industry, where low freezing points and high energy densities are key criteria, this example may be more suitable [Brennan and Owende, 2010]. Therefore the TAG composition (and their fatty acids) is directly correlated with the Biodiesel application.

1.3.5 Interesting Subproducts from the Biochemical Conversion

During the transesterification and fermentation of TAG and carbohydrates molecules into BioDiesel and BioEthanol respectively, some valuable by-products can be profited.

After cell disruption some proteins and residual biomass can be useful for food, feed, nutraceutical and oleochemical bio-products. The potential use of all the compounds from the cell, is the objective of the biorefinery approach, which underscores the full potential applications of microalgae and helps to drive the economic development bioenergy production [IEA, 2018].

The ethanol produced may also be used directly into the same BioDiesel production process to produce Fatty Acid Ethyl Ester (FAEE) instead of Fatty Acid Methyl Ester (FAME). It may reduce feedstock inputs in the BioDiesel process. However, the latter has not been done yet in practice [Mendoza *et al.*, 2020].

From the same fermentation process, the solid residue can be used for cattle-feed or for gasification. Gasification would involve the partial oxidation of biomass into a combustible gas mixture at high temperatures (800-1000°C). The biomass reacts with oxygen and steam to generate syngas (CO, H₂, CO₂, N, and CH₄). Syngas can be burnt directly or used as a fuel for gas engines or gas turbines [Mendoza *et al.*, 2020].

In addition, from the transesterification process, it is obtained glycerol. It is used in many food, cosmetics applications and also as a substitute for alcohol and glycols in the manufacturing (*eg.* paints, resins and antifreeze). Another alternative is to use it also for biogas or hydrogen production [Adhikari *et al.*, 2009].

Chapter 2

Energy-rich microalgae biomass for liquid biofuels: influence of strain selection and culture conditions

Abstract

Reserve metabolites such as neutral lipids (for BioDiesel) and carbohydrates (for BioEthanol) are valuable compounds for liquid biofuel production. This work aims to elucidate the main biological responses of two algae species known for their interest in energy-rich compound accumulation, the seawater specie *Nannochloropsis gaditana* and the freshwater specie *Parachlorella kessleri*, during N-limitation (*ie.* continuous culture) and day-night cycles. Both lipids and carbohydrates production, as well as cell resistance to mechanical disruption for intracellular compound recovery, are investigated. Batch N-depleted culture of *N. gaditana* in day-night cycles shows a low consumption of energy reserves with not significance preference for TAG or carbohydrates. However, it does accumulate significantly less carbohydrates than *P. kessleri*. Next, during chemostat cultures at four levels of nitrogen limitation, the highest levels of productivity for *N. gaditana* were 3.4 and 2.2 $\cdot 10^{-3}$ kg/m²·d for carbohydrates and TAG respectively at the 56%_{NO₃} limitation level. Contrary to *P. kessleri*, the cell disruption rate of *N. gaditana* decreases along the nitrogen limitation from 75% (at 200%_{NO₃}) to 17% (at 13%_{NO₃}). Elseways, the different dynamics of carbohydrates and TAG accumulation for both strains, exposed also different potential of total recoverable energy for biofuels. *P. kessleri* showed a good potential for BioDiesel as well as a high potential for BioEthanol; in contrast to *N. gaditana* was found more interesting for BioDiesel production.

2.1 Introduction

Nowadays, biofuels from microalgae are envisaged as contributor for replacing the use of fossil fuels and reducing the climate change effects [Brennan and Owende, 2010, Fortman *et al.*, 2008, Ponton, 2009, Timilsina and Shrestha, 2011]. BioDiesel and BioEthanol are two of the most promising liquid biofuels from microalgae to date [de Farias Silva and Bertucco, 2016, Karemore and Sen, 2016, Williams and Laurens, 2010, Zhu *et al.*, 2017]. For the production of BioEthanol and BioDiesel are needed carbohydrates (fermentable sugars) and fatty acids TFA respectively. The latter are mainly composed by triacylglycerol TAG molecules, which can be accumulated in the microalgal cell during stress conditions [Bonfond *et al.*, 2016, Breuer *et al.*, 2013, Naik *et al.*, 2010, Vitova *et al.*, 2014].

Microalgae biofuels face several challenges for efficiently produce these metabolites especially in the dynamic conditions for outdoors production. Preference on the accumulation of energy reserves of interest [Pruvost *et al.*, 2009, Vitova *et al.*, 2014], resilience to environmental changes [Caperon and Meyer, 1972] and their specific response to light and day-night cycles (DNc) [Bonfond *et al.*, 2016, Kandilian *et al.*, 2014] are some examples. Nonetheless, the potential of microalgae biodiversity offers many species with different sets of metabolite profiles capable to adapt to those outdoor situations [Ali *et al.*, 2019, Beer *et al.*, 2009, Borowitzka and Moheimani, 2013, Fischer *et al.*, 2008, Ho *et al.*, 2013, Ma *et al.*, 2014, Suganya *et al.*, 2016].

Taleb *et al.* [2016] screened fourteen microalgae strains on their TAG productivity towards BioDiesel production. The more interesting strains for BioDiesel production were *Nannochloropsis gaditana* CCMP527 and *Parachlorella kessleri* UTEX2229. They accumulated up to 56%_X and 40%_X TAG content respectively. Correspondingly, maximal areal TAG productivities were 2.3 and $2.7 \cdot 10^{-3}$ kg/m²·d for *N. gaditana* CCMP527 and *P. kessleri* UTEX2229 respectively (both at 150 μmol/m²·s).

P. kessleri has been already studied because of its capacity to grow in harsh conditions [Juárez *et al.*, 2011] and to produce large amounts of lipids and starch in regular [Li *et al.*, 2013, Příbyl *et al.*, 2012] and stress conditions [Fernandes *et al.*, 2013, Kandilian *et al.*, 2019]. Similarly, Taleb *et al.* [2018] also reported that the main physiological changes taking place on *P. kessleri* under day-night cycles are linked to energy reserves consumption and cell growth. Besides, a detailed study on *P. kessleri* response to several levels of nitrogen limitation and the relation with continuous light supply was carried out by Kandilian *et al.* [2019]. In the latter, concentrations of nitrate above 3.65 mM were found to trigger a stronger carbohydrate accumulation, and low concentrations were found to trigger higher TAG contents.

Similarly, *N. gaditana* has been studied for its lipid and carbohydrate production under stress conditions. Some authors have reported TAG content up to 40%_X in batch N-depleted cultures

at different light intensities, emphasizing the relevance of both N-depletion and light on TAG accumulation [Janssen *et al.*, 2019a, Simionato *et al.*, 2013]. Additionally, *N. gaditana* was found to produce TAG molecules by translocation of membrane lipids, *de novo* synthesis and even by recycling other energy molecules [Janssen *et al.*, 2019b, Simionato *et al.*, 2013]. Equally important, *N. gaditana* has exhibited a non-constant cell resistance in N-depleted conditions which might be linked to changes on thickness or composition of the cell wall [Beacham *et al.*, 2014, Fábregas *et al.*, 2002, Safi *et al.*, 2017, Scholz *et al.*, 2014]. Cell resistance is important since some processes used for microalgae-based in biofuels (like extraction pathways on wet biomass) rely on the disruption of the cells. Likewise, the effect of day-night cycles (DNc) on depletion of the reserve metabolites, is also relevant as it impacts the amount of biofuel during outdoors production. Studies on the physiological response of *N. gaditana* to DNc report gains of about 35% in TAG and 50% for carbohydrates during day periods, whereas losses are preferential for TAG in night periods because of respiration activity [Fábregas *et al.*, 2002].

To sum up, *P. kessleri* and *N. gaditana* are two promising microalgae species for biofuel production. Information on *P. kessleri* for different nitrogen limitation levels is already available in literature, but it is not as large for *N. gaditana*. This work aims to study the response of *N. gaditana* to various levels of nitrogen depletion and evaluate the potential of both strains as a source for biofuels, by considering their response in terms of both TAG and carbohydrates production. Likewise, it is analyzed the cells resistance to mechanical disruption, as another relevant parameter for wet-biomass downstream processing. Those result will be compared to those obtained with *P. kessleri*. finally, the potentially recoverable energy for liquid biofuels will be discussed for both strains.

2.2 Methods

2.2.1 Strains

The marine microalgae *Nannochloropsis gaditana* (Figure2.1b) was first described by Lubian [1982] as part of the *Eustigmatophyceae* class. It has been reported to reproduce asexually by fission, describing an ellipsoidal shape. It can reach 3.5-4 x 2.5-3 μm . The strain used for the experiments in this work was *N. gaditana* CCMP527 (NCMA,USA).

Besides, *Parachlorella kessleri* (Figure2.1a) is a fresh water microalgae with a spherical or ellipsoidal shape. It belongs to the *Chlorophyceae* class. It has been also described to asexually reproduce by auto-spores (2,4,6 or 8) of around of 2.5-3.5 x 3-4.5 μm . In the mature stage, it can reach 5-10 μm [Juárez *et al.*, 2011, Krienitz *et al.*, 2004, Li *et al.*, 2013]. In this work, the experiments on *P. kessleri* UTEX2229 (UTEX, USA) by Taleb *et al.* [2016] and Kandilian *et al.* [2019] were used for the comparisson with *N. gaditana*.

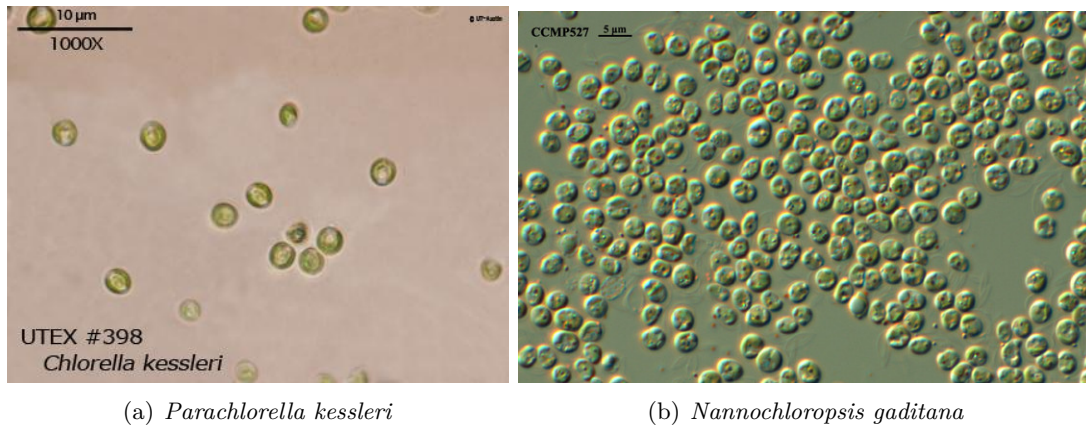


Figure 2.1: *P. kessleri* and *N. gaditana* microscopic images. Taken from UTEX [2020] and NCMA [2020] collection websites respectively.

2.2.2 Culture medium

Kandilian *et al.* [2019] used Bold Basal medium (NaNO₃, 8.02 mM), for the culture of *P. kessleri*. Meanwhile for the cultivation of *N. gaditana* in this work, Artificial Sea Water (ASW) enriched with CONWAY solution was used according to Berges *et al.* [2001]. The main medium is composed of (mM): NaCl, 248; Na₂SO₄, 17.1; KCl, 5.49; H₃BO₃, 0.259; NaF, 0.045; MgCl₂·6H₂O, 32.24; CaCl₂·2H₂O, 0.626; KBr, 0.497; SrCl₂·6H₂O, 0.056; and NaHCO₃, 1.42.

In this work four levels of nitrogen limitation and one full depletion were used to trigger lipid accumulation. These levels were established as a percentage fraction of the original NaNO₃ in the CONWAY formulation (100%_{NO₃} for 10.6 mM). The limitation levels were 200%, 56%, 46%, 29% and 13%_{NO₃} (21.2, 5.94, 4.88, 3.07 and 1.38 mM respectively) and 0%_{NO₃} (0 mM) for nitrogen depletion. These values were chosen in order to be compared with the work of Taleb *et al.* [2016] and Kandilian *et al.* [2019] on *P. kessleri*. The 200%_{NO₃} value was used to set the non-limited (replete) physiological state.

2.2.3 Culture systems

Culture systems figures are given in Fig. 1.12 at Chapter 1. Nitrogen sudden depletion culture took place in 170 L flat-panel airlift photobioreactor (HECTOR). A detailed description of the photobioreactor (PBR) can be found in Pruvost *et al.* [2011b]. The temperature of the culture was regulated to 23° C and the pH was set at 8 by automatic 98% CO₂(gas) injection. This system was operated in batch mode and supplied with artificial LED light to simulate day-night (DNc) cycles according to the average annual irradiation (photon flux density, PFD 270 µmol/m²·s) of Saint-Nazaire, France. Meteorological information of the region was obtained from an available database (Meteonorm, Switzerland). For the inoculation, a continuous culture of *N. gaditana* in non-limited conditions was established prior to initiate the batch. It provided the biomass to start the batch culture at 0.2 kg/m³.

For the nitrogen limitation studies, it was used a 1 L flat panel airlift photobioreactor described by Pruvost *et al.* [2009]. This system was operated in chemostat mode. The temperature was convectively controlled by the room temperature at 23° C and pH was set at 8 with the automatic injection of 98% CO₂ (gas). Continuous artificial LED light was supplied at 250 μmol/m²·s. Nitrogen full or limited culture media were supplied using a peristaltic pump (Reglo ICC, Ismatec, Germany) for setting a dilution rate of 0.01 h⁻¹. Similar to the batch experiment, the same non-limited continuous culture also provided the biomass for N-limited experiments.

The steady state of the limitation studies was identified when the daily determination of biomass, carbohydrates, pigment and total fatty acids, achieved no more than 5% of variation respect to the previous day and during at least 5 consecutive days. When the steady state was declared, the rest of analytic measurements were done and then a new level of nitrogen limitation tested was supplied by the correspondent medium.

2.2.4 Cell disruption rate and cell counting

Cell counting was determined by analyzing a 10 μL sample. Malassez chamber and an optical microscope equipped with camera (Axio MRC Cam at Axio Scope A1 microscope, Carl Zeiss, Germany) were used to take 40 pictures of each sample according to Zinkoné *et al.* [2018]. Then, by using an image treatment software (ImageJ v.1.52o, NIH, USA) and an own-developed algorithm in MATLAB (MathWorks, US), it was possible to treat the correspondent image information and obtain statistical information on the number and size of the cells.

To obtain the cell disruption rate, a volume of the same sample was adjusted to 30 mL at 1kg/m³ using a phosphate buffer saline (PBS) solution (to avoid the concentration effect in the disruption system). Next, the preparation was passed through a high pressure homogenization device (TS5, Constant Systems Limited, UK) at 1750 bar. Mechanical resistance of the sample was quantified by the percentage of remaining cells after homogenization. These values are reported hereafter as cell disruption rate (τ_D) .

2.2.5 Dry Weight measures

For biomass concentration analysis, triplicates of 10 mL samples were collected and passed through a pre-weighed 0.45 μm glass-fiber filter (Whatman GF/F, GE, US). Next, filters were washed with 1.19 M NH₄HCO₂ and MiliQ water to remove the remaining salts of culture medium. Filters were placed at 103 °C for about 1 h or until achieve an unvarying weight. Biomass concentration, X , is reported as the difference of weights after and before filtration in terms of the volume used. Similarly, pigment, carbohydrates, TFA and TAG contents are reported as a fraction of the biomass (% X). Biomass concentration was used for the determination of volumetric productivity, P_X and areal productivity, S_X . The corresponding relations can be found in Pruvost *et al.* [2011a] and

Chapter 1 (Table 1.3).

2.2.6 Pigment content

Pigment content analysis was followed according to Ritchie [2006] and Strickland and Parsons [1968]. Samples of 0.5 mL were centrifuged at 6,000 RFC, 4 °C during 10 min. The pellet was resuspended in 1.5 mL of methanol anhydrous 99.8%. After 1 min in sonic bath, samples were placed at 45 ° during 50 min. Then supernatant was recovered after centrifugation and light absorption at 750, 665, 652 and 480 nm was measured (V-730, Jasco, US). Following the equations from the literature previously cited, it was possible to obtain the concentration of pigments. Pigment content is expressed as the fraction of the whole dry biomass (%_X Pig).

Additionally, the ratio 480/662 nm (stress index) was calculated as a representation of the carbon/nitrogen content and the level of stress in the cell. The higher the value is, the larger the carotenoid content is compared to chlorophyll. This indicates a direct effect of nitrogen limitation, triggering the decrease of chlorophyll compared to carotenoids [Heath *et al.*, 1990].

2.2.7 Total Fatty Acid and Triacylglycerol content

The whole-cell extraction method described in Van Vooren *et al.* [2012] was applied to quantify the Total fatty acid, TFA, and triacylglycerol, TAG. According to the protocol, a sample of 30 mL was centrifuged during 10 min at 6000 RFC and 4 °C. Next, pellet was recovered and freeze-dried during 24 h. Immediately, 6 mL of chloroform/methanol 2:1 v/v (Fisher Sci, US) and 0.01% w/w of butylated hydroxytoluene were added to the samples, for then being left 6 h in incubation at 25 °. After that, the solvent supernatant was recovered and analyzed for TFA concentration by gas chromatography with flame ionization detector, GC-FID (Thermo Fisher Sci, US) and TAG concentration by high-performance thin-layer chromatography, HPTLC (CAMAG, Switzerland). TFA/TAG content is expressed as the fraction of the whole dry biomass (%_X TFA/TAG).

After valuing the TAG content, it was also calculated the correspondent volumetric and areal productivities (P_{TAG} , S_{TAG}) according to Pruvost *et al.* [2011a] and Chapter 1 (Table 1.3).

2.2.8 Total carbohydrates content

Total carbohydrates were measured following the protocol developed by DuBois *et al.* [1956]. A sample of 10 mL was centrifuged during 10 min at 6000 RFC and 4 °C. Pellet was recovered and resuspended in 1 mL of MiliQ water. A 0.5 mL aliquot was mixed with 0.5 mL of phenol solution (0.53 M) and three consecutive 2.5 mL doses of 97% H₂SO₄. Between each of the latter, the solution was vigorously agitated. Next, the reaction was left for 30 min at room temperature and then wet-bath incubated at 35 ° during 30 min. At the end, absorbance at 483 nm was measured (V-730, Jasco, US). Dilutions of a solution of glucose were prepared to calibrate the method and obtain the

total carbohydrates of the sample. Total carbohydrates content is expressed as the fraction of the whole dry biomass (%_X Sg).

It was also calculated the areal productivity based on carbohydrate content (S_{Sg}) in a similar approach as for TAG values.

2.2.9 Nitrate concentration measurement

Once the steady state of continuous cultures was reached, the outflow culture medium was recovered for nitrate measurements. A volume of 3-5 mL was filtered using 0.2 μm acetate cellulose filter (Minisart, Sartorius, Germany). The sample was injected into a ion chromatography equipment (ICS 900, Thermo Sci., USA) looking for the NO_3^- ion concentration. If needed, concentration was adjusted by dilutions with MiliQ water to be readable in the ion chromatography method. Using the NO_3^- concentration, it was calculated the Nitrogen uptake yield ($Y_{N/X}$) according to $Y_{N/X} = \Delta N_t / X$; with ΔN_t for the difference between the NO_3^- concentration in the supplied and in the worn-out culture media.

2.2.10 Potentially recoverable energy calculation

A theoretical estimated of the amount of energy which could be recovered from microalgae was calculated as the sum of the energies derived from the biofuels potentially obtained from the TAG and carbohydrates produced. It was expressed per unit of time and illuminated surface for an easy comparison to other applications.

First, the energy from BioDiesel through TAG transesterification (E_{BioD} in $\text{J}/\text{m}^2 \cdot \text{d}$) is obtained as:

$$E_{BioD} = (S_{TAG}/MW_{TAG}) \cdot \eta_{E,TAG} \cdot 3 \cdot Y_{Trans} \cdot MW_{FAME} \cdot \Delta H_{comb,BioD}^{\circ} \quad (2.1)$$

where, MW_{TAG} is the molecular weight of TAG or Fatty Acid Methyl Esters (FAME, BioDiesel) (g/mol); $\eta_{E,TAG}$ is the efficiency of TAG recovery; Y_{Trans} is the efficiency of the transesterification stage; and $\Delta H_{comb,BioD}^{\circ}$ is the heat of combustion for BioDiesel (26.7 $\text{MJ}/\text{kg}_{BioD}$). The value of 3 is the stoichiometric coefficient of FAME product in the transesterification step.

For the BioDiesel production analysis, it was proposed that about 80% of the TAG produced are actually recovered. This value could be accomplished through wet-extraction process [Angles *et al.*, 2017, Taher *et al.*, 2014]. Then transesterification was proposed based on a conversion yield of 98%. However, it has to be marked that such values requires 6 mol of alcohol per mole of triglyceride [Fukuda *et al.*, 2001]. For the molecular weight of the fatty acid methyl esters (FAME, BioDiesel), its calculation was based on the proposed fatty acid profile of *Botryococcus braunii* presented in Faried *et al.* [2017]. The corresponding heat of combustion of BioDiesel is derived from this value.

Second, the energy from BioEthanol via carbohydrates fermentation (E_{BioE} in $\text{J}/\text{m}^2 \cdot \text{d}$) is the

Table 2.1: Biochemical comparisson of *P. kessleri* and *N. gaditana* at the end of simulated DNc culture (11 days). Standard error for n=3

Strain	PBR system	Operation mode	X	Carbohydrates	TFA	TAG	Reference
			kg/m (SE)	% _X (SE)	% _X (SE)	% _X (SE)	
<i>P. kessleri</i>	Airlift	Batch	1.3 (0.04)	46 (2)	35	35	Taleb <i>et al.</i> [2018]
		Simulated DNc (11 days)					
<i>N. gaditana</i>	Airlift	Batch	0.9 (0.04)	17 (1)	26 (0.2)	18	Present study
		Simulated DNc (11 days)					

product of:

$$E_{BioE} = S_{Sg} \cdot \eta_{E,Sg} \cdot Y_{Fer} \cdot \Delta H_{comb,BioE}^{\circ} \quad (2.2)$$

where $\eta_{E,Sg}$ is the efficiency of fermentable carbohydrates recovery; Y_{Fer} is the BioEthanol conversion yield at fermentation step and $\Delta H_{comb,BioE}^{\circ}$ is the heat of combustion for BioEthanol (40.4 MJ/kg_{BioE}).

The term $\eta_{E,Sg}$ represents the recovery and acid hydrolysis of the total carbohydrates according to Karemore and Sen [2016]. The fermentation yield from the same work accounted 0.23 g of BioEthanol per each gram of fermentable sugar. BioEthanol was produced converting 90% of the fermentable sugars. The value was reported to be the 40% of the theoretical value for the *Saccharomyces cerevisiae* fermentation.

Finally, the total value of the recoverable fuel energy (J/m²·d) was estimated as:

$$E_P = E_{BioD} + E_{BioE} \quad (2.3)$$

2.3 Results and Discussions

2.3.1 Response of *N. gaditana* to Nitrogen depletion in day-night cycles

The effect of N-depletion on *N. gaditana* when cultivated in day-night cycles (DNc) and batch mode, was based on the approach described in Taleb *et al.* [2018] for *P. kessleri* in 1 L PBR. For the present study, a plateau was obtained after 168 h, indicating the N-depletion (*ie.* no growth). Then, the culture was maintained for 11 days, as done in the mentioned reference, to allow lipid accumulation during this time.

The final composition of the culture is shown in the Table 2.1. *N. gaditana* was found considerably less productive than *P. kessleri* for the same cultures conditions, with biomass concentration of 0.9 kg/m³ and 1.3 kg/m³ respectively. Energy stock molecules for *N. gaditana* attained 43%_X with 17% and 26% for carbohydrates and TFA respectively. About 70% of TFA was constituted by TAG molecules at this state (18%_X).

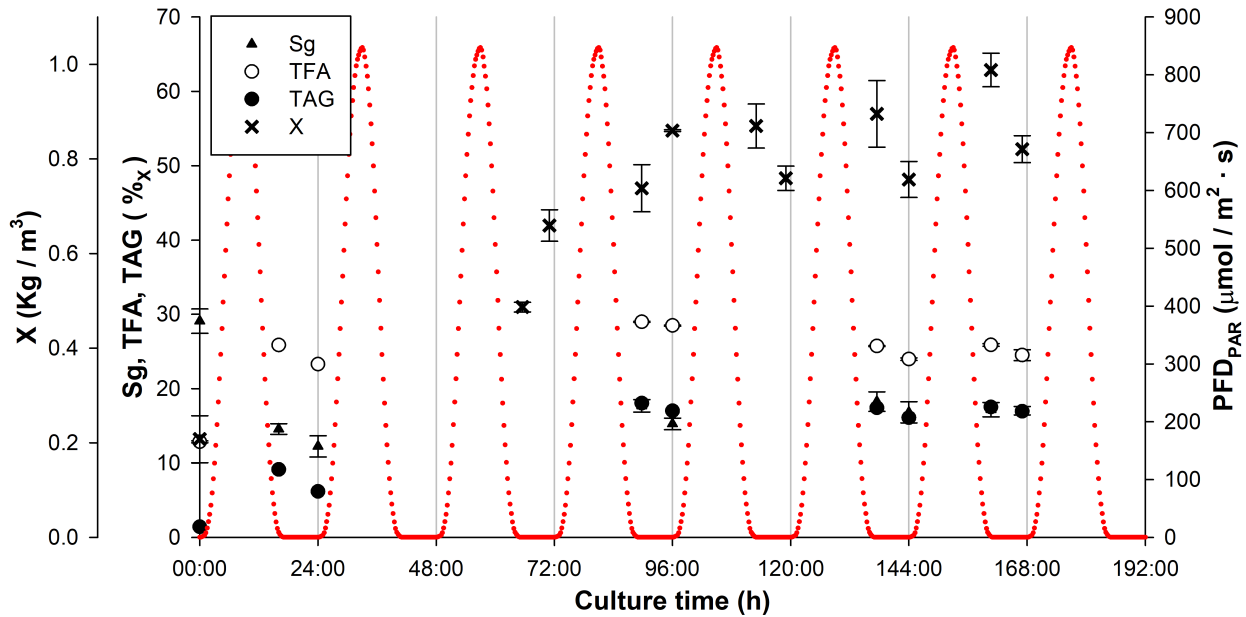


Figure 2.2: Physiological changes of *N. gaditana* under day-night cycles in depleted conditions. Triangles represents total carbohydrates; white circles are for total fatty acids; TAG are represented with black circles; and red dots correspond to the photon flux density supplied to the PBR.

It is interesting to compare the differences on the accumulation preferences for the energy reserve molecules. Carbohydrates concentration was 0.65 times less than the amount of TFA in *N. gaditana*, whereas carbohydrates of *P. kessleri* were about 1.3 times more the concentration of TFA. This difference could be explained by the preference of *P. kessleri* to accumulate carbohydrates as an energy reserve molecule, for possibly enduring the dark periods during DNc. *P. kessleri* was indeed reported to consume up to 10%_X and 5%_X of carbohydrates and TAG storage respectively in DNc (reported as not significant) [Taleb *et al.*, 2018]. Also, in the present work, *N. gaditana* was found to consume only 1.4%_X and 1%_X of carbohydrates and TAG respectively for the dark periods from 137 to 167 h (Fig. 2.2). This could also explain the difference on biomass development between the two strains in DNc. Therefore, the fact that *N. gaditana* do not strongly vary its energy-rich compounds during the night could be beneficial for the biofuel production, because the productivity would remain poorly affected during outdoors production in actual day-night cycles. More detailed studies will be required since other parameters such as temperature or night duration could also influence the dynamic of energy-rich compounds consumption.

Figure 2.3 shows the areal TAG productivity issued under DNc as obtained in the present work and from the results obtained by Taleb *et al.* [2018] for both *N. gaditana* and *P. kessleri* under continuous light and DNc regimes. From the present work, *N. gaditana* under batch sudden depletion in simulated DNc achieved $1.3 \cdot 10^{-3}$ kg/m²·d at end of 7 days. This value is around 30% less than reported final areal productivity of *P. kessleri* in the same culture conditions (DNc). It can be also observed that, under continuous light, the difference between strain is only 15%; maybe also related to the night consumption of energy reserves.

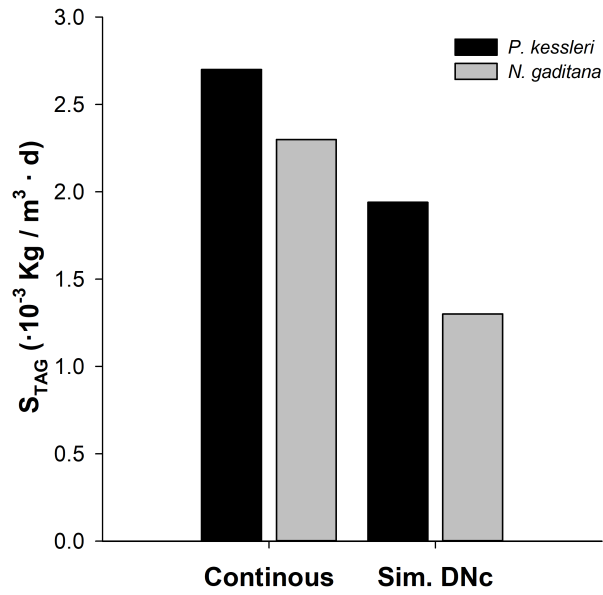


Figure 2.3: Comparison of areal productivity for batch under two light regimes for *P. kessleri* and *N. gaditana*. At left, batch cultures under continuous light, and at right cultures under simulated day-night cycles (DNC). The two continuous data and DNC for *P. kessleri* were obtained from Taleb *et al.* [2016] and Taleb *et al.* [2018] respectively.

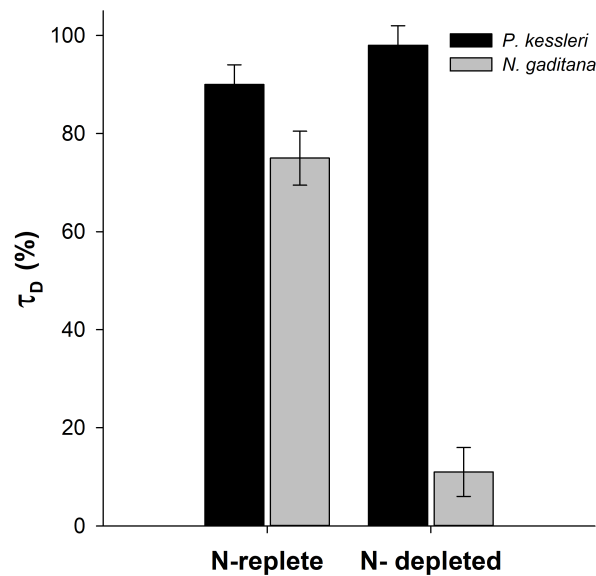


Figure 2.4: Comparison of cell disruption (at 1750 bar) for two physiological state for *N. gaditana* (white bars) and *P. kessleri* (grey bars) [Taleb *et al.*, 2016]

The figure 2.4 shows a complementary study about cell mechanical resistance. *N. gaditana*, cultivated in batch N-depleted medium and continuous light (culture data no shown) has a more marked difference in cell disruption rate when compared to N-replete conditions. In N-depleted conditions cell disruption accounted 11% (SE 5%), which is 85% less than the disruption rate found in replete conditions [Taleb *et al.*, 2016]. This trend indicating an increase of cells mechanical resistance in N-depleted conditions has also been observed by Angles *et al.* [2017].

2.3.2 *N. gaditana* culture under nitrogen limitation and continuous mode

The response of *N. gaditana* to four consecutive levels of nitrogen limitation in continuous mode (56%, 46%, 29% and 13% $_{NO_3}$) was investigated. Results were compared to the ones obtained for *P. kessleri* in same conditions as given in Kandilian *et al.* [2019]. The PBR was operated in continuous mode up to steady-state, to allow the adaptation of the microalgae to NO_3^- concentrations (around 20 days between each steady state). Continuous light (photon flux density 250 $\mu\text{mol}/\text{m}^2\cdot\text{s}$) and the CO_2 supply were established to not limit cell growth. Results are given in Table 2.2 and Figure 2.5 show the main results.

2.3.2.1 Nitrogen Uptake and Stress index

Nitrogen uptake yield ($Y_{NO_3^-/X}$) as a value rendering for the ability of the cell to assimilate the surrounding nitrogen sources, and the stress index as an indirect correlation to the C:N ratio [Heath *et al.*, 1990], were calculated at each steady state of every limitation level. It should be mentioned that all the limited cultures left an undetectable amount of NO_3^- in the media ($< 5 \text{ mg}_{NO_3}/\text{L}$, below detection limits), except for the 200% $_{NO_3}$ limitation. This corroborates the lack of nitrogen expected to stress the cultures by limiting the nitrogen source.

The non-limited culture was characterized for the highest nitrogen uptake yield, 411 $\text{g}_{NO_3}/\text{g}_X$. Next, the value declined to 189 and 201 $\text{g}_{NO_3}/\text{g}_X$ for the two subsequent limitations values 56% and 46% $_{NO_3}$ respectively. Then, values declined to the half again, for stronger nitrogen limitations, accounting 105 and 98 $\text{g}_{NO_3}/\text{g}_X$ at 29% and 13% $_{NO_3}$ respectively. Recently Rafay *et al.* [2020] calculated the maximum specific nitrate uptake of *N. gaditana* in $210 \pm 11.2 \text{ mg}_{NO_3}/\text{g}_X$ in a batch culture (F/2 medium for initial NO_3^- 100 mg/L), which falls within the range of values obtained in the present study.

It may be recalled that pigment content decrease is another physiological change taking place during N-limited cultures [Cornet *et al.*, 1992, Kandilian *et al.*, 2014]. By the cell pigment content measurement, the stress levels along N-limitation can be followed [Heath *et al.*, 1990]. Precisely, the stress index behaved in an inverted but similar trend to the previously reported nitrogen uptake values. The representative stress index for the non-limited culture was 0.55. For stronger limitations, the value increased progressively up to 1.70 at the 13% $_{NO_3}$. Dortch [1982] showed that

as soon as external nitrogen limits growth, phytoplankton may accumulate pools of unassimilated nitrogen allowing the cell to rapidly react to changes in medium composition (which may be read as small stress index or C:N ratio). Thereafter, when the surrounding nitrogen concentration is still reduced, cells consume firstly this nitrogen pool before other organic stock of nitrogen (proteins or amino acids) to then re-adapt to the new environment. This will lead to the reduction of the total nitrogen in the cell and so the stress index will increase.

2.3.2.2 Main biomass compounds

The total biomass concentration of *N. gaditana* decreased from 2.13 kg/m³ in non-limited conditions (200%_{NO₃}) to 0.89kg/m³ at 13%_{NO₃}. Total biomass did not change at the same rate that nitrogen limitation. Reducing nitrogen concentration from 200%_{NO₃} to 56%_{NO₃} only reduce 3% the biomass concentration. Meanwhile, a stronger limitation from 29%_{NO₃} to 13%_{NO₃} reduced the biomass concentration in 36%. The biomass trend is very likely to the one of *P. kessleri* presented by Kandilian *et al.* [2019]. The most notable difference between the two strains is related to the level stress needed to accumulate their energy stock molecules.

When *N. gaditana* is in favorable growth conditions, it accounts a small fraction (2%_X TAG) of the total biomass as TAG molecules (which are 16% of TFA). In comparison, when limitations begun, it can be noted in Table 2.2 that both strains gained up to 24 %_X TAG at the strongest limitation. However, both strains exhibit differences in N-limitation level: *P. kessleri* needed between 29 - 46 %_{NO₃} limitation to obtain an average 17%_X in TAG; and *N. gaditana* immediately achieved 15%_X TAG at the first limitation value (56 %_{NO₃}). This might be an interesting optimization perspective for *N. gaditana* since low limitations values do not compromise as much biomass production as higher limitations levels do.

Regarding carbohydrates, *N. gaditana* does not accumulate as much as *P. kessleri* (Table 2.2). In optimal growth conditions, it accumulates 19%_X in carbohydrates; which, at this point, are higher than TAG content. Then, 56%_X limitation triggers the maximal carbohydrates content up to 23%_X. At the lowest limitation only 18%_X in carbohydrates are accumulated, and at this point TAG molecules are already more accumulated in the cell. On the other hand, reported values for *P. kessleri*, indicates that not less than 45%_X in carbohydrates is achieved for all limitations (maximal 64%_X in carbohydrates at 46%_{NO₃}). It seems so, that *P. kessleri* has a marked storage preference for carbohydrates over TAG molecules in all N-limited conditions here tested. Meanwhile, even though *N. gaditana* has a slightly carbohydrates preference at medium limitations (56% and 46%_{NO₃}) and more for TAG at stronger limitations (29% and 13%_{NO₃}), the difference is mostly balanced between both energy reserves when comparing with *P. kessleri*. Simionato *et al.* [2013] mentioned the possibility that some sugars are being recycled into TAG molecules, which may explain the low carbohydrate content of *N. gaditana*.

Table 2.2: Physiological changes of *N. gaditana* and *P. kessleri* at steady state for several levels of nitrogen limitation. SE for the present study with n=4.

Limitation $\%_{\text{NO}_3}$	X kg/m^3 (SE)		Pigments $\%_X$ (SE)		TFA $\%_X$ (SE)		TAG $\%_X$ (SE)		Carbohydrates $\%_X$ (SE)		τ_D $\%_X$ (SE)		$Y_{\text{NO}_3^-/X}$ $\text{mgNO}_3^-/\text{gX}$		Stress Index	
	PK	NG	PK	NG	PK	NG	PK	NG	PK	NG	PK	NG	PK	NG	PK	NG
200	2.12 (0.02)	2.13 (0.04)	8.68 (0.007)	2.54 (0.12)	11.00 (0.37)	11.11 (0.60)	7.00 (0.33)	1.78 (0.10)	25.00 (0.11)	19.01 (1.77)	-	75.00 (11.00)	-	411.4	-	0.55
56	2.00 (0.02)	2.06 (0.02)	2.90 (0.005)	1.35 (0.04)	13.00 (0.08)	25.22 (0.72)	8.60 (0.30)	14.78 (1.08)	57.00 (0.00)	22.98 (0.88)	-	73.00 (2.07)	-	188.7	-	0.72
46	1.85 (0.01)	1.80 (0.03)	0.59 (0.004)	0.97 (0.04)	21.00 (0.47)	24.23 (1.00)	19.70 (0.26)	14.42 (1.01)	64.00 (1.10)	17.59 (0.58)	-	63.00 (3.43)	-	201.3	-	0.95
29	1.58 (0.02)	1.39 (0.02)	0.35 (0.004)	0.90 (0.03)	19.00 (0.31)	30.87 (1.23)	16.00 (0.31)	19.29 (0.37)	50.00 (0.77)	16.72 (0.69)	-	43.32 (3.81)	-	105.1	-	1.36
13	0.97 (0.03)	0.89 (0.02)	0.27 (0.002)	0.64 (0.02)	27.00 (0.23)	37.34 (1.72)	24.00 (0.37)	24.24 (1.06)	46.00 (0.37)	18.48 (1.33)	-	17.00 (2.91)	-	98.4	-	1.70

PK for *P. kessleri* from Kandilian et al. [2019]NG for *N. gaditana* in the present study

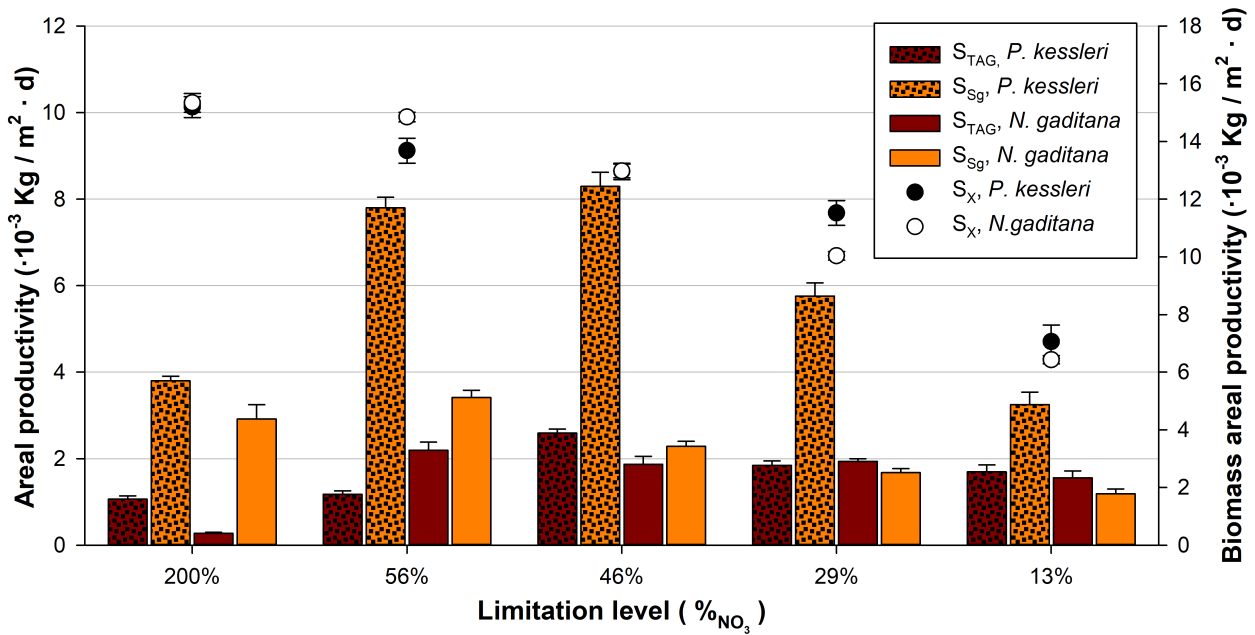


Figure 2.5: Areal productivities for TAG and carbohydrates of *N. gaditana* and *P. kessleri* at steady state in several levels of nitrogen limitation. Dotted bars are for *P. kessleri* and empties for *N. gaditana*. Bars in red color are related to TAG, while orange color are for carbohydrates (Sg). Error bars in *N. gaditana* are for SE with n=4, for the rest, refer to Kandilian *et al.* [2019]

Figure 2.5 shows the areal productivities for biomass, TAG and carbohydrates. The combined effect of *N. gaditana* biomass growth and its composition, revealed the maximal values of carbohydrate and TAG productivity at 56%_{NO₃}, equal to 3.41 and 2.19 · 10⁻³ kg/m²·d (SE 0.17 and 0.19) respectively.

Carbohydrate productivity for *N. gaditana* did not varied to much in the 56%_{NO₃} limitation related to non-limited experiment (200%_{NO₃}). However, it significantly changes at lower limitations levels, passing from 2.28 · 10⁻³ kg/m²·d at 46%_{NO₃} to 1.19 · 10⁻³ kg/m²·d at 13%_{NO₃} (SE 0.12 and 0.11 respectively). Similarly, TAG productivity remained almost unvaried for limitations at 56%, 46% and 29%_{NO₃}, achieving values of 2.19, 1.87 and 1.94 · 10⁻³ kg/m²·d (SE 0.19, 0.18, 0.07) respectively. Although the limitation level at 13%_{NO₃} triggered the highest content (24.2%_X), TAG productivity just reached 1.56 · 10⁻³ kg/m²·d (SE 0.16) as a combined with the lowest biomass productivity.

In comparison, *P. kessleri* [Kandilian *et al.*, 2019] produced the largest carbohydrate productivities (S_{Sg}) for the limitations levels from 56%_{NO₃} to 29%_{NO₃} (the highest at 8.3 · 10⁻³ kg/m²·d for a 46%_{NO₃} limitation). The maximal TAG productivity for *P. kessleri* was observed as well at the 46%_{NO₃} limitation (2.6 · 10⁻³ kg/m²·d).

It is also interesting to note that in practice and outdoor large scale production, it should be more complex to precisely apply the given imitation levels, however it remains important to know the limitation levels triggering the largest productivities in TAG and carbohydrates.

Table 2.3: Values use for the calculation of the Recoverable fuel energy.

		Units	Reference
$\Delta H_{comb, BioEthanol}^{\circ}$	26.7	<i>MJ/kg</i>	Khuong <i>et al.</i> [2016]
$\Delta H_{comb, BioDiesel}^{\circ}$	40.4	<i>MJ/kg</i>	Faried <i>et al.</i> [2017]
<i>MW algal lipids</i>	920	<i>g/mol</i>	Faried <i>et al.</i> [2017]
<i>MW of FAME</i>	299.32*	<i>g/mol</i>	Faried <i>et al.</i> [2017]
Y_{Fer}	0.23	<i>kgBioE/kgSg</i> **	Karemore and Sen [2016]
Y_{Trans}	98	%	Fukuda <i>et al.</i> [2001]
$\eta_{E, TAG}$	80	%	Proposed
$\eta_{E, Sg}$ **	89.6	%	Karemore and Sen [2016]

*based on the fatty acid profile

**Fermentable carbohydrates

2.3.2.3 Cell resistance

The fact that *N. gaditana* is more resistant to mechanical stress in N-depleted conditions has been already mentioned in the literature [Angles *et al.*, 2017, Beacham *et al.*, 2014, Scholz *et al.*, 2014] and confirmed in the presented batch experiment. Complementary, in Table 2.2, is presented a more detailed evolution of this change during different levels of nitrogen limitation.

A non limited culture of *N. gaditana* can be disrupted at 75% in a single pass through high pressure homogenization at 1750 bar. This resistance is maintained with a low limitation at 56% $_{NO_3}$. But then, in the 46% $_{NO_3}$ limitation, the disruption rate τ_D diminished at 63% for finally accounting 17% for the lowest limitation. Cell concentration as an explanation to this phenomena was discarded since sampling preparation was established always to obtain 1 kg/m³. An evolution in cell wall composition and thickness could explain this result [Beacham *et al.*, 2014, Janssen *et al.*, 2019b, 2020, Scholz *et al.*, 2014, Zhang and Volkman, 2017].

Cell resistance of microalgae cultivated in nitrogen depletion arise as an important factor for recovering TAG and carbohydrates molecules when using wet-biomass treatment. The values shown here, implies that even if productivity is high for some limitations levels, not all the compounds could be recovered if the cell resists to the disruption (or more energy will be requested to obtain sufficient cells disruption). In other words, final metabolite productivity and overall efficiency of the whole process will depend on how easy it is to recover these compounds at that physiological state. Such results will have consequences on the whole energy investment in the biofuel production process.

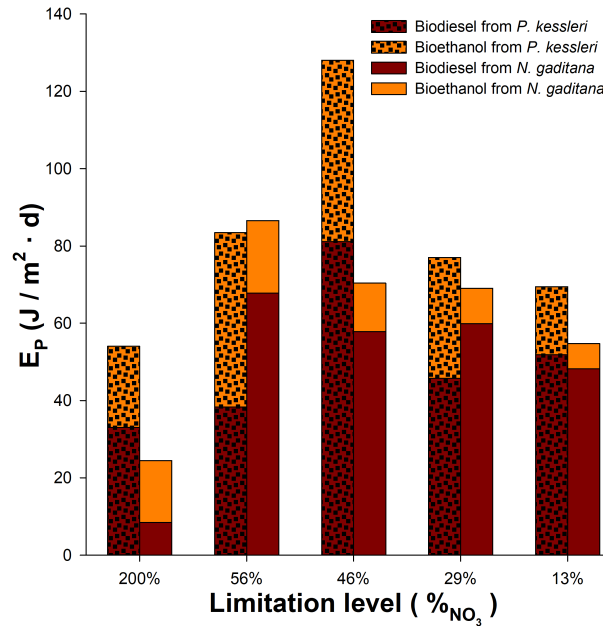


Figure 2.6: Potentially recoverable energy values for *N. gaditana* and *P. kessleri* obtained in continuous N-limited culture.

2.3.3 Potentially recoverable energy

Previous results emphasized that the applied nitrogen limitation levels may impact both TAG and carbohydrates productivities in a different manner in the microalgae cells. At some levels of limitation, there will be more production of carbohydrates than TAG, or *vice versa*. This could impact the amount of biofuel energy that may be obtained. For this reason, it is here discussed a theoretical analysis on the energy potentially recovered (E_P) from the two previous strains cultivated in N-limited conditions. This analysis is based on the equation 2.3, using the values presented in Table 2.3.

The results presented in Figure 2.6 shows the impact of the obtained TAG and carbohydrate productivities applied to a theoretical biofuel process in terms of global energy valorization. *Nannochloropsis gaditana* achieved a maximal value of energy for BioDiesel and BioEthanol of 67.8 and 18.7 J/m²·d respectively at the 56%NO₃ limitation level. Therefore, the corresponding total amount of recoverable energy E_P was 86.6 J/m²·d. To note that the E_P values for *N. gaditana* have not considered the changing disruption rates presented in Table 2.2.

For comparison, from *P. kessleri* [Kandilian *et al.*, 2019] the maximal amount of potentially recoverable energy E_P was 128 J/m²·d at the 46%NO₃ limitation level, where 47 J/m²·d was accounted by the energy obtained from BioEthanol and 81 J/m²·d by BioDiesel. It can be noticed that even if the carbohydrate productivity in *P. kessleri* at 56%NO₃ was almost twice the value of *N. gaditana* in the same limitation level, the total amount of recoverable energy from *N. gaditana* at the same level is higher because of the larger contribution from BioDiesel energy (heat of combustion of 40.4 MJ/kg) due to the also larger TAG content.

In summary, *Nannochloropsis gaditana* did not show a large productivity on carbohydrates as *Parachlorella kessleri*. The latter, has a larger potential if targeting a double biofuel valorisation (BioDiesel and BioEthanol) where more energy may be obtained for the same amount of biomass produced (due to the large accumulation of both carbohydrates and TAG); meanwhile, *N. gaditana* is interesting regarding the single BioDiesel production only. The present also show that the only option to increase the recoverable energy of *N. gaditana* seems to be by the optimization of the TAG productivity. A complete study on the optimization of both TAG production and recovery, and the related processes and variables in the BioDiesel production, are needed to really take advantage of the potential of *N. gaditana* towards the microalgal biofuel production.

2.4 Conclusions

The present study has shown the effect of nitrogen limitation on the physiology of *Nannochloropsis gaditana*. During day-night cycles, *N. gaditana* did not show preferences or a significant TAG or carbohydrate consumption during the night period. This stability could be beneficial in outdoors cultivation. Under continuous light and N-limited conditions, the highest carbohydrates and TAG productivities of *N. gaditana* accomplished 3.41 and $2.19 \cdot 10^{-3}$ kg/m²·d respectively for the 56%_{NO₃} limitation in continuous mode (PFD 250 μmol/m²·s). The disruption rate τ_D of *N. gaditana* decreased significantly in around 77% from non-limited conditions to the lowest limitation level. This trend may compromise the final recovery of metabolites. Simultaneously, the same analysis was applied on information available in literature for *Parachlorella kessleri*. Results showed that under moderate limitations levels, *P. kessleri* produce larger amounts of energy reserves which should be easier to be recovered because of the high cell disruption rate. This, combined with large production of carbohydrates, is promising for the dual valorization of both BioDiesel and BioEthanol. However, *N. gaditana* remains a promising producer of energy metabolites especially when targeting BioDiesel production using seawater.

Chapter 3

Optimization of continuous TAG production in solar nitrogen limited culture by *Nannochloropsis gaditana*

Abstract

Both nitrogen growth limitation and changing conditions of solar cultures are known to affect TAG production in microalgae. This work investigates the optimization of TAG production using a continuous nitrogen limited culture of *Nannochloropsis gaditana* in simulated day-night cycles. Such optimization is not straightforward because of the time-changing physiological state taking place in the process. Nitrogen source was supplied in a single pulse at the beginning of light period meanwhile bulk medium was supplied separately at slow but constant dilution rate of 0.005 h^{-1} . Because of the evolution of the cell fragility during culture conditions, this protocol optimization was conducted using the concept of released TAG, which represents how much of TAG production is actually recovered in downstream stages, *ie.* after cell disruption. Maximal released TAG was calculated at $0.3 \cdot 10^{-3} \text{ kg/m}^2 \cdot \text{d}$. This value is obtained based on the changes in cell disruption rate and TAG production/consumption observed under day-night cycles. Algeenan were considered to be responsible of changes in mechanical resistance during the night. An optimal harvesting time based on maximal released TAG has been suggested after 4 hr of night period.

3.1 Introduction

Actual climate change crisis and the increasing demand of energy for an always-growing society are the main reasons to keep researching on biofuels [Cavicchioli *et al.*, 2019, WMO, 2019, Zhu *et al.*, 2017]. Among these fuels, biodiesel produced from microalgae has been speculated to almost replace oil-based fuels in a near future only if better politics and technologies are implemented to improve the economics and manufacturing of biodiesel production [Baudry *et al.*, 2017, Lee, 2011]. Large scale production processes require the use of solar energy in outdoors cultivation in order to produce the triacylglycerol (TAG) molecules to be later recovered and converted into biodiesel during the downstream process. The use of photobioreactors (PBR) under day-night cycles (DNc) combined with the use of nitrogen limited/deplete cultures, appears as a good strategy for conducting TAG accumulation and reducing energy consumption by using sunlight [Chisti, 2007, Rodolfi *et al.*, 2009, San Pedro *et al.*, 2013, 2014]

Many microalgae species have been studied for biodiesel application [Mutanda *et al.*, 2011, Taleb *et al.*, 2015] but among them, *Nannochloropsis* species and particularly *Nannochloropsis gaditana* have been observed as promising TAG producer [Bouillaud *et al.*, 2019, Lubian, 1982, Matos *et al.*, 2017, Mitra *et al.*, 2015].

During outdoor cultivation several culture conditions are changing, which are known to induce metabolic responses in the cell during day and night time. Khalid *et al.* [2019] showed that light intensity and photoperiods are significant factors in the nutrient uptake rate in *Chlorella sorokiniana*. Similarly, Kandilian *et al.* [2014] showed that large accumulation of Total Fatty Acids (TFA) and TAG in *N. oculata* are strongly dependent to the photon absorption rate, not only nitrogen depletion. These results bring on the existence of an optimal photon absorption rate dependent on biomass and pigment concentration, where microalgae can effectively use light for accumulate larger amounts of TFA-TAG content. High values of light and temperature can also inhibit microalgal growth despite higher TAG accumulation [Alboresi *et al.*, 2016, Figueroa *et al.*, 1997]. Besides, TAG and biomass losses, as consequence of respiration under the night period, can reduce TAG final productivity [Bonfond *et al.*, 2016, Edmundson and Huesemann, 2015, Grobbelaar and Soeder, 1985, Lacour *et al.*, 2012, Richmond, 1996].

Initial levels of NO_3^- concentrations causes different biomass productivity with also different TAG content in *Nannochloropsis* [Taleb *et al.*, 2015] and in other species [Kandilian *et al.*, 2019]. In addition, different initial NO_3^- concentrations can trigger not only TAG accumulation but also different metabolite responses [Alboresi *et al.*, 2016, Dortch, 1982, Van Vooren *et al.*, 2012]. Thereunder Simionato *et al.* [2013] and Janssen *et al.* [2019a] revealed the reorganization of membranes during nitrogen depletion into lipids, and elucidate the *de novo* synthesis in *N. gaditana*.

Beside that, some microalgae species present some issues related to metabolite extraction with

are linked to cell wall resistance [Safi *et al.*, 2013]. Especially, *N. gaditana* has been described as particularly resistant to TAG wet-extraction process in biodiesel production when submitted to nitrogen depletion cultivation. This can be observed through the decrease of cell disruption rate when cells are nitrogen depleted [Angles *et al.*, 2017, Scholz *et al.*, 2014]. Alginate presence in *N. gaditana* could explain this. *Nannochloropsis* algaenan comprises long-chain aliphatic hydrocarbons linked with up to three ether bonds mostly presented in outer cell wall [Gelin *et al.*, 1999, Scholz *et al.*, 2014]. In some microalgae, some of these molecules can be composed by a trilaminar structure up to C₈₀ long fatty acid chains [Allard *et al.*, 2002, Dunker and Wilhelm, 2018, Kodner *et al.*, 2009]. This compound could protect microalgae against fungal parasitism, desiccation or even high concentration of detergents [Allard *et al.*, 2002, Scholz *et al.*, 2014]. However, algaenan are very difficult to be extracted or quantified due to the nonhydrolyzable nature of these biomacromolecules [Kodner *et al.*, 2009, Zhang and Volkman, 2017].

Nowadays, the simplest approach to produce TAG molecules using microalgae is by coupling two stages of culture in continuous light: one culture in optimal growing conditions followed by a batch culture in nitrogen depletion. Van Vooren *et al.* [2012] used a continuous culture of *Nannochloropsis oculata* for the biomass production stage and then two possible strategies of starvation (*ie.* sudden and progressive starvation) in batch mode for the second one. This method accomplished a TAG productivity up to 0.0036 and 0.0028 kg/m²·d for the sudden and progressive batch starvation respectively. Semi-continuous culture mode can be used as well for the biomass production stage as showed by Taleb *et al.* [2015]. During a semi-continuous cultures a part of culture volume is replaced with fresh media, enabling to establish the periodic cycles of growth and harvest. In the mentioned study, after the semi-continuous production stage, the collected biomass was washed and re-cultivated in a second nitrogen-free batch (sudden starvation) to induce TAG accumulation. Under this system *N. gaditana* accounts around 0.013 kg/m³·d volumetric TAG productivity (surface TAG productivity 1.63 kg/m²·d).

High TAG productivity under two-stages culture systems is reached because biomass production and lipid accumulation are uncoupled one from each other, which allow to profit of the maximal cell growth in the first stage, and then starve those cells in the second one to trigger the TAG accumulation. However, such a protocol involves large surfaces, as two culture systems are needed for a given production.

Parallel to the two-stages approach, it seems plausible to produce TAG molecules using a single operation, either by using batch or semi-continuous mode [Benvenuti *et al.*, 2016a]. Benvenuti *et al.* [2016b] simulated how single batches can beat semi-continuous system for TAG production using *Nannochloropsis* sp. These results are argued on the limited photosynthetic efficiency at the beginning of each new replenishment during semi-continuous operation, which decreases cell growth potential for the next cycle. Therefore, the significant TAG productivity by *N. gaditana* in

a batch mode could be achieved by a good balance between the *de novo* synthesis of fatty acids and a controlled diversion of the preexisting membrane lipids leaving almost intact those in the photosynthetic apparatus. This mechanisms may result into a yet effective light absorption, which is sufficient to sustain for both lipid accumulation and cell growth even during nitrogen starvation [Simionato *et al.*, 2013].

Continuous production under day-night cycles, was investigated by Bonnefond *et al.* [2016]. A culture of *Dunaliella salina* was operated in a classical turbidostat mode, with the only variant that dilution rate was manually adjusted when necessary to maintain a constant daily cell concentration. This approach allowed to obtain daily and repetitive variations, very similar to a steady state in a classical continuous mode. As expected, TAG reserves were consumed in the dark period (when there is no source of energy), and renewed during light period.

If continuous TAG-rich biomass production is intended during day-night cycles (DNc), three factors are directly related: light, nitrogen supply/uptake and harvesting frequency.

In continuous mode, biomass produced during light period (*ie.* day), should be equal to the amount of harvested and consumed biomass during night period (*ie.* night). Which implies that, in order to obtain a steady state for continuous harvesting under DNc, dilution rate D , must be a) small enough to allow cell growth during day period and b) not too large to wash out the culture when is combined with night biomass losses during night period.

Establishing such protocol during nitrogen limitation is not straightforward: the specific growth rate will be influenced by nitrogen supply/uptake and time-varying light absorption. Both will be related to the nitrogen source availability because of the decrease in pigment concentration when cell is exposed to nitrogen limitation [Kandilian *et al.*, 2014, 2019]

This research is lead by the interest in proposing a nitrogen limited continuous culture protocol under DNc for optimized continuous TAG production by *Nannochloropsis gaditana*. Multiple aspects are expected to change during DNc, which could impact biomass growth and concentration, TAG content, cell wall composition and nitrogen uptake. In the same way, the present work aims to elucidate if these variations could be exploitable for the TAG recovery process.

The proposed approach is divided in two main experimental sets: (I) analysis of released TAG (after cell disruption) produced in sudden starvation and under day-night cycles, in order to elucidate if there is an impact of those cycles over cell mechanical resistance, and (II) establishment of a continuous TAG production protocol in nitrogen-limited culture conditions and during day-night cycles, taking advantage of the time-varying physiological changes identified in the DNc study, for optimization of TAG production and recovery in wet-extraction process.

3.2 Materials and Methods

3.2.1 Culture medium

Nannochloropsis gaditana CCMP527 (NCMA, USA) was cultivated using Artificial Sea Water (ASW) [Berges *et al.*, 2001] as main medium with CONWAY solution for nutrient enrichment. The former is composed as follow (mM): NaCl, 248; Na₂SO₄, 17.1; KCl, 5.49; H₃BO₃, 0.259; NaF, 0.045; MgCl₂·6H₂O, 32.24; CaCl₂·2H₂O, 0.626; KBr, 0.497; SrCl₂·6H₂O, 0.056; NaHCO₃, 1.42. Originally CONWAY solution uses 10.6 mM of NaNO₃ as nitrogen source.

For prepared media with different NO₃⁻ concentrations, CONWAY solution is still used but the relative amount of NaNO₃ was varied. Hereafter, these values will be so expressed as percentage of the original formulation (100%_{NO₃} for 10.6 mM NaNO₃) as a representation of the depletion level. For example, depending on the experiment, systems were prepared either with media solutions at 200%, 100%, 56%, 46%, 29%, 0%_{NO₃} (21.2, 10.6, 5.94, 4.88, 3.07 and 0 mM of NO₃⁻ respectively). As well, the culture at 200%_{NO₃} is referred as *replete* (it was considered for assuring optimal growth by avoiding nitrogen limitation). Likewise, cultures mentioned as *depleted* had no nitrogen sources added (0%_{NO₃}).

For punctual addition of NO₃⁻, an independent solution at 126 mM of NaNO₃ was prepared and added separately of the nitrogen culture media.

3.2.2 Outdoor Reactors

Outdoors studies were carried out in two identical 170 L (5 cm thick) flat-panel airlift PBRs (Subitec, Germany; Fig. 3.1a) installed at Saint-Nazaire, France (47°15'06.5"N, 2°15'34.5"W). Cultures were conducted during late summer 2018. Instrumentation for temperature and pH were shared between both reactors. The pH was regulated by manual 98% CO₂ (gas) injections. Temperature was controlled to not overpass 32° C using water sprays on the outer PBR surface. Solar PAR irradiation, pH and internal temperature were monitored and plotted in figure 3.2a. After sterilization, these systems were identified as replete or depleted reactors and filled with the corresponding media. Then, both reactors were inoculated (10%v/v) at 0.2 kg/m³ using *N. gaditana* seed culture in exponential growth phase. Next, systems were run in batch mode during 11 days.

3.2.3 Indoor Reactor

For the study on depleted culture in simulated DNc, a 170 L (5 cm thick) flat-panel airlift PBR (HECTOR, Fig. 3.1b) was operated in batch mode. The pH was automatically regulated at 8 by automatic 98% CO₂(gas) injection. The temperature of the culture was regulated to 23°C. More details on the PBR are available in Pruvost *et al.* [2011b].

Indoor experiments on the establishment of the continuous TAG production in nitrogen depletion

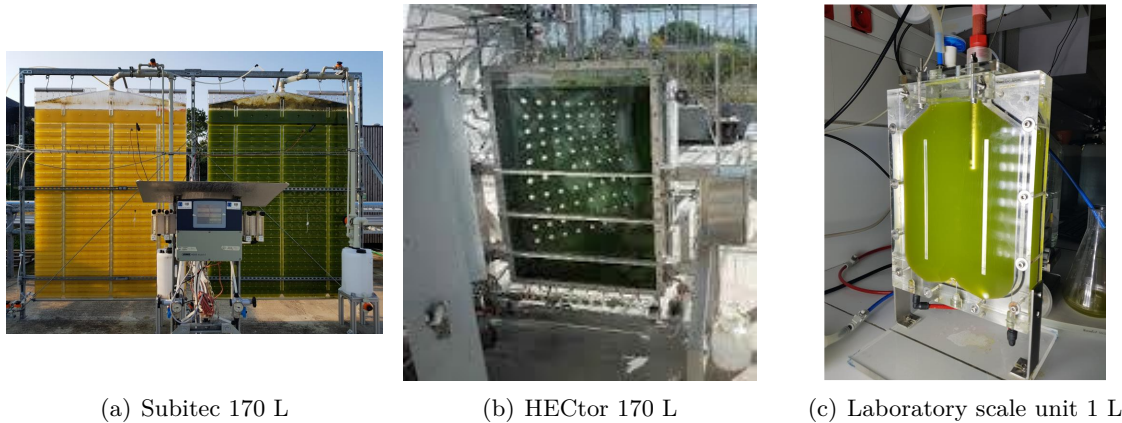


Figure 3.1: Flat-panel airlift PBRs systems used for outdoor (a) and indoor (b,c) cultivations

and DNc, were performed in 1 L (3 cm thick) flat-panel airlift PBRs (Fig. 3.1c). More information is detailed by Pruvost *et al.* [2009]. Temperature was controlled convectively at 23° C with the temperature of the room and pH was set at 8 using automatic 98% CO₂ (gaz) injections. After sterilization, PBR was either filled with the corresponding depleted medium for batch culture or adapted to be operated in continuous mode using peristaltic pump for feeding (Reglo ICC, Ismatec, Germany).

3.2.4 Day-night cycles

3.2.4.1 Actual solar cycles

Solar irradiation data was obtained from a weather station (Vantage Pro2 Plus, Davis, US) in W/m^2 . Values were multiplied by 4.57 factor and then converted into $\mu\text{mol}/m^2\cdot\text{s}$ according to Thimijan and Heins [1983] to obtain the photon flux density (PFD). Next, values were adjusted considering that just 42.9% of solar energy is photosynthetically active radiation, PAR. Hence, all irradiation values are reported here as PFD for PAR, (PFD_{PAR} , $\mu\text{mol}/m^2\cdot\text{s}$).

Averaged solar PFD of $111.5 \mu\text{mol}/m^2\cdot\text{s}$ (night included) was registered for the 11 days of outdoors experimentation. Day-to-Night ratio was 15:9 h. The lowest PFD ($370 \mu\text{mol}/m^2\cdot\text{s}$) was obtained after 48 h and 240 h, and the highest ($\approx 500 \mu\text{mol}/m^2\cdot\text{s}$) at around 72 h, 96 h and 144 h (Fig. 3.2).

3.2.4.2 Simulated Cycles

Solar cycles simulations for the indoor PBR system were emitted by LED PAR-light panel. Calibration between light received by the PBR and LED power supply was performed using a quantum sensor for the PAR spectrum (LI-190-SA sensor with LI-250-A meter, LI-COR, Germany) placed in the inner side of the PBR. Once calibration was established, day-night cycles (DNc) were programmed (Arduino, US) by varying the supplied light to the culture every 15 min in a 24 h loop.

Values were obtained from a meteorological database (Meteonorm, Switzerland) for the averaged PFD_{PAR} in an entire year at Saint-Nazaire, France. The final DNc averaged $269 \mu\text{mol}/\text{m}^2 \cdot \text{s}$, a maximum at noon of $847 \mu\text{mol}/\text{m}^2 \cdot \text{s}$ and Day-to-Night ratio of 16:8 h. For convenience, DNc started at 00:00 h with the first light and ended at 23:59 with the last hour of the night period.

3.2.5 Experimental layout

The experiments performed during this work can be detailed as follows:

I. *Study of released TAG in batch culture during DNc:*

- (a) *Depleted culture in actual DNc.* The two outdoor PBR were filled with replete media or depleted media respectively. Replete media culture was used as control. Both cultures were run in batch mode during 11 days, which is the time when the depleted reactor reached the maximal biomass concentration. During the first three days of it, biomass concentration, cell disruption rate and stress index were analyzed.
- (b) *Depleted culture in simulated DNc.* Indoor 170 L PBR was filled with depleted media. Reactor was also run in batch mode during 11 days (and monitored for biomass concentration, cell disruption rate and pigment concentration. Culture entered in stationary phase after the fifth day. This data was used to calculate productivity and released TAG.

II. *Study of released TAG during continuous N-limited culture and simulated DNc:*

The 1L indoor PBR in DNc simulation was run in continuous mode. It was only changed the way how nitrate was added into the PBR.

- (c) *Minimal Nitrate (NO_3^-) concentration for sustain biomass growth and TAG accumulation.* During this experiment continuous reactors were arranged at different nitrogen concentration in the feeding media (N_0) with multiple dilution rates D each, as follows: for $56\%_{\text{NO}_3}$: 0.04, 0.03, 0.02, 0.01 and 0.005 h^{-1} ; for $46\%_{\text{NO}_3}$: 0.013, 0.01 and 0.007 h^{-1} ; and for $29\%_{\text{NO}_3}$: 0.013, 0.01, 0.007 and 0.005 h^{-1} . For every set of experiments, biomass concentration and residual NO_3^- were monitored. Eventually, biomass concentration, TFA/TAG and pigment content were measured once the periodic regime was obtained. These values were used for calculations on nitrate daily consumption and TAG and biomass productivities.
- (d) *TAG production under punctual nitrate addition.* Once dilution rate and daily nitrate consumption were established, it was opted to turn nitrate continuous addition into a punctual addition. For that, as well as in continuous addition, ASW + CONWAY media was supplied but this time without nitrate source. An individual NaNO_3 solution was prepared and added separately. Bulk media was constantly supplied at $0.078 \text{ mL}/\text{min}$

and nitrate at the same ratio but only during 34 min just before starting a new day period (*ie.* started at 23:26 h of the previous night). But inlet rates were adjusted to match the chosen dilution rate, issued from the previous section ($D= 0.005 \text{ h}^{-1}$). The latter was chosen based on the amount of nitrate needed to sustain cell growth everyday and the limits of pumping device. Residual nitrogen, biomass concentration, cell disruption rate and TAG content were followed.

Note that the term *periodic regime* considers the repetitive and unvaried changes in cell physiology, occurring every day-night cycle during a continuous PBR culture mode. It was considered after measures of biomass concentration, nitrogen uptake or TFA/TAG content remained unvaried at each sunset- sunrise cycle.

3.2.6 Cell disruption rate

A sample of 30 mL at biomass concentration of around $1\text{kg}/\text{m}^3$ (adjusted with phosphate buffer saline (PBS)) was passed through a high pressure homogenization device (TS5, Constant Systems Limited, UK) at 1750 bar. Cells number before and after disruption were counted via image analysis. For each sample, 40 pictures were taken from a Malassez chamber using an optical microscope coupled to camera (Axio MRC Cam at Axio Scope A1 microscope, Carl Zeiss, Germany). Samples were prepared based on the protocol by Zinkoné *et al.* [2018]. Image pretreatment software (ImageJ v.1.52o, NIH, USA) allowed to calculate cell surfaces for each picture based on distance to pixel proportion. This information was analyzed with a MATLAB (MathWorks, US) algorithm to obtain cells number and statistical information of the sample. Microalgal cells disruption rate (τ_D) is reported as the complementary proportion of cells counted after disruption relative to those counted before.

3.2.7 Dry Weight measures

Samples of 10 mL were filtered using glass-fiber filters ($0.45 \mu\text{m}$, Whatman GF/F, GE, US) previously weighed. Filters were then washed using 1.19 M NH_4HCO_2 and MiliQ water. Filters with retained biomass were dried at $103 \text{ }^\circ\text{C}$ during 1 hr (no more time needed to achieve weight stabilization) and then weighed. Values reported here as biomass concentration, X , correspond to the mean values for a triplicate assay. These were calculated base on the weight difference between dry-biomass and clean filters per unit of culture volume used. Additionally, biomass volumetric productivity, P_X and areal productivity, S_X were calculated according to Pruvost *et al.* [2011a] and given in Chapter 1 (Table 1.3).

3.2.8 Stress Index

For comparison reasons among the different physiological states, stress index was measured based on the pigment content quantification developed by Ritchie [2006] and Strickland and Parsons [1968]. Stress index assess the carotenoids to chlorophyll ratio as an indicator of nitrogen depletion. It has been also found to have correlation with the carbon to nitrogen ratio content in the cell [Heath *et al.*, 1990].

First, samples of 0.5 mL were collected and centrifuged at 6,000 RFC, 4 °C during 10 min. Supernatant was disposed and replaced with 1.5 mL of methanol anhydrous 99.8%. Samples were then sonicated during 1 min and incubated in the dark during 50 min at 45 °C. Intermediately after, samples were again centrifuged and light absorption of the supernatant was measured (V-730, Jasco, US). The stress index, the ratio 480/662 nm minus the background absorption at 750 nm, was then calculated.

3.2.9 Total Fatty Acid/Triacylglycerol content measurement

Total fatty acid (TFA) and triacylglycerol (TAG) cell content were measured using the whole cell method and analysis published by Van Vooren *et al.* [2012]. Shortly, samples were centrifuged 10 min at 3,600 RFC and 4 °C and then freeze-dried for posterior batch analysis at the end of each experimental run. At that time, dried biomass was mixed with 6 mL of chloroform/methanol 2:1 v/v (Fisher Sci, US) and 0.01% w/w of butylated hydroxytoluene. Then, it was incubated in agitation during 6 h and 25 °C. Extracts were recovered and analyzed for: TFA by gas chromatography with flame ionization detector, GC-FID (Thermo Fisher Sci, US) and TAG by high-performance thin-layer chromatography, HPTLC (CAMAG, Switzerland). TFA or TAG measures are so expressed as a percentage of grams relative to algal biomass treated, TFA%_X or TAG%_X. Then, it was also possible to calculate volumetric and areal productivities for TAG (P_{TAG} , S_{TAG}) according to Pruvost *et al.* [2011a] and Chapter 1 (Table 1.3). Additionally, released TAG was expressed either in kg/m³·d or kg/m²·d, as the product of TAG productivity (in kg/m³·d or kg/m²·d) and the cell disruption rate ($P_{TAG} \cdot \tau_D$).

3.2.10 Nitrate concentration measurement

In order to measure nitrate (NO₃⁻) concentration, it was followed the protocol proposed in the Standard Methods for the Examination of Water and Wastewater document [American Public Health Association, 1999]. It is based on the ultraviolet light absorbance of NO₃⁻ at 220 nm using silica cells of 1 cm light-path. Organic matter may absorb ultraviolet light at the same wavelength. To prevent this, an additional measurement at 275 nm and previous filtration is required.

As a protocol, 1.5 mL of culture were diluted 20 times using highly purified water and then

centrifuged during 10 min at 3,600 RFC and 4 °C. Then, supernatant was filtered using 0.2 μm acetate cellulose filter (Minisart, Sartorius, Germany). Immediately, ultraviolet absorbance (V-730, Jasco, US) was measured at the established wavelengths. Corrected sample absorbances were calculated following the relation $ABS_{220nm} - 2 \cdot ABS_{275nm}$. Values were then transposed into mM with a standard curve ($r^2=0.999$) which used 1:20 diluted ASW depleted media as blank and individual additions of NaNO_3 in 0 - 200 μM range.

Values shown as N_t are for NO_3^- concentration in the culture for a given sampling time.

3.3 Results and Discussion

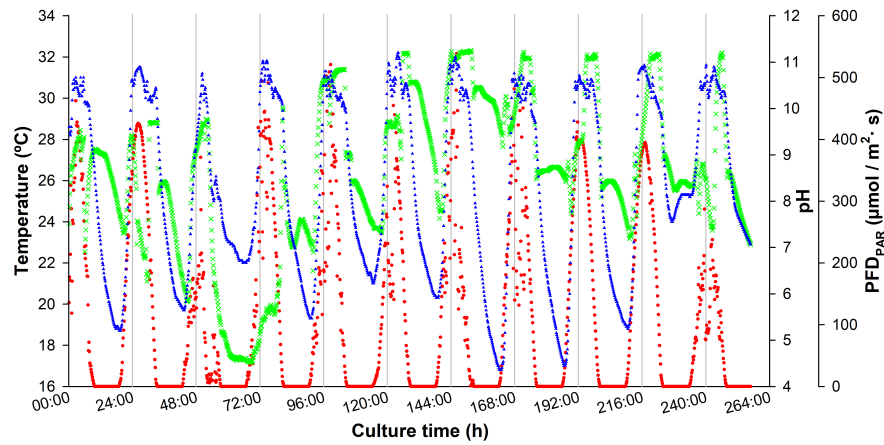
3.3.1 Released TAG in batch mode and day-night cycles

3.3.1.1 Depleted batch culture at actual Day-Night cycles

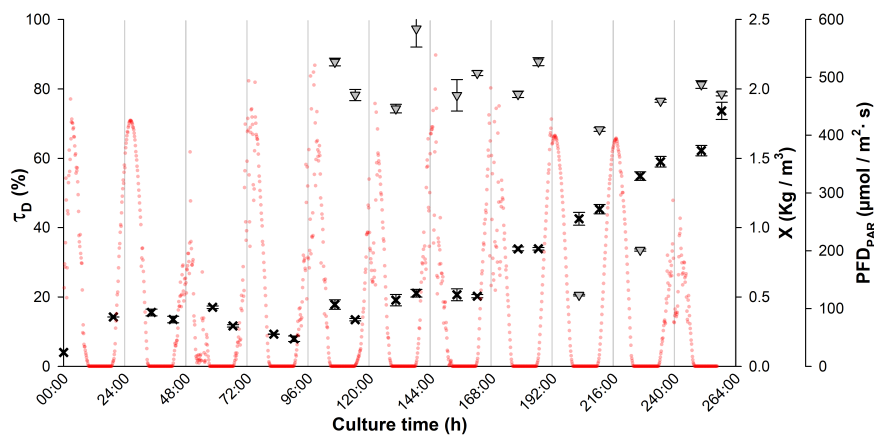
Replete culture, as a control system, allowed to assess the maximal cell growth attended during actual outdoors conditions (Fig. 3.2). For comparison, after batch culture for 11 days, depleted and replete reactors reached 0.5 kg/m^3 and 1.8 kg/m^3 (SE=0.02 and 0.06) of biomass concentration respectively. Exponential growth started at 168 hr for both cultures. The increase of biomass concentration for the depleted culture (Fig. 3.2c) was of 0.3 kg/m^3 , meanwhile replete culture increased to 1.6 kg/m^3 . Besides, stress index (which is also related with the carbon/nitrogen ratio in cell and it is independent of nitrate in the medium) for depleted and replete cultures reached 1.83 and 0.51 at the end of the culture respectively, indicating a marked effect of nitrogen depletion on pigment composition for the N-depleted culture..

As the depleted culture presented barely-unvarying biomass concentration during the last four days of stationary phase, disruption rate was measured at this time to avoid as much as possible the impact of biomass concentration in the disruption process. During these last days of the stationary phase, significant differences were observed in disruption rate values not only between physiological states (replete and depleted cultures), but also during the DnC itself. In one side, replete culture exhibited a rapid increase in disruption rate from 21% to 68% and from 34% to 77% (SE \approx 2%, n=3) during the night periods at 202 hr and 226 hr respectively (Fig. 3.2b). It corresponded to an averaged daily increase of 45% and 13% for replete and depleted cultures respectively. These results then confirm those by Angles *et al.* [2017], about changes in mechanical resistance with the physiological state, but here also showing large variations during day-night cycles.

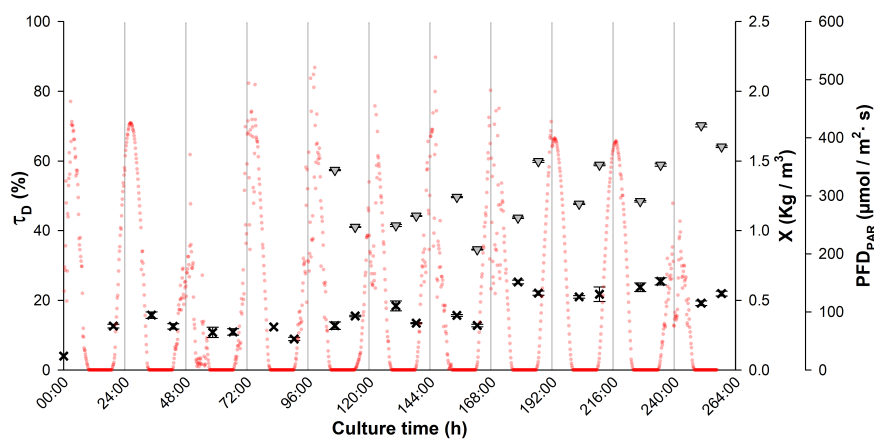
In the other side, depleted culture were also found to increase disruption rate from 44% to 60%, 48% to 59% and 48% to 59% (SE \approx 2%, n=3) at 178 hr, 202 hr and 226 hr night periods respectively (Fig. 3.2c). By comparing the averaged variations of 45.37% for replete culture and 12.6% for depleted culture, it is possible to confirm the results of Angles *et al.* [2017] in continuous light (150 $\mu\text{mol}/\text{m}^2 \cdot \text{s}$) about changes in mechanical resistance due to physiological state but now also during



(a) Outdoor culture conditions



(b) Replete culture



(c) Depleted culture

Figure 3.2: Culture conditions, biomass concentration and disruption rate τ_D under outdoor conditions for Replete and Depleted cultures. Plots for a) Daily solar PFD (red dot), pH (green X) and culture temperature (blue triangle). Also, cell disruption rate (grey triangles) and biomass concentration (black X) for b) Replete and c) Depleted culture. Error bars for SE, $n=3$.

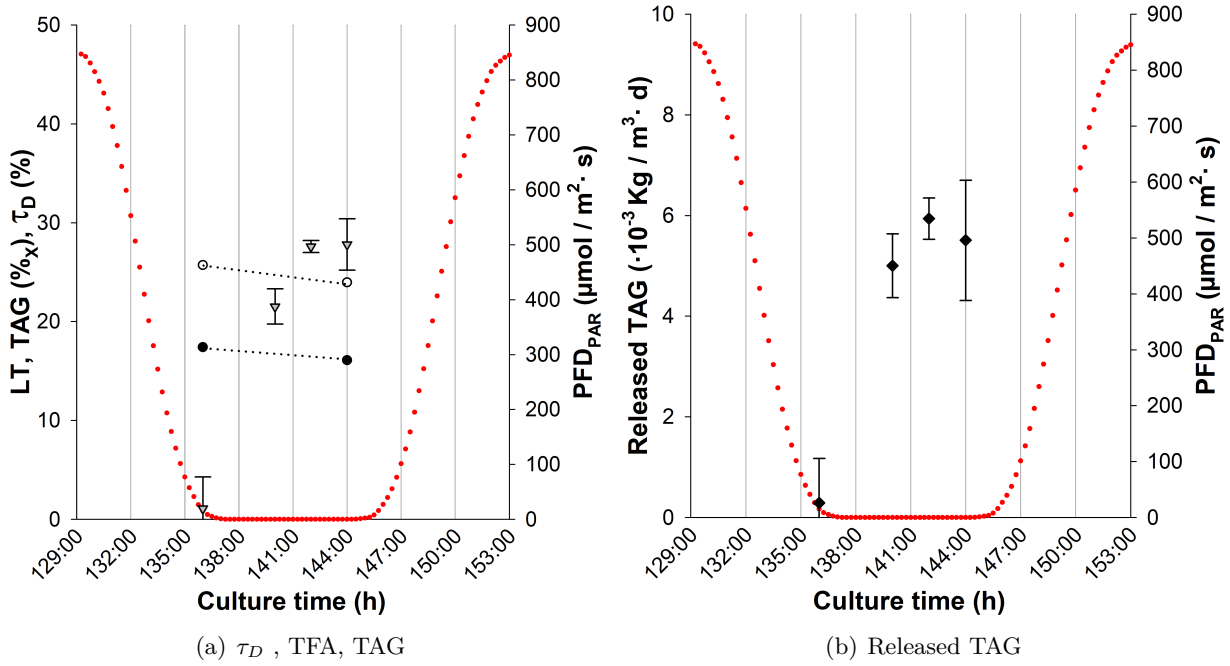


Figure 3.3: Released TAG under day-night simulated cycles in batch culture. The time range stands as a sample of the periodic regime. Subfigure a) shows TFA, TAG content as well as τ_D . Grey triangles stands for τ_D , white circles for TFA content and black circles for TAG content. Subfigure b) presents released TAG value in black diamonds. Error bars for SE (n=3).

DNc.

It has been demonstrated that besides nutrient limitation, also light, pH and temperature have an impact on cellular growth and lipid production [Bonfond *et al.*, 2016, Breuer *et al.*, 2013, Grobbelaar and Soeder, 1985, Kandilian *et al.*, 2019, Lacour *et al.*, 2012, Renaud *et al.*, 1995]. These factors are constantly varying during DNc (Fig. 3.2a) and bring out physiological changes. The presented results suggest that they could also impact mechanical resistance of the cells. These characteristics of the biomass during the production stage are very likely to impact the recovery of lipids in the following downstream process, unraveling the existence of an optimal harvesting point under actual DNc.

3.3.1.2 Depleted batch culture at simulated Day/Night cycles

In order to estimate the optimal harvesting time during DNc regimes, the time-varying mechanical resistance was investigated in well-controlled DNc at laboratory scale regarding the release of TAG.

Depleted batch culture under simulated DNc arrived to stationary phase after 120 hr. The last three night periods (from 112 to 168 hr) were considered as stable cycles since biomass concentration was kept everyday between 0.9 - 0.8 kg/m^3 (SE=0.04, n=3). In the same way, during the night period TFA, TAG and τ_D also varied (Fig. 3.3a). As consequence, the released TAG were not constant (Fig. 3.3b).

Fig. 3.3a shows TFA and TAG were consumed every night from 25 to 23 %X and from 17

to 16 %_X respectively. These consumption values are in accordance with the trends published by several works for different microalga species [Edmundson and Huesemann, 2015, Grobbelaar and Soeder, 1985, Lacour *et al.*, 2012]. TAG volumetric and surface productivities for these consumption ranges, were calculated then in $26 - 19 \cdot 10^{-3} \text{ kg/m}^3 \cdot \text{d}$ (SE 2.2) and $1.3 - 0.9 \cdot 10^{-3} \text{ kg/m}^2 \cdot \text{d}$ (SE 0.1) respectively .

Similar to actual DNc, cell disruption rate τ_D was also found varying in simulated DNc. Cell disruption rate increased from 1.1% at the end of the day, to 27.8% at the end of the night period (Fig. 3.3a). We can note a large variation in the culture obtained in actual outdoor conditions. This could be attributed to the variation of growing parameters, like temperature which was not controlled in the outdoor culture.

It is indeed not expected that microalgae have an unique and stable physiological state during DNc. Beacham *et al.* [2014] revealed that some of the *Nannochloropsis* genus increase the thickness of the cell wall as a physiological response to stress conditions, impacting directly the lipid recovery. In the same manner Scholz *et al.* [2014] have proposed algaenan synthesis to be responsible of cell's mechanical resistance in *Nannochloropsis gaditana*. All of these responses could be affected by light, temperature and nitrate availability.

The change in algaenan could be specially relevant. Scholz *et al.* [2014] indeed analyzed cell wall composition in *N. gaditana*. Cell wall was described as a bilayer structure 75% composed of a cellulosic inner wall covered by an external hydrophobic algaenan layer. In some *Nannochloropsis* species, algaenan are shown to be formed by long monohydroxy fatty acid of C₂₈-C₃₄ long chain [Gelin *et al.*, 1997, 1999, Zhang and Volkman, 2017].

Scholz *et al.* [2014] proposed algaenan of *N. gaditana* to have similar biosynthesis as cutan from some drought-resistant plants. Because of this similarity, it is hypothesized that C₁₈ fatty acid may be derivated into classical C₂₈-C₃₄ algaenan constitutes. To support this, it has been found C₁₈ fatty acids accumulation during media depletion in *N. gaditana* [Janssen *et al.*, 2019b], and also a pyrolysis analysis of *Nannochloropsis oculata* in *log phase* (with confirmed presence of algaenans) showed the presence of C₁₈ fatty acids [Zhang and Volkman, 2017].

It must be recall, that in optimal growing conditions, *Nannochloropsis* species are know to mainly produce C_{16:0}, C_{16:1} and C_{20:5} fatty acids. Then when nitrogen starts to be consumed, these fatty acids species start to accumulate in neutral and polar fractions. Moreover, a new fatty acid C₁₈ long chain was also found to accumulate [Beacham *et al.*, 2014, Janssen *et al.*, 2019b, Navarro López *et al.*, 2015, Taleb *et al.*, 2015, Zhang and Volkman, 2017].

In addition, Janssen *et al.* [2019b] has discovered two interesting mechanism in *N. gaditana* during nitrogen starvation which could also support this hypothesis. Firstly, the verification of the transposition and *de novo* synthesis of some fatty acids between the TAG and PL fractions (mainly Eicosapentanoic acid C_{20:5n-3}, EPA); and secondly, the increase of C₁₈ fatty acids in the polar

lipid fraction (membrane associated). It is interesting to note that the rest of the studied fatty acids seems to be present and then transposed at the onset of starvation but not C₁₈ fatty acid. Contrary, the latter started to be mainly synthesized *de novo* in both TAG and PL fraction only during nitrogen starvation.

The hypothesis on algeenan also can be supported by the presence *in vivo* of some enzyme related with elongation of C₁₈ fatty acids during nitrogen starvation (like polyketide synthases). An increased activity of this enzyme during this period will be determinant in the theory of elongation of C₁₈ into C₂₈-C₃₄ [Gelin *et al.*, 1997]. Some enzymes participating in long chain lipids elongation in *N. gaditana* have been already described by Janssen *et al.* [2020], however there were only confirmed for C_{20:5} fatty acids. For enzymes associated to longer chains metabolism, Scholz *et al.* [2014] has analyzed *in situ* some of them.

However, neither C₁₈ changes nor long chain elongation enzymes have been tested during DNc in the consulted bibliography or the present work. It suggests an interesting departure for future research.

The combined results for TAG consumption and cell disruption changes allow to calculate the released TAG (3.3b). Released TAG represents the TAG molecules that could actually be recovered for further steps during wet-extraction process (or any other process aimed to recover microalgae components). It was estimated by fixing the cell disruption conditions, as presented in Section 3.2.6.

A maximal released TAG value of $5.9 \cdot 10^{-3} \text{ kg/m}^3 \cdot \text{d}$ (SE=0.41, n=3) ($0.3 \cdot 10^{-3} \text{ kg/m}^2 \cdot \text{d}$) was reached at 270 min after the end of the day. In other words, once the day period is ended, cell have not started respiration yet and so the TAG content is maximal. However, not all TAG can be recovered because cells are more resistant to mechanical disruption at this point. Then, by the end of the night, cells are less resistant but they have catabolized already a portion of TAG. This dynamic stand out the optimal harvesting time here found after 4.5 h (270 min) where TAG released was found maximal during DNc. If the biomass is harvested and disrupted at the onset of night, around 90% of the TAG production may be lost, because of a too large mechanical resistance of the cell.

The concept of released TAG, presented by this work as function of variations in mechanical resistance during DNc, is therefore found relevant to optimize the TAG production.

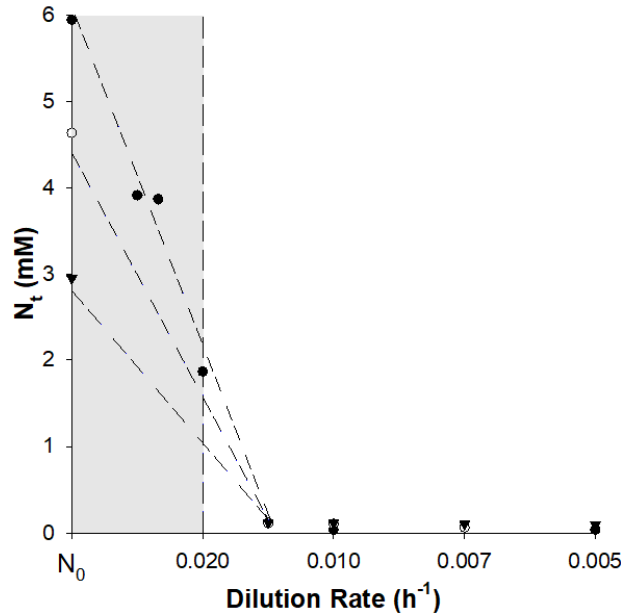


Figure 3.4: Residual NO_3^- concentration at the periodic regimes of multiple dilution rates during simulated day-night cycles. Plots are for three different initial nitrate concentrations at continuous addition: 56% (5.94mM) (black dot), 46% (4.63mM) (white dots) and 29% (2.95mM) (black triangle). Grey zone represents dilutions rates where culture was washed out. (n=1)

3.3.2 Released TAG during continuous N-limited culture and simulated day-night cycles

3.3.2.1 Minimal initial NO_3^- concentration for TAG accumulation

The next part of the study aimed to explore the possibility of setting a culture operated in continuous mode (for continuous production), under nitrogen limitation (for simultaneous TAG accumulation and cell division) and during simulated DNc (for outdoors cultivation).

The first approach tested for the purpose of the present work was to look for the minimal initial nitrate concentration N_0 at the maximal dilution rate that allows to simultaneously accumulate TAG and sustain cell growth without washing out the system during simulated DNc. Figure 3.4 shows the trend of residual nitrogen N_t observed in the periodic regime for three different initial nitrogen concentrations (56% $_{\text{NO}_3}$, 46% $_{\text{NO}_3}$ and 29% $_{\text{NO}_3}$) for 6 different dilution rates. When dilution rate was higher than 0.02 h^{-1} cultures washed out even at higher nitrate concentrations. The rest of cultures, with dilution rate equal or slower than 0.013 h^{-1} , arrived to the periodic regime with residual nitrogen N_t close to zero (about to 0.03 mM for 56% $_{\text{NO}_3}$, 0.11 - 0.06 mM for 46% $_{\text{NO}_3}$ and 0.2 - 0.10 mM for 29% $_{\text{NO}_3}$). These differences are mainly based on the combined effect of dilution rate and the growth rate resulting from each nutrient limitations. When dilution rate is large enough, biomass losses will impose over cell growth (due to large biomass losses through harvesting); but when dilution rate is lower than 0.02 h^{-1} , the growth rate compensates biomass losses (due to both harvesting and night catabolism) and then the culture is able to attain the periodic regime.

Table 3.1: Biomass concentration and TFA and TAG content during a simulated day-night cycles for two dilution rates. Initial NO_3^- concentration was set at 29% (2.95 mM).

D (h^{-1})	Sampling	X	TFA	TAG	Stress
	time	kg/m^3 (SE)	$\%_X$ (SE)	$\%_X$ (SE)	Index
0.005	sunset	2.5 (0.04)	34 (2.3)	33 (3.0)	0.75
	sunrise	2.3 (0.05)	34 (1.6)	30 (1.7)	0.72
0.013	sunset	1.3 (0.04)	25 (1.4)	24 (1.0)	0.68
	sunrise	1.2 (0.05)	23 (0.9)	20 (3.3)	0.61

However, the highest TAG productivities were only found for cultures with initial nitrogen concentration $29\%_{\text{NO}_3}$. For this condition, results for the large (0.013 h^{-1}) and low (0.005 h^{-1}) dilution rates are presented in Table 3.1. These culture reached the periodic regime after 16 days and remained in that regime until the end of the experiment, 15 days latter. The system at 0.013 h^{-1} produced 2.9 and $2.3 \cdot 10^{-3} \text{ kg}/\text{m}^2 \cdot \text{d}$ of TAG surface productivity at sunset and sunrise sampling times respectively. Likewise, the system at 0.005 h^{-1} slightly obtained a higher TAG surface productivity with 3.0 and $2.5 \cdot 10^{-3} \text{ kg}/\text{m}^2 \cdot \text{d}$ for the same sampling times.

Variations on productivity values are consequences of the DNc and the stress caused by different levels of nitrogen depletion in both systems. As a result, cells grow during the day period and consume energy reserves during night period (losing about 3 - $4\%_X$ of TAG). For a comparison of the stress level, it has to be remained the previous experiments for batch outdoor cultures under actual DNc, which reached 1.82 and 0.53 stress index for a depleted and replete cultures respectively. The present cultures (from sunset to sunrise) remained in the range 0.75 - 0.72 for the 0.005 h^{-1} condition, and from 0.68 - 0.61 for 0.013 h^{-1} condition. This comparison emphasizes that the present culture strategy allows an equilibrium of physiological states that lets cells to both divide and accumulate lipids in day-night cycles and continuous mode. Condition at dilution rate of 0.005 h^{-1} obtained the highest productivity because of this compromise, producing 2.5-2.3 kg/m^3 in biomass concentration (biomass surface productivity of 9 - $8.2 \cdot 10^{-3} \text{ kg}/\text{m}^2 \cdot \text{d}$) with high TAG content at 33 - $30\%_X$, compared to its analogous at 0.013 h^{-1} producing only 1.3 - $1.2 \text{ kg}/\text{m}^3$ of biomass concentration with lower TAG content at 24 - $20\%_X$.

Differences in TAG content could also have been due to the time lapse that cells experienced in nitrogen starvation. Figure 3.5 shows a sample of residual nitrogen N_t during DNc. In a 24 h cycle, a minimal N_t value around 0.07 mM is obtained. This could be due to the existence of a basal nitrogen concentration for allowing cell growth, or the minimal detection range of the analytic method. Whatever the reason, four daily phases can be observed. These phases were found to be repeated and unvaried from the beginning of the periodic regime until the end of the culture (15 days):

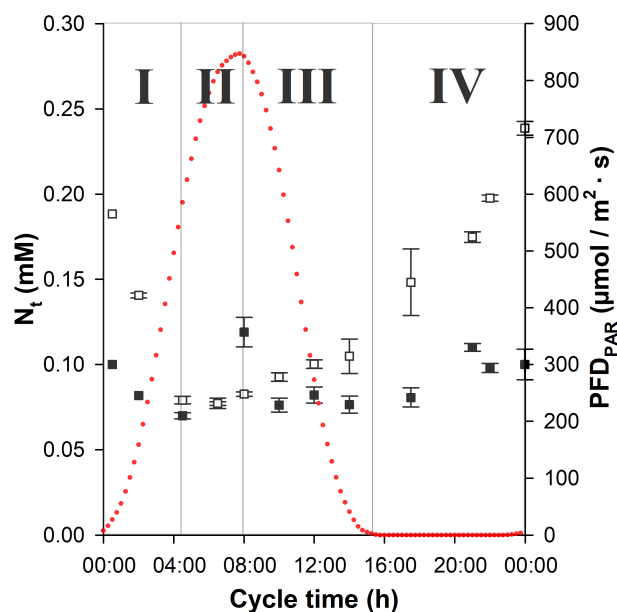


Figure 3.5: Residual NO_3^- concentration at the periodic regime during DNc simulated cycles for two dilution rates. Plots are for 0.005 h^{-1} (black squares) and 0.013 h^{-1} (white squares) dilutions rates. Initial NO_3^- concentration was set at 29% (2.95 mM). Red dots represent a simulated day-night cycle. Error bars for SE, $n=3$

Phase I. *Fast nitrogen consumption.* Beginning at a maximal nitrogen concentration and with a rising source of light (onset of the day), microalgae start the metabolic activity. As a result, nitrogen concentration decreases while biomass increase.

Phase II. *Late nitrogen consumption.* Residual nitrogen arrived to a minimal value after 4 hr of enlightening (midday). For achieving nitrogen depletion cells may metabolize at a maximal rate or very close to it.

Phase III. *Early nitrogen accumulation.* As consequence of a reduced photosynthetic activity after the peak of light (photosaturation), metabolic activity is slower and nitrogen starts to concentrate again due to the constant supply, but it is still consumed (end of the day).

Phase IV. *Full nitrogen accumulation.* At this point, with no longer light source to activate growth metabolism, photosynthetic growth stops, respiration is induced and nitrogen starts to accumulate almost linearly due to the constant feeding (night period).

Likewise, Figure 3.5 shows how most of nitrogen consumption occurs during the light period. Besides, all along the 24 h cycle, cultures were found to consume 0.33 mM (28.29 mg) and 0.84 mM (71.73 mg) of NaNO_3 at 0.005 and 0.013 h^{-1} respectively.

3.3.2.2 TAG production under punctual NO_3^- addition

Based on the observations of nitrate consumption phases, the previous operative parameters were modified in a further optimization. The objective was to still add NaNO_3 but also to avoid its accumulation during the cycle, for letting cells to starve more than in the previous experiments. In order to accomplish this objective, the known amount of NaNO_3 consumed in 24 h, was added separately from the bulk medium, in a single pulse and just in the onset of day period (*ie.* at the begin of the phase I: fast consumption stage). This was applied once the stability of the PBR under DnC, 29% $_{\text{NO}_3}$ limitation and continuous mode at 0.005 h^{-1} was achieved.

Janssen *et al.* [2018] run a similar protocol but for a *N. gaditana* batch culture. Punctual doses of KNO_3^- , (0.23 M) were added at the beginning of each night during stationary growth phase. For night period 498.5 and 674.3 mg of the solution were added under the hypothesis of helping photosystem recovery which had been compromised due to lipid transposition. Contrary, the present study adds NaNO_3 based on the demand of nitrogen previously determined with the aim to be entirely consumed before sunset.

This culture protocol took 28 days to reach the periodic regime and continued like this for 29 days more, emphasizing a stable regime despite the stress conditions here applied. Similarly to previous experiments, once in this state, the culture measurements prevailed unvaried and cycling until the end of the experiment. Those repetitive cycles are discussed below.

Figure 3.6a shows the residual nitrogen N_t during 24 h of monitoring. As expected, it took 4 hours for microalgae culture to consume the supplied nitrogen. It was similar to the same phase I (from 00:00 to 04:00 h) as described in the previous section. Then, as there is no more continuous nitrogen supply, N_t remains at a minimal level of 0.04 mM.

Biomass growth is shown in Figure 3.6b. It seems to also confirm the previous phases under DnC. It can be distinguished a like-lag phase (Phase I, from 00:00 to 04:00 h) where cells might repair photosystems and used the consumed nitrogen source to presumably synthesize new proteins [Janssen *et al.*, 2018]. Then, an exponential phase, Phase II (04:00 to 10:00 h) can be observed by the rapid increase of biomass concentration from 1.7 to 2.1 kg/m^3 . This separation of the growth phase from the nitrogen uptake phase may be caused by the use of nitrogen pools [Dortch, 1982] accumulated when nitrogen is available and then used by cells when there is still light available for photosynthesis but no nitrogen in the medium. Rafay *et al.* [2020] also showed a similar result by *N. gaditana* in a repeated batch culture at $395 \mu\text{mol/m}^2 \cdot \text{s}$. Next, Phase III and IV (from 10:00 to 24:00 h) are observed by following the decrease in biomass concentration from 2.1 kg/m^3 to the lowest level of 1.4 kg/m^3 , corresponding to the effect of diminishing light and nitrogen absence in the PBR.

Figure 3.6c, also shows the cell disruption rate τ_D and the TFA and TAG cell content. It can be differentiated the effect of light on mechanical resistance. Firstly, it has to be marked

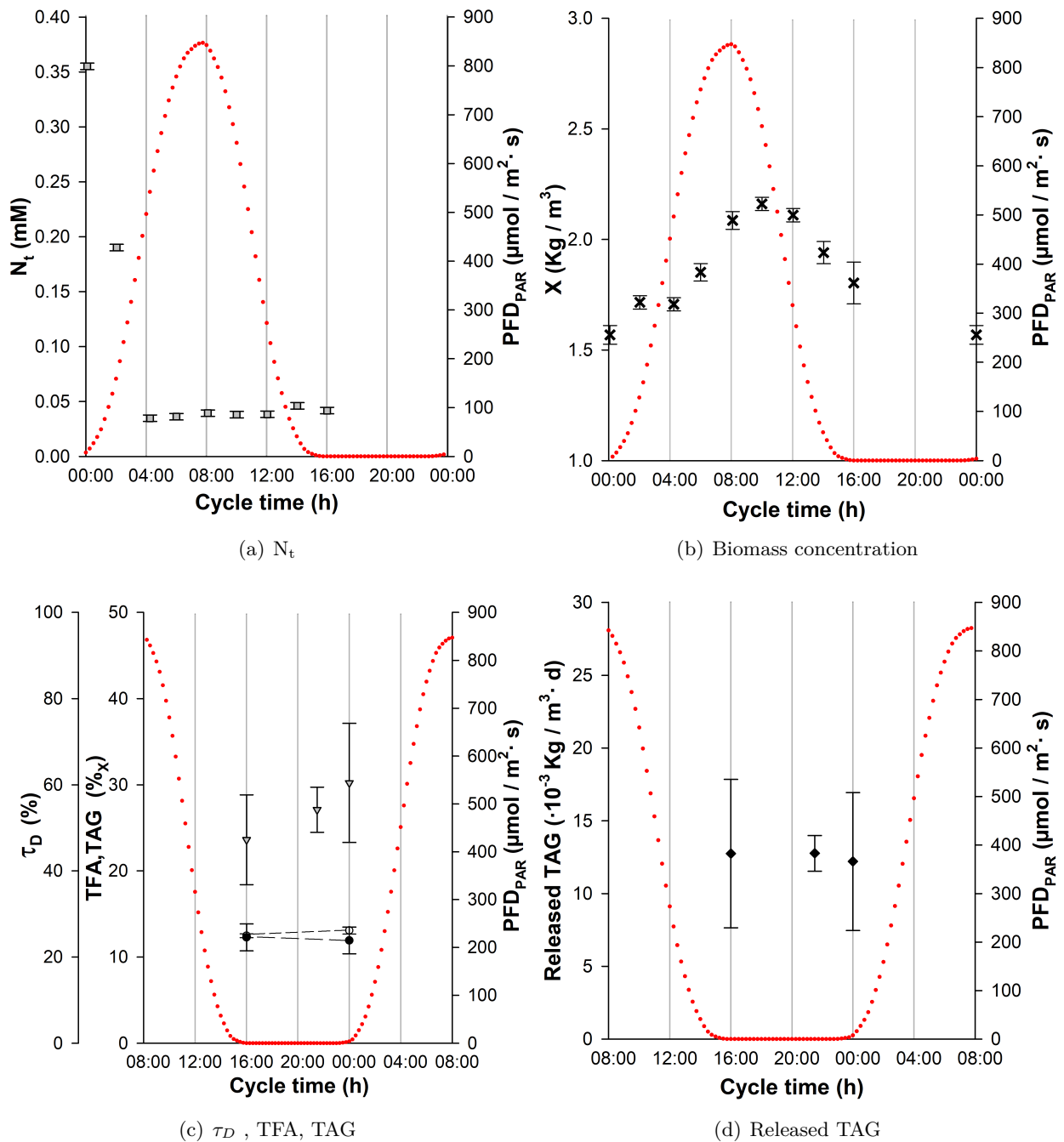


Figure 3.6: Culture changes for punctual addition of NO_3^- in continuous mode during day-night cycles. At a) grey squares represent residual nitrogen N_t (Error bars for SE, $n=3$); at b) black cross represent dry weight biomass measurement (Error bars for SE, $n=3$); at c) grey triangles stands for cell disruption rate τ_D (Error bars for SE, $n \approx 25$) while white and black circles are for TFA and TAG content respectively (Error bars for SE, $n=3$); and at d) Released TAG are represented by black diamonds (Error bars for SE, $n=23$).

that, TFA and TAG are not varying as much as in previous experiments during the night period. However disruption rate does but in a different range. The TFA values reported here, slightly changed during night period from 12.5 to 13.1%_X (SE=0.67% and 1.25%, n=3) and TAG from 12.3 to 11.9%_X (SE=1.57% and 1.55%, n=3). In this case, TAG represents about 90% of TFA. In addition, disruption rate is still increasing in 13%, by going from 47% to 60% during night period. These values are similar to those obtained in actual DNc, but now for a continuous culture. Nonetheless, it might be noted that the standard error of the measurements (SE=10%, n=3) do not allow to be certain about variations. However, it could still being discussed that algenean (as a possible explanation to changes in mechanical resistance) might be affected by DNc or by nitrogen depletion and they could account in cell wall composition. Therefore, changes of long chain hydrocarbons in cell wall composition under DNc, need to investigated in further research to confirm our hypothesis.

TAG volumetric and surface productivities were calculated from 27.0 to 20.2 ·10⁻³ kg/m³·d and 0.8 to 0.6 ·10⁻³ kg/m²·d respectively. These results are very close to those from batch outdoor in simulated DNc. However the present protocol leads to more interesting values regarding cell disruption rate. As a result of the combination of TAG production and recovery, in the figure 3.6d are presented the released TAG of the experiment. The recoverable TAG are constant around 12.6 ·10⁻³ kg/m³·d (SE=3.7, n=3) (0.4 ·10⁻³ kg/m²·d) which is about the double than the achieved value for the batch outdoor PBR in simulated DNc. The former is higher not only due to the differences in TAG content, but also because disruption rate is not affected as much as in a normal batch depletion (Fig. 3.3), and because of the higher biomass concentration reached in the continuous culture.

Additionally to this experiment, a final experience was conducted supplying half of the nitrogen dose under exactly the same conditions (data not shown). The aim was to look if lower nitrogen concentrations would impact TAG content under this protocol. Surprisingly, after stabilization (31 days), TFA and TAG content did not significantly change (12.4% and 12.1% respectively; SE=0.23% and 0.82%, n=2) but biomass concentration diminished to 0.7 kg/m³ (2.5 and 2.1 kg/m³ for continuous and full dose punctual protocols respectively). Reducing to the half of nitrogen needs, diminished surface TAG productivity to 0.3 ·10⁻³ kg/m²·d, which is also about the half of the surface TAG productivity of the full previous dose.

Comparing the latter value for half punctual nitrogen addition (0.3 ·10⁻³ kg/m²·d) with the productivity results from the experiments under continuous addition (3 to 2.5 ·10⁻³ kg/m²·d) and with full addition (0.8 to 0.6 ·10⁻³ kg/m²·d), it can be concluded that the highest productivity (and the highest TAG content) was achieved under continuous addition; with 70% and 90% more than punctual and half punctual addition protocols respectively. It is hypothesized that little excess of nitrogen in media, in relation to a fully starved culture, is somehow still needed for the synthesis of

TAG during the day period. It is possible that some translocation or *de novo* synthesis pathways are switching on/off to allow the cell to survive or starve during DNc. Therefore, the decrease of productivity under punctual addition would be due to an imbalance of TAG synthesis because of the lack of nitrogen when triggering a N-deprivation during day period. Then, a residual nitrate concentration could have a positive effect on TAG productivity.

0.01

3.4 Conclusions

The present work investigated a nitrogen limited continuous culture protocol to take advantage of the night dynamic of *N. gaditana* culture in DNc, notably phases of biomass growth and losses (TAG consumption) and variations in cell disruption rate. About the latter, algalan accumulation in cell wall was hypothesized to be responsible of the mechanical resistance changes observed in night period. Using the proposed concept of released TAG, it was calculated the optimal harvesting time of a solar culture (batch N-depleted) at 4 hr after sunset (with released TAG of $0.3 \cdot 10^{-3}$ kg/m²·d at sunset and $0.01 \cdot 10^{-3}$ kg/m²·d at sunset). As well, it has been showed that reducing dilution rate in a continuous microalgal culture (0.005 h^{-1}) with a limited nitrogen supply, can balance cell growth and TAG metabolism to establish a periodic regime which was demonstrated stable under simulated DNc. In the same manner, a single dose of the nitrogen source applied in the onset of light period was found less effective. The best TAG productivity was achieved with continuous addition of a N-limited media (around $3 \cdot 10^{-3}$ kg/m²·d; and $9 \cdot 10^{-3}$ kg/m²·d of biomass surface productivity). The estimated released TAG was around $1.4 \cdot 10^{-3}$ kg/m²·d.

Chapter 4

Optimization of lipid recovery from *Nannochloropsis gaditana* via wet-centrifugal extraction

Abstract

The aim of this work is to track and optimize lipid recovery from *Nannochloropsis gaditana* in wet extraction operations. No significant differences were found when disrupting microalgal suspensions using biomass concentrations of up to 30 g/L dry-weight, but were found between physiological states. A nitrogen-depleted culture needed 5.8 min in a bead milling device to disrupt 80% of the cells, compared to 4.8 min for a nitrogen-replete culture. The released lipids were then recovered by two different methods: one using a Centrifugal Partition Extractor device and one using a Continuous Centrifugal Extractor device. For the latter, ANOVA analysis of a Box-Behnken RSM showed that the interaction between biomass concentration and solvent inlet rate influences lipid recovery the most. A quadratic regression model also revealed that 84% of triacylglycerol was recovered using 7.9 g/L of algal suspension at 5.4 mL/min treated with 8.9 mL/min of 2-methyl-tetra-hydrofuran.

4.1 Introduction

Over about the last two decades, biofuels such as biodiesel from microalgae lipids have been considered an option with regard to climate change and the energy-supply crisis [Chisti, 2007]. However, although many technologies have been developed for this purpose [Axelsson and Gentili, 2014, Chisti, 2007, Halim *et al.*, 2012b, Scott *et al.*, 2010, Tan *et al.*, 2018], not all of them can be applied in the biodiesel context. This is mainly because the choice of process is expected to be energy efficient, sustainable and economically viable.

Cell disruption coupled with wet extraction (liquid-liquid extraction) is a tested option for developing an energy-efficient process [Angles *et al.*, 2017, Dong *et al.*, 2016, Ghasemi Naghdi *et al.*, 2016, Lee *et al.*, 2012, Taher *et al.*, 2014]. Total Fatty Acids (TFA) are released through cell disruption, which prepares them for contact with the solvent. By using liquid-liquid extraction, the drying or dewatering step is therefore avoided and the impact on the overall output of biodiesel energy is greatly reduced [Amaro *et al.*, 2011, Halim *et al.*, 2011, Lee *et al.*, 2010, Taher *et al.*, 2014].

The *Nannochloropsis* genus is a diverse collection of microalgae comprising 6 species with several sub-strains. Most of these have been widely studied for biodiesel production due to their high lipid content under stress conditions [Beacham *et al.*, 2014, Bouillaud *et al.*, 2019, Ma *et al.*, 2016, 2014]. *Nannochloropsis gaditana* is one of the most promising strains that produces high levels of lipids [Taleb *et al.*, 2015]. It is well known that cell stresses like nitrogen limitation and high light exposure trigger the accumulation of TFA, in particular Triacylglycerol molecules (TAG) [Camacho-Rodríguez *et al.*, 2014, Flynn *et al.*, 1993, Taleb *et al.*, 2015]. Stress also seems to affect cell resistance to disruption. It has been shown that the *Nannochloropsis* genus has a relatively narrow cell wall in optimal growing conditions, but during nitrogen limitation the cell's mechanical resistance is somehow increased [Angles *et al.*, 2017, Beacham *et al.*, 2014]. This effect could be linked to the effect of its size or the translocation of lipids to the cell wall [Janssen *et al.*, 2019b, Montalescot *et al.*, 2015].

Lipid recovery can therefore be carried out by solvent extraction. Although non-polar solvents like CHCl_3 have a high lipid extraction yield, using them on an industrial scale would increase environmental and health problems [Watts, 2004]. A viable option in this context consists of using solvents like heptane, ethyl acetate and 2-methyl-tetra-hydrofuran (the latter two considered green solvents). These solvents and 8 others have been previously screened for their efficiency with short-time wet extraction, in particular 2-methyl-tetra-hydrofuran, which minimizes the energy needed for solvent recycling and presents low solubility in water [Angles *et al.*, 2017].

One approach for intensifying wet extraction is to use processes based on centrifugal force for improved mixing and separation. Systems like Continuous Centrifugal Extraction (CCE) are

designed for continuous liquid-liquid extraction and simultaneous separation of phases [Bojczuk *et al.*, 2017]. CCE allows the input of two solutions - solvent and algal culture feed (rich in lipids) - in a common rotary chamber, the speed of which can be modulated. Under the right conditions, two well-separated outlet flows are recovered during extraction: the raffinate fraction - which is mostly lean culture, and the extract fraction, which is mostly solvent. This equipment is promising for reducing solvent consumption and simplifying scaling-up of the wet-extraction process due to the adjustable flow-rate capacity and ability to connect several modules in series. However, the use of centrifugal continuous extraction has not been reported for pure biotechnological applications or biofuel production [Schügerl, 1994, Seyfang *et al.*, 2019].

Another interesting wet extraction approach is to use a Centrifugal Partition Extraction (CPE) device. These devices have been widely used for separation and recovery purposes in the biotechnology and nutrition industries [Bojczuk *et al.*, 2017]. The principle is based on liquid-liquid chromatography with no solid support to extract the solutes, based on the partition coefficient between two non-miscible solvents. CPE devices, like CPC columns, have a series of small chambers filled with solvent as a stationary phase. The stationary phase is maintained by applying a centrifugal force to the entire series of chambers. A mobile phase is then pumped into the system, enabling interaction with the solvent. This way, the solvent elutes the solutes every time it enters the device chambers. With this technology, the amount of solvent used and the operating time are considerably reduced compared to conventional extraction processes, including CCE. For this reason CPE is a useful comparison point for efficiency.

In order to scale-up centrifugal extraction for biodiesel production, many variables still need to be adjusted. For example, the availability of lipids during extraction will rely essentially on the biomass concentration (and TFA/TAG content) and the percentage of disrupted biomass. There is also an ideal solvent-to-feed-rate ratio for optimal mass transfer of lipids; however, when these two currents are stirred vigorously, emulsification may be assisted by the natural presence of algal proteins and pH changes following disruption.

Consequently, analyzing the role of the above variables separately could be disadvantageous in terms of time, resources and unknown related interactions. One strategy for analyzing and optimizing the multiple factors that interact in the phenomenon is Response Surface Methodology (RSM), specifically Box-Behnken design [Box and Behnken, 1960, Ferreira *et al.*, 2007] which is arranged as a spherical set of variables, which means that extreme interaction vertices are not considered. This is advantageous since certain combinations of factors could be physically restrictive or expensive to operate; with this methodology, a response surface can be obtained that can be modeled and analyzed using the ANOVA method, which looks for the greatest interaction impacting the response. However, prior to running a RSM it is recommended to conduct some exploratory experiments to understand the trend of the variables.

The aim of this work is therefore to enhance lipid recovery from *Nannochloropsis gaditana* by first maximizing lipid availability via bead milling, then optimizing the main parameters using CCE technology. The optimal lipid recovery obtained is then compared with a reference CPE and the resulting operational problems discussed in terms of biodiesel application.

4.2 Materials and Methods

4.2.1 Microalgal Cultures

The microalga *Nannochloropsis gaditana* CCMP527 (NCMA, USA) was grown using Artificial Sea Water (ASW) (Berges et al., 2001) enriched with CONWAY solution as the culture medium. ASW is prepared using (mM): NaCl, 248; Na₂SO₄, 17.1; KCl, 5.49; H₃BO₃, 0.259; NaF, 0.045; MgCl₂·6H₂O, 32.24; CaCl₂·2H₂O, 0.626; KBr, 0.497; SrCl₂·6H₂O, 0.056; NaHCO₃, 1.42. CONWAY solution has NaNO₃ as the source of nitrogen at 10.6 mM. However for experiments referred to as N-replete (optimal conditions), the NO₃⁻ was doubled to 21.2 mM to ensure there was no nitrogen limitation. For the cultures referred as N-depleted (starved conditions) a CONWAY solution without NO₃⁻ was prepared and added in the same quantity as for the replete culture.

Three photobioreactors (PBRs) were used to supply enough biomass for this work. For early experiments related to cell disruption optimization and solvent choice, two were set outdoors in France in late summer 2018 (47° 15' 06.5" N, 2° 15' 34.5" W) in 170-litre flat-panel airlift PBRs (Subitec, Germany). These reactors were operated in batch mode with the pH regulated at 8 by manual injection of 98% CO₂ (gas). For the experiments related to Box-Behnken RSM, a single 170-litre flat-panel airlift PBR (HECTOR PBR) was operated indoors in batch mode. A description of the reactor is given by Pruvost *et al.* [2011b]. This reactor was irradiated with artificial LED light, simulating the average annual irradiation (photon flux density 269 μmol/m²·s) and solar cycles of the above outdoors conditions. The pH was also set at 8 by automatic CO₂(gas) injection.

The biomass from the depleted and replete cultures was harvested using a continuous centrifuge (DRA320VX Rousselet Robatel, France) at 6,000 rpm. The sludge (biomass concentration 40 g/L) was then diluted using a phosphate buffer saline (PBS) solution at 1, 5, 10, 20 and 30 g/L for cell disruption optimization, and 2, 5 and 10 g/L for RSM.

4.2.2 Dry-Weight Analysis

Glass fiber filters with a pore diameter of 0.45 μm (Whatman GF/F) were pre-weighed. Samples of 10 mL were taken from the PBRs and filtered in triplicate. The filtered biomass was then washed with 3 equal volumes of NH₄HCO₂ 1.19 M, and 3 equal volumes of MiliQ water. The filters were dried at 103 °C for 1 h (no further time needed to achieve weight stabilization) and then weighed. The biomass concentration (represented by X) was considered as the weight difference between

the dry biomass and the empty filters for each culture volume. All reported values in this work correspond to the mean values in a triplicate dry-weight assay.

4.2.3 Bead Milling

To carry out cell disruption, a continuous bead mill was used in the laboratory (DYNO-Mill KD, Multilab, WAB, Switzerland). The grinding chamber (≈ 0.561 L) connected to an agitator disc (64 mm diameter) was filled to 80% with 0.5 mm diameter glass grinding beads. During the process, milling was carried out at 14 m/s impeller tip speed and a flow biomass inlet rate of 9 L/h with reference to Zinkoné *et al.* [2018].

Three dilutions (10, 20, 30 g/L) for each N-depleted and N-replete culture were passed through the bead milling device between 1 and 5 times. At the end of each pass, the corresponding aliquot was analyzed to determine the associated disruption rate.

4.2.4 Quantification of Cell Disruption

Cells were counted digitally using image analysis and a Malassez cell-counting chamber under microscope. First, a diluted sample was prepared to avoid saturating the number of cells per image, but enough to provide a representative aliquot of the culture [Zinkoné *et al.*, 2018]. Then a Malassez double chamber was prepared and focused at 40 x using an optical microscope connected to a camera (Axio MRC Cam at Axio Scope A1 microscope, Carl Zeiss, Germany). The camera took 40 pictures of each sample which were then analyzed using image-analysis software (ImageJ v.1.52o, NIH, USA) to discriminate images-like-noise and cells. The cell surface was calculated in μm^2 for all images-like-cells based on the distance-to-pixel proportion.

The cell count and statistical information was then gathered using a MATLAB (Math-Works, US) algorithm. The microalgal cell disruption rate τ_D was defined as the proportion of additional cells counted after bead milling in relation to those counted before the process.

4.2.5 Total Fatty Acid (TFA) and Triacylglycerol (TAG) extraction efficiency and quantification

4.2.5.1 Solvent Choice and Standard Extractions

To find out either the TFA or TAG content, $CHCl_3$ /Methanol 2:1 v/v (Fisher Sci, US) was used as a reference solvent for extractions. Other solvents used for comparison assays were heptane, Hep (Emsure-Merck, Germany), ethyl acetate, EtoAc (Fisher Sci, US) and 2-methyl-tetra-hydrofuran, Me-THF (Acros Organics-Thermo Fisher Sci, US). Their main properties are summarized in 4.1.

First, the three biomass samples from the depleted cultures were passed three times through a cell disruptor (Constant Systems Ltd, UK) at 2.7 Kbar and 10 °C. Passing the samples through

Table 4.1: Main physicochemical properties of Heptane, Ethyl Acetate and 2-Methyl-tetrahydrofuran

	Hep	EtoAc	Me-THF
<i>Molecular Formula</i>	C ₇ H ₁₆	C ₄ H ₈ O ₂	C ₅ H ₁₀ O
<i>Density at 20° C - ρ_S (g/mL)</i>	0.684	0.902	0.854
<i>Vapor pressure at 20° C (mmHg)</i>	34.5	73	102
<i>Boiling temperature at P_{atm} (° C)</i>	98.4	77.1	80.2
<i>Viscosity at 25° C (cP)</i>	0.376	0.423	0.46
<i>Solubility in water at 20° C (wt%)</i>	2.2 (25° C)	8.7	14.1
<i>Reference</i>	[Kim <i>et al.</i> , 2019]	[Kim <i>et al.</i> , 2019]	[Sicaire <i>et al.</i> , 2014]

the equipment three times ensures total destruction of the cells, which was verified by microscope observation. The suspension was mixed with solvent at $S/F = 0.5$ v/v (solvent per aqueous phase) for 4 hours at 23 °C. To measure the TFA content, the organic fractions were recovered, transesterified and measured by Gas Chromatography with a Flame Ionization Detector (GC-FID) (Thermo Fisher Sci, US). Next, to quantify the TAG content, an aliquot of the last extract was processed by HPTLC (CAMAG, Switzerland) using a mix of polar and non-polar lipids (Merck, Germany) as a marker reference. The results for TFA or TAG per gram of algal biomass treated are shown as TFA%_X or TAG%_X.

Then extraction efficiency is defined as:

$$\eta_{E,i} = (i_j)/(i_{CHCl_3/MeOH}) \quad (4.1)$$

with i is either extractions TFA%_X or TAG%_X carried out with a specific solvent, j .

Thus the Specific Solvent Consumption, can be also defined as follows:

$$\Gamma_j = (S \cdot \rho_j)/(F \cdot X \cdot \eta_{E,i}) \quad (4.2)$$

with S is the solvent inlet rate and F the feed inlet rate (both in mL/min); ρ_j is for solvent density in g/L, X is the biomass concentration in the feed in g/L and $\eta_{E,i}$ is the extraction efficiency. In this work, Γ_j was only calculated for the optimized condition in the CCE and for the comparison analysis with CPE.

4.2.5.2 Continuous Centrifugal Extraction

The extraction system used was a mono-stage Continuous Centrifugal Extraction (CCE) device - Type BXP 012 (Rousselet Robatel, France) using N-depleted biomass from a HECtor PBR. The rotary speed was set beforehand at between 2000-4000 rpm (107-430 ref) depending on the

experimental run. After approximately 20 s, the latter was stable and the solvent and feed inlet rates (S and F) were set at the established flow rate into the system. After an additional 30 - 60 s, the extract and raffinate fractions (E and R) began to flow out normally and were recovered at the same inlet flow rate, which also enabled verification of the total flow supplied ($T_oT = S + F = E + R$). Around 30 mL from each outlet current was then collected and analyzed identically by GC-FID and HPTLC to obtain the TFA/TAG extraction efficiency $\eta_{E,i}$ for the actual experimental run.

4.2.5.3 Centrifugal Partition Extraction

Two liters of N-depleted culture at 5 g/L biomass concentration X were passed several times through the bead milling device until a cell disruption rate τ_D of more than 90% was obtained. This suspension was treated with Centrifugal Partition Extraction (CPE). The device (model A, Kromaton, France) was equipped with a short column (231 chambers) to carry out TAG extraction with Me-THF. The equipment was set for 1 stage at 900 rpm in non-continuous mode for a column volume of 270 mL and a solvent volume of 140 mL. The disrupted culture suspension was then passed through the system at 25 mL/min allowing 5 min of residence time for the extraction. The extracted fraction was recovered and analyzed for TAG content and therefore TAG extraction efficiency ($\eta_{E,TAG}$).

4.2.6 Response surface methodology for Continuous Centrifugal Extraction

The Box-Benhken RSM was chosen to optimize the operative parameters of the CCE. This type of design includes 15 observation units (OUs) for three independent factors and one response variable: 12 OUs derived from independent variables around 3 more OUs as replicates of the central point. The variables and ranges chosen for the CCE device were: biomass concentration (from bead milling) $X = 2, 5, 10$ g/L; and solvent and feed inlets S and $F = 5, 7.5, 10$ mL/min each. All the runs were batched-executed at 25°C (three rounds, according to the range in the biomass concentration) for the first 30 min after milling, to avoid undesirable reactions due to interaction between medium and cytoplasmic ions. Samples from each OU were stored at -80°C for determination of further TFA/TAG extraction efficiency ($\eta_{E,i}$).

For cases where emulsification was unavoidable, samples were still taken but centrifuged at 6000 rpm and 4°C for 10 min (Hettich, Germany), to separate the phases from the two outlets. The organic phase was then analyzed by the same methods as above and the 15 OU efficiencies processed using Design Expert V11 (Stat-Ease, US). For some analyses, the variables were coded as follows: X as A, S as B and F as C. The software provided random experimental design, statistical analysis and numerical and graphical optimization.

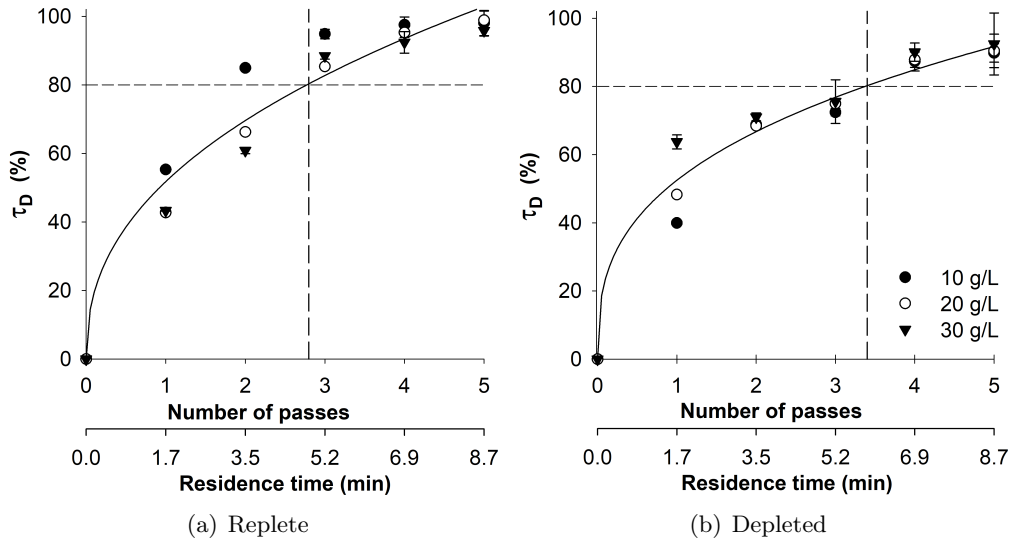


Figure 4.1: Physiological state and disruption kinetics at bead milling. The disruption rate τ_D is plotted for each biomass concentration condition X , and the two-parameter power regression for each physiological state. Error bars for CI ($n \approx 20$, $\alpha = 0.05$)

4.3 Results and Discussion

4.3.1 Final Culture Conditions

After 11 days, the final biomass concentration for N-depleted and N-replete outdoor cultures was 0.54 and 2.29 g/L respectively, with 28.1% $_X$ and 8.7% $_X$ of TFA and 13.4% $_X$ and 2.2% $_X$ of TAG respectively. As a reference to compare stress levels among PBRs, the absorbance 480/662 nm index was measured [Heath *et al.*, 1990]. N-depleted and N-replete values at the final day were 1.83 and 0.51 respectively, indicating, as expected, a large influence in carotenoids to chlorophyll ratio for N-depleted culture.

Indoor PBR system was ended after 13 days. The final biomass concentration was 1.52 g/L with 32.2% $_X$ TFA and 28.6% $_X$ TAG. The 480/662 nm index was 3.34 at the end of the culture.

4.3.2 Cell Disruption Optimization

Fig. 4.1 plots the cell disruption rate as a function of the physiological state (as a consequence of cells adapting to the culture medium) and biomass concentration, throughout the operating period; three different biomass concentrations from two different medium conditions (replete and depleted) were treated in a bead milling device to find out the residence time (number of passes) required to achieve a cell disruption rate of 80%. One-way analysis of the variance applied to each physiological state revealed that the differences between the biomass concentration groups at disruption rate τ_D (replete: $F(2, 12) = 0.31$, $p = 0.74$; depleted: $F(2, 12) = 0.22$, $p = 0.81$) were not statistically significant. Based on this consideration, the whole data set for each physiological state was arranged in a two-parameter power regression as shown in Fig. 4.1 ($R^2 = 0.9619$ for replete, $R^2 = 0.9776$

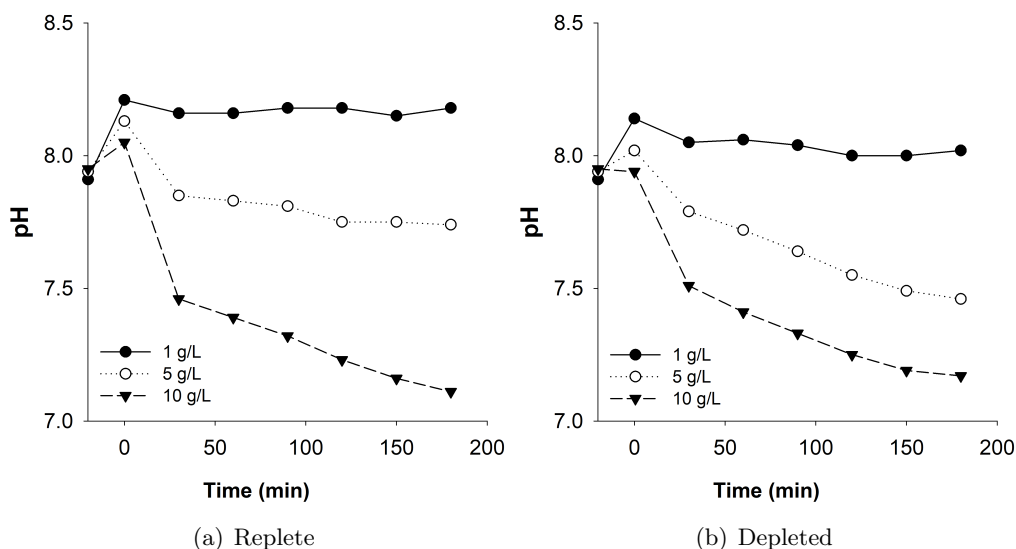


Figure 4.2: pH value of microalgae suspension after bead milling for N deplete (a) and N depleted (b) cultures. For each graph, the value on the left represents pH before milling; the value at zero represents the moment immediately after milling. ($n = 1$)

for depleted), and the regression equation thereby enabled calculation of the exact residence time needed for bead milling to disrupt 80% of the cells. These values are 4.8 min for replete culture and 5.8 min for depleted culture. The difference is more evident when looking for the values at the curve where $\tau_D > 80\%$. At least three passes are required for replete culture (Fig. 4.1a) and four passes for depleted culture (Fig. 4.1b). A comparison of the τ_D from different physiological states shows that *N. gaditana* presents more mechanical resistance to milling when it is harvested in nitrogen-depleted conditions. A similar result using *Nannochloropsis sp.* was obtained by Angles *et al.* [2017].

The final pH value after bead milling is important to preserve the integrity of the molecules to be recovered and also the workability of the suspension for further steps, which mainly include emulsification of the lipids and proteins released during the process. For this reason, the pH was monitored after cell destruction for biomass concentrations 1, 5 and 10 g/L and for the two physiological conditions. The initial pH was 7.9 for each of them, as shown in Fig. 4.2. The suspensions for both physiological conditions stabilized the pH almost immediately after disruption (8.2 for replete and 8.0 for depleted). In addition, the 5 g/L suspension for N-replete culture had a stable and lower pH of 7.8 after 120 minutes. In the same period and for the same concentration, the N-depleted condition did not reach stability (around pH 7.5). The same was observed for the highest suspension concentrations (10 g/L) for both physiological conditions during the 180 min test. These conditions tended to attain even lower pH values (around pH 7). This could be explained by the fact that when 5 and 10 g/L cultures are milled, ions like H^+ and other organic compounds are released in proportion to cell concentration and stress level (these compounds possibly being accumulated during stress conditions as a cell regulation mechanism [Borowitzka,

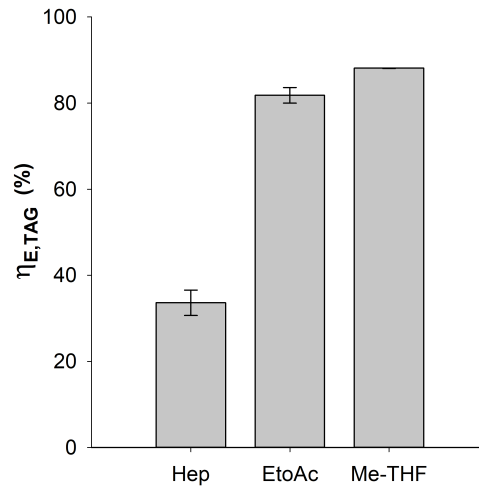


Figure 4.3: Triacylglycerol extraction efficiency for heptane, ethyl acetate and 2-methyl-tetrahydrofuran. Error bars for SE ($n = 2$)

2018]). Presumably, the liberation of these ions and molecules, added to the rest of the culture medium, could interact until the whole solution reaches an equilibrium. The pH stabilization time would depend on the abundance of these molecules and their interaction in the final mixture. It would therefore appear that the suspension needs to be processed for the first 50 minutes at most after cell disruption to avoid any undesired interaction, which could affect the recovery process.

4.3.3 Choice of Solvent for Extraction

Fig. 4.3 shows the extraction efficiency results for N-depleted biomass using the three solvents tested. Me-THF and EtoAc showed similar extraction efficiency $\eta_{E,TAG}$: up to 88% and 82% respectively. Heptane had the lowest at 34%. In all cases, TAG represented 89% of TFA, showing that the solvents used have no relevant selectivity for TAG.

In addition, by using cell destruction prior to extraction, the solvents (or mixtures) did not depend on their ability to draw lipids from the cell (such as 2:1 v/v $\text{CHCl}_3/\text{MeOH}$ [Bligh and Dyer, 1959]) but simply on their affinity with lipid molecules, since TAG molecules were already released in the medium. This enabled maximization of extraction efficiency and thereby reduction of the amount of solvent used; which can also significantly reduce the investment required in solvent for the whole wet extraction process.

As a result, Me-THF will be chosen as the best of the three solvents for recovering TAG in future experiments.

4.3.4 Centrifugal Partition Extraction

Centrifugal partition Extraction CPE has been used as a reference to compare the specific solvent consumption (Γ_{Me-THF}) of CCE.

For one single TAG extraction performed at CPE device it was possible to treat 2 L at biomass

concentration 5 g/L with only 140 mL of solvent. These values leads to TAG extraction efficiency $\eta_{E,TAG}$ of 83% (SE= 3%, n=3), which corresponds to a specific solvent consumption Γ_{Me-THF} of 27.7 g_{Me-THF}/g_{TAG}.

4.3.5 Response surface methodology for Continuous Centrifugal Extraction optimization

The Box-Benhken RSM was chosen as the method for optimizing the main CCE parameters as a strategy for reducing the number of experimental runs and simultaneously analyzing multi-parameter interactions. The optimal value obtained with this method, added to the bead milling results, was expected to provide relevant information on the overall efficiency of the wet-extraction method in the biodiesel context.

However, prior to starting the RSM, some pre-tests were run to clarify the operating work-zone. Emulsions were easily obtained where the rotary speed of the CCE device exceeded some limits. These limits varied for each observation unit (OU), but the lowest limit was always the rotary speed which allowed outlet flows to be recovered at the same rate as inlet flows (5000-6000 rpm /670-966 rcf). A relationship was observed between total supplied flow (ToT) for the different substances used and this rotary speed limit. Higher speeds promoted separation of the phases, but also the consistency of the emulsion. This phenomenon could be due to Taylor-vortexes during centrifugal extractions driving more complex variations in fluid dynamics when the rotary speed was increased [Nakase and Takeshita, 2012, Stuart, 1986]. There is therefore a compromise between emulsification and separation when using a CCE module.

Another factor that could influence emulsification and therefore extraction efficiency ($\eta_{E,i}$) is the release of intracellular material into the medium. It has been shown that some microalgae proteins have emulsifying properties [Ebert *et al.*, 2019]. The biomass concentration and disruption rate, therefore, also influence this phenomenon: for a given high biomass suspension, increasing the disruption rate τ_D will also release emulsifying molecules. Accordingly, some pre-tests were run to clarify the biomass concentration range to be used in RSM to avoid emulsification as far as possible. Normally, cultures above 10 g/L are unmanageable for extraction because of the immediate appearance of an emulsion, even when working at low S/F ratios or low rotary speed (< 4000 rpm / 429 rcf). For example, when working with suspensions above 10 g/L of biomass, emulsion appeared from 3500 rpm (329 rcf); a higher rotary speed was therefore required for recovering the same outlet flow rates (since $ToT = S + F = E + R$), although no solvent was recovered, just an enhanced emulsion. These pre-tests defined the operational range of biomass concentration as between 2-10 g/L for RSM analysis. However, protein content and operational pH were not considered as variables for RSM.

After running the Design Expert Software, the data were found to fit well with a quadratic-

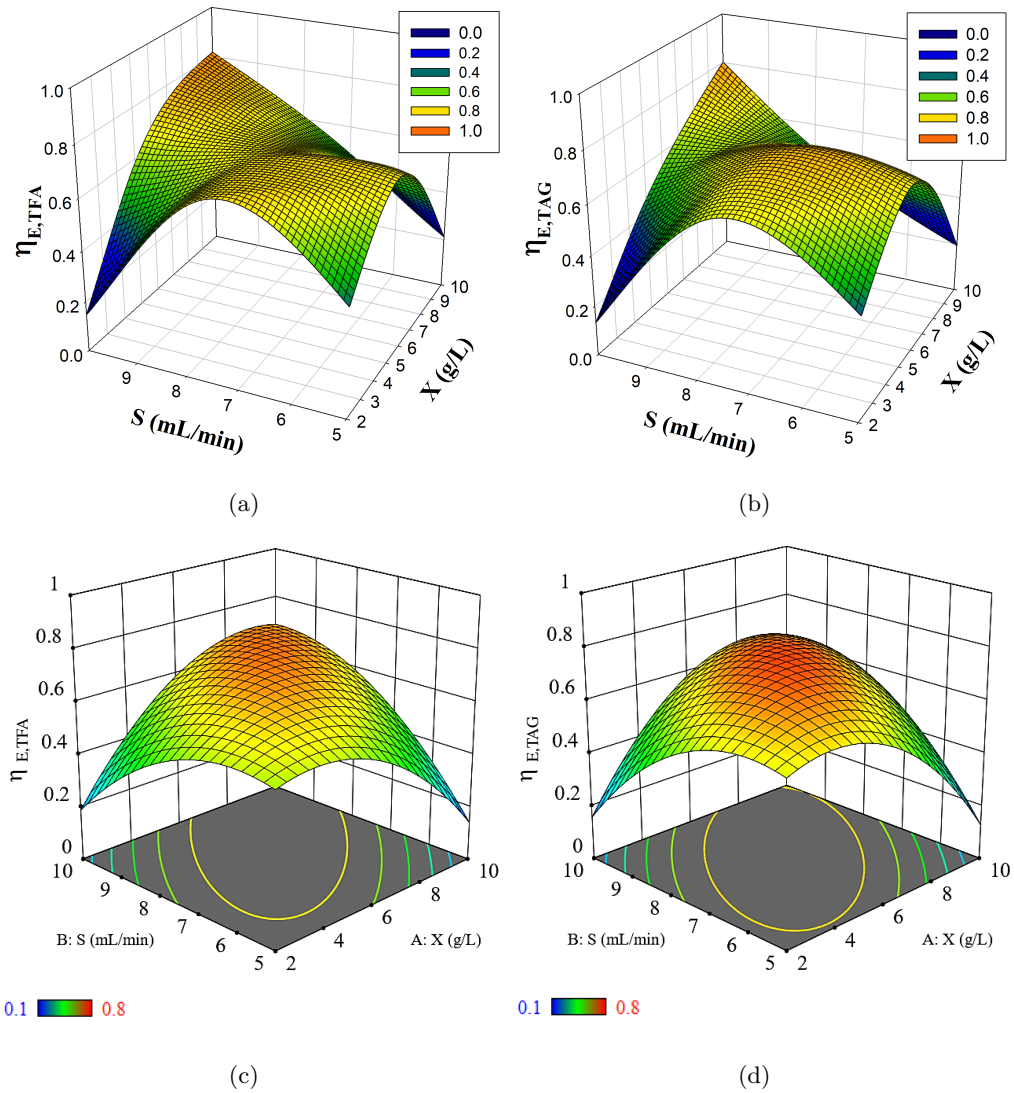


Figure 4.4: Raw experimental data and quadratic model 3D mesh for solvent-to-biomass concentration influence on extraction efficiency, $\eta_{E,i}$. a) and b) unprocessed data for TFA and TAG respectively. c) and d) data obtained after modeling

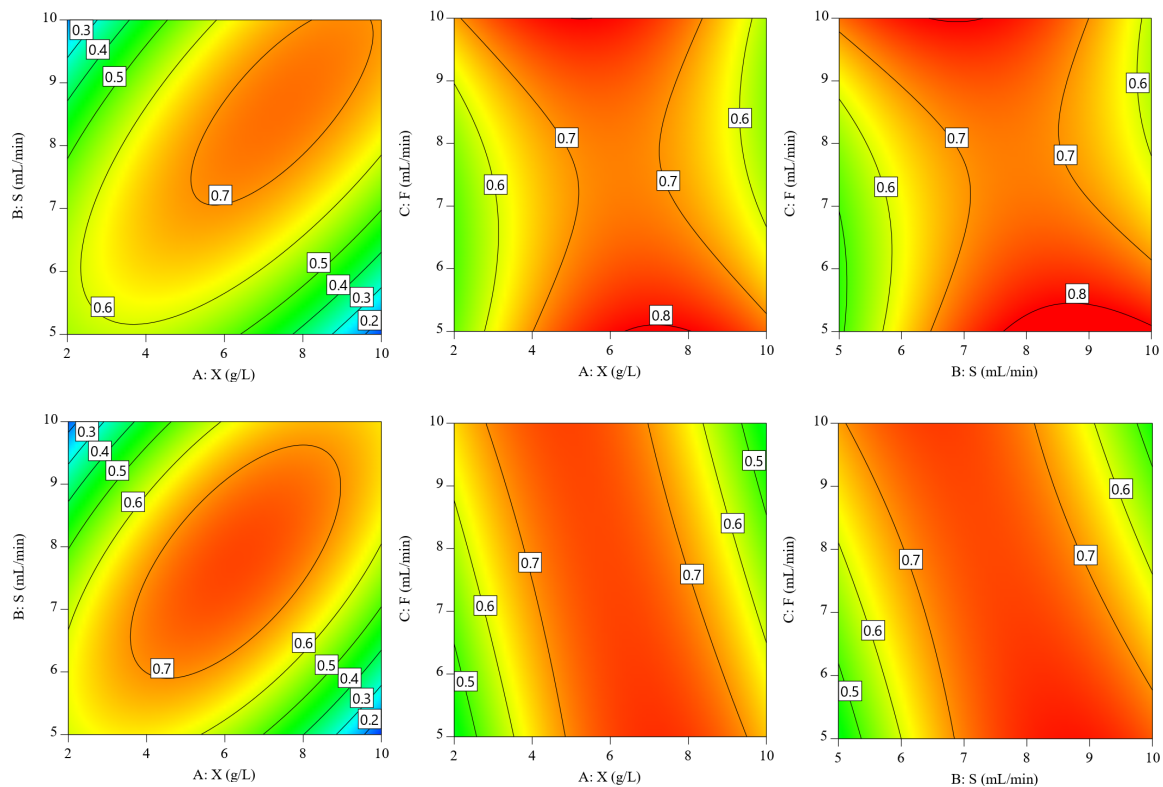


Figure 4.5: Contour graphs for each interaction among sources for the regression model obtained by Box-Behnken for extraction efficiency, $\eta_{E,i}$ response. Contour lines mark extraction efficiency, $\eta_{E,i}$ levels. a), b) and c) for TFA and d), e) and f) for TAG

Table 4.2: Analysis of variance (ANOVA) for a quadratic order modeling. Values for surface response on TFA and TAG extraction efficiency are shown.

Source	AGT					TAG				
	SS	df	Mean Square	F-value	p-value	SS	df	Mean Square	F-value	p-value
<i>Model</i>	0.4980	9	0.0553	2.730	0.141	0.5790	9	0.0643	2.150	0.207
<i>A-Biomass conc.</i>	0.0033	1	0.0033	0.164	0.702	0.0001	1	0.0001	0.003	0.962
<i>B-Solvent</i>	0.0156	1	0.0156	0.770	0.420	0.0026	1	0.0026	0.088	0.779
<i>C-Feed</i>	0.0001	1	0.0001	0.001	0.977	0.0003	1	0.0003	0.010	0.925
<i>AB</i>	0.2179	1	0.2179	10.740	0.022	0.2303	1	0.2303	7.700	0.039
<i>AC</i>	0.0279	1	0.0279	1.380	0.294	0.0557	1	0.0557	1.860	0.231
<i>BC</i>	0.0553	1	0.0553	2.730	0.160	0.0727	1	0.0727	2.430	0.180
<i>A²</i>	0.0892	1	0.0892	4.400	0.090	0.1307	1	0.1307	4.370	0.091
<i>B²</i>	0.0765	1	0.0765	3.770	0.110	0.1006	1	0.1006	3.360	0.126
<i>C²</i>	0.0246	1	0.0246	1.210	0.321	0.0002	1	0.0002	0.007	0.937
<i>Std.Dev.</i>	0.142					0.173				
<i>Mean</i>	0.582					0.546				
<i>C.V.%</i>	24.482					31.700				
<i>R²</i>	0.831					0.795				

Table 4.3: Estimated regression coefficients in terms of coded factors and final equation coefficients in terms of actual factors, both obtained from the quadratic model obtained for TFA and TAG wet-extraction efficiency.

Factor	TFA		TAG	
	Coefficient estimate	Final equation coefficient	Coefficient estimate	Final equation coefficient
<i>Intercept</i>	0.712	-0.792	0.753	-1.973
<i>A- Biomass conc.</i>	0.020	0.0206	0.003	0.0634
<i>B-Solvent</i>	0.045	0.3667	0.018	0.4235
<i>C-Feed</i>	0.002	-0.005	-0.006	0.247
<i>AB</i>	0.230	0.023	0.236	0.0236
<i>AC</i>	-0.082	-0.008	-0.116	-0.012
<i>BC</i>	-0.118	-0.019	-0.135	-0.022
<i>A²</i>	-0.168	-0.011	-0.204	-0.013
<i>B²</i>	-0.144	-0.023	-0.165	-0.026
<i>C²</i>	0.082	0.0131	-0.008	-0.001

order model. Fig. 4.4 shows that with the experimental extraction efficiency $\eta_{E,i}$, which corresponds with a high biomass concentration, X and S cannot actually be fitted into a model because of the sudden increase (mainly due to the unexpected appearance of emulsion at these values). Carrying out ANOVA (Table 4.2) showed that first-order sources (A , B and C) seem to have less significance than second-order sources (AB , AC , BC , A^2 , B^2 and C^2). Interactions and additives mainly affected the model response over the effect of isolated variables: AB and A^2 are the only ones below $\alpha = 0.1$. The same trends were obtained for TFA and TAG.

The estimated coefficients are shown in table 4.3. These represent the expected shift in response per unit factor value when the rest of factors are constant. To obtain these coefficients using the Box-Benhken RSM, the values of the source had to be coded as +1 for the higher levels and -1 for the lower ones. This kind of analysis enables identification of the relative impact of the factors by comparing their coefficients. The equation produced with these coefficients could be used to predict the effects in the response but only within the coded limits of each source.

By ignoring the additive variables, for example, the source AB (Coeff_{TFA}: 0.230, Coeff_{TAG}: 0.236) was shown to have the greatest proportional effect on extraction efficiency $\eta_{E,i}$, followed by an inverse-proportional effect on the relationship between S and F (Coeff_{TFA}: -0.118, Coeff_{TAG}: -0.135). This simply means that if more lipids are to be recovered, a higher S should also be used, but the effect is diminished if F is increased in relation to S . A high concentration will require more time and interface contact with the solvent, which can be achieved by reducing the feed rate for CCE. On the other hand, the effect of the additive variables is also the highest for A^2 and B^2 .

Table 4.3 also shows the coefficients for the equation in terms of actual factors. This could be used to predict the extraction efficiency $\eta_{E,i}$ for given levels of each factor. Here, the levels should be specified in the original units for each factor.

Nevertheless, neither type of coefficient obtained for regression in this work can be used to predict extraction efficiency $\eta_{E,i}$ precisely, due to the low R^2 and moderate p-value of the model itself. However, R^2 (0.831 for TFA and 0.795 for TAG) indicates only a reasonable correlation between the experimental and predicted values of the response. Despite this, the model still provides important information on the relationship between the parameters, which is clearer when the contour graphs are analyzed.

Contour graphics (Fig. 4.5) can be useful to navigate within the limits of the operational variables during CCE. Using the AB interaction as a first reference, Fig. 4.4 a and d shows a maximal extraction efficiency $\eta_{E,i}$ with S : 7-10 mL/min and X : 5-10 g/L. This zone can therefore be transposed to the X - F and S - F interactions (Fig. 4.4 b, c, e, f) where higher efficiencies are found at a low feed rate. The Design Expert Software also provides a tool for numerically locating the optimal point for the three simultaneous sources. Using $\alpha = 0.05$ for maximum extraction efficiency in the model, it was found that $\eta_{E,TFA} = 0.93$ at $X = 8.3$ g/L, $S = 9.2$ mL/min, $F = 5.0$ mL/min and $\eta_{E,TAG} = 0.84$ at $X = 7.9$ g/L, $S = 8.9$ mL/min, $F = 5.4$ mL/min. Both efficiency points were consistent with the previous analyses. The values obtained were higher than with the $CHCl_3$ /Methanol wet extraction (extraction efficiency, $\eta_{E,i} = 50\%$) performed by Angles *et al.* [2017]. However, it should be recalled that the values correspond to the 80% lipids released in the bead milling operation.

With the optimal point obtained by the experiment design, the specific solvent consumption for continuous centrifugal extraction CCE could be determined as $\Gamma_{Me-THF} = 213.8$ g_{Me-THF}/g_{TAG}.

Note that Γ_{Me-THF} is linked to the energy consumption for the whole biodiesel process, since more energy is required for distilling each gram of solvent used to produce each liter of biodiesel. These values show that CPE technology, as a scaled-up process, could save 7.8 times more solvent than CCE even though the two technologies have similar extraction efficiencies.

However, the results for CCE could be improved. On the one hand, this work has demonstrated the relationship between stress levels, biomass concentration and the release of intracellular material with the formation of emulsion, and shown the work-zone to be avoided when carrying out CCE. In this regard, more research on the optimization of hydrodynamics in the CCE chamber could permit working with higher biomass concentrations, which would increase recovery. On the other hand, CCE efficiency can also be improved by using several devices connected in series (the present work relating to a single module). This approach is also interesting in terms of the scalability of the operation, which is one of the biggest advantages of CCE over CPE.

The reason for using Box-Behnken RSM for this work was to determine the general trend of

extraction as a function of the main operative parameters (such as biomass concentration and solvent and biomass flow rates) and also to determine an operational CCE work-zone. As stated, many other factors other than those related to the appearance of emulsification (not studied in detail in the RSM presented, such as pH and temperature) interact during centrifugal extraction and should be investigated for future experiments in biodiesel production.

The optimal wet extraction yield of 73% obtained with bead milling combined with CCE (using Me-THF) has been demonstrated as a high-performance TAG recovery technology with the advantages of scalability for the biodiesel process. The process may perform better compared to extraction yields in the literature. For example, different solvent mixtures and cell disruption for *N. gaditana* were tested by Ryckebosch *et al.* [2014], where solvents such as hexane/isopropanol, ethyl acetate/hexane and ethanol were found to be the best of six, with extraction yields of 58%, 46% and 52% respectively. Similarly, Sati *et al.* [2019] reviewed extraction yields from other pre-extraction treatments such as mechanical (35%), surfactant (78%) and enzymatic lysis (73%). There are other interesting technologies for biodiesel application too, such as the simultaneous distillation and extraction process which gave a 24% extraction yield with *N. oculata* [Dejoye Tanzi *et al.*, 2013] and microwave combined with super-critical CO₂ extraction, which achieved a 30% extraction yield with *N. salina* [Patil *et al.*, 2018].

4.4 Conclusion

Wet-extraction operations (bead milling combined with centrifugal extraction) achieved 73% final TAG recovery using CCE technology on *Nannochloropsis gaditana* cultivated in N-depleted media. Physiological variables such as cell fragility and process operating conditions such as harvesting concentration were found to affect the whole process. The key variables and their interactions during lipid recovery were determined and optimized by RSM analysis. However, CPE saves around eight times more solvent than CCE. Consequently, further intensification of the extraction step is required to combine scalability (*ie.* the CCE process) with a reduction in solvent consumption and emulsification issues for biodiesel production.

Chapter 5

Energy-driven biorefinery approach for double Biofuel recovery from microalgae

Abstract

Microalgal biofuels have been subject of discussion concerning energy efficiency. Sustainability objectives request an overall positive energy balance of the biofuel process which is dependent of the efficiency of each process unit and also on the amount of biofuel produced. Strain selection and the development of dedicated, efficient and low-energy production process (culture systems and wet-biomass treatment) are here of primary relevance. Relevant approaches in the BioDiesel production are simulated and discussed in terms of their impact on the Net Energy Ratio. Next, as a further attempt of optimization, it is also included the co-production of BioEthanol, as allowed by a microalgae strain exhibiting simultaneous lipids and carbohydrates accumulation (*P. kessleri*). Solar light co-valorization by using a photovoltaic panel is also discussed. From the five simulation cases compared, it has been concluded the relevance of photovoltaic energy co-generation (*eg.* up to 67 504 MJ for a reference case of 1 ton/y of biomass production) for sustaining energy consumption in downstream operations related to lipid recovery and their conversion into BioDiesel (*eg.* 41 201 MJ/y and 67 404 MJ/y respectively for the corresponding case). Even if the co-production of BioEthanol was not found to substantially increase the net energy ratio of the full process (0.68 for the best case), the presented double Biofuel recovery approach allows to increase the fuel valorisation by producing up to 50% more liquid fuel than for a single biofuel process. Improvements in solvent recovery, product purification, culture protocol and strain choice are suggested for further research.

5.1 Introduction

During the last decade, biofuels from microalgae have been shown as alternative for supplying the over-growing energy demand while contributing to the CO₂ emissions decrease [Alalwan *et al.*, 2019, Chisti, 2007, 2008, Shuba and Kifle, 2018]. However, production process sustainability and economics are still challenging for large scale implementation [Collet *et al.*, 2014, Ponton, 2009]. Regarding sustainability, energy is the final product; therefore for energy balance it is crucial that energy inputs are lower than energy outputs [Batan *et al.*, 2010].

For this objective, the production process of biofuel has to be optimized in several of the production stages involved. First, the strain choice is key for the large accumulation of energy rich metabolites. Several works have described culturing protocols and screening systems to choose the most interesting strain with high triacylglycerol TAG (for BioDiesel) or carbohydrates (for BioEthanol) contents [Benvenuti *et al.*, 2015, Ma *et al.*, 2014, Moutel *et al.*, 2016, Song *et al.*, 2013, Taleb *et al.*, 2015, 2016]. Precisely, *Parachlorella kessleri* and *Nannochloropsis gaditana* have been described to accumulate TAG, both up to 24%_X; and 64%_X and 23% of carbohydrates respectively under nitrogen limitation, chemostat mode and continuous light (Chapter 2 for *N. gaditana*; and [Kandilian *et al.*, 2019] for *P. kessleri*). At the same time, it has been studied for *N. gaditana*, the nitrogen limitation interaction with the day-night cycles (Chapter 3 and Janssen *et al.* [2019a], Rafay *et al.* [2020], Simionato *et al.* [2011], Taleb *et al.* [2018]).

Similarly, the design and operation of culture systems including photobioreactors (PBR) for culturing microalgae for outdoors conditions are decisive [Lee *et al.*, 2014, Pruvost *et al.*, 2015]. In terms of energy investment, solar cultures are preferred over continuously light-supplied cultures at larger scales. Thus, location is relevant. For example, even though some outdoors conditions have been shown to positive influence the accumulation of TAG molecules (and therefore BioDuel production) [Breuer *et al.*, 2013, Venkata Subhash *et al.*, 2014], according to the region in the globe, high solar radiance and temperatures may be challenging for an optimized culture [Pruvost *et al.*, 2019]. Nwoba *et al.* [2020] recently reported an alternative to reduce the energy input in the biomass production stage by using a flat panel photobioreactor constructed of insulated glass units (IGUs, for Infrared light filtering) with an integrated energy-generating photovoltaic (PV) panel. With this technology it is argued to isolate the microalgae culture of >90% of the ultraviolet and infrared spectral components, while still letting pass >75% of visible light; and, as a result, reducing strongly the energy needs for thermal regulation while producing in parallel electricity from the PV panel.

Regarding downstream processing of the biomass, the so-called Wet-pathway [Angles *et al.*, 2017] has been shown to reduce energy consumption by the avoidance of around 17.71 MJ/kg biomass, in drying process [Yuan *et al.*, 2015]. In wet-pathway, the wet harvested biomass is

treated by cell disruption methods in order to release the TAG and carbohydrates molecules into the liquid medium. Safi *et al.* [2017] and Halim *et al.* [2012b] compared several methods to disrupt the cells regarding energy consumption, and concluded that High Pressure Homogenization and Bead-Milling processes required less intensive operating conditions (like operating time or pressures) which impacts directly the energy cost of the operation.

To recover the released metabolites, several methods have been studied [Balasubramanian *et al.*, 2013, Halim *et al.*, 2012a]. However, in the BioDiesel context, extraction after cell disruption is still a bottleneck in the production process. The chosen method is expected to optimize the extraction of targeted compounds while being sufficiently metabolite-selective in order to minimize the purification steps before final BioDiesel conversion, and, moreover, energy efficient [Halim *et al.*, 2012a]. It has been studied the importance of solvent choice on the process, their interaction with the products and their extraction efficiency with wet biomass [Angles *et al.*, 2017, Balasubramanian *et al.*, 2013]. On this matter, the centrifugal extraction technologies combined with appropriate solvent choice arises as a promising technology capable to simultaneously perform extraction and separation operations [Bojczuk *et al.*, 2017, Seyfang *et al.*, 2019].

Another option to optimize the biofuel process, is to maximize the energy output by leading an energy-driven biorefinery approach. So far, the biorefinery concept has been increasingly considered as one of the strategies to exploit the highest value of microalgal cultures [Chew *et al.*, 2017, Gifuni *et al.*, 2019, Naik *et al.*, 2010, Suganya *et al.*, 2016]. Nowadays, biorefinery is mainly proposed as an strategy to recover by-products towards other market fields (*eg.* nutraceuticals or cosmetics). In this work, it is simulated the double recovery of energy reserve molecules (lipids and carbohydrates) towards the conversion into BioEthanol and BioDiesel. Recently, Sivaramakrishnan and Incharoensakdi [2018] and Karemore and Sen [2016] have shown the viability of the double biofuel production at lab scale using microalgae biomass. They yielded 4-6 kg/m³ of ethanol during the fermentation of lipid-extracted and hydrolyzed biomass. By itself the BioEthanol production process from microalgae manifested a net energy ratio of 0.45 with -2 749.6 GJ/y (for 200 Tn/y biomass production) for the net energy balance according to Hossain *et al.* [2019]. Similarly, Yuan *et al.* [2015] showed a net energy ratio <1 for BioDiesel only, implying that the chosen production system is not capable of producing more energy than it consumes. In this last study, cultivation and oil extraction dominated the energy use.

The benefits of the energy-driven biorefinery approach have been already showed by Harun *et al.* [2010], arguing a substantial process cost reduction by the co-production of methane, BioEthanol and BioDiesel. Likewise, according to Sander and Murthy [2010], each 24 kg (28 L, 1 GJ of energy) of algal BioDiesel, produces as well 34 kg of byproducts. If a cellulose-to-ethanol yield of 85% was assumed on the byproducts, it may result in additional 6.28 L of ethanol. Borowitzka and Moheimani [2013] also argued that an average yield of 0.13 L bioethanol kg⁻¹ algal biomass and

0.12 L biodiesel kg^{-1} algae biomass, may appear to be reasonable for biofuel valorisation.

In this work, it will be simulated the conjunction of known and optimized protocols and technologies for the biofuel application, proposing also a integrated energy biorefinery approach. The suggested process will be mainly focused in the BioDiesel production with the supplemental inclusion of BioEthanol as byproduct. There will be also shown the impact of innovative culturing technologies, such as High Volumetric PBR (AlgoFilm) and hybrid photovoltaic (PV)-PBR, on the net energy ratio of the full biofuel process.

5.2 Materials and Methods

5.2.1 Process description and System boundaries

An algorithm sequence in Excel (Microsoft, USA) has been used to simulate the liquid wet-pathway biofuel production process. Four operation blocks (each with its corresponding operation units) have been arranged for the overall production process (Fig. 5.1): Biomass production (Prod-100), Metabolite recovery (Rec-200), BioDiesel conversion (BioD-300) and BioEthanol conversion (BioE-400). Biomass production block encompasses the Photobioreactor (PBR-101) and Centrifugation (C-102); Metabolite recovery block includes Bead-Milling (BM-201) and Centrifugal Continuous Extraction (CX-202); the BioDiesel conversion block comprises a first Solvent Recovery (D-301), then Transesterification (R-302) and BioDiesel recovery (D-302); and finally the BioEthanol conversion block covers the Fermentation unit (R-401) and Ethanol recovery (D-402).

The system only considers four general mass inputs by the streams (S): culture medium (S-101), 2-methyl-tetra-hydrofuran, Me-THF (S-203), Methanol, Me-OH (S-303) and water dilution streams (S-202 and S-401). It also considers three outputs: BioDiesel (S-305), BioEthanol (S-403) and waste stream. Similarly, the only energy inputs considered were those related to electric operation of units. Energy outputs were Photovoltaic Energy (E_{PV}) and Energy from BioDiesel and BioEthanol (E_{BioD} and E_{BioE} respectively). Inputs like embodied energies, labour, pumping, inoculum and medium production, plant deconstruction and other maintenance sub-operations were not considered here.

Simulations were conducted for 1 Tn/y of dried biomass and operating full process time (t_{OP}) of 365 d. Therefore, the simulated continuous production process can be described as follows:

- 1) First, biomass is grown in PBR-101 (Flat panel) using S-101 as mass input. Main equipment description, protocols and strains are described in Table 5.1. For the PBR-101, besides electric energy for culture mixing, Passive Evaporative Cooling (PEC) and photovoltaic energy co-generation (PV) may be considered in some scenarios to impact the energy balance.
- 2) Next biomass is continuously harvested and may be concentrated using a continuous cen-

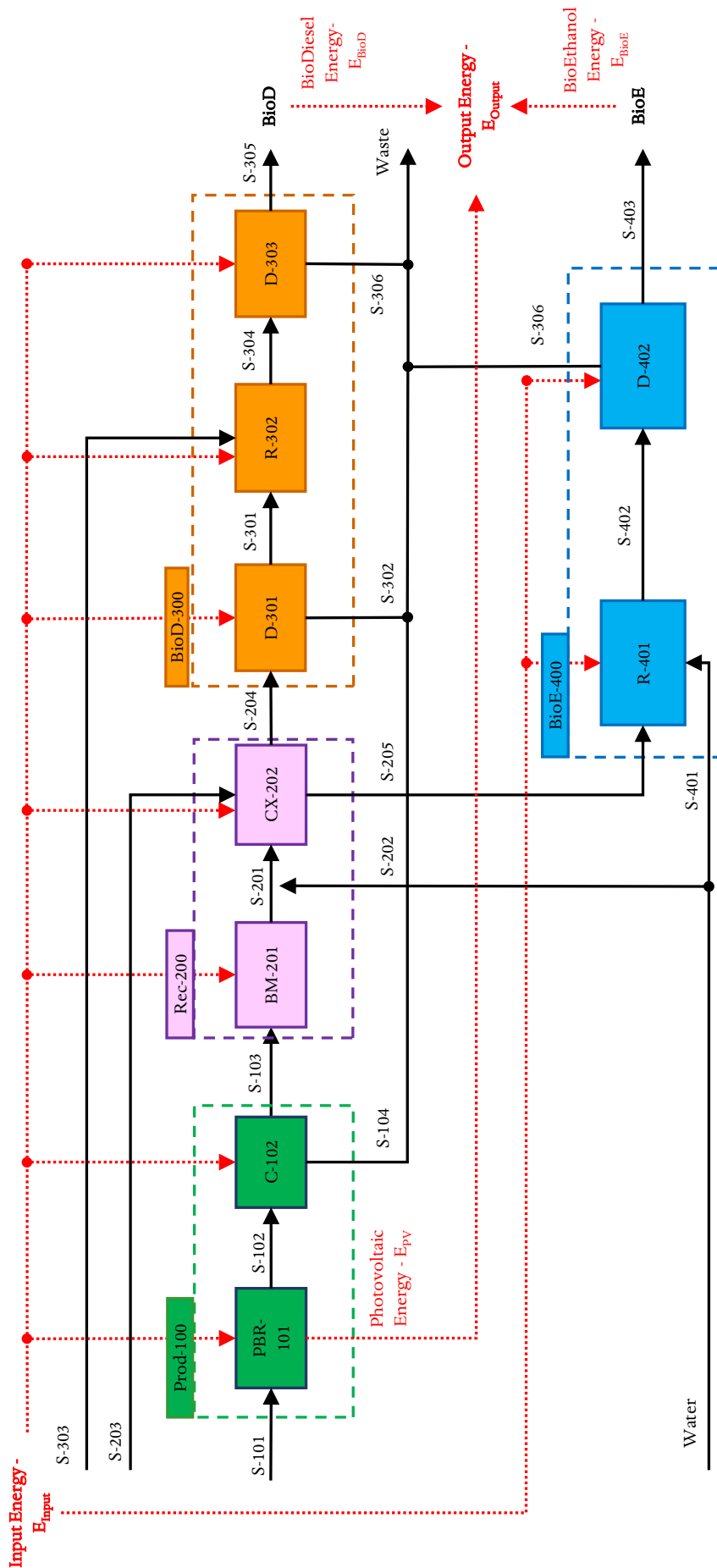


Figure 5.1: Mass and Energy scheme for the double biofuel recovery simulation. Red-dotted lines represent the energy input/output and black-continuous lines for the mass flow between operation units. Only when both red and black circles are indicated, split or mixing points should be assumed. Non-continuous lines (in four different colors) encompass the four operation blocks. Code: PBR: photobioreactor, C: centrifuge, BM: Bead Milling, CX: Continuous centrifugal extraction, D: Solvent recovery, R: Stirred reactor and S: stream.

trifuge. The mass outputs S-103 and S-104 go out directly to the disruption process and waste respectively. Energy input is here related to the centrifuge power.

- 3) The collected biomass pass into a vessel to be further batched to the cell disruption equipment BM-201 (Bead milling). Process output S-201 is then directed to CX-202. Energy consumption was considered only for impeller speed of the bead milling unit.
- 4) Then, stream S-201 is diluted for being used in the continuous centrifugal extraction equipment CX-202. During the operation Me-THF (S-203), is used to triacylglycerol (TAG) extraction. Then by centrifuge force action, two outputs are recovered: the stream S-204 which, full of solvent and TAG, is conducted to the BioDiesel conversion block; and the S-205 with the rest of polar components (carbohydrates among them) to the BioEthanol conversion block. Energy Input consider the power for the rotation of the mobile chamber of the centrifugal continuous extraction.
- 5) In the BioD-300 block, the solvent previously used may be recovered in D-301 by evaporation. Therefore the content of the stream S-301 is considered to be entirely composed by TAG molecules heading towards R-302; and S-302 only composed by Me-THF going to waste stream. Energy input only includes the theoretical latent heat for solvent evaporation.
- 6) Next transesterification reaction takes place in the stirred reactor R-302 using the TAG molecules and the Me-OH required for the reaction (S-301 and the S-303 respectively). Raw Fatty Acid Methyl Esters, FAME's (BioDiesel) then go to D-303 for the final treatment. Stirring and heating were considered for the energy input calculation.
- 7) BioDiesel final treatment occurs in the BioDiesel recovery unit D-303, separating residual Me-OH and the fatty acid methyl esters, FAME. The BioDiesel product is recovered in the stream S-305 and residual Me-OH in the S-306. No particular technology has been proposed in this operation (standard separation).
- 8) The local output stream S-401 containing polar component and carbohydrates is used as input of the Fermentor R-401 for the BioEthanol conversion block. Simulation considers also a dilution stream S-401 to regulate the carbohydrate concentration if needed. S-402 directs Bioethanol enriched stream into the D-402 operation unit.
- 9) Finally, D-402 stands for the BioEthanol recovery unit. Also, no particular technology has been proposed for this operation (standard separation). Fermentation subproducts are part of the S-404 stream, while the refined BioEthanol is harvested in the S-403 stream.

Table 5.1: Description of operations used for 1 Tn/y biomass production at the PBR-101 unit.

Case	1 - 2 - 3	4	5
Operation mode	Nitrogen Limitation, Chemostat/continuous mode, continuous light	Nitrogen Limitation, Chemostat/continuous mode, day-night cycles (DNc)	Nitrogen Limitation, Chemostat/continuous mode, continuous light
Strain	<i>Nannochloropsis gaditana</i>	<i>Nannochloropsis gaditana</i>	<i>Parachlorella kessleri</i>
Surface Productivity - S_X (kg/m²·d)	0.0148	0.009	0.01296
Dilution rate - D (h⁻¹)	0.01	0.005	0.01
TAG content - %_X TAG	15	30	20
Carbohydrates content - %_X Sg	23	20	64
Recoverable fuel energy, 100% efficiency - E_P (MJ/y)	9 090	14 641	16 599
<i>Recoverable BioDiesel energy, at 100% efficiency - $E_{P,BioD}$ (MJ/y)</i>	5 943	11 901	7 886
<i>Recoverable BioEthanol energy, at 100% efficiency - $E_{P,BioE}$ (MJ/y)</i>	3 147	2 740	8 714

5.2.2 Operation Units description

For all the streams, the total mass flow rate (M_T , kg/d) may be calculated as:

$$M_T = M_X + M_W + M_S + M_{Me-OH} + M_{BioD} + M_{BioE} + M_Z \quad (5.1)$$

$$M_X = M_{TAG} + M_{Sg} + M_{XR}$$

where M_W is for water, M_S for solvent, M_{Me-OH} for Me-OH, M_{BioD} for BioDiesel, M_{BioE} for BioEthanol, M_Z for waste and M_X for biomass. The latter divided in sub-fractions of TAG (M_{TAG}), carbohydrates (M_{Sg}) and residual biomass (M_{XR}).

5.2.2.1 Photobioreactor, PBR-101

For all the simulated scenarios, the culture was supposed in continuous mode. According to the culture protocol used and simulation cases, the values set as inputs were surface productivity, S_X (kg/m²·d); TAG and carbohydrate contents as fraction of the dry biomass concentration (%_XTAG and %_XSg respectively); dilution rate, D (h⁻¹); and specific illuminated area, a_s (1/m). Then, using the S-101 flow rate Q_{S101} the following equations were calculated:

$$P_X = S_X \cdot a_s$$

$$L = 1/a_s$$

$$V_{Op} = Q_{S101}/D$$

$$A^* = V_O/L \quad (5.2)$$

$$Q_{S101} = Q_{S102}$$

$$X_{S102} = S_X \cdot a_s/D$$

where P_X is biomass volumetric productivity ($\text{kg}/\text{m}^3 \cdot \text{d}$), V_{Op} is the culture operating volume (m^3), A^* is the illuminated surface (m^2) and X is the dry biomass concentration (kg/m^3). Production volume was adjusted for achieving 1 Tn/y of dry biomass at the S-102 stream, depending of volumetric productivity value.

Two main energy consumptions may be considered for culture stage: energy for agitation by air injection E_{El} (MJ/y) and energy for pumping fresh water for the passive evaporative cooling system (PEC) E_Q (MJ/y). The PEC is a system utilizing freshwater spray on the illuminated surface of the PBR to regulate the temperature by evaporation, as described in Nwoba *et al.* [2020].

The total energy input of the operation $E_{Input,PBR101}$ is the sum of these two values. These were obtained by:

$$\begin{aligned} E_{El,PBR101} &= P_{El,PBR101} \cdot V_O \cdot t_{OP} \\ E_{Q,PBR101} &= P_{Q,PBR101} \cdot V_O \cdot t_{OP} \\ E_{Input,PBR101} &= E_{El,PBR101} + E_{Q,PBR101} \end{aligned} \quad (5.3)$$

$P_{El,PBR101}$ and $P_{Q,PBR101}$ are the related specific power (1.8 and 1.2 kWh/ $\text{m}^3 \cdot \text{d}$ respectively) based on the power values reported by Nwoba *et al.* [2020] and Tredici *et al.* [2015].

5.2.2.2 Centrifugation, C-102

Centrifugation process was considered as a continuous process. The mass balance inputs were flow rate and biomass components of the stream S-102 (Q_{S102} and $M_{X,102}$), as well as centrifuge efficiency (η_{C102} of 95%) and moisture percentage for the output ($\%_W$ at 5% w/w). Therefore the process was represented as follows:

$$\begin{aligned} M_{X,103} &= M_{X,102} \cdot \eta_{C102} \\ M_{W,103} &= M_{W,102} \cdot \%_W \\ Q_{103} &= M_{T,103} / \rho_W \end{aligned} \quad (5.4)$$

where ρ_W (water density, 1000 kg/m^3) was considered as an average density of culture broth.

Total energy for this operation was determined from:

$$E_{Input,C102} = Q_{103} \cdot P_{El} \cdot t_{OP} \quad (5.5)$$

using P_{El} as 2.07 kWh/ m^3 as calculated from Nwoba *et al.* [2020] and Tredici *et al.* [2015].

5.2.2.3 Bead-Milling, BM-201

Bead-Milling was simulated as batch process. Harvested biomass in S-103 stream was stored in a intermediate tank to be further processed at BM-201. From Chapter 4, it is known that a highly resistant microalgae strain, such as *N. gaditana* at 10-30 kg/m³ dry biomass concentration, may achieve more than 80% disruption rate (τ_D) in 0.004 d (0.097 h). From the same work it is also possible to calculate the process time for the S-103 treatment by using the available information from the same bead-milling supplier (DYNO-Mill KD, WAB, Switzerland):

$$\begin{aligned}
 V_{eff,BM201} &= V_{BM201} \cdot T_{ff} \\
 Q_{103a} &= V_{eff,BM201}/t_D \\
 Q_{103} &= V_{Op,Tank} \\
 t_{Op,BM201} &= V_{Op,Tank}/(Q_{103a} \cdot N_{OEq,BM201})
 \end{aligned} \tag{5.6}$$

where $V_{eff,BM201}$ is the effective grinding chamber volume (m³) for a particular bead-milling device with nominal grinding chamber volume V_{BM201} (m³) and filled percentage value T_{ff} of 45.4%; Q_{103a} stands for a theoretical stream going out from the tank; and t_D is the disruption residence (d) with value of 0.004 d.

Then, considering that the S-103 flow rate must be processed in a day, it can be assumed equal to the tank volume $V_{Op,Tank}$ (m³). Therefore, the operating time for the BM-201, $t_{Op,BM201}$, takes in count the tank volume, the theoretical stream Q_{103a} and an iterative value for the number of equipments, $N_{OEq,BM201}$, to adjust the operating time.

The energy consumption, can be calculated by using the nominal power $P_{El,BM201}$, (kW) for a particular device (also provided by the supplier):

$$E_{Input,BM201} = P_{El,BM201} \cdot N_{OEq,BM201} \cdot t_{Op,BM201} \tag{5.7}$$

5.2.2.4 Centrifugal Continuous Extraction, CX-202

The centrifugal continuous extraction device was considered as a continuous process. Input values are for the optimized protocol from Chapter 4. There the process needs to consider the dilution of S-201 stream (to 7.9 kg/m³ biomass concentration) for archiving 89% of TAG extraction efficiency $\eta_{E,TAG}$ using an optimal solvent to feed inlet ratio (S/F) of 1.65. Using the latter, it is calculated the amount fo solvent Me-THF to be used in the S-203. The calculations describing this operation

unit were:

$$\begin{aligned}
 Q_{203} &= S/F \cdot Q_{201a} \\
 ToT &= Q_{203} + Q_{201a} = Q_{204} + Q_{205} \\
 M_{TAG,204} &= M_{TAG,201a} \cdot \eta_{E,TAG} \cdot \tau_D \\
 M_{Sg,205} &= M_{TAG,201a}
 \end{aligned} \tag{5.8}$$

where the stream S-201a is the dilution of S-201, and τ_D corresponds to the disruption rate achieved in BM-201. The process was considered to not create emulsions, and so streams S-204 and S-205 will only contain TAG and cell debris (carbohydrates among them) respectively. ToT is the total flow supplied and determine the size and nominal power $P_{El,CX202}$ (kW). Such values are provided by the centrifugal continuous extraction supplier (Rousselet Robatel, France). Then, the energy consumption is calculated as follows:

$$E_{Input,CX202} = P_{El,CX202} \cdot N_{oEq,CX202} \cdot t_{OP} \tag{5.9}$$

where $N_{oEq,CX202}$ is the number of devices used for the extraction and t_{OP} the operating full process time.

5.2.2.5 Solvent Recovery, D-301

The Me-THF used during the CX-202 process is continuously recovered in the solvent recovery unit D-301. Simulation considers a perfect separation of the components by evaporation. Therefore it is assumed:

$$\begin{aligned}
 M_{TAG,204} &= M_{TAG,301} \\
 M_{S,302} &= M_{S,204}
 \end{aligned} \tag{5.10}$$

For energy consumption calculation it was only assumed the theoretical latent heat required for phase change:

$$E_{Input,D301} = \Delta H_{vap} \cdot M_{S,204} \cdot t_{OP} \tag{5.11}$$

with ΔH_{vap} as the specific latent heat of Me-THF (375 MJ/kg_{MeTHF} [Sicaire *et al.*, 2014]); and t_{OP} the operating full process time.

5.2.2.6 Transesterification, R-302

Me-OH Continuous conversion of TAG into fatty acid methyl esters (FAME, Biodiesel) takes place in the stirred reactor R-302. The process is described by the following equations:

$$\begin{aligned}
 M_{BioD,304} &= (M_{TAG,301}/MW_{AlgLip}) \cdot 3 \cdot Y_{Trans} \cdot MW_{FAME} \\
 M_{T,303} &= (M_{TAG,301}/MW_{AlgLip}) \cdot (Me-OH/TAG) \cdot MW_{Me-OH}
 \end{aligned}
 \tag{5.12}$$

where MW is the molecular weight of algal lipids, FAME or Me-OH (920, 299.32, 32.04 g/mol respectively) based on Faried *et al.* [2017]. The value of 3 in the first equations, represents the stoichiometric coefficient of FAME products during transesterification. It has been shown that high transesterification yields Y_{Trans} may only be achieved when using a 6 or 12 Me-OH-to-TAG-moles ratio ($Me-OH/TAG$) [Faried *et al.*, 2017, Fukuda *et al.*, 2001]. For the purpose of this work it has been used a ratio of 6 $Me-OH/TAG$ yielding 98% conversion in the reaction.

For the calculation of energy consumption, the work of Batan *et al.* [2010] has been used as reference. The author has reported specific energies for stirring and heating based on the amount of biodiesel produced, leading to:

$$E_{Input,R302} = (P_{El,R302} + P_{Q,R302}) \cdot M_{BioD,304} \tag{5.13}$$

with $P_{El,R302}$ and $P_{Q,R302}$ for the specific energies for stirring and heating respectively with values of 0.03 kWh/kg $_{BioD} \cdot y$ and 2.1 MJ/kg $_{BioD} \cdot y$ respectively.

5.2.2.7 Fermentation, R-401

Another stirred reactor R-401 was considered to perform the fermentation reaction. It takes as input the mass of carbohydrates contained in the S-205 stream, $M_{Sg,205}$. The simulation used the values reported by Karemore and Sen [2016], which also deal with lipid extraction followed by chemical pretreatment of the residual biomass with H_2SO_4 (not simulated) and fermentation by *Saccharomyces cerevisiae*. Under this protocol 90% of carbohydrates $\eta_{Fer,Sg}$, were converted into BioEthanol with a yield Y_{Fer} , 0.23 kg $_{BioE}/kg_{Sg}$ (theoretical yield of Ethanol conversion, 0.51 kg $_{BioE}/kg_{Sg}$ [Lee *et al.*, 2001, Okamoto *et al.*, 2014]). Calculations used to describe the fermentation process were:

$$\begin{aligned}
 M_{BioE,402} &= M_{Sg,205} \cdot Y_{Fer} \\
 M_{Sg,402} &= M_{Sg,205} \cdot (1 - \eta_{Fer,Sg})
 \end{aligned}
 \tag{5.14}$$

The energy consumption was based on the specific power $P_{El,R401}$ related to the algal biomass

produced in PBR-101, accounting 0.05 MJ/kg_X:

$$E_{Input,R401} = (P_{El,R401} \cdot M_{X,102} \cdot t_{OP}) \quad (5.15)$$

5.2.2.8 BioEthanol and BioDiesel recovery, D-402 and D-303

The final stages in the BioEthanol and BioDiesel production (D-402 and D-302 respectively) involve the same process inputs for the mass balance simulation. It was considered the operation efficiency (η_{D402} or η_{D303}) and the purity achieved with that process (Pu_{D402} or Pu_{D303}). The final liquid biofuel is recovered in the streams S-403 and S-305 for BioEthanol ($M_{BioE,403}$, kg/d) and BioDiesel ($M_{BioD,305}$, kg/d) respectively. This leads to the following equations:

$$\begin{aligned} M_{BioD,305} &= M_{BioD,304} \cdot \eta_{D303} \cdot Pu_{D303} \\ M_{TAG,305} &= M_{TAG,304} \cdot \eta_{D303} \cdot (1 - Pu_{D303}) \end{aligned} \quad (5.16)$$

$$\begin{aligned} M_{BioE,403} &= M_{BioE,402} \cdot \eta_{D402} \cdot Pu_{D402} \\ M_{Sg,403} &= M_{Sg,402} \cdot \eta_{D402} \cdot (1 - Pu_{D402}) \end{aligned} \quad (5.17)$$

No particular technology for both recoveries was suggested in calculations. Energy consumption was then not considered. Note that some purification processes for BioEthanol, like distillation, which could be high energy-consuming, were not included here. This aspect will be discussed later.

5.2.3 Output Calculations

Recoverable Fuel energy E_P (MJ/y) was described as the energy that can be recovered in a 100% efficient process, and so it shows the maximal energy achievable for the biomass produced. It sums the Recoverable BioDiesel energy $E_{P,BioD}$ (MJ/y) and the Recoverable BioEthanol energy $E_{P,BioE}$ (MJ/y). Calculations of Recoverable BioDiesel and BioEthanol energies considered, in addition, the maximal theoretical yield in the stoichiometric reactions. This leads to:

$$E_{P,BioD} = (S_X \cdot \%_X TAG / MW_{AlgLip}) \cdot \eta_{E,TAG} \cdot 3 \cdot Y_{Trans} \cdot MW_{FAME} \cdot \Delta H_{comb,BioD}^\circ \cdot A^* \cdot t_{OP} \quad (5.18)$$

$$E_{P,BioE} = (S_X \cdot \%_X Sg) \cdot \eta_{E,Sg} \cdot Y_{Fer} \cdot \Delta H_{comb,BioE}^\circ \cdot A^* \cdot t_{OP} \quad (5.19)$$

$$E_P = E_{P,BioD} + E_{P,BioE} \quad (5.20)$$

As it can be noted, equations considered the extraction recovery efficiency of the full process for TAG and carbohydrates ($\eta_{E,TAG}$ and $\eta_{E,Sg}$) as 100%. The same was considered for the transesterification yield Y_{Trans} , but not for the fermentation yield Y_{Fer} where Lee *et al.* [2001], Okamoto *et al.* [2014]

have referred a $0.51 \text{ kg}_{BioE}/\text{kg}_{Sg}$ for the theoretical value. For Heat of combustion for BioDiesel and BioEthanol ΔH_{comb}° were 40.4 and 26.7 MJ/kg $_{BioFuel}$ respectively [Faried *et al.*, 2017, Khuong *et al.*, 2016, Xu *et al.*, 2006]; Note that the illuminated surface A^* of the culture system is specific for each simulation case.

Likewise, with the mass and energy balances, it was calculated the actual energy obtained from the liquid biofuels produced and the total energy invested for the process involved. The energy obtained from BioDiesel E_{BioD} (MJ/y) and BioEthanol E_{BioE} (MJ/y) was calculated as follows:

$$E_{BioD} = M_{BioD,305} \cdot \Delta H_{comb,BioD}^{\circ} \cdot t_{OP} \quad (5.21)$$

$$E_{BioE} = M_{BioE,403} \cdot \Delta H_{comb,BioE}^{\circ} \cdot t_{OP} \quad (5.22)$$

Some simulations include the co-generation of photovoltaic energy E_{PV} in the PBR-101. This was calculated based on the values reported by Nwoba *et al.* [2020], where each installed PBR of 1.8m^2 produced 110.2 kWh/y (for solar irradiance 16–28 MJ/m 2 ·y and 7–9 sunlight hours per day). This brings a photovoltaic specific power $P_{PV,PBR101}$ of 61.23 kWh/m 2 ·y. The photovoltaic energy recovered from the culture unit may be simply calculated by:

$$E_{PV} = P_{PV,PBR101} \cdot A^* \quad (5.23)$$

Therefore, the total energy produced by the simulated process is the sum of the latter equations including, if mentioned, the photovoltaic energy produced in PBR-101. Final energy output is then:

$$E_{Output} = E_{BioD} + E_{BioE} + E_{PV} \quad (5.24)$$

Finally, the net energy ratio NER was calculated as follows:

$$NER = E_{output}/E_{input} \quad (5.25)$$

where E_{input} accounts the sum of all the energy inputs from each equipment along all the process.

Because simulations were conducted for the same produced biomass (1 Tn/y), different NER were obtained for the simulations cases, but differing only in the values used as energy output. It was also calculated the different NER values considering the Recoverable Fuel energies (100% efficiency) to know the maximal potential of each simulation case. These are referred as:

- a) NER_{BioD} , 100% eff., for only the BioDiesel production process and photovoltaic energy production (Prod-100 + Rec-200 + Bio-300 inputs energies and $E_{P,BioD} + E_{PV}$ output energies);
- b) NER_T , 100% eff., for double biofuel recovery and photovoltaic energy production (Prod-100 + Rec-200 + Bio-300 + BioE-400 inputs energies and $E_{P,Output} = E_{P,BioD} + E_{P,BioE} + E_{PV}$

Table 5.2: Simulated characteristics for the PBR-101 unit for 1 Tn/y of produced biomass. FP is for Flat Panel; HVP is High Volumetric Productivity PBR; PEC is Passive Evaporative Cooling; IGU is Insulated Glass Unit.

Case	1	2	3	4	5
PBR Technology	FP	FP	HVP	HVP	HVP
Heat control technology	PEC	IGU	IGU	IGU	IGU
Photovoltaic generation	no	yes	yes	yes	yes
Illuminated surface, A^* (m²)	185.42	185.42	185.42	306.25	211.27
Operating Volume, V_{Op} (m³)	18.54	18.54	0.37	0.61	0.42
Specific Illuminated area, a_s (1/m)	10	10	500	500	500
PBR culture depth, L (m)	0.100	0.100	0.002	0.002	0.002

output energies);

- c) NER_T ($-E_{PV}$), 100% eff., also for double biofuel recovery but without considering the photovoltaic energy produced (Prod-100 + Rec-200 + Bio-300 + BioE-400 inputs energies and $E_{P,Output} = E_{P,BioD} + E_{P,BioE}$ output energies).

Similarly, the same relations have been used to describe the actual NER when considering process efficiencies, NER_{BioD} , NER_T , NER_T ($-E_{PV}$). In this case, the actual energies from liquid biofuels (E_{BioD} , E_{BioE} and E_{PV}) obtained after process efficiencies, were used for calculations instead of the Recoverable Fuel energies.

5.2.4 Simulation Cases Description

Five cases have been proposed in this work in order to simulate 1 Tn/y of microalgae culture. Downstream technologies for operation blocks Rec-200, BioD-300 and BioE-400 have been maintained for all the cases. Minor considerations regarding the size, number and power of the equipments may have been adapted at each case to treat the resultant flow rate. In contrast, the operation block Prod-100 varied relative to the technologies used at the PBR-101. The main characteristics of the latter in the simulated cases are presented in Table 5.2. Likewise operations mode, strains and culture productivities are summarized in Table 5.1. The simulated cases are then:

Case 1: The Prod-100 block is a Flat Panel photobioreactor FP-PBR of 10 cm depth, air injection for culture mixing and heat control by passive evaporative cooling (PEC), [Nwoba

et al., 2020]. It represents the culture of *Nannochloropsis gaditana* under continuous mode/chemostat (dilution rate D , 0.01 h^{-1}), continuous light ($250 \mu\text{mol}/\text{m}^2\cdot\text{s}$) and nitrogen limitation ($56\%_{NO_3}$ of the original medium formulation) according to the results of Chapter 2.

Case 2: The Prod-100 block is a FP-PBR of 10 cm depth and air injection for culture mixing. Heat control was simulated using the insulated glass unit IGU, with an integrated energy-generating photovoltaic PV, as presented by Nwoba *et al.* [2020]. Same protocol used in case 1 was applied: culture of *N. gaditana* under continuous mode/chemostat (D , 0.01 h^{-1}), continuous light ($250 \mu\text{mol}/\text{m}^2\cdot\text{s}$) and nitrogen limitation ($56\%_{NO_3}$) for *N. gaditana*.

Case 3: A High Volumetric Productivity photobioreactor HVP-PBR [Pruvost *et al.*, 2016] was simulated for the Prod-100 block. The HVP-PBR was considered to have 2 mm depth, air injection for culture mixing, the IGU for heat control and the co-generation of PV energy. Similar to cases 1 and 2, this scenario included the same culture protocol for *N. gaditana*, *ie.* culture of *N. gaditana* under continuous mode/chemostat (D , 0.01 h^{-1}), continuous light ($250 \mu\text{mol}/\text{m}^2\cdot\text{s}$) and nitrogen limitation ($56\%_{NO_3}$).

Case 4: The fourth simulation included a HVP-PBR of 2 mm depth, air injection for culture mixing, the IGU for heat control and the co-generation of PV energy. In this case, the protocol used to grow *N. gaditana* was based on protocol proposed in the Chapter 3. It uses the simultaneous use of continuous production at dilution rate D of 0.005 h^{-1} , nitrogen limitation at $29\%_{NO_3}$ and light supply in simulated day-night cycles with average photon flux density of $269 \mu\text{mol}/\text{m}^2\cdot\text{s}$.

Case 5: For the last scenario, the Prod-100 used the same PBR unit (HVP-PBR of 2 mm depth, air injection, IGU+PV) as for case 4, but a culture of *Parachlorella kessleri* producing simultaneously large amounts of TAG and carbohydrates was considered based on the results obtained by Kandilian *et al.* [2019]; *ie.* continuous mode operation under a dilution rate D of 0.01 h^{-1} , continuous light at $250 \mu\text{mol}/\text{m}^2\cdot\text{s}$ and nitrogen limitation at $46\%_{NO_3}$ of the original medium formulation.

5.3 Results and Discussion

5.3.1 Analysis of Culture system impact

Results from the five simulation cases are presented in Tables 5.3 and 5.4.

Cases 1, 2 and 3 allowed to compare the three productive systems for the BioDiesel production

Table 5.3: Liquid biofuel produced volumes and Input/Output Energies for the five simulation cases. All the values correspond to a total production of 1 Tn/y of microalgal biomass.

Case		1	2	3	4	5					
Total Processes Energy-E_{Input} (MJ/y)											
Prod-100	PBR-101	85 292	73 188	55 739	43 635	873	873	1 441	1 441	995	995
	C-102		12 104		12 104		0		0		0
Rec-200	BM-201	63 845	63 056	63 845	63 056	25 733	24 945	41 989	41 201	29 225	28 437
	CX-202		788		788		788		788		788
BioD-300	D-301	64 159	63 954	64 159	63 954	67 535	67 320	67 835	67 404	67 278	66 992
	R-302		205		205		215		431		286
BioE-400	R-401	50	50	50	50	50	50	50	50	50	50
	Total E_{Input}	213 345		183 793		94 191		111 316		97 548	
Biofuel volume produced (L/y)											
	BioD		93		93		98		196		130
	BioE		52		52		55		48		152
	Total biofuel		145		145		153		244		282
Produced Energy (MJ/y)											
	E_{BioD}		3 201		3 201		3 369		6 746		4 470
	E_{BioE}		1 100		1 100		1 158		1 008		3 206
	$+E_{PV}$		0		40 870		40 870		67 504		46 592
	E_{Output}		4 300		4 300		4 527		7 754		7 676
	$E_{Output} (+E_{PV})$				45 170		45 397		75 259		54 268

only. The main differences were related to biomass concentration as obtained from PBR intensification and energy consumption by heat control.

Flat-Panel PBR (cases 1 and 2) used 18.5 m^3 of operating volume and 185.4 m^2 of illuminated surface to produce 1 Tn/y of biomass. In contrast, the HVP-PBR (case 3) only required 0.4 m^3 for the same production surface. Since the three technologies used the same surface productivity for the simulations, they were expected to have equal values of produced biomass and illuminated surface. However, at the end of the Prod-100 block, the impact of the HVP-PBR regarding the achievement of high biomass concentrations (31 kg/m^3 , Eq. 5.2) during the culture, made unnecessary the use of a centrifuge stage to concentrate the biomass and, consequently, it is also avoided the mass losses linked to centrifugation efficiency. FP-PBR achieved a final concentration of 0.62 kg/m^3 , which would be concentrated up to 11.6 kg/m^3 (955 kg/y after centrifugation). Just by adding a centrifuge unit, the input energy for FP-PBR adds $12\,104 \text{ MJ/Tn.y}$ to the final input energy of the Prod-100 block. This energy is then avoided when using the HVP-PBR system.

Regarding the heat control system, the FP-PBR with the PEC system (case 1) consumed $73\,188 \text{ MJ/y}$, of which $29\,552$ were for spraying water for the PEC, and $43\,635$ for mixing by air injection. This consumption was the largest in all the simulated operations. Some energy can be saved if the PEC system is replaced for the insulated glass unit IGU. This leads to avoid the passing of $>90\%$ of UV-IR spectral light components, while still letting pass more than 75% of visible light through the PBR [Nwoba *et al.*, 2020]. By the use of this technology, it was possible to consume in case 2 only $43\,635 \text{ MJ/y}$ as required for mixing by air injection. Notably, the specific energies linked to the PBR-101 are dependent of the volume of culture and so if the volume is reduced, as in case 3, the energy input will be also reduced. As consequence, the HVP-PBR required only 873 MJ/y for mixing by air injection.

Another interest of using the IGU, is the partial photovoltaic conversion of filtered light. The system FP-PBR of case 2 and the HVP-PBR (case 3) then included the co-generation of photovoltaic energy, adding $40\,870 \text{ MJ/y}$ to the total energy production.

For the Prod-100 block only and for the first three cases, it can be simulated the NER_{BioD} by considering as constant all the energy inputs and without biomass losses. In this optimal conditions, the FP-PBR+PEC can only achieve 0.07 , contrasting with the optimal value for FP-PBR+IGU+PV at 0.84 ; closer to energy neutrality. When introducing the HVP-PBR+IGU+PV (case 3), it significantly increased the NER_{BioD} with an optimal value of 53.6 . The main difference relates on the co generation of photovoltaic energy and the avoidance of energy input for heat control. The same trend can be found when taking into account the actual biomass losses by device efficiency: FP-PBR+PEC reached 0.04 , FP-PBR+IGU+PV obtained 0.8 while the HVP-PBR+IGU+PV system still have the largest ratio at 50.7 .

It can clearly be noticed that the system FP-PBR+PEC (case 1) is energetically unsustainable

because of its heat control system (besides the fact that it also consume excessive amounts of water to the task; not considered in this work). Meanwhile, the use of PBR constructed on insulated glass with photovoltaic panels may bring a substantial increase of the energy ratio, with a energy surplus that may be used to sustain other operations along the full production process (see later).

By adding downstream processing units (Rec-200 and BioD-300), it can be noticed the decrease of NER (Table 5.4).

For both 1 and 2 cases, equal energies of 63 845 and 64 159 MJ/y were consumed for the operation blocks Rec-200 and BioD-300 respectively. Bead milling operation BM-201 and solvent evaporation after extraction D-301 were found to contribute the most with 63 845 and 64 159 MJ/y respectively (>98% of their respective production blocks). Meanwhile, because of the increase in the biomass concentration, case 3 (HVP-PBR+IGU+PV) only used 25 733 and 67 535 MJ/y for Rec-200 and BioD-300 respectively.

Adding the entire downstream operations to the FP-PBR+PEC culture system, the NER_{BioD} 100% eff. diminishes from 0.07 to 0.03. The same trend occurs even with the FP-PBR+IGU+PV: the entire downstream units reduce the NER_{BioD} 100% eff. from 0.84 to 0.25. On the contrary the excess of energy generated by the HVP-PBR+IGU+PV system, could be used to endure some of the downstream operations. When just adding the metabolite recovery block Rec-200 to the latter, the energy balance is still positive (NER_{BioD} 100% eff. > 1) passing from 53.64 to 1.76; and from 50.69 to 1.66 when considering efficiency losses; *ie.* corresponds approximately to 30 times less the NER at the Prod-100 block only. Next, when adding the BioDiesel conversion BioD-300 block, the NER_{BioD} 100% eff. turned to 0.50 (0.47 with efficiency losses). It evidences the high impact of downstream processing on the biofuel production process, even if the production block has a large energy surplus. Systems generating PV energy (+40 870 MJ/y) may compensate some of the energy of downstream, however it is still not enough to turn positive the energy balance.

Meanwhile, it may be concluded that PEC and PV addition to FP system (FP+PEC or FP+IGU+PV) are still far of providing enough energy saving to improve the NER_{BioD} in the full production process. So far in this work, the HVP-PBR+IGU+PV seems to be most promising regarding the objective of NER > 1 (positive energy balance). However it is still necessary to improve the energy production or energy savings, either by applying novel production protocols, more promising strains or replacing operation units in the downstream block for others less energy-consuming ones, as it is investigated later.

Table 5.4: Net Energy Ratio for the five simulation cases. For each simulation case, each column of the resulting NER is accumulative over the precedent, *i.e.* the third column is the modified NER value for Prod-100, after the inclusion of the rest of downstream stages in the NER calculation.

Case	1		2		3		4		5						
	Prod-100	+Rec-200	+BioD-300 +BioE-400												
NER_{BioD} , 100% eff.	0.07	0.04	0.03	0.84	0.39	0.25	53.64	1.76	0.50	55.09	1.83	0.71	54.76	1.80	0.56
$NER_T (+E_{BioE})$, 100% eff.	0.11	0.06	0.04	0.90	0.42	0.27	57.25	1.88	0.53	56.99	1.89	0.74	63.52	2.09	0.65
$NER_T (-EPV)$, 100% eff.				0.16	0.08	0.05	10.42	0.34	0.10	10.16	0.34	0.13	16.68	0.55	0.17
NER_{BioD}	0.04	0.02	0.02	0.79	0.37	0.24	50.69	1.66	0.47	51.51	1.71	0.67	51.32	1.69	0.52
$NER_T (+E_{BioE})$	0.05	0.03	0.02	0.81	0.38	0.25	52.02	1.71	0.48	52.21	1.73	0.68	54.55	1.80	0.56
$NER_T (-EPV)$				0.08	0.04	0.02	5.19	0.17	0.05	5.38	0.18	0.07	7.72	0.25	0.08

5.3.2 Analysis of culture protocol and double biofuel conversion

5.3.2.1 Outdoors culture protocol

Chapter 3, suggests an interesting protocol based on the continuous production under nitrogen limitation and day-night cycles. This protocol is also closer to actual operative outdoors conditions (*ie.* solar culture). This protocol was combined in case 4 with the HVP-PBR+IGU+PV system to be compared with the protocol established in case 3, which also includes continuous mode and nitrogen limitation in the same culture system but under continuous light. It has to be noted that continuous light is commonly used to characterize strain growth performances, including lipid production. However, such conditions are far to the actual outdoors conditions, where light is changing as consequence of day-night cycles and climate events.

The comparison will also include the possibility of recovering the carbohydrates of the cell to be transformed into BioEthanol, in addition to the TAG molecules for BioDiesel. This, as part of an energy-driven biorefinery approach aimed to increase the energy output of the biofuel production process [Harun *et al.*, 2010, Karemore and Sen, 2016, Sivaramakrishnan and Incharoensakdi, 2018].

Outdoors conditions lead to an inferior biomass surface productivity ($0.009 \text{ kg/m}^2\cdot\text{d}$) which makes it to require 65% more illuminated surface and operating volume (306 m^2 and 0.61 m^3) than for the continuous light protocol (185 m^2 and 0.37 m^3) to produce 1 Tn/y of biomass. With a larger illuminated surface, the PV energy generated using the outdoors protocol, add up 67 504 MJ/y to the final energy output. Nevertheless more energy will be consumed during the processing because of the increased operating volume mainly for Prod-100 and Rec-200 blocks. Outdoors protocol would require 1 441 and 41 201 MJ/y for the mentioned blocks, while for the continuous light protocol in case 3, it would be required about 40% less energy input.

If it is considered both results in terms of TAG accumulation for BioDiesel production only, as obtained with *N. gaditana*, the resulting biomass from the outdoors protocol has 30%_X TAG content, which is the double than for the continuous light protocol (Table 5.1). More available TAG in the former leads to produce as well two times more BioDiesel volume (196 L/y , $6\,746 \text{ MJ/y}$) than for the latter protocol (98 L/y , $3\,369 \text{ MJ/y}$).

If NER_{BioD} is then calculated, the BioDiesel production process under the two mentioned protocols in cases 3 and 4 reveals energy-efficient ($NER > 1$) for the operation blocks of production and metabolite recovery (Prod-100 + Rec-200). Particularly, the obtained NER_{BioD} for the culture protocol under simultaneous nitrogen limitation and day-night cycles, retrieved 51.5 for the Prod-100 block; which decreased to 1.7 when the downstream process Rec-200 was added. However, by adding the final conversion into BioDiesel retrieved NER_{BioD} of 0.67 (NER_{BioD} 100% eff. of 0.71). These values are similar to those already discussed for the protocol and system in case 3, but with the convenience that the former protocol takes into account the day-night cycles for an

actual outdoors biofuel production.

5.3.2.2 Double Biofuel valorization

The presented outdoors protocol may achieve a larger recoverable fuel energy when the full conversion of all the energy stock molecules into biofuels is considered. Table 5.1 presents for 1 Tn of produced biomass, 14 641 MJ/y from energy by liquid biofuels; *ie.* BioDiesel (11 901 MJ/y) and BioEthanol (2 740 MJ/y). Meanwhile, the protocol under continuous light (cases 1,2,3) may produce 9 090 MJ/y (5 943 MJ/y for BioDiesel and 3 147 MJ/y for BioEthanol) from energy by liquid biofuels. The differences are mainly due to the content of TAG/carbohydrates available in the cell and the surface productivity, as obtained here from *P. kessleri* in DNe.

In second instance, if it is considered the addition of BioEthanol (issued from the conversion of carbohydrates from a *P. kessleri* culture) to the outdoors protocol simulation, it may be added up 1 008 MJ/y. With this inclusion the entire process invest 111 316 MJ/y of energy. The $NER_T(+E_{BioE})$ associated to this double biofuel recovery slightly increases to 0.68 for the full production process (NER_{BioD} 100% eff. of 0.74). If the PV energy is not considered in the calculations, the $NER_T(-E_{PV})$ would sharply decrease to 0.07, revealing again the importance of PV energy co-generation in the Prod-100 block. However, the recovery of 48 L/y of BioEthanol in the outdoors protocol, increases 24% the product valorization of the process, to finally produce 244 L/y; *ie.* 7 754 MJ/y for liquid fuels only and 75 259 MJ/y when including PV energy.

Notably, the double biofuel recovery approach takes advantage of the amount of carbohydrates and lipids available in the cell to be converted into liquid biofuels. Therefore, microalgae culture protocols where biomass accumulates larges amounts of these molecules, are ideal for the process. Strains such as *Parachlorella kessleri* are then of interest. As detailed by Kandilian *et al.* [2019], *P. kessleri* accumulates 64%_X carbohydrates and 20%_X TAG of biomass for a continuous nitrogen limitation and continous light (Table 5.1).

The total recovered liquid biofuel volume from *P. kessleri* was larger than previous simulations with *N. gaditana*, allowing to recover 282 L/y in total; of which 130 L/y corresponds to BioDiesel and 152 L/y corresponds to BioEthanol. These volumes were found to be 3.2 times larger for the BioEthanol and 0.66 times less for BioDiesel than the volumes recovered with *N. gaditana* in the most productive simulation here presented (case 4).

For a 100% efficiency process as described for simulation case 5, recoverable fuel energy with *P. kessleri* has been calculated in 16 599 MJ/y; of which $E_{P,BioD}$ is 7 886 MJ/y, and $E_{P,BioE}$ is 8 714 MJ/y. The process restricted to BioDiesel would have a final NER_{BioD} , 100% eff. of 0.65 and the process considering the double biofuel valorization will have $NER_T(+E_{BioE})$, 100% eff. of 0.65. This indicates no significant increase in the net energy ratio. Likewise, when efficiency losses along the process are considered, similar results are obtained (NER_{BioD} of 0.52 and $NER_T(+E_{BioE})$

of 0.56). This results also indicate that the co-production of BioEthanol does not increase the energy balance, but only increases the amount of biofuel produced. This increase is compensated by the additional energy investment from the processes used to obtain BioEthanol. Furthermore, note that energies for both BioDiesel and BioEthanol purification were not considered here. Those purification steps would be different for both. Recovering the BioEthanol from the fermentation broth could request a distillation process, which should be much more energy-consuming than for Me-OH and FAME separation.

It can be noticed from Tables 5.1 and 5.3, that there exists a difference between the recoverable fuel energy and the actual recovered energy (E_{Output} of 7 676 MJ/y), losing about 65% of the recoverable energy only by BioEthanol. This is explained for the fermentation yield used in the operation unit R-401, which described a two-stages fermentation protocol for lipid-extracted biomass. For the simulations presented in this work, the carbohydrates concentrations going out from CX-202 device, were in the range of 0.6 to 5.1 kg/m³ depending on the production technology considered. In these conditions microalgal biomass hydrolysis yield, and therefore the BioEthanol conversion, might be significantly lower than the theoretic value, even if separate hydrolysis and fermentation may seem to be the best pretreatment for microalgal biomass [de Farias Silva and Bertucco, 2016, Ho *et al.*, 2013]. Furthermore, microalgae hydrolysate may contain inhibitory chemicals of ethanol fermentation which also would reduce the yield [Klinke *et al.*, 2004]. In practice, the BioEthanol recovery may also contribute in the final volume of the process. Since with lower carbohydrates concentrations, the BioEthanol concentrations at the end of fermentation also gets affected, a distillation process applied to the D-402 recovery unit, will not be energy efficient enough for the task, investing more energy to recover. Then, membrane technologies like those presented by Lewandowicz *et al.* [2011], Wei *et al.* [2014] may be suitable for a more energy-efficient biofuel process.

One of the main conclusion of this analysis is that even if the fermentation and recovery process are optimized, the maximum yield included in the net energy ratio at 100% efficiency for the full double biofuel recovery with *P. kessleri* remains below the energy neutrality ($NER_T(+E_{BioE})$, 100% eff. of 0.65). When using the energy output for the operation units described in this work, and the potentially recoverable fuel energy for *N. gaditana* from case 4 (14 641 MJ/y) and *P. kessleri* in case 5 (16 599 MJ/y), it has been calculated that the present protocols require a energy saving (or energy output) of at least 29 171 MJ/y and 34 357 MJ/y for the simulations in case 4 and 5 respectively. Such energy may be saved from the solvent recovery unit D-301 (which is the most energy-intensive of all the presented operations).

Likewise, it would be expected that further research may still be focused in the design of culture protocols enhancing the accumulation of energy stock molecules, metabolic engineering, exploring the strain potential of other microalgae species towards biofuel applications or the recovery of other sources of energy from a energy-biorefinery approach (*eg.* biohydrogen, methanization) [Adhikari

et al., 2009, Alalwan *et al.*, 2019, Brennan and Owende, 2010, Vitova *et al.*, 2014].

5.4 Conclusion

Simulations on the double biofuel recovery from microalgae allow to increase in 24-56% the volume liquid fuel produced depending on the chosen protocol, with similar overall NER. It has been shown that HPV-PBR combined with wet-biomass treatment, as well as the inclusion of insulated glass unit IGU and photovoltaic co-generation system is crucial to improve the NER. Reducing the input energy for cooling while simultaneously supplying more energy (photovoltaic) could be used to compensate the more energy-intensive of the downstream processes. These operations were found to be key option of the design of a sustainable microalgae-based biofuel process. Likewise, both *P. kessleri* and *N. gaditana* potentially recoverable energies under two different culture protocols lead closer to the energy neutrality only when also photovoltaic energy is co-generated. However even for the best simulated cases in this work, the NER gets drastically decreased by the extraction solvent recovery and the cell disruption units. Additional optimization for downstream processing and strain choice is then suggested.

Chapter 6

General Conclusion

Main results and discussion

The production process of liquid biofuels by microalgae is based on the biological production of energy reserve molecules (TAG and carbohydrates) stored by the cell, which amount is increased in non-optimal growth conditions. Optimally producing and recovering such molecules are challenging stages in the perspective of a large scale energy efficient process, especially when considering the context of outdoor culture which induces time-varying growth conditions. The present work aimed to optimize key aspects of culturing energy-rich microalgae and the wet-extraction pathway to recover energy metabolites, for finally integrate them into an energy-drive biorefinery approach including a global NER analysis.

Chapter 2 has compared the potential of two promising strains for the biofuel production: *Nannochloropsis gaditana* and *Parachlorella kessleri*. There, *N. gaditana* has shown stability for the TAG/carbohydrate consumption during dark periods of day-night cycles, where *P. kessleri* did not. Such characteristic could be relevant for the outdoors production since it avoids large losses of metabolite during dynamic light regimes.

Then, a nitrogen-limited culture was investigated with the aim to set a continuous production of TAG enriched biomass. Here, *N. gaditana* was firstly investigated under continuous light and it revealed relevant TAG productivities besides a dynamic cell disruption rate, both along the nitrogen limitation levels. This also revealed the compromise for the final TAG/carbohydrate recovery, since for larger limitations levels (and so higher TAG/carbohydrate contents), also high mechanical resistance values were found.

Based on those results, the calculation of the potentially recoverable energy of the strain was proposed. It considers the TAG/carbohydrate productivity on a specific nitrogen limitation level, the cell disruption rate associated and the transposition of both into a 100% efficient simultaneous BioEthanol and BioDiesel production process. With this approach it was possible to determinate that a nitrogen limitation level of 56% $_{NO_3}$ generated an equivalent of 86.6 J/m²·d of energy from liq-

uid biofuels from *N. gaditana* (67.8 and 18.7 J/m² · d from BioDiesel and BioEthanol respectively). Meanwhile through a bibliographic comparison and the same calculation of the potentially recoverable energy, *P. kessleri* was found to produce 128 J/m² · d at 46%_{NO₃} level (47 and 81 J/m² · d from BioDiesel and BioEthanol respectively), which makes it a suitable strain for the dual valorization of the biomass into both BioDiesel and BioEthanol. *N. gaditana* remained of interest when targeting BioDiesel production using seawater resource in the perspective of avoid from using freshwater as should be using *P. kessleri*.

N. gaditana has been investigated in Chapter 3 towards the nitrogen limited continuous culture protocol during day-night cycles. During this chapter it was proposed the concept of released TAG, which includes the effect of cell disruption rate on the final TAG productivity.

Since, microalgae may consume energy-stored metabolites in absence of light and *N. gaditana* showed a marked decrease of mechanical resistance during day-night cycles, the concept of released TAG was found an option to find the optimal compromise between TAG productivity and their release into the liquid broth. By using the released TAG approach, it was retrieved the optimal harvesting time for nitrogen starved batched cultures of *N. gaditana* under day-night cycles, at 4 hr after sunset, leading to a released TAG of 0.27 · 10⁻³ kg/m² · d. Algeenan accumulation in cell wall was hypothesized to be responsible of the mechanical resistance changes observed in night period.

Similarly, a continuous nitrogen limitation protocol under day-night cycles was proposed. It was demonstrated that the reduction of the dilution rate (at 0.005 h⁻¹ in simultaneous continuous mode and nitrogen limitation), was able to compensate the biomass losses occurring during dark times of day-night cycles, as a consequence of the slower cellular growth. Released TAG under this protocol achieved 1.4 · 10⁻³ kg/m² · d (Biomass surface productivity of 9 · 10⁻³ kg/m² · d). The protocol enabled the continuous outdoors production of TAG molecules from microalgae in nitrogen limited conditions.

However, there exists some other bottlenecks to undertake on the way to an energy-efficient biofuel production process. The wet-extraction pathway is precisely a set of technologies that avoid a substantial energy investment in the recovery production block. The Chapter 4 aimed to optimize two of these technologies: bead milling and continuous centrifugal extraction; both over a *N. gaditana* wet biomass.

It was found that biomass concentrations around 10-30 g/L of nitrogen-depleted culture need 5.8 min in a bead milling device (grinding chamber ≈ 0.561 L, filled at 80% and inlet rate of 9 L/h) to disrupt 80% of the cells. Meanwhile, a significance difference was found when treating a nitrogen-repleted culture; requiring only 4.8 min of treatment. The results were in accordance to those in Chapter 3, describing the increase of mechanical resistance when cells are close to nitrogen depletion.

This information stressed the energy balance issue, revealing that not all the physiological states

of a strain might require the same energy input during downstream operations; *ie.* for *N. gaditana* it exists a marked relation in terms of operational parameters, between the culture stage and the bead milling operation that might impact the final recovered energy in terms of biofuel.

The disrupted biomass (rich in TAG molecules) was used to optimize the continuous centrifugal extraction; an intensified technology that takes advantage of centrifugal forces to separate and extract compounds by the use of solvents. A Box-Behnken response surface methodology showed that the interaction between biomass concentration and solvent inlet rate influences the centrifugal extraction the most. The optimal process was determined to use 7.9 g/L biomass concentration at 5.4 mL/min inlet rate and 8.9 mL/min inlet rate of 2-methyl-tetra-hydrofuran, to extract a final TAG recovery of 84%. The combined effect of bead milling and centrifugal extraction achieved 73% final TAG recovery. However the use of solvent still being elevated in 214 g of 2-methyl-tetra-hydrofuran per each gram of recovered TAG, therefore further research on the solvent consumption and other operative concerns (*eg.* emulsification) are here suggested.

The results of this chapter show how important it is to obtain optimized protocols that take into consideration not only the operational parameters, but also the final state of the biomass at the end of the culture; *ie.* changes in mechanical resistance, biomass concentration and availability of metabolites of interest.

It is important to mention that the another extraction output (aqueous phase supposed without lipids) contains carbohydrate molecules and residual biomass. This process stream was thought to be a valuable source to simultaneously produce BioEthanol in parallel to BioDiesel. The Chapter 5 proposed a energy-driven biorefinery approach to investigate different scenarios of microalgal biomass production and conversion into biofuel. For that purpose, this final chapter bring together the concepts and results from all the previous chapters to evaluate the potential of the culture technologies and operational protocols for culture and downstream processing, on the final net energy ratio of the overall biofuel process.

Through five simulations, results have shown that the most energy-intensive process are, in order, the culture stage, metabolite recovery, BioDiesel conversion and finally the BioEthanol conversion blocks. The culture process might save about 50% of the energy input by using high volumetric photobioreactors combined with the insulated glass unit and the integrated energy-generating photovoltaic module. The high volumetric photobioreactor allows to significantly increase the biomass concentration, while reducing culture volume and then energy consumption. It enables to avoid harvesting/concentration unit and reduce the final energy input. In the same manner, the insulated glass unit avoids solar radiation to heat the system and then the use of energy-intensive heat control systems. Meanwhile, the integrated energy-generating photovoltaic module was demonstrated to be crucial for producing energy for maintaining downstream process units and increase then the overall net energy ratio.

Using the above mentioned processes it was also simulated the comparison of *P. kessleri* and *N. gaditana* for the double biofuel production from 1 Tn/y of dry algal biomass. The net energy ratio for the culture protocol of Chapter 3 using *N. gaditana* was 0.68; recovering 7 754 MJ/y issued from 244 L/Tn·y of liquid biofuels (53% of the potentially recovered fuel energy). Meanwhile, *P. kessleri* (with higher carbohydrate content) under continuous light protocol produced similar energy (7 676 MJ/y; 46% of the potentially recovered fuel energy) with a net energy ratio of 0.56 and producing up to 282 L/Tn·y of liquid biofuels.

Even though the simulated net energy ratios for all the simulated cases were below 1 even for the entire double biofuel production, results allowed to identify the key energy-intensive process blocks and their effect on the overall process. The importance of the co-production of other energy sources (photovoltaic and simultaneous BioDiesel and BioEthanol) in the final input energy and net energy ratio of the process was shown. From a energy-driven biorefinery approach, the double biofuel production looks interesting to be further researched; it might assist to diminish the costs of the process and to value more the biomass.

Conclusion

Along the present manuscript it has been discussed several key aspects of the biofuel production process and their interactions. Here are some highlights of the work:

- Insights to the strain prospection through their energy potential,
- a protocol for continuous production under simultaneous nitrogen limitation and day-night cycles,
- insights on the physiological changes (mechanical resistance and TAG consumption) of microalgae in nitrogen depletion and day-night cycles and how these directly impact the downstream processing for recovering interesting molecules,
- the double biofuel recovery perspective, and
- insights for developing and intensifying downstream technologies for the final net energy ratio and valorisation of algal biomass. The last presented simulations reveal that the suggested technologies are still far from energy neutrality, however recent technologies and new culture and downstream optimization protocols, as those presented here, bring us even closer to the goal of producing sustainable energy to help solve the environment and modern society challenges.

Nomenclature

Variables

$\%X$	biomass fraction on dry weight basis, %
A^*	illuminated surface, m^2
a_s	specific illuminated area, $1/m$
D	dilution rate, h^{-1}
ΔH_{comb}°	Heat of combustion, MJ/kg
E	(with subscript) Recoverable Energy, $J/m^2 \cdot d$
E	(no subscript) Extract flow rate, mL/min
E	Energy, MJ
E_{EI}	operative energy, MJ/y
E_Q	cooling energy, MJ/y
F	Feed of Biomass flow rate, mL/min
I	Irradiance, $\mu mol/m^2 \cdot s$
M	Mass flow rate, kg/d
MW	(with subscript) Molecular weigh, (g/mol)
N	NO_3^- concentration, mM
P	volumetric productivity, $kg/m^3 \cdot d$
$PF D$	Photon Flux Density, $\mu mol/m^2 \cdot s$
Pu	Purity, %
Q	Volume flow rate, m^3
R	Raffinate flow rate, mL/min
S	(with subscript) Surface productivity, $kg/m^2 \cdot d$
S	(with numerical subscript), assigns a stream
S	(no subscript) Solvent flow rate, mL/min
t	Time, h/d/y
V	Volume, m^3
X	biomass concentration, kg/m^3
Y	Yield of two variables, units depends on the variables

Greek symbols

Γ	Specific solvent consumption, dimensionless
Δ	Difference between a reference and sampling value, dimensionless
$\eta_{j,i}$	Efficiency in the process/operation j , for the i component, dimensionless
μ	Specific growth rate, 1/h
ρ	Density, g/mL or kg/L
τ_D	Disruption Rate, %

Subscripts

0	refers to initial
<i>BioD</i>	refers to Biodiesel
<i>BioE</i>	refers to Bioethanol
<i>D</i>	Refers to disruption process
<i>dark</i>	refers to night period in a day-night cycle
<i>E</i>	refers to the extraction
<i>FAME</i>	refers to fatty acid methyl esters
<i>Fer</i>	refers to fermentation
<i>i, j</i>	related to a specific subject
<i>light</i>	refers to day period in a day-night cycle
Me-OH	Refers to Methanol
Me-THF	Refers to 2-methyl-tetra-hydrofuran
NO_3	refers to nitrate concentration
N/X	refers to nitrate consumption to biomass production ratio
<i>P</i>	refers to sum of energies recovered from biodiesel and bioethanol
<i>PAR</i>	refers to photosynthetically active radiation
<i>OP</i>	Refers to a full process operating property
<i>Op</i>	Refers to particular Operating property
<i>PV</i>	Refers to Photovoltaic
<i>S</i>	Refers to the solvent
<i>Sg</i>	refers to carbohydrates
<i>T</i>	Refers to the total
<i>t</i>	refers to a particular instant
<i>TAG</i>	refers to triacylglycerol

<i>TFA</i>	refers to total fatty acid
<i>Trans</i>	refers to transesterification
<i>W</i>	Refers to the water
<i>X</i>	refers to biomass
<i>XR</i>	Refers to the residual biomass
<i>Z</i>	Refers to waste

Acronyms and abbreviations

AFOLU	Agriculture, forestry and other land use
ASW	Artificial sea water
BECCS	Bioenergy with carbon dioxide capture and storage
BM	Bead-Milling
C	Centrifugation
CCE	Continuous Centrifugal Extraction
CCX	Centrifugal Continuous Extraction
CDR	Carbon Dioxide Removal
CPE	Centrifugal Partition Extraction
D	Solvent Recovery
DNc	Day-night cycle(s)
EtoAc	Ethyl Acetate
FP-PBR	Flat Panel Photobioreactor
GHGs	Greenhouse gases
Hep	Heptane
HVP-PBR	High Volumetric Productivity photobioreactor
IEA	International Energy Agency
Me-THF	2-Methyl-tetra-hydrofuran
NER	Net Energy ratio
OU	Observation units for DoE
PAR	Photosynthetically Active Radiation
PBR	Photobioreactor
PEC	Passive Evaporative Cooling
PFD	Photon Flux Density
Prod	Production zone
R	Stirred reactor
Rec	Recovery zone

RSM	Response Surface Methodology
TAG	Triacylglycerol
TFA	Total fatty acid
WMO	World Meteorological Organization

Bibliography

- Adhikari, S., Fernando, S. D., and Haryanto, A. (2009). Hydrogen production from glycerol: An update. *Energy Conversion and Management*, 50(10), 2600–2604.
- Alalwan, H. A., Alminshid, A. H., and Aljaafari, H. A. (2019). Promising evolution of biofuel generations. Subject review. *Renewable Energy Focus*, 28(March), 127–139.
- Alam, M. A., Xu, J. L., and Wang, Z. (2020). *Microalgae biotechnology for food, health and high value products*.
- Alboresi, A., Perin, G., Vitulo, N., Diretto, G., Block, M., Jouhet, J., Meneghesso, A., Valle, G., Giuliano, G., Maréchal, E., and Morosinotto, T. (2016). Light remodels lipid biosynthesis in *Nannochloropsis gaditana* by modulating carbon partitioning between organelles. *Plant Physiology*, 171(4), 2468–2482.
- Ali, A., Qadir, A., Kuddus, M., Saxena, P., and Abdin, M. Z. (2019). Production of biodiesel from algae: An update. *Handbook of Ecomaterials*, 3(April), 1953–1964.
- Allard, B., Rager, M. N., and Templier, J. (2002). Occurrence of high molecular weight lipids (C80+) in the trilaminar outer cell walls of some freshwater microalgae. A reappraisal of algaenan structure. *Organic Geochemistry*, 33(7), 789–801.
- Amaro, H. M., Guedes, A. C., and Malcata, F. X. (2011). Advances and perspectives in using microalgae to produce biodiesel. *Applied Energy*, 88(10), 3402–3410.
- American Public Health Association (1999). *4500 NO3 NITROGEN (NITRATE)*.
- Angles, E., Jaouen, P., Pruvost, J., and Marchal, L. (2017). Wet lipid extraction from the microalga *Nannochloropsis* sp.: Disruption, physiological effects and solvent screening. *Algal Research*, 21, 27–34.
- Axelsson, M. and Gentili, F. (2014). A single-step method for rapid extraction of total lipids from green microalgae. *PLoS ONE*, 9(2), 17–20.
- Balasubramanian, R. K., Yen Doan, T. T., and Obbard, J. P. (2013). Factors affecting cellular lipid extraction from marine microalgae. *Chemical Engineering Journal*, 215–216, 929–936.
- Balasundaram, B., Harrison, S., and Bracewell, D. G. (2009). Advances in product release strategies and impact on bioprocess design. *Trends in Biotechnology*, 27(8), 477–485.
- Batan, L., Quinn, J., Willson, B., and Bradley, T. (2010). Net energy and greenhouse gas emission evaluation of biodiesel derived from microalgae. *Environmental Science and Technology*, 44(20), 7975–7980.
- Baudry, G., Delrue, F., Legrand, J., Pruvost, J., and Vallée, T. (2017). The challenge of measuring biofuel sustainability: A stakeholder-driven approach applied to the French case. *Renewable and Sustainable Energy Reviews*, 69, 933–947.
- Beacham, T. A., Bradley, C., White, D. A., Bond, P., and Ali, S. T. (2014). Lipid productivity and cell wall ultrastructure of six strains of *Nannochloropsis*: Implications for biofuel production and downstream processing. *Algal Research*, 6(PA), 64–69.
- Beer, L. L., Boyd, E. S., Peters, J. W., and Posewitz, M. C. (2009). Engineering algae for biohydrogen and biofuel production. *Current Opinion in Biotechnology*, 20(3), 264–271.
- Benvenuti, G. (2016). *Batch and repeated-batch oil production by microalgae*. Ph.D. thesis, Wageningen University.

- Benvenuti, G., Bosma, R., Cuaresma, M., Janssen, M., Barbosa, M. J., and Wijffels, R. H. (2015). Selecting microalgae with high lipid productivity and photosynthetic activity under nitrogen starvation. *Journal of Applied Phycology*, 27(4), 1425–1431.
- Benvenuti, G., Bosma, R., Ji, F., Lamers, P., Barbosa, M. J., and Wijffels, R. H. (2016a). Batch and semi-continuous microalgal TAG production in lab-scale and outdoor photobioreactors. *Journal of Applied Phycology*, 28(6), 3167–3177.
- Benvenuti, G., Lamers, P. P., Breuer, G., Bosma, R., Cerar, A., Wijffels, R. H., and Barbosa, M. J. (2016b). Microalgal TAG production strategies: Why batch beats repeated-batch. *Biotechnology for Biofuels*, 9(1), 1–17.
- Berger, A. (1988). Milankovitch Theory and climate. *Reviews of Geophysics*, 26(4), 624–657.
- Berges, J. A., Charlebois, D. O., Mauzerall, D. C., and Falkowski, P. G. (1996). Differential Effects of Nitrogen Limitation on Photosynthetic Efficiency of Photosystems I and II in Microalgae. *Plant Physiology*, 110(2), 689–696.
- Berges, J. A., Franklin, D. J., and Harrison, P. J. (2001). Evolution of an artificial seawater medium: Improvements in enriched seawater, artificial water over the last two decades. *Journal of Phycology*, 37(6), 1138–1145.
- Bligh, E. G. and Dyer, W. J. (1959). A Rapid Method Of Total Lipid Extraction And Purification. *Canadian Journal of Biochemistry and Physiology*, 37(8), 911–917.
- Blokker, P., Schouten, S., Van den Ende, H., De Leeuw, J. W., Hatcher, P. G., and Sinninghe Damsté, J. S. (1998). Chemical structure of algaenans from the fresh water algae *Tetraedron minimum*, *Scenedesmus communis* and *Pediastrum boryanum*. *Organic Geochemistry*, 29(5-7-7 pt 2), 1453–1468.
- Bojczuk, M., Żyźelewicz, D., and Hodurek, P. (2017). Centrifugal partition chromatography – A review of recent applications and some classic references. *Journal of Separation Science*, 40(7), 1597–1609.
- Bond, G., Showers, W., Cheseby, M., Lotti, R., Almasi, P., DeMenocal, P., Priore, P., Cullen, H., Hajdas, I., and Bonani, G. (1997). A pervasive millennial-scale cycle in North Atlantic Holocene and glacial climates. *Science*, 278(5341), 1257–1266.
- Bonnefond, H., Moelants, N., Talec, A., Bernard, O., and Sciandra, A. (2016). Concomitant effects of light and temperature diel variations on the growth rate and lipid production of *Dunaliella salina*. *Algal Research*, 14(MARCH), 72–78.
- Borowitzka, M. A. (2018). The ‘stress’ concept in microalgal biology—homeostasis, acclimation and adaptation. *Journal of Applied Phycology*, 30(5), 2815–2825.
- Borowitzka, M. a. and Moheimani, N. R. (2013). *Algae for Biofuels and Energy*.
- Bouillaud, D., Heredia, V., Castaing-Cordier, T., Drouin, D., Charrier, B., Gonçalves, O., Farjon, J., and Giraudeau, P. (2019). Benchtop flow NMR spectroscopy as an online device for the in vivo monitoring of lipid accumulation in microalgae. *Algal Research*, 43(July), 101624.
- Box, G. E. P. and Behnken, D. W. (1960). Some New Three Level Designs for the Study of Quantitative Variables. *Technometrics*, 2(4), 455.
- Brennan, L. and Owende, P. (2010). Biofuels from microalgae—A review of technologies for production, processing, and extractions of biofuels and co-products. *Renewable and Sustainable Energy Reviews*, 14(2), 557–577.
- Breuer, G., Lamers, P. P., Martens, D. E., Draaisma, R. B., and Wijffels, R. H. (2013). Effect of light intensity, pH, and temperature on triacylglycerol (TAG) accumulation induced by nitrogen starvation in *Scenedesmus obliquus*. *Bioresource Technology*, 143, 1–9.
- Camacho-Rodríguez, J., González-Céspedes, A. M., Cerón-García, M. C., Fernández-Sevilla, J. M., Acien-Fernández, F. G., and Molina-Grima, E. (2014). A quantitative study of eicosapentaenoic acid (EPA) production by *Nannochloropsis gaditana* for aquaculture as a function of dilution rate, temperature and average irradiance. *Applied Microbiology and Biotechnology*, 98(6), 2429–2440.

- Caperon, J. and Meyer, J. (1972). Nitrogen-limited growth of marine phytoplankton-I. changes in population characteristics with steady-state growth rate. *Deep-Sea Research and Oceanographic Abstracts*, 19(9), 601–618.
- Cavicchioli, R., Ripple, W. J., Timmis, K. N., Azam, F., Bakken, L. R., Baylis, M., Behrenfeld, M. J., Boetius, A., Boyd, P. W., Classen, A. T., Crowther, T. W., Danovaro, R., Foreman, C. M., Huisman, J., Hutchins, D. A., Jansson, J. K., Karl, D. M., Koskella, B., Mark Welch, D. B., Martiny, J. B., Moran, M. A., Orphan, V. J., Reay, D. S., Remais, J. V., Rich, V. I., Singh, B. K., Stein, L. Y., Stewart, F. J., Sullivan, M. B., van Oppen, M. J., Weaver, S. C., Webb, E. A., and Webster, N. S. (2019). Scientists' warning to humanity: microorganisms and climate change. *Nature Reviews Microbiology*, 17(9), 569–586.
- Chew, K. W., Yap, J. Y., Show, P. L., Suan, N. H., Juan, J. C., Ling, T. C., Lee, D. J., and Chang, J. S. (2017). Microalgae biorefinery: High value products perspectives. *Bioresource Technology*, 229, 53–62.
- Chisti, Y. (2007). Biodiesel from microalgae. *Biotechnology Advances*, 25(3), 294–306.
- Chisti, Y. (2008). Biodiesel from microalgae beats bioethanol. *Trends in Biotechnology*, 26(3), 126–131.
- Chua, E. T. and Schenk, P. M. (2017). A biorefinery for Nannochloropsis: Induction, harvesting, and extraction of EPA-rich oil and high-value protein. *Bioresource Technology*, 244, 1416–1424.
- CNRS (2020). Microalgues: les coulisses d'une révolution.
- Collet, P., Lardon, L., Hélias, A., Bricout, S., Lombaert-Valot, I., Perrier, B., Lépine, O., Steyer, J. P., and Bernard, O. (2014). Biodiesel from microalgae - Life cycle assessment and recommendations for potential improvements. *Renewable Energy*, 71, 525–533.
- Cornet, J. F., Dussap, C. G., and Dubertret, G. (1992). A structured model for simulation of cultures of the cyanobacterium *Spirulina platensis* in photobioreactors: I. Coupling between light transfer and growth kinetics. *Biotechnology and Bioengineering*, 40(7), 817–825.
- Cuellar-Bermudez, S. P., Garcia-Perez, J. S., Rittmann, B. E., and Parra-Saldivar, R. (2015). Photosynthetic bioenergy utilizing CO₂: an approach on flue gases utilization for third generation biofuels. *Journal of Cleaner Production*, 98, 53–65.
- de Farias Silva, C. E. and Bertucco, A. (2016). Bioethanol from microalgae and cyanobacteria: A review and technological outlook. *Process Biochemistry*, 51(11), 1833–1842.
- Dejode Tanzi, C., Abert Vian, M., and Chemat, F. (2013). New procedure for extraction of algal lipids from wet biomass: A green clean and scalable process. *Bioresource Technology*, 134, 271–275.
- Dien, B. S., Cotta, M. A., and Jeffries, T. W. (2003). Bacteria engineered for fuel ethanol production: current status. *Applied Microbiology and Biotechnology*, 63(3), 258–266.
- Dineshababu, G., Vijayan, D., Uma, V. S., Makut, B. B., and Das, D. (2019). Microalgal Systems for Integrated Carbon Sequestration from Flue Gas and Wastewater Treatment. In *Application of Microalgae in Wastewater Treatment*, pages 339–370. Springer International Publishing, Cham.
- Dong, T., Knoshaug, E. P., Pienkos, P. T., and Laurens, L. M. (2016). Lipid recovery from wet oleaginous microbial biomass for biofuel production: A critical review. *Applied Energy*, 177, 879–895.
- Dortch, Q. (1982). Effect of growth conditions on accumulation of internal nitrate, ammonium, amino acids, and protein in three marine diatoms. *Journal of Experimental Marine Biology and Ecology*, 61(3), 243–264.
- DuBois, M., Gilles, K. A., Hamilton, J. K., Rebers, P. A., and Smith, F. (1956). Colorimetric Method for Determination of Sugars and Related Substances. *Analytical Chemistry*, 28(3), 350–356.
- Dunker, S. and Wilhelm, C. (2018). Cell wall structure of coccoid green algae as an important trade-off between biotic interference mechanisms and multidimensional cell growth. *Frontiers in Microbiology*, 9(APR).

- Ebert, S., Grossmann, L., Hinrichs, J., and Weiss, J. (2019). Emulsifying properties of water-soluble proteins extracted from the microalgae: *Chlorella sorokiniana* and *Phaeodactylum tricornutum*. *Food and Function*, 10(2), 754–764.
- Edmundson, S. J. and Huesemann, M. H. (2015). The dark side of algae cultivation: Characterizing night biomass loss in three photosynthetic algae, *Chlorella sorokiniana*, *Nannochloropsis salina* and *Picochlorum* sp. *Algal Research*, 12, 470–476.
- Edwards, R., Hass, H., Larivé, J.-F., Lonza, L., Mass, H., Rickeard, D., Larive, J.-F., Rickeard, D., and Weindorf, W. (2013). *Well-to-Wheels analysis of future automotive fuels and powertrains in the European context WELL-TO-TANK (WTT) Report. Version 4.*
- Edwards, R., Hass, H., Larivé, J.-F., Lonza, L., Mass, H., Rickeard, D., Larive, J.-F., and Rickeard, D. (2014). *Well-To-Wheels Report Version 4.a. JEC Well-to-wheels Analysis.*
- Fábregas, J., Maseda, A., Domínguez, A., Ferreira, M., and Otero, A. (2002). Changes in the cell composition of the marine microalga, *Nannochloropsis gaditana*, during a light:dark cycle. *Biotechnology Letters*, 24, 1699–1703.
- Fariéd, M., Samer, M., Abdelsalam, E., Yousef, R. S., Attia, Y. A., and Ali, A. S. (2017). Biodiesel production from microalgae: Processes, technologies and recent advancements. *Renewable and Sustainable Energy Reviews*, 79(May), 893–913.
- Farrar, W. V. (1966). Tecuitlatl; A Glimpse of Aztec Food Technology. *Nature*, 211(5047), 341–342.
- Fernandes, B., Teixeira, J., Dragone, G., Vicente, A. A., Kawano, S., Bišová, K., Příbyl, P., Zachelder, V., and Vítová, M. (2013). Relationship between starch and lipid accumulation induced by nutrient depletion and replenishment in the microalga *Parachlorella kessleri*. *Bioresource Technology*, 144, 268–274.
- Ferreira, S. L., Bruns, R. E., Ferreira, H. S., Matos, G. D., David, J. M., Brandão, G. C., da Silva, E. G., Portugal, L. A., dos Reis, P. S., Souza, A. S., and dos Santos, W. N. (2007). Box-Behnken design: An alternative for the optimization of analytical methods. *Analytica Chimica Acta*, 597(2), 179–186.
- Figuroa, F. L., Jimenez, C., Lubian, L. M., Montero, O., Lebert, M., and Hader, D. P. (1997). Effects of high irradiance and temperature on photosynthesis and photoinhibition in *nannochloropsis gaditana* lubian (eustigmatophyceae). *Journal of Plant Physiology*, 151(1), 6–15.
- Fischer, C. R., Klein-Marcuschamer, D., and Stephanopoulos, G. (2008). Selection and optimization of microbial hosts for biofuels production. *Metabolic Engineering*, 10(6), 295–304.
- Flynn, K. J., Davidson, K., and Cunningham, A. (1993). Relations between carbon and nitrogen during growth of *Nannochloropsis oculata* (Droop) Hibberd under continuous illumination. *New Phytologist*, 125(4), 717–722.
- Fortman, J. L., Chhabra, S., Mukhopadhyay, A., Chou, H., Lee, T. S., Steen, E., and Keasling, J. D. (2008). Biofuel alternatives to ethanol: pumping the microbial well. *Trends in Biotechnology*, 26(7), 375–381.
- Foster, G. L., Royer, D. L., and Lunt, D. J. (2017). Future climate forcing potentially without precedent in the last 420 million years. *Nature Communications*, 8, 1–8.
- Fukuda, H., Kondo, A., and Noda, H. (2001). Biodiesel fuel production by transesterification of oils. *Journal of Bioscience and Bioengineering*, 92(5), 405–416.
- Gelin, F., Volkman, J. K., De Leeuw, J. W., and Sinninghe Damsté, J. S. (1997). Mid-chain hydroxy long-chain fatty acids in microalgae from the genus *Nannochloropsis*. *Phytochemistry*, 45(4), 641–646.
- Gelin, F., Volkman, J. K., Largeau, C., Derenne, S., Sinninghe Damsté, J. S., and De Leeuw, J. W. (1999). Distribution of aliphatic, nonhydrolyzable biopolymers in marine microalgae. *Organic Geochemistry*, 30(2-3), 147–159.
- Ghasemi Naghdi, F., González González, L. M., Chan, W., and Schenk, P. M. (2016). Progress on lipid extraction from wet algal biomass for biodiesel production. *Microbial Biotechnology*, 9(6), 718–726.

- Gifuni, I., Pollio, A., Safi, C., Marzocchella, A., and Olivieri, G. (2019). Current Bottlenecks and Challenges of the Microalgal Biorefinery. *Trends in Biotechnology*, 37(3), 242–252.
- Grobbelaar, J. U. and Soeder, C. J. (1985). Respiration losses in planktonic green algae cultivated in raceway ponds. *Journal of Plankton Research*.
- Halim, R., Gladman, B., Danquah, M. K., and Webley, P. A. (2011). Oil extraction from microalgae for biodiesel production. *Bioresource Technology*, 102(1), 178–185.
- Halim, R., Danquah, M. K., and Webley, P. A. (2012a). Extraction of oil from microalgae for biodiesel production: A review. *Biotechnology Advances*, 30(3), 709–732.
- Halim, R., Harun, R., Danquah, M. K., and Webley, P. A. (2012b). Microalgal cell disruption for biofuel development. *Applied Energy*, 91(1), 116–121.
- Hamje, H. D. C., HASS, H., LONZA, L., MAAS, H., REID, A., D.ROSE, K., and VENDERBOSCH, T. (2014). EU renewable energy targets in 2020: Revised analysis of scenarios for transport fuels. Technical report, Publications Office of the European Union, Luxembourg.
- Hansen, J. E. and Sato, M. (2012). Paleoclimate implications for human-made climate change. *Climate Change: Inferences from Paleoclimate and Regional Aspects*, pages 21–47.
- Harris, J., Viner, K., Champagne, P., and Jessop, P. G. (2018). Advances in microalgal lipid extraction for biofuel production: a review. *Biofuels, Bioproducts and Biorefining*, 12(6), 1118–1135.
- Harun, R. and Danquah, M. K. (2011). Influence of acid pre-treatment on microalgal biomass for bioethanol production. *Process Biochemistry*, 46(1), 304–309.
- Harun, R., Danquah, M. K., and Forde, G. M. (2010). Microalgal biomass as a fermentation feedstock for bioethanol production. *Journal of Chemical Technology and Biotechnology*, 85(2), 199–203.
- Harun, R., Jason, W. S., Cherrington, T., and Danquah, M. K. (2011). Exploring alkaline pre-treatment of microalgal biomass for bioethanol production. *Applied Energy*, 88(10), 3464–3467.
- Heath, M. R., Richardson, K., and Kirboe, T. (1990). Optical assessment of phytoplankton nutrient depletion. *Journal of Plankton Research*, 12(2), 381–396.
- Ho, S. H., Huang, S. W., Chen, C. Y., Hasunuma, T., Kondo, A., and Chang, J. S. (2013). Bioethanol production using carbohydrate-rich microalgae biomass as feedstock. *Bioresource Technology*, 135, 191–198.
- Ho, S. H., Ye, X., Hasunuma, T., Chang, J. S., and Kondo, A. (2014). Perspectives on engineering strategies for improving biofuel production from microalgae - A critical review. *Biotechnology Advances*, 32(8), 1448–1459.
- Hossain, N., Zaini, J., and Indra Mahlia, T. M. (2019). Life cycle assessment, energy balance and sensitivity analysis of bioethanol production from microalgae in a tropical country. *Renewable and Sustainable Energy Reviews*, 115(April), 109371.
- IEA (2018). Market Report Series Renewables 2018 Analysis and Forecast to 2023. *International Energy Agency*, page 211.
- IEA (2019). Global Energy & CO2 Status Report 2019. Technical report, Paris.
- IEA (2020). Oil Market Report: 9 March 2020. Technical Report 9 March 2020.
- IPCC (2007). Climate Change 2007: Synthesis Report. Technical report, IPCC, Valencia, Spain.
- IPCC (2014). Climate Change 2014 Synthesis Report. Technical report, IPCC, Geneva, Switzerland.
- IPCC (2018). Summary for Policymakers, In: Global Warming of 1.5°C. An IPCC Special Report on the impacts of global warming of 1.5°C above pre-industrial levels and related global greenhouse gas emission pathways, in the context of strengthening the global response to.
- Janssen, J. H., Kastenhofer, J., de Hoop, J. A., Lamers, P. P., Wijffels, R. H., and Barbosa, M. J. (2018). Effect of nitrogen addition on lipid productivity of nitrogen starved *Nannochloropsis gaditana*. *Algal Research*, 33(May), 125–132.

- Janssen, J. H., Wijffels, R. H., and Barbosa, M. J. (2019a). Lipid production in *nannochloropsis gaditana* during nitrogen starvation. *Biology*, 8(1), 1–13.
- Janssen, J. H., Lamers, P. P., de Vos, R. C., Wijffels, R. H., and Barbosa, M. J. (2019b). Translocation and de novo synthesis of eicosapentaenoic acid (EPA) during nitrogen starvation in *Nannochloropsis gaditana*. *Algal Research*, 37(November 2018), 138–144.
- Janssen, J. H., Spoelder, J., Koehorst, J. J., Schaap, P. J., Wijffels, R. H., and Barbosa, M. J. (2020). Time-dependent transcriptome profile of genes involved in triacylglycerol (TAG) and polyunsaturated fatty acid synthesis in *Nannochloropsis gaditana* during nitrogen starvation. *Journal of Applied Phycology*.
- Janssen, M. (2002). *Cultivation of microalgae : effect of light / dark cycles on biomass yield*. Ph.D. thesis, Wageningen University.
- Juárez, Á. B., Vélez, C. G., Iñiguez, A. R., Martínez, D. E., Rodríguez, M. C., Vigna, M. S., and De Molina, M. D. C. R. (2011). A *Parachlorella kessleri* (Trebouxiophyceae, Chlorophyta) strain from an extremely acidic geothermal pond in Argentina. *Phycologia*, 50(4), 413–421.
- Kandilian, R., Pruvost, J., Legrand, J., and Pilon, L. (2014). Influence of light absorption rate by *Nannochloropsis oculata* on triglyceride production during nitrogen starvation. *Bioresource Technology*, 163, 308–319.
- Kandilian, R., Taleb, A., Heredia, V., Cogne, G., and Pruvost, J. (2019). Effect of light absorption rate and nitrate concentration on TAG accumulation and productivity of *Parachlorella kessleri* cultures grown in chemostat mode. *Algal Research*, 39(October 2018), 101442.
- Karemore, A. and Sen, R. (2016). Downstream processing of microalgal feedstock for lipid and carbohydrate in a biorefinery concept: a holistic approach for biofuel applications†. *RSC Advances*, 6(35), 29486–29496.
- Khalid, A. A., Yaakob, Z., Abdullah, S. R. S., and Takriff, M. S. (2019). Analysis of the elemental composition and uptake mechanism of *Chlorella sorokiniana* for nutrient removal in agricultural wastewater under optimized response surface methodology (RSM) conditions. *Journal of Cleaner Production*, 210, 673–686.
- Khuong, L. S., Zulkifli, N. W., Masjuki, H. H., Mohamad, E. N., Arslan, A., Mosarof, M. H., and Azham, A. (2016). A review on the effect of bioethanol dilution on the properties and performance of automotive lubricants in gasoline engines. *RSC Advances*, 6(71), 66847–66869.
- Kim, D. Y., Vijayan, D., Praveenkumar, R., Han, J. I., Lee, K., Park, J. Y., Chang, W. S., Lee, J. S., and Oh, Y. K. (2016). Cell-wall disruption and lipid/astaxanthin extraction from microalgae: *Chlorella* and *Haematococcus*. *Bioresource Technology*, 199(August), 300–310.
- Kim, S., Chen, J., Cheng, T., Gindulyte, A., He, J., He, S., Li, Q., Shoemaker, B. A., Thiessen, P. A., Yu, B., Zaslavsky, L., Zhang, J., and Bolton, E. E. (2019). PubChem 2019 update: improved access to chemical data. *Nucleic Acids Research*, 47(D1), D1102–D1109.
- Klinke, H. B., Thomsen, A. B., and Ahring, B. K. (2004). Inhibition of ethanol-producing yeast and bacteria by degradation products produced during pre-treatment of biomass. *Applied Microbiology and Biotechnology*, 66(1), 10–26.
- Kodner, R. B., Summons, R. E., and Knoll, A. H. (2009). Phylogenetic investigation of the aliphatic, non-hydrolyzable biopolymer algaenan, with a focus on green algae. *Organic Geochemistry*, 40(8), 854–862.
- Krienitz, L., Hegewald, E. H., Hepperle, D., Huss, V. A., Rohr, T., and Wolf, M. (2004). Phylogenetic relationship of *Chlorella* and *Parachlorella* gen. nov. (Chlorophyta, Trebouxiophyceae). *Phycologia*, 43(5), 529–542.
- Krzemińska, I., Pawlik-Skowrońska, B., Trzcińska, M., and Tys, J. (2014). Influence of photoperiods on the growth rate and biomass productivity of green microalgae. *Bioprocess and Biosystems Engineering*, 37(4), 735–741.
- Lacour, T., Sciandra, A., Talec, A., Mayzaud, P., and Bernard, O. (2012). Diel variations of carbohydrates and neutral lipids in nitrogen-sufficient and nitrogen-starved cyclostat cultures of *isochrysis* sp. *Journal of Phycology*, 48(4), 966–975.

- Lee, A. K., Lewis, D. M., and Ashman, P. J. (2012). Disruption of microalgal cells for the extraction of lipids for biofuels: Processes and specific energy requirements. *Biomass and Bioenergy*, 46, 89–101.
- Lee, D. H. (2011). Algal biodiesel economy and competition among bio-fuels. *Bioresource Technology*, 102(1), 43–49.
- Lee, E., Pruvost, J., He, X., Munipalli, R., and Pilon, L. (2014). Design tool and guidelines for outdoor photobioreactors. *Chemical Engineering Science*, 106, 18–29.
- Lee, J. Y., Yoo, C., Jun, S. Y., Ahn, C. Y., and Oh, H. M. (2010). Comparison of several methods for effective lipid extraction from microalgae. *Bioresource Technology*, 101(1 SUPPL.), S75–S77.
- Lee, S. Y., Cho, J. M., Chang, Y. K., and Oh, Y. K. (2017). Cell disruption and lipid extraction for microalgal biorefineries: A review. *Bioresource Technology*, 244, 1317–1328.
- Lee, T. H., Kim, M. Y., Ryu, Y. W., and Seo, J. H. (2001). Estimation of theoretical yield for ethanol production from D-xylose by recombinant *Saccharomyces cerevisiae* using a metabolic pathway synthesis algorithm. *Journal of Microbiology and Biotechnology*, 11(3), 384–388.
- Legrand, J. (2013). ADVANCES IN CHEMICAL ENGINEERING Photobioreaction Engineering. In *Journal of Chemical Information and Modeling*, volume 43, pages 1689–1699.
- Leong, W. H., Lim, J. W., Lam, M. K., Uemura, Y., and Ho, Y. C. (2018). Third generation biofuels: A nutritional perspective in enhancing microbial lipid production. *Renewable and Sustainable Energy Reviews*, 91(July 2017), 950–961.
- Lewandowicz, G., Białas, W., Marczewski, B., and Szymanowska, D. (2011). Application of membrane distillation for ethanol recovery during fuel ethanol production. *Journal of Membrane Science*, 375(1-2), 212–219.
- Li, X., Příbyl, P., Bišová, K., Kawano, S., Cepák, V., Zachleder, V., Čížková, M., Brányiková, I., and Vítová, M. (2013). The microalga *Parachlorella kessleri*—A novel highly efficient lipid producer. *Biotechnology and Bioengineering*, 110(1), 97–107.
- Lindsey, R. (2020). Climate Change: Atmospheric Carbon Dioxide.
- Lubian, L. M. (1982). *Nannochloropsis gaditana* sp. nov., a new Eustigmatophyceae marina. *Lazaroa*, 4, 287–293.
- Ma, X., Liu, J., Liu, B., Chen, T., Yang, B., and Chen, F. (2016). Physiological and biochemical changes reveal stress-associated photosynthetic carbon partitioning into triacylglycerol in the oleaginous marine alga *Nannochloropsis oculata*. *Algal Research*, 16, 28–35.
- Ma, Y., Wang, Z., Yu, C., Yin, Y., and Zhou, G. (2014). Evaluation of the potential of 9 *Nannochloropsis* strains for biodiesel production. *Bioresource Technology*, 167, 503–509.
- Matos, Â. P., Cavanholi, M. G., Moecke, E. H. S., and Sant’Anna, E. S. (2017). Effects of different photoperiod and trophic conditions on biomass, protein and lipid production by the marine alga *Nannochloropsis gaditana* at optimal concentration of desalination concentrate. *Bioresource Technology*, 224, 490–497.
- Mendoza, Á., Morales, V., Sánchez-Bayo, A., Rodríguez-Escudero, R., González-Fernández, C., Bautista, L. F., and Vicente, G. (2020). The effect of the lipid extraction method used in biodiesel production on the integrated recovery of biodiesel and biogas from *Nannochloropsis gaditana*, *Isochrysis galbana* and *Arthrospira platensis*. *Biochemical Engineering Journal*, 154(July 2019), 107428.
- Mitra, M., Patidar, S. K., George, B., Shah, F., and Mishra, S. (2015). A euryhaline *nannochloropsis gaditana* with potential for nutraceutical (EPA) and biodiesel production. *Algal Research*, 8, 161–167.
- Montalescot, V., Rinaldi, T., Touchard, R., Jubeau, S., Frappart, M., Jaouen, P., Bourseau, P., and Marchal, L. (2015). Optimization of bead milling parameters for the cell disruption of microalgae: Process modeling and application to *Porphyridium cruentum* and *Nannochloropsis oculata*. *Bioresource Technology*, 196, 339–346.
- Moutel, B., Gonçalves, O., Le Grand, F., Long, M., Soudant, P., Legrand, J., Grizeau, D., and Pruvost, J. (2016). Development of a screening procedure for the characterization of *Botryococcus braunii* strains for biofuel application. *Process Biochemistry*, 51(11), 1855–1865.

- Mutanda, T., Ramesh, D., Karthikeyan, S., Kumari, S., Anandraj, A., and Bux, F. (2011). Bioprospecting for hyper-lipid producing microalgal strains for sustainable biofuel production. *Bioresource Technology*, 102(1), 57–70.
- Naik, S. N., Goud, V. V., Rout, P. K., and Dalai, A. K. (2010). Production of first and second generation biofuels: A comprehensive review. *Renewable and Sustainable Energy Reviews*, 14(2), 578–597.
- Nakase, M. and Takeshita, K. (2012). Numerical and Experimental Study on Oil-water Dispersion in New Countercurrent Centrifugal Extractor. *Procedia Chemistry*, 7, 288–294.
- Navarro López, E., Robles Medina, A., González Moreno, P. A., Jiménez Callejón, M. J., Esteban Cerdán, L., Martín Valverde, L., Castillo López, B., and Molina Grima, E. (2015). Enzymatic production of biodiesel from nannochloropsis gaditana lipids: Influence of operational variables and polar lipid content. *Bioresource Technology*, 187, 346–353.
- NCMA (2020). *Microchloropsis gaditana* CCMP527.
- Nwoba, E. G., Parlevliet, D. A., Laird, D. W., Alameh, K., Louveau, J., Pruvost, J., and Moheimani, N. R. (2020). Energy efficiency analysis of outdoor standalone photovoltaic-powered photobioreactors coproducing lipid-rich algal biomass and electricity. *Applied Energy*, 275(March), 115403.
- Okamoto, K., Uchii, A., Kanawaku, R., and Yanase, H. (2014). Bioconversion of xylose, hexoses and biomass to ethanol by a new isolate of the white rot basidiomycete *Trametes versicolor*. *SpringerPlus*, 3(1), 1–9.
- Orijel, C., Gomez-Sanchez, C., Rios-Lozano, M., Guerrero-Torres, J., Rossano-Becerril, S., Herrera Ramirez, A., Rocha Ruiz, P., Chauvin, A., Badillo-Corona, J., de la Peña-Mireles, I., and Garza-Rodriguez, J. (2020). Enzymatic Methods for Isobutanol Production.
- Otterstedt, K., Larsson, C., Bill, R. M., Ståhlberg, A., Boles, E., Hohmann, S., and Gustafsson, L. (2004). Switching the mode of metabolism in the yeast *Saccharomyces cerevisiae*. *EMBO Reports*, 5(5), 532–537.
- Pan, Z., Huang, Y., Wang, Y., and Wu, Z. (2017). Disintegration of *Nannochloropsis* sp. cells in an improved turbine bead mill. *Bioresource Technology*, 245, 641–648.
- Patil, P. D., Dandamudi, K. P. R., Wang, J., Deng, Q., and Deng, S. (2018). Extraction of bio-oils from algae with supercritical carbon dioxide and co-solvents. *Journal of Supercritical Fluids*, 135(September 2017), 60–68.
- Přibyl, P., Cepák, V., and Zachleder, V. (2012). Production of lipids in 10 strains of *Chlorella* and *Parachlorella*, and enhanced lipid productivity in *Chlorella vulgaris*. *Applied Microbiology and Biotechnology*, 94(2), 549–561.
- Plouviez, M., Shilton, A., Packer, M. A., and Guieysse, B. (2017). N₂O emissions during microalgae outdoor cultivation in 50 L column photobioreactors. *Algal Research*, 26, 348–353.
- Ponton, J. W. (2009). Biofuels: Thermodynamic sense and nonsense. *Journal of Cleaner Production*, 17(10), 896–899.
- Pruvost, J. and Cornet, J.-F. (2012). Knowledge models for the engineering and optimization of photobioreactors. In C. and C. Walter, editor, *Microalgal Biotechnology: Potential and Production*, number January 2012, pages 181–224. De Gruyter.
- Pruvost, J., Van Vooren, G., Cogne, G., and Legrand, J. (2009). Investigation of biomass and lipids production with *Neochloris oleoabundans* in photobioreactor. *Bioresource Technology*, 100(23), 5988–5995.
- Pruvost, J., Cornet, J. F., Goetz, V., and Legrand, J. (2011a). Modeling dynamic functioning of rectangular photobioreactors in solar conditions. *AIChE Journal*, 57(7), 1947–1960.
- Pruvost, J., Van Vooren, G., Le Gouic, B., Couzinet-Mossion, A., and Legrand, J. (2011b). Systematic investigation of biomass and lipid productivity by microalgae in photobioreactors for biodiesel application. *Bioresource Technology*, 102(1), 150–158.
- Pruvost, J., Cornet, J. F., Le Borgne, F., Goetz, V., and Legrand, J. (2015). Theoretical investigation of microalgae culture in the light changing conditions of solar photobioreactor production and comparison with cyanobacteria. *Algal Research*, 10, 87–99.

- Pruvost, J., Le Borgne, F., Artu, A., Cornet, J.-F., and Legrand, J. (2016). Industrial Photobioreactors and Scale-Up Concepts. pages 257–310.
- Pruvost, J., Le Borgne, F., Artu, A., and Legrand, J. (2017). Development of a thin-film solar photobioreactor with high biomass volumetric productivity (AlgoFilm©) based on process intensification principles. *Algal Research*, 21, 120–137.
- Pruvost, J., Goetz, V., Artu, A., Das, P., and Al Jabri, H. (2019). Thermal modeling and optimization of microalgal biomass production in the harsh desert conditions of State of Qatar. *Algal Research*, 38(December 2018), 101381.
- Rafay, R., Uratani, J. M., Hernandez, H. H., and Rodríguez, J. (2020). Growth and Nitrate Uptake in *Nannochloropsis gaditana* and *Tetraselmis chuii* Cultures Grown in Sequential Batch Reactors. *Frontiers in Marine Science*, 7(February), 1–9.
- Renaud, S. M., Zhou, H. C., Parry, D. L., Thinh, L. V., and Woo, K. C. (1995). Effect of temperature on the growth, total lipid content and fatty acid composition of recently isolated tropical microalgae *Isochrysis* sp., *Nitzschia closterium*, *Nitzschia paleacea*, and commercial species *Isochrysis* sp. (clone T.ISO). *Journal of Applied Phycology*, 7(6), 595–602.
- Richmond, A. (1996). Efficient utilization of high irradiance for production of photoautotrophic cell mass: A survey. *Journal of Applied Phycology*, 8(4-5), 381–387.
- Richmond, A. (2004). *Handbook of Microalgal Culture: Biotechnology and Applied Phycology*. Wiley-Blackwell, Oxford, 1 edition.
- Ritchie, R. J. (2006). Consistent sets of spectrophotometric chlorophyll equations for acetone, methanol and ethanol solvents. *Photosynthesis Research*, 89(1), 27–41.
- Rodolfi, L., Zittelli, G. C., Bassi, N., Padovani, G., Biondi, N., Bonini, G., and Tredici, M. R. (2009). Microalgae for oil: Strain selection, induction of lipid synthesis and outdoor mass cultivation in a low-cost photobioreactor. *Biotechnology and Bioengineering*, 102(1), 100–112.
- Ruangsomboon, S. (2012). Effect of light, nutrient, cultivation time and salinity on lipid production of newly isolated strain of the green microalga, *Botryococcus braunii* KMITL 2. *Bioresource Technology*, 109, 261–265.
- Ryckebosch, E., Bermúdez, S. P. C., Termote-Verhalle, R., Bruneel, C., Muylaert, K., Parra-Saldivar, R., and Foubert, I. (2014). Influence of extraction solvent system on the extractability of lipid components from the biomass of *Nannochloropsis gaditana*. *Journal of Applied Phycology*, 26(3), 1501–1510.
- Safi, C., Charton, M., Pignolet, O., Silvestre, F., Vaca-Garcia, C., and Pontalier, P. Y. (2013). Influence of microalgae cell wall characteristics on protein extractability and determination of nitrogen-to-protein conversion factors. *Journal of Applied Phycology*, 25(2), 523–529.
- Safi, C., Cabas Rodriguez, L., Mulder, W. J., Engelen-Smit, N., Spekking, W., van den Broek, L. A., Olivieri, G., and Sijtsma, L. (2017). Energy consumption and water-soluble protein release by cell wall disruption of *Nannochloropsis gaditana*. *Bioresource Technology*, 239, 204–210.
- San Pedro, A., González-López, C. V., Ación, F. G., and Molina-Grima, E. (2013). Marine microalgae selection and culture conditions optimization for biodiesel production. *Bioresource Technology*, 134, 353–361.
- San Pedro, A., González-López, C. V., Ación, F. G., and Molina-Grima, E. (2014). Outdoor pilot-scale production of *Nannochloropsis gaditana*: Influence of culture parameters and lipid production rates in tubular photobioreactors. *Bioresource Technology*, 169, 667–676.
- Sander, K. and Murthy, G. S. (2010). Life cycle analysis of algae biodiesel. *International Journal of Life Cycle Assessment*, 15(7), 704–714.
- Sati, H., Mitra, M., Mishra, S., and Baredar, P. (2019). Microalgal lipid extraction strategies for biodiesel production: A review. *Algal Research*, 38(January), 101413.
- Scholz, M. J., Riley, M. R., and Cuello, J. L. (2013). Acid hydrolysis and fermentation of microalgal starches to ethanol by the yeast *Saccharomyces cerevisiae*. *Biomass and Bioenergy*, 48, 59–65.

- Scholz, M. J., Weiss, T. L., Jinkerson, R. E., Jing, J., Roth, R., Goodenough, U., Posewitz, M. C., and Gerken, H. G. (2014). Ultrastructure and composition of the *Nannochloropsis gaditana* cell wall. *Eukaryotic Cell*, 13(11), 1450–1464.
- Schügerl, K. (1994). *Solvent Extraction in Biotechnology*, volume 8. Springer Berlin Heidelberg, Berlin, Heidelberg.
- Scott, S. A., Davey, M. P., Dennis, J. S., Horst, I., Howe, C. J., Lea-Smith, D. J., and Smith, A. G. (2010). Biodiesel from algae: Challenges and prospects. *Current Opinion in Biotechnology*, 21(3), 277–286.
- Seyfang, B., Klein, A., and Grützner, T. (2019). Extraction Centrifuges—Intensified Equipment Facilitating Modular and Flexible Plant Concepts. *ChemEngineering*, 3(1), 17.
- Shuba, E. S. and Kifle, D. (2018). Microalgae to biofuels: ‘Promising’ alternative and renewable energy, review. *Renewable and Sustainable Energy Reviews*, 81(August 2017), 743–755.
- Sicaire, A.-G., Vian, M. A., Filly, A., Li, Y., Bily, A., and Chemat, F. (2014). 2-Methyltetrahydrofuran: Main Properties, Production Processes, and Application in Extraction of Natural Products. pages 253–268.
- Simionato, D., Sforza, E., Corteggiani Carpinelli, E., Bertucco, A., Giacometti, G. M., and Morosinotto, T. (2011). Acclimation of *Nannochloropsis gaditana* to different illumination regimes: Effects on lipids accumulation. *Bioresource Technology*, 102(10), 6026–6032.
- Simionato, D., Block, M. A., La Rocca, N., Jouhet, J., Maréchal, E., Finazzi, G., and Morosinotto, T. (2013). The response of *Nannochloropsis gaditana* to nitrogen starvation includes de novo biosynthesis of triacylglycerols, a decrease of chloroplast galactolipids, and reorganization of the photosynthetic apparatus. *Eukaryotic Cell*, 12(5), 665–676.
- Sivaramakrishnan, R. and Incharoensakdi, A. (2018). Utilization of microalgae feedstock for concomitant production of bioethanol and biodiesel. *Fuel*, 217(December 2017), 458–466.
- Song, M., Pei, H., Hu, W., and Ma, G. (2013). Evaluation of the potential of 10 microalgal strains for biodiesel production. *Bioresource Technology*, 141, 245–251.
- Strickland, J. D. H. and Parsons, T. R. (1968). *A Practical Handbook of Seawater Analysis*. Number 167. Fisheries Research Board of Canada, Ottawa, second ed edition.
- Stuart, J. T. (1986). Taylor-Vortex Flow: A Dynamical System. *SIAM Review*, 28(3), 315–342.
- Suganya, T., Varman, M., Masjuki, H. H., and Renganathan, S. (2016). Macroalgae and microalgae as a potential source for commercial applications along with biofuels production: A biorefinery approach. *Renewable and Sustainable Energy Reviews*, 55, 909–941.
- Swings, J. and De Ley, J. (1977). The biology of *Zygomonas mobilis*. *Bacteriological reviews*, 41(1), 1–46.
- Taher, H., Al-Zuhair, S., Al-Marzouqi, A. H., Haik, Y., and Farid, M. (2014). Effective extraction of microalgae lipids from wet biomass for biodiesel production. *Biomass and Bioenergy*, 66, 159–167.
- Taleb, A., Pruvost, J., Legrand, J., Marec, H., Le-Gouic, B., Mirabella, B., Legeret, B., Bouvet, S., Peltier, G., Li-Beisson, Y., Taha, S., and Takache, H. (2015). Development and validation of a screening procedure of microalgae for biodiesel production: Application to the genus of marine microalgae *Nannochloropsis*. *Bioresource Technology*, 177(January), 224–232.
- Taleb, A., Kandilian, R., Touchard, R., Montalescot, V., Rinaldi, T., Taha, S., Takache, H., Marchal, L., Legrand, J., and Pruvost, J. (2016). Screening of freshwater and seawater microalgae strains in fully controlled photobioreactors for biodiesel production. *Bioresource Technology*, 218, 480–490.
- Taleb, A., Legrand, J., Takache, H., Taha, S., and Pruvost, J. (2018). Investigation of lipid production by nitrogen-starved *Parachlorella kessleri* under continuous illumination and day/night cycles for biodiesel application. *Journal of Applied Phycology*, 30(2), 761–772.
- Tan, X. B., Lam, M. K., Uemura, Y., Lim, J. W., Wong, C. Y., and Lee, K. T. (2018). Cultivation of microalgae for biodiesel production: A review on upstream and downstream processing. *Chinese Journal of Chemical Engineering*, 26(1), 17–30.

- Thimijan, R. and Heins, R. (1983). Photometric, radiometric, and quantum light units of measure: a review of procedures for interconversion. *HortScience*, 18(6), 818–822.
- Timilsina, G. R. and Shrestha, A. (2011). How much hope should we have for biofuels? *Energy*, 36(4), 2055–2069.
- Tredici, M. R., Bassi, N., Prussi, M., Biondi, N., Rodolfi, L., Chini Zittelli, G., and Sampietro, G. (2015). Energy balance of algal biomass production in a 1-ha "Green Wall Panel" plant: How to produce algal biomass in a closed reactor achieving a high Net Energy Ratio. *Applied Energy*, 154, 1103–1111.
- United-Nations (2015). Accord de Paris. *21ème Conférence des Parties*, pages 1–18.
- UTEX (2020). *Chlorella kessleri* 2229.
- Van Vooren, G., Le Grand, F., Legrand, J., Cuiné, S., Peltier, G., and Pruvost, J. (2012). Investigation of fatty acids accumulation in *Nannochloropsis oculata* for biodiesel application. *Bioresource Technology*, 124, 421–432.
- Venkata Subhash, G., Rohit, M. V., Devi, M. P., Swamy, Y. V., and Venkata Mohan, S. (2014). Temperature induced stress influence on biodiesel productivity during mixotrophic microalgae cultivation with wastewater. *Bioresource Technology*, 169, 789–793.
- Vitova, M., Bisova, K., Kawano, S., and Zachleder, V. (2014). Accumulation of energy reserves in algae: From cell cycles to biotechnological applications. *Biotechnology Advances*, 33(6), 1204–1218.
- Vítová, M., Goecke, F., Sigler, K., and Řezanka, T. (2016). Lipidomic analysis of the extremophilic red alga *Galdieria sulphuraria* in response to changes in pH. *Algal Research*, 13, 218–226.
- Voiland, A. (2010). Aerosols: Tiny Particles, Big Impact.
- WATSON, R. A. and OSBORNE, P. L. (1979). An algal pigment ratio as an indicator of the nitrogen supply to phytoplankton in three Norfolk broads. *Freshwater Biology*, 9(6), 585–594.
- Watts, P. (2004). Chloroform. Technical Report 58, World Health Organization, Geneva, Switzerland.
- Wei, P., Cheng, L. H., Zhang, L., Xu, X. H., Chen, H. L., and Gao, C. J. (2014). A review of membrane technology for bioethanol production. *Renewable and Sustainable Energy Reviews*, 30, 388–400.
- Wilhelm, C., Büchel, C., Fisahn, J., Goss, R., Jakob, T., LaRoche, J., Lavaud, J., Lohr, M., Riebesell, U., Stehfest, K., Valentin, K., and Kroth, P. G. (2006). The Regulation of Carbon and Nutrient Assimilation in Diatoms is Significantly Different from Green Algae. *Protist*, 157(2), 91–124.
- Willeit, M., Ganopolski, A., Calov, R., and Brovkin, V. (2019). Mid-Pleistocene transition in glacial cycles explained by declining CO₂ and regolith removal. *Science Advances*, 5(4), 1–9.
- Williams, P. J. B. and Laurens, L. M. (2010). Microalgae as biodiesel & biomass feedstocks: Review & analysis of the biochemistry, energetics & economics. *Energy and Environmental Science*, 3(5), 554–590.
- WMO (2019). WMO Statement on the State of the Global Climate in 2018. Technical Report 1233.
- WMO (2020). WMO statement on the status of the global climate in 2019. Technical Report 1248.
- Xu, H., Miao, X., and Wu, Q. (2006). High quality biodiesel production from a microalga *Chlorella protothecoides* by heterotrophic growth in fermenters. *Journal of Biotechnology*, 126(4), 499–507.
- Yang, S., Fei, Q., Zhang, Y., Contreras, L. M., Utturkar, S. M., Brown, S. D., Himmel, M. E., and Zhang, M. (2016). *Zyomonas mobilis* as a model system for production of biofuels and biochemicals. *Microbial Biotechnology*, 9(6), 699–717.
- Yoon, K., Han, D., Li, Y., Sommerfeld, M., and Hu, Q. (2012). Phospholipid:Diacylglycerol Acyltransferase Is a Multifunctional Enzyme Involved in Membrane Lipid Turnover and Degradation While Synthesizing Triacylglycerol in the Unicellular Green Microalga *Chlamydomonas reinhardtii*. *The Plant Cell*, 24(9), 3708–3724.

- Yousuf, A. (2012). Biodiesel from lignocellulosic biomass - Prospects and challenges. *Waste Management*, 32(11), 2061–2067.
- Yuan, J., Kendall, A., and Zhang, Y. (2015). Mass balance and life cycle assessment of biodiesel from microalgae incorporated with nutrient recycling options and technology uncertainties. *GCB Bioenergy*, 7(6), 1245–1259.
- Zalasiewicz, J. A., Williams, M., Steffen, W., and Crutzen, P. (2010). The new world of the anthropocene. *Environmental Science and Technology*, 44(7), 2228–2231.
- Zhang, Z. and Volkman, J. K. (2017). Algaenan structure in the microalga *Nannochloropsis oculata* characterized from stepwise pyrolysis. *Organic Geochemistry*, 104, 1–7.
- Zhu, L., Nugroho, Y. K., Shakeel, S. R., Li, Z., Martinkauppi, B., and Hiltunen, E. (2017). Using microalgae to produce liquid transportation biodiesel: What is next? *Renewable and Sustainable Energy Reviews*, 78(May 2016), 391–400.
- Zinkoné, T. R., Gifuni, I., Lavenant, L., Pruvost, J., and Marchal, L. (2018). Bead milling disruption kinetics of microalgae: Process modeling, optimization and application to biomolecules recovery from *Chlorella sorokiniana*. *Bioresource Technology*, 267(July), 458–465.

Titre : Optimisation de la production de biocarburants par microalgues en conditions solaires

Mots clés : Biocarburants, Extraction voie-humide, Microalgues, Cycles jour-nuit, Efficience énergétique

Résumé : La biodiversité des microalgues offre un grand nombre d'espèces pouvant être utilisées comme source de sucres et de triacylglycérol pour biocarburants. *Parachlorella kessleri* et *Nannochloropsis gaditana* sont deux souches prometteuses pour cet usage. Différentes dynamiques d'accumulation en sucres et TAG ont été mesurés en avant pour ces deux souches, menant à un potentiel différent d'énergie totale récupérable. *P. kessleri* a montré un bon potentiel pour le biodiesel et un fort potentiel pour le bioéthanol, contrairement à *N. gaditana* qui nécessite une optimisation préférentielle de la production et de la récupération de TAG pour le biodiesel, principalement en raison d'un plus forte teneur en TAG mais aussi de l'augmentation de la résistance mécanique dans des conditions de stress et des cycles jour-nuit.

Il a été proposé un protocole pour produire du TAG sous limitation d'azotée, cycles jour-nuit et mode de production continu. Dans le cadre de ce dernier protocole, les TAG libérés pour l'extraction par voie humide ont été de 1,4 g/m²-j. Le processus d'extraction humide en soit a également été optimisé. Le broyage des billes a permis de détruire 80 % des cellules carencées pour un temps de séjour d'environ 6 minutes. Ensuite, l'extraction centrifuge en continu a permis de récupérer les 84 % de TAG libérés en utilisant 8,9 ml/min de 2-méthyl-tétra-hydrofurane. Ces résultats ont été intégrés dans une simulation du procédé global, permettant d'identifier les opérations critiques basé sur l'analyse du NER, ainsi qu'en proposant une double récupération de biocarburants liquides (BioEthanol + BioDiesel)

Title : Optimization of Biofuel production in Solar conditions by Microalgae

Keywords : Biofuels, Wet-extraction, Microalgae, Day-Night Cycles, Energy efficiency

Abstract : Microalgae biodiversity offers large number of species with the potential to be used as source of carbohydrates and triacylglycerol for biofuels. *Parachlorella kessleri* and *Nannochloropsis gaditana* are two promising strains for biofuel production. The different dynamics of carbohydrates and TAG accumulation for both strains, exposed also different potential of total recoverable energy for biofuels. *P. kessleri* showed a good potential for biodiesel and high potential for bioethanol; in contrast to *N. gaditana* which presented larger TAG content but also requires a preferential optimization on the TAG production and recovery for biodiesel mainly because of the increase in mechanical resistance during stress conditions and day-night cycles.

It was proposed a protocol to produce TAG under nitrogen limitation, day-night cycles and continuous production mode. Under the latter protocol, released TAG for the Wet-extraction downstream were 1.4 g/m²-d. Downstream wet-extraction process was also optimized. Bead milling disrupted 80% of the starved cells in ~6 min residence time. Then, by the following continuous centrifugal extraction, it was recovered the 84% of released TAG using 8.9 mL/min of 2-methyl-tetra-hydrofuran. These results were integrated in a whole-process simulation, allowing to identify the critical operations based on NER analysis, and proposing, as well, a double liquid biofuel recovery (BioEthanol + BioDiesel).